Elucidating the role of dipeptidyl peptidase 4 in cancer metabolism and biology using in vitro and in vivo models

By

Lisa Pogson
Bachelor of Science (Honours)

Thesis
Submitted to Flinders University
for the degree of

Doctor of Philosophy

College of Science and Engineering
1 December 2021

Declaration

I certify that this thesis does not incorporate, without acknowledgment, any material

previously submitted for a degree or diploma in any university. To the best of my knowledge

and belief it does not contain any material previously published or written by another person

except where due reference is made in the text.

Lisa Dawn Pogson

Date 03/05/2021

Acknowledgements

I would first and foremost like to thank my supervisor Professor Catherine Abbott for providing me with the opportunity to undertake this project and for her guidance, encouragement, time and never-ending patience throughout this study. I also would like to acknowledge the contribution of an Australian Postgraduate Award Scholarship which allowed me to undertake the research required to complete this thesis.

The work described in this thesis could not have been completed without significant help from a number of people. I would like to thank Andrew Boslem for lending us the Seahorse XFe analyser and providing the training and support that contributed to the results presented in chapter two. I would like to thank Professor Mark Gorrell and Sumaiya Chowdhury for maintaining the knockout mouse breeding stock and providing us with the DPP4 and FAP knockout mice, Dr Hanna Krysinska for her assistance in setting up the animal model and Dr David Rudd for his support, advice and assistance with sacrifice and tissue collection. I would also like to thank Professor Catherine Abbott for going above and beyond in helping me with my animal monitoring and management when I broke my elbow and could not enter the animal facility. I would like to thank Dr Ying Hu and Julian Di Ubaldo for their assistance in the histological evaluation and classification of the colonic tumours. I would finally like to thank Dr Daniel Jardine for training and technical advice at Flinders Analytical (Flinders University) and Dr Cindy Macardle for kindly providing me with THP-1 cells.

I would finally like to thank the past and present members of the Abbott laboratory for their help and support throughout my research and would like to thank Hanna and David for their ongoing encouragement, support, and friendship. I would finally like to give a special thanks to my family, my Mum, and my three beautiful children Jessica, James and Jason. Thank you all for your love and support and for your understanding of what I was trying to achieve. Thank you for always understanding my commitment during months where all family events were impacted by mouse monitoring, and for supporting me through trying to write while working a high stress full time job, I could not have finished this thesis without you. I must also give special thanks to my Mum, who has worked tirelessly supporting both me and my children, keeping our lives running smoothly especially when my work and writing left me little time for anything else. Thank you Mum you are truly awesome.

Contents

List of Figures

List of Tables

Abbreviations

ACF	Aberrant crypt foci
ADA	Adenosine deaminase
ADP	Adenosine diphosphate
AK2	Adenylate Kinase 2
Akt	Protein kinase B
ALT	Alanine aminotransferase
AML	Acute myeloid leukaemia
AMP	Adenosine monophosphate
AMPK	AMP-activated protein kinase
ANOVA	Analysis of variance
AOM	Azoxymethane
APAF	Australian Proteome Analysis Facility
AST	Aspartate aminotransferase
ATP	Adenosine triphosphate
B-CLL	B cell chronic lymphocytic leukemia
BPH	Benign prostatic hyperplasia
BSA	Bovine serum albumin
CAFs	Cancer-associated fibroblasts
CD9	Tetraspanin
CD24	Cluster of differentiation 24
CML	Chronic myeloid leukemia
CO_2	Carbondioxide
CSC	Cancer stem cells
CRC	Colorectal cancer
CXC	Chemokine receptor
DMSO	Dimethyl sulfoxide
ECAR	Extracellular acidification rate
ESFT	Ewing's sarcoma family of tumours
ETC	Electron transport chain
DMH	1,2-Dimethylhydrazine
DNA	Deoxyribonucleic acid

DPP	Dipeptidyl peptidase
DPP4/CD26	Dipeptidyl peptidase 4
DPP6	Dipeptidyl peptidase 6
DPP8	Dipeptidyl peptidase 8
DPP9	Dipeptidyl peptidase 9
DPP10	Dipeptidyl peptidase 10
ECAR	Extracellular acidification rate
ECL	Enhanced chemiluminescence
ECM	Extracellular matrix
EDTA	Ethylenediaminetetraacetic acid
EMT	Epithelial–mesenchymal transition
ETC	Electron transport chain
FAP	Fibroblast activation protein
FBS	Fetal bovine serum
FCCP	Carbonyl cyanide-4-(trifluoromethoxy)phenylhydrazone
FDA	U.S. Food and Drug Administration
FDG-PET	Fluorodeoxyglucose positron emission tomography
GIP	Glucose-dependent insulinotropic peptide
GLP-1	Glucagon-like peptide-1
GLP-2	Glucagon-like peptide-2
GM-CSF	Granulocyte-macrophage colony-stimulating factor
H_2O	Hydrogen dioxide
HEPA	High Efficiency-Particulate Air
HEPES	4-(2-hydroxyethyl)-1-piperazineethanesulfonic acid
HPLC	High-performance liquid chromatography
HRP	Horseradish peroxidase
hVSMCs	Human vascular smooth muscle cells
IFN-γ	Interferon gamma
IGF-1	insulin-like growth factor 1
IL	Interleukin
IMS	Mitochondrial intermembrane space
IP-10	Interferon gamma-induced protein 10

K_2HPO_4	Dipotassium hydrogen phosphate
LIX	C-X-C motif chemokine 5
MAb	Monoclonal antibody
MALDI	Matrix-assisted laser desorption/ionisation
MAM	Methylazoxymethanol
MAP2K1	Mitogen-activated protein kinase 1
MAPK	Mitogen-activated protein kinase
MCP-1	Monocyte chemoattractant protein-1
MDF	Mucin-depleted foci
ME	Metabolizable energy
MIP-1α	Macrophage inflammatory protein
miRNAs	Micro ribonucleic acid
MMP	Matrix metalloproteinase
MMP-2	Matrix metalloproteinase-2
MPM	Malignant pleural mesothelioma
mRNA	Messenger RNA
MSI	Mass spectrometry imaging
MT-1	Membrane type 1
NAFLD	Nonalcoholic fatty liver disease
NK cells	Natural killer cells
NPC	Nuclear pore complex
NPY	Neuropeptide Y
NOD-SCID	Non-obese diabetic background severe combined immunodeficiency mice
NSCLC	Non-small cell lung cancers
OD	Optical density
OCR	Oxygen consumption rate
pAMPK	Phosphorylated AMP-activated protein kinase
PBS	Phosphate buffered saline
PI-3K	Phosphoinositide 3-kinase
PP	Pancreatic polypeptide hormone
PYY	Peptide tyrosine tyrosine
RANTES	Regulated on activation normal T cell expressed and secreted

RCC	Renal Cell Carcinoma
RNA	Ribonucleic acid
RPMI	Roswell Park Memorial Institute Medium
RT	Room temperature
RT-PCR	Reverse transcription polymerase chain reaction
SALDI	Surface-assisted laser desorption/ionisation
SCID	Severe combined immunodeficiency
SDF-1	Stromal-cell-derived factor-1-α
SDS-PAGE	Sodium dodecyl sulphate–polyacrylamide gel electrophoresis
SEM	Standard error
T2DM	Type 2 diabetes mellitus
T-ALCL	T-anaplastic large cell lymphomas
T-ALL	T-acute lymphoblastic leukemias
TEMED	Tetramethylethylenediamine
T-LBL	T lymphoblastic lymphomas
T-LGLLPD	T-large granular lymphocyte lymphoproliferative disorder
TNF	Tumor necrosis factor
VbP	L-valinyl-L-boroproline
VEGF	Vascular endothelial growth factor
WT	Wildtype
XF	Extracellular Flux
XFe	Extracellular Flux analyser

Abstract

Diabetes and cancer are two diseases with significant impact on worldwide health that share many mutual risk factors and biological links. While both disease states involve significant metabolic change as well as activation of inflammatory and stress-related pathways, a causal relationship between diabetes and cancer is yet to be identified. Patients with diabetes have a significantly higher risk of developing certain cancer types including colorectal cancer, the second leading cause of cancer related deaths worldwide with about 1 million cases and >500,000 deaths annually. Furthermore, an increase in colorectal cancer incidence is associated with western diet and lifestyle, factors that are also linked with increased insulin resistance and predisposition to type 2 diabetes mellitus (T2DM), such as high calorie intake, low physical activity and excess abdominal fat. Recent observational studies suggest that some medications used to treat hyperglycaemia and T2DM are associated with a reduced risk of cancer. Given this association, there is a growing interest in determining the impact of T2DM treatment targets on tumorigenesis.

Sitagliptin is a selective dipeptidyl peptidase-4 (DPP4) inhibitor also used for the treatment of T2DM. The insulinotropic action of sitagliptin involves the increase of nutrient-stimulated insulin release through inhibition of DPP4 enzymatic degradation of the active form of incretins, glucose-dependent insulinotropic peptide (GIP) and glucagon-like peptide-1 (GLP-1). Sitagliptin is one of the most readily available DPP4 inhibitors in Australia, in the 2019/20 financial year 1.5 million pharmaceutical scripts for sitagliptin were claimed in Australia amassing a total cost of $82 million dollars. However, in addition to its insulinotropic action, the enzymatic activity of DPP4 is shown to be involved in a diverse range of biological processes associated with neoplastic transformation, including cell differentiation and adhesion, immune modulation and apoptosis. This raises some well warranted concerns within the research and medical community on whether DPP4 inhibition will have a positive or negative effect on the initiation and progression of different cancers, particularly colorectal cancer. The overall aim of this thesis was to determine the role DPP4 inhibitors play in the control of the metabolic needs of cancer cells and establish a relationship between DPP4 and colorectal cancer development and progression.

In chapter two sitagliptin was used to examine the possible effects of DPP4 inhibition on the regulation of cellular metabolism and the AMP-activated protein kinase (AMPK) signalling pathway in two lymphocyte cell lines. The actions of sitagliptin were compared to metformin a known AMPK regulator and front line T2DM treatment associated with a reduced cancer burden in diabetic patients. *In vitro* analysis of mitochondrial respiration and glycolysis demonstrated that sitagliptin alters the bioenergetic profile of both T lymphocyte cells and

human acute monocytic leukemia cells, reducing both oxidative phosphorylation and glycolysis in a similar fashion to metformin. Additionally, metabolic reprogramming by sitagliptin was associated with increased AMPK and activated AMPK presence, indicating that DPP4 imparts control over cellular metabolism through AMPK associated actions.

In chapter three a chemically induced colon carcinogenesis model using azoxymethane (AOM) was established in DPP4 genetic knockout mice (Dpp4-/-) on a the C57Bl/6 background. In this work the closely related DPP4 protein family member fibroblast activation protein (FAP) was also targeted using the same model of carcinogenesis in FAP genetic knockout mice (Fap-/-). FAP shares a close sequence identity to DPP4 and is believed to arise from gene duplication due to its gene proximity and is identified as a potential pharmaceutical target in several types of cancers including colon carcinogenesis. Chapter three is the first study to utilise the AOM model of colorectal cancer in Dpp4-/- and Fap-/- mice and establishes that this model of colorectal cancer is suitable for use with these genetic knockouts. In chapter three a monitoring refinement was established that led to improvements in animal welfare by reducing the weight loss cut off point for euthanasia. This enabled identification of a subset of mice where AOM treatment led to severe liver damage allowing elimination of these mice earlier from the study. This modification ties into the refinement alternative of the three R's principal of animal experimentation reducing animal distress and enhancing the welfare of experimental animals. Additionally, this study indicates that DPP4 and FAP ablation is protective against severe AOM driven liver injury and less mice in these groups were removed from the trial as they were less likely to reach the 10% weight loss cut-off for euthanasia after AOM treatment.

In chapter four the refined AOM model described in chapter three was used to examine the role of DPP4 and FAP in CRC progression. Chapter four provides further evidence that both DPP4 and FAP play a role in tumour pathogenesis. With exposure to AOM, Dpp4-/- mice develop a significantly increased number of adenomas and adenocarcinomas while both Dpp4-/- and Fap-/- mice have significantly increased tumour growth and penetrance. Dpp4-/- mice also show a significant reduction in total numbers of ACF which indicates that in the absence of DPP4 tumour progression is occurring at a faster rate. Dpp4-/- and Fap-/- mice have reduced plasma levels of CXCL10 indicating a reduced ability to recruit immune cells into the tumour site, additionally, Dpp4-/- mice have significantly reduced lymphocyte numbers indicating that both phenotypes have an impaired immune response which may be contributing to increased tumour growth. The results from this work confirm that both DPP4 and FAP are involved in CRC tumour development and highlights the need for further work

to identify the mechanisms through which ablation of DPP4 and FAP increases tumorigenesis.

The significant original contribution of knowledge in this thesis is that it is the first study to demonstrate using the AOM chemically induced carcinogenesis model in Dpp4-/- and Fap-/- mice, that both DPP4 and FAP play a role in tumour incidence and development and that DPP4 plays a significant role in tumour prevalence. In contrast chapter two indicates that sitagliptin may provide a novel therapeutic approach for targeted metabolic reprogramming of cancer cells positioning DPP4 inhibitors as potential anti-cancer agents for some specific tumour types. These findings are in direct contradiction to recently published animal studies suggesting that DPP4 inhibitors either have no effect on tumour development or decrease overall tumour number. However, DPP4 has two domains, an enzyme active domain, which DPP4 inhibitors act upon, and another domain that is able to mediate protein-protein interactions that are involved in the cancer process. This paradox suggests that although inhibition of DPP4 enzyme activity may be protective against CRC development, DPP4 direct protein interactions may be involved in a much more significant way in control of colorectal cancer development and progression.

Chapter 1

Literature Review

1.1 Introduction

Dipeptidyl peptidase-4 (DPP4) also known as the T-cell activation antigen CD26, is a serine exopeptidase belonging to a class of proteases that cleave a dipeptide from proteins and peptides with a penultimate proline residue (Abbott et al., 2006; Hopsu-Havu and Glenner, 1966; Matteucci and Giampietro, 2009). DPP4 is the foremost member of the S9B or DPP4 protein family, a subgroup of the prolyl-oligopeptidase family of enzymes, which includes DPP4, fibroblast activation protein alpha (FAP or seprase), dipeptidyl peptidase 8 (DPP8) and dipeptidyl peptidase 9 (DPP9) (Abbott et al., 2006; Gorrell, 2005; Yazbeck et al., 2009; Yu et al., 2010). There are also two non-enzymatic family members that function as brain localised potassium channel modulators, DPP6, previously called DPL1 (DP-like 1) and DPP10 (DPL2 or DPPX), both DPP6 and DPP10 are enzymatically inactive due to a mutation of the catalytic serine and its bordering tryptophan residues (Ansorge et al., 2011; Kirby et al., 2010).

The members of the DPP4 gene family consist of both membrane-bound and soluble forms which cover an expansive range of expression patterns, tissue distributions and localization. While each has its own unique substrate specificity, they all have similar structural elements within their catalytic domains (Abbott et al., 1999). The family are considered non-classical serine proteases, they have a serine nucleophile like other serine proteases but their catalytic triad has an amino acid order of serine, aspartic acid, histidine, which is reversed from that seen for classical serine proteases like those found in the trypsin and subtilisin families (Rosenblum and Kozarich, 2003). The DPP4 protein structure is a homodimer with each protein monomer comprising two distinct domains, an N-terminal localised 8-bladed propeller domain and a C-terminal hydrolase domain. The propeller domain sits against the hydrolase domain with the catalytic triad localised at the interface (Aertgeerts et al., 2004; Nardini and Dijkstra, 1999).

The enzyme active members of the DPP4 gene family are distinguished from other endopeptidases able to hydrolyse post-proline bonds by a pair of glutamate residues located in the propeller domain. These residues found at position 205 and 206 in human DPP4 are essential for dipeptidyl peptidase activity, they are isolated from the catalytic serine in the primary structure, but located within the catalytic pocket in the tertiary structure and are most likely essential factors effecting substrate entry (Abbott et al., 1999).

DPP4 enzyme activity removes an X-Pro or X-Ala dipeptide from the N-terminus of small peptide substrates containing on average 30 residues (Abbott et al., 1999). Peptide bonds that comprise proline residues are less affected by enzymatic degradation through general

peptidase activity as the distinct cyclic structure of the proline amino acid manipulates the structural conformation of the peptide chain and provides protection against degradation by most other proteases (Mentlein, 1988). The reduced susceptibility of prolyl carrying peptides to proteolytic hydrolysis offers a mechanism of safeguard against degradation (Cunningham and O'Connor, 1997). The ability of the DPP4 enzyme family to specifically target and augment these prolyl carrying peptides sets them apart from other proteases and highlights the importance of their function. After nearly 40 years of investigation on this enzyme family and their actions *in vivo*, their diverse functionality means that much more research is required before their functions are fully elucidated. Investigation into N-terminal processing of polypeptides via dipeptidyl peptidase activity has associated this processing activity with the augmentation of function in a variety of substrates including chemokines, neuropeptides, and peptide hormones (Yazbeck et al., 2009; Yu et al., 2010). Ongoing study of this family of enzymes has identified their involvement in cancer progression and metabolism and highlighted the possibility of their use in future treatments targeted at oncology and other chemotherapeutic interventions (Matteucci and Giampietro, 2009; Wagner et al., 2016; Waumans et al., 2015; Yu et al., 2010).

The altered expression of DPP4 and associated protein family members is observed in a number of human tumour types identifying their pathogenic relevance in carcinogenesis (Yazbeck et al., 2018). The archetypal family member DPP4 has an important role in metabolism, maintaining glucose homeostasis through the *in vivo* stabilization of the incretins GIP and GLP-1, gut-regulatory peptides that control blood sugar levels through postprandial insulin secretion and glucose clearance (De et al., 2018; Mulvihill and Drucker, 2014). DPP4 inhibitors have been in clinical use for treatment of type 2 diabetes mellitus (T2DM) for over a decade and are now widely accepted as an antidiabetic therapeutic approach (Mulvihill and Drucker, 2014). In addition to its known role in metabolism, DPP4 plays a complicated and conflicting role in cancer growth, acting as both a tumour suppressor and a tumour promoter dependent on tumour type (Sulda et al., 2006). The associated enzyme family member FAP is expressed at sites of tissue remodelling and on reactive stromal fibroblasts of epithelial cancers, and its overexpression is associated with increased tumour growth and invasion (Puré and Blomberg, 2018). In this review the current understanding of the action of DPP4 and FAP will be summarised in respect to their possible role in cancer biology.

1.2 Dipeptidyl Peptidase 4

Dipeptidyl peptidase 4 (DPP4) (EC 3.4.14.5) was originally identified in 1966 (Hopsu-Havu and Glenner, 1966) and is characterised as a homodimeric type 2 transmembrane glycoprotein that has a molecular mass of 220–240 kDa. It is also known as the leukocyte surface antigen CD26 (Fleischer, 1994; Tanaka, 1993). Human DPP4 is comprised of 766 amino acids, it has a short cytoplasmic tail consisting of six NH_2-terminal amino acids, a 23 amino acid transmembrane domain and an extracellular domain comprised of the remaining 737 amino acids (Misumi et al., 1992; Ogata et al., 1989). It is the extracellular domain that exhibits the dipeptidyl peptidase enzyme activity, selectively removing N-terminal dipeptides from peptide substrates containing a penultimate proline or alanine residue (Matteucci and Giampietro, 2009).

DPP4 is found in body fluids such as serum and seminal plasma, this soluble form is lacking the transmembrane domain and intracellular NH_2 terminal tail thus is thought to result from proteolytic cleavage of DPP4 from the cell membrane (Iwaki-Egawa et al., 1998; Lambeir et al., 2003). DPP4 enzyme activity associated with its soluble form has been described in human serum as well as in other bodily fluids including, saliva, urine, synovial fluid and at very low levels in cerebrospinal fluid (Yazbeck et al., 2018). Highest levels of soluble DPP4 enzyme activity is found to be associated with prostasomes or prostrate localised vesicles found in seminal plasma (Kotackova et al., 2009; Vanhoof et al., 1992).

1.2.1 DPP4 mRNA expression and protein presence

DPP4 mRNA in normal adult tissue shows high expression in the placenta and the kidney, moderate expression in the lung and liver, and low-level expression in skeletal muscle, the heart, pancreas and the brain (Abbott et al., 1994). In rats immunoblot in conjunction with mRNA expression analysis demonstrates high DPP4 presence and expression in the kidney and small intestine, moderate levels in the lung, liver, and spleen and low levels in the stomach, testis and heart, with no DPP4 protein or mRNA found in the brain or muscle (Hong et al., 1989). Quantitative histochemical studies using the Gly-Pro-4-methoxy-2-naphthalenyl substrate have identified DPP4 activity in unfixed and freeze-dried cryostat tissue sections from rats, mice, guinea-pigs, cats, rabbits and hamsters. These studies have led to the visualisation of DPP4 enzyme activity in capillary endothelium of the blood vascular system, liver sinusoidal endothelial cells, the perineurium of the peripheral nervous system, epithelial cells of the salivary glands, microvillous zone of intestinal crypts and villi, in the ductus epididymis and proximal renal tubules in the kidney, in the uterus, fallopian
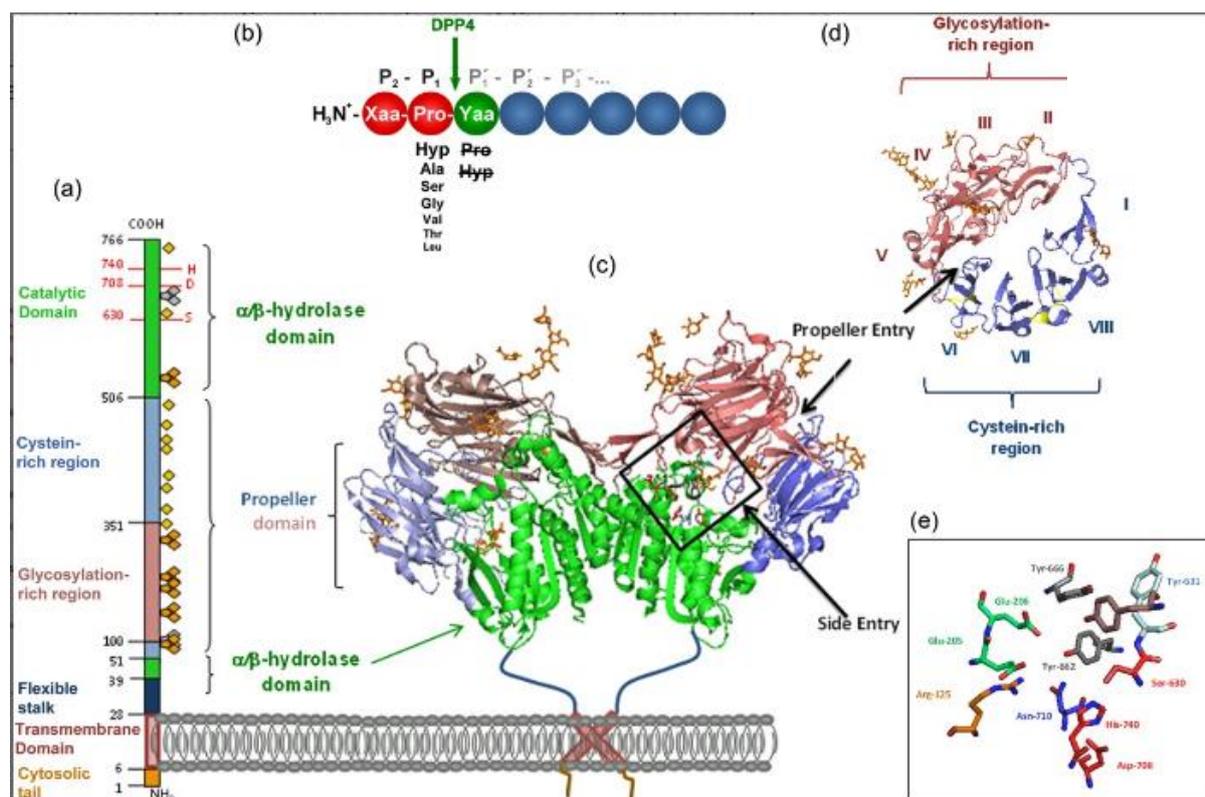
Figure 1.1. Primary and quaternary structure of human dipeptidyl peptidase 4 (DPP4). (a) DPP4 subunit primary structure with red numbers and letters indicating the catalytic triad. (b) DPP4 substrate specificity. Cleavage site indicated by arrow. Xaa and Yaa indicate any amino acid and decreasing amino acid font at the P1 position represents declining rate of hydrolysis. Crossed out amino acids cannot occupy P1′. (c) quaternary structure of the human DPP4 homodimer determined by Weihofen et al., 2004, showing the α/β-hydrolase domain (aa 39–51 and 506–766) in green and propeller domain (aa 55–497) with the glycosylation-rich subdomain (red) and the cystein-rich subdomain (blue). (d) Top view of the propeller domain with the eight propeller blades identified with roman numbers and the two subdomains identified, glycosylation-rich subdomain (red) and the cystein-rich subdomain (blue). (e) A depiction of the DPP4 active site zoomed in, residues involved in catalysis, Ser630, Asp708, His740 are shown in red. Image adapted from Klemann et al., 2016 based on Protein Data Bank: 1W1I (Klemann et al., 2016; Weihofen et al., 2004) reprinted with permission from John Wiley & Sons, Inc.

tubes, hepatocyte and lymphocyte membrane in the liver, in the plasma membrane of epithelia and in the interstitium of many organs (Gossrau, 1979). These findings highlight the widespread distribution of DPP4 expression and enzyme activity in many organs with maximal DPP4 activity measured using Gly-Pro-MNA seen within the Cortex and microvillus brush border of the kidney (Gossrau, 1979; Gutschmidt and Gossrau, 1981).

1.2.2 DPP4/CD26 costimulatory function

DPP4 plays a role in T cell activation through co-stimulation and association with, adenosine deaminase (ADA), caveolin-1, CARMA-1, CD45, mannose26-phosphate/insulin growth factor-II receptor (M6P/IGFII-R) and C-X-C motif receptor 4 (CXC-R4) (Ohnuma and Morimoto, 2013; Torimoto et al., 1991; Wagner et al., 2016). In the hematopoietic system DPP4 is a leukocyte antigen identified as CD26 and found on subsets of CD4+ and CD8+ T cells. Thus CD26/DPP4 is also known as a T cell activation antigen, as its expression level is dependent on the differentiation and activation stage of the cell and is connected with the capacity of a T cell to produce interleukin-2 (Scholz et al., 1985). In CD4+ T cells, CD26/DPP4 expression is restricted to a subset of the CD4 population, the CD45RO+CD29+ memory helper cell populace. This subsection of CD4+ T cells expressing CD26/DPP4 are shown to be distinctive in their ability to respond to recall antigens, induce B-cell immunoglobulin (IgG) synthesis and activate MHC-restricted cytotoxic T cells (Dang et al., 1990; Klemann et al., 2016; Morimoto et al., 1989). CD26/DPP4 expression has been connected to other hematopoietic cells including, natural killer cells, which exhibit low levels of DPP4 expression which is increased after stimulation with interleukin-2 (Buhling et al., 1994), B lymphocytes with increased expression seen after stimulation with St. aureus protein or pokeweed mitogen (Bühling et al., 1995), and myeloid cells with increased expression upon maturation to normal monocytes directed toward the macrophage pathway but not the granulocyte lineage (Laouar and Bauvois, 1992).

1.2.3 DPP4 regulation of glucose homeostasis

DPP4 is the most widely studied of the DPP4 family as its inhibition has been identified as prolonging the *in vivo* action of glucagon-like peptide-1 (GLP-1) and glucose-dependent insulinotropic polypeptide (GIP) (Matteucci and Giampietro, 2009; R Mentlein et al., 1993). GLP-1 and GIP are rapidly inactivated via the enzymatic activity of DPP4, resulting in a half-life of just a few minutes. Inhibiting DPP4 activity decreases the enzymatic processing and eventual inactivation of these incretins and increases their biological availability. This ultimately has provided an excellent therapeutic pathway for the treatment of T2DM as the immediate effect of active GLP-1 and GIP is to stimulate insulin secretion in a glucose-

dependent manner lowering blood glucose. GLP-1 also inhibits glucagon secretion, delays gastric emptying, provides a decrease in appetite, and is shown experimentally to increase beta cell mass and survival (Kirby et al., 2010; Stulc and Sedo, 2010).

1.2.4 DPP4 inhibitors for the treatment of type 2 diabetes

Many DPP4 inhibitors have entered the pharmaceutical market targeted at treatment of T2DM. Commonly referred to as gliptins these drugs mimic the end of the incretin hormones and block the DPP4 active site though each has discrete structural differences and binding mechanisms (Yazbeck et al., 2021). Of these inhibitors, sitagliptin was the first to be approved for use by the U.S. Food and Drug Administration (FDA) in October 2006 and is now also approved for use in Europe, and over 40 other countries (US Food and Drug Administration, 2016; Yazbeck et al., 2009). Recent reviews by others provides a comprehensive summary of DPP4 inhibitors currently in use including the benefits and potential issues relating to their use and will not be reviewed here (Deacon and Lebovitz, 2016; Mulvihill and Drucker, 2014).

1.3 DPP4 Involvement in immune function

Previous studies into DPP4 and its possible in vivo actions have indicated its involvement in many biological processes. The enzymatic activity of DPP4 has been shown to play a significant role in augmenting cellular responses to external stimuli. A T-cell receptor (TCR) complex reacting to specific peptide antigens or antibodies is in general unable to induce T-cell proliferation and lymphokine secretion on its own but requires a second costimulatory signal. DPP4 is identified as being one of the T-cell surface expressed molecules that can exhibit this costimulatory activity and is also found to show enhanced expression following T-cell activation (Dang et al., 1990; Klemann et al., 2016; Tanaka, 1993). The monoclonal antibody-mediated crosslinking of DPP4 with CD3 T-cell receptors on Jurkat T-cell lines induces production of interleukin 2 (IL-2). Jurkat cells used in the same study also produce substantially more IL-2 after stimulation with anti-CD26 and anti-CD3 antibodies than those transfected with mutated DPP4 lacking enzymatic activity. Mutated DPP4 with no enzymatic activity did however produce more IL-2 than DPP4 negative controls indicating that DPP4 enzyme activity plays a significant but not absolute role in T-cell costimulation (Ohnuma et al., 2008; Tanaka, 1993).

Yu, et al., 2011 examined the mechanism through which DPP4 aids in T-cell proliferation by using wild type soluble recombinant human DPP4, a DPP4 enzyme inactive mutant and a DPP4 ADA non-binding mutant, using *in vitro* T-cell proliferation assays with peripheral

blood mononuclear cells (PBMC). These PMBCs were stimulated with phytohaemagglutinin (PHA), muromonab-CD3 or Herpes simplex virus antigen (HSV Ag). Both wild type and enzyme negative DPP4 enhanced PHA-induced T-cell proliferation dose-dependently, while wild type and ADA negative DPP4 had no overall effect on anti-CD3-stimulated PBMC proliferation. Both enzyme negative and ADA negative DPP4 had mixed results in relation to HSV Ag, PBMC proliferation was induced in low responders to HSV Ag, but had no effect or inhibited proliferation in HSV-high responders. The ability of DPP4 to stimulate human T-cell proliferation in this work is identified as being the most likely mechanistically independent of both DPP4 enzyme activity and ADA-binding capability (Yu et al., 2011).

In similar studies Scho¨n et al., 1985 showed that N-Ala-Pro-O-(nitrobenzoyl)-hydroxylamine an irreversible DPP4 inhibitor suppresses proliferation of human PBMCs stimulated with mitogens and further studies undertaken by Reinhold et al., 1977 and 1988 showed that the reversible DPP4 inhibitors Lys(Z(NO2))-thiazolide and Lys(Z(NO2))-pyrrolidide, inhibit leukocyte proliferation, suppress DNA synthesis and also suppress IL-2, IL-10, IL-12 and IFN-γ cytokine production in mitogen or antigen stimulated human and mouse T-cells (Reinhold et al., 2005, 1998, 1997; Schon et al., 1984). Through these findings it can be seen that DPP4 plays a part in cellular response to external stimulation and that DPP4 enzymatic activity may or may not be involved. The pathway of DPP4 participation in these processes is yet to be identified.

The effect of DPP4 inhibitors on T-cell activation and function has led to their evaluation and indicated success in providing immunosuppressive therapies in vivo animal models of human disorders such as transplantation, rheumatoid arthritis, multiple sclerosis, autoimmune encephalomyelitis and inflammatory bowel diseases (Chen et al., 2020; Reinhold et al., 2005; S et al., 1997; Shao et al., 2020; Yazbeck et al., 2009). Elevated numbers of DPP4 T-cells have been observed in patients with autoimmune diseases such as rheumatoid arthritis and multiple sclerosis, with the DPP4 expression in T-cells from multiple sclerosis sufferers found to be three to four fold higher than in peripheral blood T-cells retrieved from healthy persons. In T-cells from multiple sclerosis sufferers DPP4 inhibitors suppressed DNA synthesis as well as production of IFN-γ, IL-4 and TNF-α. In an animal model of T-cell mediated disease, autoimmune encephalomyelitis, administration of a DPP4 inhibitor prevented central nervous system inflammation, demyelization as well as other clinical and neuropathological signs characteristic of the autoimmune encephalomyelitis disease course (Reinhold et al., 2011, 2005).

In animal and in vitro models of rheumatoid arthritis, inhibition of DPP4 enzyme activity led to increased levels of stromal cell-derived factor-1 (SDF-1) and the downstream effectors of

SDF-1 signalling, matrix metalloproteinase-1(MMP-1) and matrix metalloproteinase-3 (MMP-3). These are proteins known to be involved in the breakdown of the extracellular matrix in both normal physiological processes and disease states such as arthritis and cancer metastasis. The role of DPP4 enzymatic activity in the progress of rheumatoid arthritis was further investigated using SCID mice xenotransplanted with human rheumatoid arthritis synovial fibroblasts (RASFs), the known active driver of joint destruction in rheumatoid arthritis, and co-transplanted with human cartilage. *In vivo* inhibition of DPP4 enzymatic activity in this model significantly promoted RASFs invasion and produced higher accumulation of MMP-1 and MMP-3 compared with controls (Ospelt et al., 2010; U et al., 2007). This work indicates that DPP4 and more specifically DPP4 enzymatic activity may be playing an essential role in the protection of articular cartilage against invasion by synovial fibroblasts in rheumatoid arthritis and that the inhibition of DPP4 activity may exacerbate disease progression in sufferers.

The effect of DPP4 inhibition in inflammatory bowel diseases (IBD) has not been widely studied; there is however mounting evidence that suggests DPP4 activity plays a role in the pathogenesis of IBD. An investigation into changes in serum DPP4 activity in adult patients showed that DPP4 serum activity levels in IBD sufferers with either Crohn's disease (CD) or Ulcerative colitis (UC) were significantly decreased compared to healthy controls. DPP4 activity levels in serum also correlated inversely with the disease severity for both disease states (Cohen, 2003). Dpp4-/- mice given dextran sulphate sodium (DSS) to induce colitis show greater disease severity and reduced crypt area which is a histological marker for increased disease state. Wildtype mice administered DPP4 inhibitors in conjunction with the DSS treatment however show significantly decreased disease activity and improved crypt depth. Treatment of Dpp4-/- mice receiving DSS with the same DPP4 inhibitors provided no protective effects providing evidence that it is interaction between DPP4 and the inhibitor that is required for the reduced inflammatory response (Roger Yazbeck et al., 2008; Yazbeck et al., 2009).

There is mounting evidence that DPP4 activity plays many varied and often crucial roles in immunomodulation and augmentation of cellular responses to external stimuli. It is these biological processes involving DPP4 and the possible long term effects of their modification that need to be taken into consideration when investigating dipeptidyl peptidase inhibition as a therapy. It is also not clear the impact that these immune modulating roles identified for DPP4 will have on the initiation and progression of cancers. There is still much more research required to fill in these knowledge gaps and provide a more complete picture of the *in vivo* role of DPP4 and how it's effect on immunity and inflammatory responses potentially

impact disease progression in cancer and the possible long term effects of using DPP4 inhibition as a treatment.

1.4 DPP4 and Cancer

The role played by DPP4 in cancer is not clearly defined, it has been identified as both a tumour suppressor and a tumour promoter dependant on tumour type and tissue of origin. This indeterminate relationship is in part due to varied expression levels of DPP4 associated with differing cancer states but also the impact of its presence or absence on tumour development. DPP4 is shown to be strongly expressed in colorectal cancer, malignant mesothelioma, haematological malignancies and Ewing's sarcoma, with its presence linked to aggressive tumour growth. In contrast its low expression or absence is associated with increased tumour development in melanoma, ovarian cancer, non-small cell lung cancer, endometrial and prostate cancer, neuroblastoma, glioma and renal cell carcinoma (Enz et al., 2019; Pro and Dang, 2004). The inability to define a singular role for DPP4 in tumour biology is largely due to the multifaceted actions of the protein. DPP4 exhibits enzymatic action through serine peptidase activity as well as non-enzymatic actions including its ability to bind extracellular matrix components (Boonacker and Van Noorden, 2003). As previously outlined the protein structure of DPP4 includes two distinct domains, an N-terminal localised 8-bladed propeller domain involved in protein binding and a C-terminal hydrolase domain containing the enzymatic active site (Aertgeerts et al., 2004; Engel et al., 2003; Nardini and Dijkstra, 1999). Many of the varied functions of DPP4 are associated with actions from the differing domains of the protein (Engel et al., 2003; Wesley et al., 1999). The multiple actions of DPP4 may also work synergistically, independently, or even in opposition to each other, depending on the cell type and localised microenvironment.

In addition to its known regulation of the bioactivity of GLP-1 and GIP, the enzymatic action of DPP4 is involved in the activation or deactivation of many chemokines, integrins and neuropeptides, while its non-enzymatic actions and cellular binding are involved in immune modulation through activation of antigen-specific T cell proliferation (Cordero et al., 2009; Vanhoof et al., 1995). Moreover, DPP4 is shown to play a role in regulation of inflammation, ontogenesis, cell migration, protein turnover and tissue re-modelling, as well as the pro-oncogenic regulation of signal transduction, cell adhesion and apoptosis (Aytac et al., 2001; Cheng et al., 1998; De et al., 2018; Pethiyagoda et al., 2000; Wesley et al., 1999). DPP4 through heterodimeric complexing with FAP is also associated with tissue repair and remodelling of the extracellular matrix (ECM) as well as malignant transformation and cancer

progression in the tumour microenvironment (Cordero et al., 2009; Ghersi et al., 2002; Javidroozi et al., 2012).

Given the diverse function of DPP4 coupled with its varied expression in cancer it is not surprising that the defined role for DPP4 in tumour biology is yet to be elucidated. Below DPP4 and its identification as both a tumour suppressor and a tumour promoter in differing types of cancer is discussed, highlighting the potential role for this multifunctional protein in cancer development and identifying its importance as a promising therapeutic target.

1.4.1 DPP4 as a tumour suppressor

Reduced DPP4 expression is correlated with increased tumorigenesis in several cancer types including melanoma, ovarian cancer, lung cancer, endometrial cancer, prostate cancer, neuroblastoma, glioma and renal cell carcinoma. Work undertaken on these cancer types show that the malignant phenotype can be reverted with increased DPP4 expression, indicating that DPP4 plays a significant role in control of cancer cell growth, invasion and metastasis (Arscott et al., 2009; Morrison et al., 1993; Wesley et al., 2004). Further to these findings, work comparing the effects of increased DPP4 expression using both wildtype and enzyme inactive mutant DPP4 show that in the inhibition of tumour progression is not related to DPP4 enzyme activity in ovarian and lung cancer (Kajiyama et al., 2002; Wesley et al., 2004). However, enzyme activity was important for loss of tumorigenicity but not growth factor independence or invasive phenotype in melanoma (Wesley et al., 1999). While enzyme activity was required for tumour suppressive actions through regulation of stromal-cell-derived factor-1-α (SDF-1/CXCL12) in endometrial cancer, prostate cancer, and neuroblastoma (Arscott et al., 2009; Mizokami et al., 2004; Sun et al., 2005, 2003).

1.4.1.1 Melanoma

DPP4 is highly expressed in normal melanocytes but this expression is lost during malignant transformation with this loss occurring concurrently with exogenous growth factor independence (Houghton et al., 1988; Wesley et al., 1999). In an *in vivo* model of tumour development using human melanoma cell lines, MEL-22a, SK-MEL-28, and SK-MEL-29, injected subcutaneously into nude mice, re-expression of wt DPP4 at similar level to that seen in normal melanocytes introduced a reversal of the malignant phenotype (Wesley et al., 1999). Re-expression of DPP4 lead to loss of tumorgenicity through anchorage independent growth as well as re-establishment of growth factor dependence. This suppression of tumorigenicity was shown to be dependent on DPP4 enzyme activity, however the expression of an enzyme inactive DPP4 mutant with a serine/alanine substitution was able

to reinstate dependence on growth factors (Wesley et al., 1999). It is of note that the expression of enzyme active DPP4 did alter cellular proliferation, but the effect was seen not in the logarithmic growth phase but during the lag period once a confluent state had been reached thereby reducing the total number of cells (Wesley et al., 1999). Re-expression of both enzyme active and mutant DPP4 was also shown to rescue FAP expression, the ability of FAP and DPP4 to create heterodimers may indicate that the re-expression of one protein is able to regulate the localization of the other, this signifies a coordinated role for both DPP4 and FAP in malignancy and substantiates FAP involvement in regulating tumorigenesis in melanocytic cells which is discussed later (Havre et al., 2008; Wesley et al., 1999; Yu et al., 2006).

Investigation into the mechanism involved in the loss of DPP4 protein expression using a panel of melanoma cell lines showed that DPP4 loss occurs at the RNA level via aberrant methylation of the DPP4 gene promoter. Subsequent treatment of these DPP4 negative melanoma cell lines with the demethylating agent, 5-aza-2′-deoxycytidine (5-AZA-Cdr) increased DPP4 expression and was correlated with growth inhibition and increase in apoptosis (McGuinness and Wesley, 2008). Invasion assays conducted using melanoma cell lines LOX and C8161 showed that parental cells and cells transfected with vector only were highly invasive, while a 75% reduction in invasiveness was seen in cells transfected with DPP4. Additionally, loss of invasiveness in melanoma cells did not require DPP4 enzyme activity or the DPP4 cytoplasmic domain (Pethiyagoda et al., 2000). The highly invasive phenotype in melanoma cells may be due to the reduced expression of DPP4 being counteracted by an increase in the expression of FAP. LOX cells naturally expressing high levels of FAP are shown to be significantly more invasive than LOX cells with lower FAP expression (Enz et al., 2019; Goldstein et al., 1997; Monsky et al., 1994). These findings not only suggest that DPP4 plays a defined anti-tumorigenic role in melanoma, it identifies FAP as a regulator of tumorigenesis in melanocytic cells and highlights the need for further investigation into the entanglement between DPP4 and FAP in malignancy.

1.4.1.2 Ovarian cancer

Work conducted on ovarian cancer cell lines has identified DPP4 as a potential tumour suppressor. An *in vitro* study by Kajiyama et al., (2002) using the ovarian cancer cell line SKOV3 has demonstrated that increasing DPP4 expression in cells with low levels of DPP4 results in a less invasive phenotype, decreasing both migration and invasion and producing a defined change in cellular morphology. Additionally, it was shown *in vivo* that nude mice inoculated with SKOV3 cells transfected with wt DPP4 had decreased tumour dissemination and increased survival time (Kajiyama et al., 2002). Inhibition of DPP4 enzyme activity by

diprotin-A (H-Ile-Pro-Ile-OH) was unable to reverse the reduction in migration or invasion *in vitro*, indicating that the antitumorigenic effect of DPP4 was not related to its proteolytic activity (Kajiyama et al., 2002). Additional work on SKOV3 cells with low DPP4 expression showed that induction of DPP4 expression increased expression of E-cadherin and β-catenin and altered cell morphology, moving cells to a more epithelial phenotype displaying tighter cell to cell adhesion thereby reducing their metastatic potential (Kajiyama et al., 2003). Transfection of wt DPP4 in SKOV3 cells also decreased the expression of two known markers of invasive metastasis, matrix metalloproteinase 2 (MMP-2), and membrane type 1 matrix metalloproteinase (MT1-MMP), and increased the presence of tissue inhibitors of matrix metalloproteinases (Kajiyama et al., 2003). Increase in DPP4 expression was also correlated with greater adhesion to collagen and fibronectin, again indicating a tumour suppressive role for DPP4 in preventing metastasis through increased cellular adhesion (Kikkawa et al., 2003). Follow on work conducted on SKOV3 cells transfected with wt DPP4 showed a positive correlation between DPP4 expression and sensitivity to the standard treatment for epithelial ovarian carcinoma, paclitaxel-platinum-based chemotherapy, identifying DPP4 as a promising therapeutic target for treatment of ovarian cancer. Again, the presence of a DPP4 enzyme inhibitor diprotin-A did not alter paclitaxel sensitivity in DPP4 transfected cells indicating that the non-proteolytic actions of DPP4 are associated with the increased responsiveness to chemotherapeutic treatment (Kajiyama et al., 2010).

Although DPP4 in ovarian cancer has been associated with tumour suppressive actions *in vitro*, *in vivo* studies using patient samples show that DPP4 expression is significantly higher in ovarian carcinomas. Zhang et al., (2015) studied 128 samples of epithelial ovarian cancer and identified that 106 were positive for DPP4 presence (determined via immunohistochemical analysis), and the number of DPP4 positive cells were higher than seen in borderline ovarian tumour or benign ovarian tumour samples (Zhang et al., 2015). Of the 106 DPP4 positive ovarian samples, 78 patients showed moderate to high DPP4 expression, and although DPP4 was present in both cancerous and reactive mesothelial cells, DPP4 levels were consistently higher in the carcinoma cells. Furthermore, while DPP4 expression did not correlate with histological grade, tumour type or disease free survival, it was significantly higher in patients with lymph node metastasis (Zhang et al., 2015). Zhang et al's., (2015) *in vivo* results are surprising as increased DPP4 presence *in vitro* was associated with prevention of metastasis through increased cell to cell adhesion. Previous work conducted by the same group using immunohistochemical analysis to detect DPP4 presence in 378 epithelial ovarian carcinomas and 42 samples of normal ovarian tissue identified that 92% of the ovarian cancer samples were positive for DPP4 while only 59% of the normal tissue samples were DPP4 positive (Zhang et al., 2008). DPP4 expression was

not correlated with age, tumour stage or histological grade, but was significantly correlated with histological type and high DPP4 expression was identified as a marker for poor prognosis in terms of overall survival (Zhang et al., 2008). The findings taken from work conducted on ovarian cancer cell lines *in vitro* produce conflicting results when compared to results obtained from *in vivo* analysis. Although opposing, the outcomes from both forms of analysis do indicate a role for DPP4 in cancer progression and identify its potential as a prognostic biomarker in ovarian cancer.

1.4.1.3 Lung cancer

Lung neoplasms have two main histological subtypes, small cell lung cancer and non-small cell lung cancers (NSCLC), nearly 85% of all lung cancers are NSCLC (Chang et al., 2018; Enz et al., 2019). In normal bronchial and alveolar epithelium cells, DPP4 protein expression as well as enzyme activity is detected but DPP4 mRNA and protein expression is notably reduced in all NSCLC cell lines indicating that DPP4 may be tumour suppressive in this cell type (Asada et al., 1993; Wesley et al., 2004). Re-expression of wt DPP4 in the NSCLC cell line SK-LUC-8 resulted in morphological changes in cultured cells with transfected cells taking on a defined epithelial morphology that would not reach confluency due to contact inhibition. SK-LUC-8 cells transfected with wt DPP4 also showed growth inhibition with a longer lag period between plating and entering into the logarithmic phase and a reduced ability to perform anchorage-independent growth (Wesley et al., 2004). In a xenograft model using SK-LUC-8 cells transplanted into athymic nude mice, increased expression of wt DPP4 in SK-LUC-8 cells reduced tumorgenicity with vector only control cells producing significantly larger tumours when compared to DPP4 transfected cells (Wesley et al., 2004). Consistent with the DPP4 tumour supressing activity observed in both melanoma and ovarian cancer cells, the reduced tumorigenicity in NSCLC is not reliant on DPP4 enzyme activity with similar results seen when cells are transfected with wt DPP4 or mutant DPP4 lacking enzyme activity (Wesley et al., 2004).

To date there is very limited work reporting on the relationship between DPP4 and lung neoplasms *in vivo*. The nonselective DPP4, FAP, DPP8, and DPP9 inhibitor Val-Boro-Pro (also known as PT-100 or talabostat) has been used in clinical trials to determine its effectiveness in treating advanced stage NSCLC (Eager et al., 2009; Nemunaitis et al., 2006). Eager et al., (2009) demonstrated that inhibition via Val-Boro-Pro was unable to inhibit NSCLC progression in patients and did not merit further clinical development. These results are not surprising given that the anti-tumorigenic actions of DPP4 are not associated with DPP4 enzyme action in melanoma or ovarian cancer (Eager et al., 2009). In a more recent study, the DPP4 specific inhibitor vildagliptin was able to significantly reduce tumours

in a murine xenograft model using human lung adenocarcinoma cells, although the anti-tumorigenic effect in this work was determined to be associated with a significant increase in macrophages and NK cells and not the direct effect of inhibition of DPP4 enzyme activity within the tumour cells (Jang et al., 2019). Additionally, in relation to general lung cancer, DPP4 is identified as a potential auxiliary marker to identify patients as high-risk for lung cancer development (Blanco-Prieto et al., 2015). Collectively research to date highlights DPP4 as a promising therapeutic target in NSCLC although as with melanoma and ovarian cancers, the mechanism by which DPP4 imparts its suppression of tumorigenesis in NSCLC is still unclear.

1.4.1.4 Endometrial cancer

Immunohistochemical analysis has demonstrated high DPP4 expression in normal endometrial glandular cells which is down regulated in endometrial adenocarcinomas with an inverse correlation between DPP4 immunoreactivity and tumour grading (Khin et al., 2003). Khin et al., (2003) identified that the DPP4 substrate, *regulated on activation normal T cell expressed and secreted* (RANTES), was overexpressed in endometrial carcinoma, although there was no significant correlation between RANTES expression and tumour grade. RANTES was shown to induce cell proliferation in the endometrial adenocarcinoma cell lines, HEC1A and ISHIKAWA in a concentration-dependent manner (Khin et al., 2003). These findings indicate that DPP4 may act as a tumour suppressor in endometrial cancer through degradation of pro-proliferative substrates such as RANTES and identifies a potential anti-tumorigenic role played by DPP4 proteolytic activity in this form of cancer.

Additional work on the role of DPP4 proteolysis in endometrial cancer has demonstrated that the DPP4 substrate, C-X-C motif chemokine 12 (SDF-1/CXCL12), and its associated receptor CXCR4, are both expressed in endometrial cancer tissue and the concentration of SDF-1/CXCL12 in endometrial cancer cells was significantly lower in cells transfected with DPP4 (Mizokami et al., 2004). The actions of SDF-1/CXCL12 are shown to stimulate tumour cell proliferation, migration and angiogenesis in thyroid, ovarian and breast cancers, this is in line with findings on endometrial cancer cells where SDF-1/CXCL12 was shown to stimulate proliferation (Hall and Korach, 2003; Hwang et al., 2003; Mizokami et al., 2004; Scotton et al., 2002). The pro-proliferative actions of SDF-1/CXCL12 was significantly lower in endometrial cancer cells transfected with DPP4 when compared to vector transfected cells suggesting that DPP4 mediated degradation of SDF-1/CXCL12 may be able to down regulate tumour growth in endometrial cancer. This Mizokami et al., (2004) study was the first to define a relationship between SDF-1/CXCL12, CXCR4 and DPP4 in solid tumours (Mizokami et al., 2004). Later Tan et al., (2014) demonstrated loss of DPP4 expression in

endometrial stromal cells under hypoxia is associated with up-regulation of angiogenic factors leading to increased migration, invasion, and angiogenesis, and promotion of endometrial lesion development. In this study the proteolytic activity of DPP4 and its regulation of SDF-1/CXCL12 was again associated with tumour suppression as treatment with DPP4 inhibitor diprotin-A in combination with addition of the chemokine SDF-1/CXCL12 enhanced cell migration and invasion providing further evidence that the proteolytic activity of DPP4 may play a role in tumour suppression in endometrial cancer (Tan et al., 2014).

1.4.1.5 Prostate cancer

In the prostate gland the regulation of normal epithelium and progression to malignancy is associated with changes to the expression levels of a specific growth factor, basic fibroblast growth factor (bFGF), which is a potent mitogen and angiogenic agent (Chodak et al., 1992; Dow and Devere White, 2000; Giri et al., 1999). The expression pattern of both DPP4 and bFGF was assessed in, normal prostate epithelial cells (NPrEC), non-tumorigenic epithelial prostate cell line RWPE-1, tumorigenic human prostate adenocarcinoma cell line LNCaP, and tumorigenic and metastatic prostate cancer cell line DU-145. Analysis by flow cytometry showed decreasing DPP4 expression with increasing tumorigenesis in these prostate cell lines, with high DPP4 cell surface expression seen in NPrEC cells, moderate expression in RWPE-1 and LNCaP cells, and very low expression in DU-145 cells. Northern blot analysis of the cells confirmed that this reduction occurs at the transcriptional RNA level (Wesley et al., 2005). Western blot analysis of the prostate cells for bFGF presence showed low levels of bFGF in NPrEC, RWPE-1, and LNCaP cells, but high levels in the highly tumorigenic DU-145 cells, indicating an inverse correlation between DPP4 and bFGF expression (Wesley et al., 2005). Induction of wt DPP4 expression in DU-145 cells using a tetracycline inducible expression system resulted in a change in morphology with cells exhibiting a more organised epithelial like growth with increased doubling time and contact inhibition. The increased expression of wt DPP4 in DU-145 cells was also shown to reduce bFGF presence, inhibit cell proliferation, migration, and invasion, and also induce apoptosis and cell cycle arrest (Wesley et al., 2005).

Additional work on prostate cancer cell lines has associated the DPP4 enzymatic degradation of SDF-1/CXCL12 with reduced invasion and metastasis. SDF-1/CXCL12 and associated receptors, CXCR4 and CXCR7/RDC1, have been determined to be key elements for metastasis of prostate cancer (Sun et al., 2005, 2003; Taichman et al., 2002; Wang et al., 2008). As previously reported in endometrial cancer, SDF-1/CXCL12 is known to be inactivated via DPP4 enzymatic cleavage (De La Luz Sierra et al., 2004; Lambeir et al., 2001; Mizokami et al., 2004). In the human prostate cell lines, PC-3 and LNCaP, both

established from metastatic human prostatic cancers, SDF-1/CXCL12 expression is associated with enhanced adhesion and invasion into the extracellular matrix (Chu et al., 1983; Kaighn et al., 1979; Sun et al., 2008) The effect of SDF-1/CXCL12 on prostate cancer cell migration and invasion was shown to be regulated via DPP4 enzymatic degradation of the chemokine, as inhibition of DPP4 enzyme activity via diprotin-A was able to increase the invasive activity in PC-3 and LNCaP cells. In follow on work using a xenograft model in immune deficient mice where primary tumours were established subcutaneously via injection of prostate cancer cells, inhibition of DPP4 by diprotin-A was shown to facilitate prostate cancer cell migration into the marrow and metastasis through the SDF-1/CXCL12 and CXCR4 chemokine axis (Sun et al., 2008). Findings from this work reflect results taken from studies into endometrial cancer where DPP4 proteolysis is shown to be involved in control of tumour progression and metastasis through the regulation of chemokine SDF-1/CXCL12.

Nazarian et al., (2014) conducted studies on serum samples from 144 patients with prostate cancer, solid-phase peptide extraction and mass spectrometric analysis of patient serum showed no significant difference in DPP4 presence between non-metastasising prostate cancer and normal controls (Nazarian et al., 2014). However, serum DPP4 enzyme activity was shown to be reduced in patients with metastatic disease progression when compared to patients with localized disease or healthy controls (Nazarian et al., 2014). In contrast an immunohistochemical study of 36 prostate cancer biopsies from patients associated higher levels of DPP4 expression with cancer tissue when compared to normal tissue (Lu et al., 2013). A similar study by Wilson et al., (2000) undertook immunohistochemical studies of frozen tissue from nine benign prostatic hyperplasia (BPH) and 13 prostate cancer biopsies, and showed DPP4 activity to be elevated in prostate cancer tissue (Lu et al., 2013; Wilson et al., 2000). Although these results appear to contradict Nazarian et al., (2014) they do demonstrate that DPP4 presence was unchanged regardless of tumour progression and only DPP4 enzyme activity was decreased in metastatic cancer. It is of note that in other work reporting on DPP4 activity in prostate cancer a comparison in metastasising and non-metastasising cancers was not undertaken (Lu et al., 2013; Nazarian et al., 2014; Wilson et al., 2000). Lu et al., (2013) showed expression levels of the SDF-1/CXCL12 receptor, CXCR4, were significantly higher in prostate cancer tissue when compared to normal tissue, substantiating a potential relationship between SDF-1/CXCL12, DPP4 and prostate cancer progression *in vivo* as observed *in vitro* in cell lines (Lu et al., 2013).

1.4.1.6 Neuroblastoma

Comparison of a panel of human neuroblastoma-derived cell lines (SK-N-SH, SH-SY5Y, SMS-KCNR, SK-N-MC, SK-N-DZ, SK-N-AS, and SK-N-F1) with normal neural crest-derived

structures via flow cytometry has determined that DPP4 expression is present in neural crests but is significantly decreased in all neuroblastoma-derived cell lines (Arscott et al., 2009). Transfection and restoration of wt DPP4 expression in SK-N-SH and SK-N-AS cells resulted in a morphological change, moving the cells from growing in disorganized focal clumps to a more neuronal morphology presenting a flat epithelial phenotype. Re-expression of wt DPP4 in neuroblastoma-derived cells was also associated with a decrease in cell proliferation, invasion and angiogenesis, and was shown to decrease SDF-1/CXCL12 mediated migration and increase apoptosis. In addition, the anti-tumorigenic action of DPP4 in neuroblastoma cells was associated with its enzyme activity as targeted inhibition of DPP4 by diprotin-A was able to restore the malignant phenotype of the cells (Arscott et al., 2009). *In vivo* the anti-tumorigenic actions of DPP4 have been investigated using a model of xerograph tumour formation in nude mice. Tumours grew in all mice injected with vector control SK-N-AS cells, but mice injected with SK-N-AS cells re-expressing wt DPP4 had no tumour growth (Arscott et al., 2009).

As reported for previous cancer types where DPP4 is associated with tumour suppression, the ability of DPP4 to control malignant progression in neuroblastoma appears to be associated with its regulation of the chemokine SDF-1/CXCL12. In the study by Arscott et al., (2009) increased expression of DPP4 was associated with a down regulation of SDF-1/CXCL12 and its receptor CXCR4, this association between DPP4, SDF-1/CXCL12, CXCR4 and carcinogenesis is confirmed in Russell et al., (2004) who demonstrated expression levels of SDF-1/CXCL12 and CXCR4 in neuroblastoma were significantly increased in patients with high-stage disease as well as bone and bone marrow metastases, with increased expression signifying poorer clinical outcomes (Arscott et al., 2009; Russell et al., 2004).

1.4.1.7 Glioma

The tumour suppressing activities of DPP4 in neuroblastoma, endometrial and prostate cancers, and its actions on SDF-1/CXCL12 have also been observed in the regulation of malignant glioblastoma progression (Barbero et al., 2003). In glioma cell lines U373 and T98G, DPP4 enzymatic activity was shown to influence the regulation of SDF-1/CXCL12 and substance P, substrates that are associated with modulation of the biological processes involved in the progression of gliomas (Bušek et al., 2008). Further work conducted on the human glioma cell lines U373, T98G and U87, which have low to undetectable levels of endogenous DPP4, increasing wt DPP4 expression was correlated with reduced cellular growth and delayed progression through the cell cycle (Busek et al., 2012). Increased DPP4 expression also results in reduced cell proliferation *in vitro* and subsequently *in vivo,* tumour

xenotransplantation of wt DPP4 transfected U373 cells with increased DPP4 expression led to suppression of glioma growth (Busek et al., 2012). Furthermore, these *in vitro* and *in vivo* results were observed in cells transfected with both enzyme active, and inactive DPP4, indicating that the effect on cellular proliferation was associated with the non-enzymatic actions of the protein (Busek et al., 2012).

Stremenova et al., (2007) demonstrated that DPP4 presence in healthy human brain tissue is low with DPP4-like activity predominantly linked to the activity of associated S9B family proteins DPP8 and DPP9, but in patient derived human glioma tissue DPP4 is upregulated with its expression level directly correlated with tumour grade (Stremenova et al., 2007). Stremenova et al., (2007) also correlated upregulation of DPP4 expression with a parallel increase in the SDF-1/CXCL12 chemokine receptor, CXCR4. The increase in CXCR4 is likely related to tumorigenicity as it would facilitate an increase in the pro-oncogenic activities of SDF-1/CXCL12. On the other hand DPP4 inactivates SDF-1/CXCL12, the increased expression of the CXCR4 receptor may be a compensatory activity undertaken by the glioma cells to counteract increased DPP4 expression in an attempt to maintain tumorgenicity (Stremenova et al., 2007).

The anti-tumorigenic actions of DPP4 in glioma have been correlated with differential expression of Ki67, a marker of tumour cell proliferation and growth. In human brain gliomas an inverse correlation was determined between DPP4 and Ki67 with an increase in DPP4 activity associated with decreased Ki67 expression. Furthermore, low DPP4 enzyme activity was correlated with shorter survival in patients presenting with glioma (Mareš et al., 2012). The connection of an increase in DPP4 activity with a decrease in the expression of known tumour promotor Ki67 presents yet another alternate route of action through which DPP4 may prevent the inappropriate proliferation of malignant cells (Busek and Sedo, 2013).

1.4.1.8 Renal Cell Carcinoma (RCC)

Human renal cell cancers encompass several different histological types arising from distinctive cells that originate from differing parts of the nephron. Clear cell and papillary renal cell cancers develop from the epithelium of the proximal tubule, while collecting duct and chromophobe renal cell cancer, as well as oncocytoma develop from the epithelium of the collecting tubule in the distal nephron (Cairns, 2011). Each tumour type demonstrates differing genetics, biology and behaviour although the most common histological type accounting for 80% of all diagnosed renal cell cancers is clear cell carcinoma, also known as conventional RCC (Cairns, 2011).

In an assessment of samples collected from normal and renal tumour patients, DPP4 expression and enzyme activity was identified on healthy epithelial cells of the proximal tubule but this expression and activity was reduced in RCC (Kehlen et al., 1998; Varona et al., 2010). Immunostaining in normal renal tissue for DPP4 expression demonstrated that DPP4 is exclusively located in the proximal nephron, as RCCs are derived from cells of the proximal nephron, the strong DPP4 expression in this area coupled with the reduction in its expression and enzyme activity with development of RCC suggest that a decrease in DPP4 presence is required for malignant progression of RCC (Varona et al., 2010).

In an alternate study using surgically resected human RCC tissues and renal carcinoma cell lines (Caki-1, Caki-2, VMRC-RCW and ACHN), DPP4 was shown to be highly expressed on RCC tissues when compared to normal renal cells surrounding the RCC. DPP4 expression on all RCC cell lines was also shown to be high when compared to prostate cancer cell lines DU-145 and LNCap (Inamoto et al., 2006). Treatment of renal carcinoma cells with high expression of DPP4 using an anti-CD26 monoclonal antibody resulted in growth inhibition and cell cycle arrest and cells were able to internalise cell surface DPP4, leading to decreased binding on collagen and fibronectin. Follow on work using a mouse xenograft model with renal carcinoma cells demonstrated that treatment with the anti-CD26 monoclonal antibody considerably reduced tumour growth in tumour-bearing mice affording enhanced survival (Inamoto et al., 2006). The ability of DPP4 to act as tumour promoter in RCC is supported by a study on RCC resected tissues and normal renal tissue were increased cytoplasmic DPP4 activity in RCC was associated with significantly shorter five-year survival rate (Larrinaga et al., 2012).

Clearly different researchers have obtained conflicting results in renal cell carcinoma with DPP4 acting as a tumour suppressor in some studies and as a promotor in others. These contradictory findings may not only be related to the multifunctional role of DPP4 but also with the multifaceted nature of renal cell cancers. The differing actions of DPP4 in renal carcinomas may be due to variations in cancer types where the parental cells are established from different parts of the nephron (Cairns, 2011). Although DPP4 is shown to play a varying role these results do indicate that modification to the expression and activity profile of DPP4 is a key event in the malignant progression of renal cell carcinoma.

1.4.2 DPP4 as a tumour promoter

Although increased DPP4 expression is correlated with decreased tumorigenesis in some cancer types, its presence is similarly related to increased tumour cell migration and invasion and it is also identified as a marker of cancer stem cells (CSCs) in differing types of cancer

(Ghani et al., 2011; Herrmann et al., 2014). Additionally, in colorectal cancer DPP4 has been identified as a specific marker for a subpopulation of CSCs associated with increased metastasis and enhanced chemotherapeutic resistance, results that when surmised together suggest that DPP4 is a pro-tumorigenic marker of more aggressive tumour progression in certain cancer types (Pang et al., 2010).

1.4.2.1 Colorectal Cancer

Analysis of the expression of DPP4 in human epithelial cells sourced from different regions of the small intestine and colon indicates that DPP4 activity is highest in ileum and jejunum, decreases to low in duodenum and is not detectable in colon (Darmoul et al., 1994). Although DPP4 is shown to be absent in normal colon epithelia, DPP4 expression is correlated with the clinical and pathological features of CRC. Through analysis of tissue samples collected from 143 CRC patients undergoing colonic resection, Lam et al., (2014) showed DPP4 is expressed in adenocarcinomas of the colon and its expression is correlated with disease progression (Lam et al., 2014). Lam et al., (2014) correlated increased DPP4 expression in CRC patients with progression to distant metastasis, advanced tumour staging and worse overall patient survival (Lam et al., 2014). Larrinaga et al., (2015) assessed DPP4 activity and mRNA expression in, adenocarcinomas, adenomas, and normal colorectal mucosa, from 116 patients with CRC who were undergoing partial colectomies and found similar results. They established a relationship between DPP4 expression and tumorigenesis in CRC with increased DPP4 activity and mRNA expression associated with both adenocarcinomas and adenomas of the colon but not with the adjacent non-carcinogenic colorectal mucosa (Larrinaga et al., 2015).

In addition, Larrinaga et al., (2015) showed that DPP4 expression in CRC tissues did not correlate with overall patient five-year survival or disease reoccurrence, however plasma DPP4 activity was shown to inversely correlate with patient survival. High plasma DPP4 activity was correlated with a significant increase in disease reoccurrence and overall poor prognosis (Larrinaga et al., 2015). De Chiara et al., (2014) examined serum samples taken pre- and postoperatively from 43 patients with primary colorectal cancer and provided further evidence for this association. Patients with low stable pre-operative serum levels of soluble DPP4 remained disease free after resection, while patients presenting with high or unstable DPP4 serum levels were found to have recurrence of tumour growth. High levels of post-operative DPP4 serum levels was also shown to predict metastatic disease progression (De Chiara et al., 2014). The results correlating plasma and serum DPP4 with overall survival in CRC highlight DPP4 as a potential biomarker for assessing prognosis in CRC patients (Yazbeck et al., 2018).

In line with its association with CRC in patients, *in vitro* work undertaken in colon cancer cell lines substantiate these findings and demonstrate a role for DPP4 in modulation of CRC cells. In colon carcinoma cell lines Caco-2 and HT-29, DPP4 expression is increased during enterocyte differentiation a relationship that has highlighted DPP4 as a marker of differentiation in intestinal epithelia (Darmoul et al., 1992; Ducarouge et al., 2017). A confluence dependent increase in DPP4 mRNA and protein is seen in colon cancer cell lines HCT-116 and HCT-15. In conjunction with the increase in DPP4, confluence in HCT-116 and HCT-15 cell cultures also correlates with a decrease in c-MYC a transcription factor associated with regulation of cellular proliferation, growth, differentiation, and apoptosis (Abe et al., 2011; Vita and Henriksson, 2006). Furthermore, re-expression of c-MYC in both cell lines was shown to suppress DPP4 expression (Abe et al., 2011). Confluence in HCT-15 cells was shown to increase caudal type homeobox protein 2 (Cdx2), a transcription factor involved in the regulation of intestinal cell differentiation, and this increase induced DPP4 expression (Abe et al., 2011; Silberg et al., 2000). These findings establish a relationship between DPP4, and transcription factors involved in the regulation of cellular proliferation, growth, differentiation and apoptosis, highlighting DPP4 for further investigation as a potential therapeutic target.

Much of the current work on colorectal cancer focuses on the identification of cancer stem cells (CSC), a subpopulation of cells responsible for initiation of tumour growth in CRC (Yeung et al., 2010). Markers of CSC in colorectal cancer include CD133+, CD166+ and CD44+, although no one marker has been proven to reliably distinguish CSC from regular cancer cells (Gemei et al., 2013; Pang et al., 2010). Recent work has focused on DPP4 as a marker for CSC subsets. Pang et al., (2010) identified a subpopulation of DPP4 positive CSCs that are consistently present in both the primary and metastatic colorectal tumours of CRC patients with liver metastasis. Furthermore, it was established that in patients with DPP4 positive cells in their primary tumour but without liver metastasis at the time of assessment, the presence of DPP4 in their primary tumour predicted the development of distant metastasis on follow-up (Pang et al., 2010). In follow on work using subcutaneous injection of DPP4 positive and negative tumour cells into SCID mice, injection of DPP4 positive cells induced tumour formation and development of distant metastasis, while DPP4 negative cells from the same human tumour did not result in tumour formation (Pang et al., 2010). DPP4 presence in CSC cells is also associated with enhanced chemoresistance, treatment of primary tumour cell culture with 5-fluorouracil (5-FU) or oxaliplatin leads to enrichment of DPP4 positive cells, in primary cell culture. Eighty percent of tumour cells were DPP4 positive 15 days after treatment. When transplanted subcutaneously into SCID mice that received 5-FU or oxaliplatin treatment, 80% of mice transplanted with DPP4

positive cancer stem cells were shown to have viable cancer cells remaining eight weeks post treatment that initiated tumour regrowth (Pang et al., 2010).

In summary, although DPP4 is absent in normal colonic tissue it has increased expression in colon cancer and its presence is correlated with increase metastasis and poorer overall survival in patients. It has been highlighted as a marker of differentiation and a potential transcriptional regulator involved in the control of cellular proliferation, growth, differentiation an apoptosis, and has been identified as a marker of colonic tumour stem cells able to impart resistance to chemotherapeutic treatment. The action of DPP4 in colorectal cancer indicates it is pro-oncogenic in this tumour type however the mechanisms contributing to its pro-oncogenic action are not fully understood. Combined, this highlights the potential of DPP4 as a therapeutic target and prognostic marker in colon cancer, but further work is required to develop a better understanding of DPP4 and its involvement in this cancer type.

1.4.2.2 Malignant mesothelioma

Malignant pleural mesothelioma (MPM) is an aggressive malignancy of the lung arising from mesothelial lining of the pleura (Komiya et al., 2014). Immunohistochemical analysis of surgically resected human malignant mesothelioma tissues showed high expression of DPP4 in malignant mesothelioma cells but very low expression in benign adenomatoid or normal mesothelial cells (Inamoto et al., 2007). The correlation between DPP4 and malignancy in mesothelioma was conducted on a relatively small patient cohort of 12. Aoe et al., (2012) undertook a study on a larger sample size of 79 mesothelioma patients who had undergone biopsy at surgery and showed that DPP4 is expressed differentially dependant on primary cell type. They also showed that DPP4 expression is associated with the epithelial and biphasic mesothelioma, but not with the sarcomatoid type of mesothelioma (Aoe et al., 2012). Immunohistochemical analysis showed that DPP4 cytoplasmic expression levels differed to that seen for membrane expression. In a study involving patient tissue samples from 81 cases of epithelioid mesothelioma, 34 cases of sarcomatoid mesothelioma and 19 cases of biphasic mesothelioma, using eight different DPP4 specific antibodies showed that DPP4 cytoplasmic expression was present in all histological types of mesothelioma, while membrane expression of DPP4 was not seen in sarcomatoid mesothelioma, and was only found in 88% of differentiated and 69% of less differentiated epithelioid mesothelioma (Amatya et al., 2011). As DPP4 is a membrane bound protein its presence within the cell is unusual and may be as a result of membrane digestion, it is however noted by Amatya et al., (2011) that mesothelioma cells when grown in culture medium grow as spindled cells with an inconspicuous cell membrane. It may be that the

cytoplasmic location of DPP4 in mesothelioma is related to the absence of a defined cell membrane.

In vitro DPP4 expression is upregulated upon reaching confluence in the mesothelioma cell line JMN (Abe et al., 2011). When mesothelioma JMN cells are treated with an anti-DPP4 monoclonal antibody (MAb) they demonstrate reduced binding to fibronectin and type I collagen, indicating DPP4 acts as an ECM-binding protein in mesothelioma (Inamoto et al., 2007). Additionally, in a JMN xenograft model using NOD-SCID mice, treatment with anti-DPP4 MAb was shown to inhibit tumour growth and enhance survival *in vivo* (Inamoto et al., 2007).

The identification of DPP4 as a marker of cancer stem cells (CSC) in colon cancer is replicated in mesothelioma where it has been identified as a marker of CSC in addition to CD9 and CD24 (Ghani et al., 2011; Yamazaki et al., 2012). CD24+ cells are shown to increase tumour formation *in vitro* and *in vivo* and DPP4/CD26 is directly correlated to CD24 expression in sarcomatoid cell lines signifying that targeted therapy using DPP4/CD26 monoclonal antibodies may eliminate CD24+ CSCs in this mesothelioma subtype (Ghani et al., 2011). An *in vitro* study focused on the interaction of CD9 and DPP4/CD26 in mesothelioma showed co-precipitation of CD9 and CD26 in mesothelioma cell lines. Using siRNA methods, downregulation of DPP4/CD26 led to increased CD9 expression, while downregulation of CD9 increased DPP4/CD26 expression. Additionally, cell invasion assays showed that overexpression of DPP4/CD26 coupled with downregulation of CD9 led to enhanced invasiveness. Depletion of DPP4/CD26 reduced cellular invasiveness through interaction with α5ß1, an integrin demonstrated to play a key role in cancer metastasis and invasion (Barkan and Chambers, 2011; Okamoto et al., 2014).

In mesothelioma JMN cells, DPP4 has also been associated with the secretion of ECM protein and integrin adhesion molecule periostin. When DPP4 and periostin expression correlated in JMN cells, an increase in migration and invasion via tyrosine kinase Src phosphorylation induced nuclear translocation of the transcription factor Twist-related protein 1 (Twist1) was observed (Komiya et al., 2014). The cytoplasmic region of DPP4 associates with somatostatin receptor 4 (SSTR4) in human mesothelioma cells an action which is correlated with increased cell migration, invasion, colony formation, and *in vivo* tumour growth. Additionally, extracellular binding of an anti-CD26 antibody combined with SSTR4 agonist resulted in an antitumorigenic molecular signalling that were associated with the actions of the cytoplasmic region of DPP4 (Yamamoto et al., 2014).

DPP4 expression is connected to increased sensitivity to chemotherapy and improved median survival time in patients undergoing chemotherapeutic treatment. *In vitro* and microarray mesothelioma studies associate high levels of DPP4 expression with high cellular proliferation and increased chemosensitivity as highly proliferative cells are typically more sensitive to chemotherapeutic treatment (Aoe et al., 2012). These combined results strongly position DPP4 as an important diagnostic and prognostic biomarker for identification of CSC in mesothelioma as well as a predictor for response to chemotherapy.

1.4.2.3 Haematological malignancies

Due to its role in regulation of intracellular signal transduction in T cells, the expression of DPP4 in association with haematological malignancies has been extensively studied. DPP4 is shown to be a tumour promotor in haematological malignancy and DPP4 expression is a marker of aggressive cancer progression and poor survival prognosis in T lymphoblastic lymphomas (T-LBL), T-acute lymphoblastic leukemias (T-ALL), T-anaplastic large cell lymphomas (T-ALCL), and T-large granular lymphocyte lymphoproliferative disorder (T-LGLLPD) (Carbone et al., 1995; Dang et al., 2003). DPP4 also shows variable expression in B cell chronic lymphocytic leukemia (B-CLL) and is identified as a predictive marker in B-CLL patients with increased DPP4 expression associated with poor therapeutic outcomes (Cro et al., 2009). This correlation between DPP4, cancer progression and poor survival prognosis, targets DPP4 as a potential prognostic marker of aggressive haematological diseases.

In T and B cell malignancy DPP4 is associated with protumorigenic increase in cellular adhesion to the extracellular matrix (ECM). Depletion of DPP4 in T-ALCL cell line Karpas 299 via small interfering RNA transfection as well as treatment with anti-CD26 antibody results in decreased adhesion to fibronectin and type I collagen. The reduction in cellular adhesion is linked with dephosphorylation of both integrin β1 and p38 mitogen-activated protein kinase (p38MAPK) indicating that DPP4 mediates cellular adhesion in T-ALCL cells through phosphorylation of integrin β1 via p38MAPK (Sato et al., 2005). The relationship between DPP4 and p38MAPK phosphorylation is also seen in the Burkitt B cell lymphoma cell line Jiyoye, where increased DPP4 expression is shown to enhance phosphorylation of p38MAPK. DPP4 expression in Jurkat T-cell line (Aytac et al., 2003), and B-cell lines, Jiyoye (Yamochi et al., 2005) and Karpas 299 (Sato et al., 2003), is also positively related to topoisomerase IIα expression an enzyme identified as an notable therapeutic target in cancer treatment shown to play an essential role in control of cellular proliferation. In a xenotransplantation model using Karpas 299 T-ALCL cells transplanted into the anterior abdominal wall in SCID mice, DPP4 depletion via knockout RNAi resulted in decreased tumorigenicity and increased survival with no tumour development seen in mice inoculated

with DPP4 deficient T-ALCL cells (Sato et al., 2005). This decreased tumorgenicity was related to the reduced ability of DPP4 deleted tumour cells to bind to ECM proteins (Sato et al., 2005). In additional studies using Karpas 299 T-ALCL cells, depletion of DPP4 was associated with downregulation of proteoglycan versican, an extracellular matrix regulator known for its involvement in cell adhesion, migration, and proliferation. DPP4 depletion in T-ALCL cells was also associated with reduced collagenase I activity and a reduced ability to adhere to type I collagen (Havre et al., 2013; Wight et al., 2020).

DPP4 presence has also been linked to increased disease aggression in T-cell malignancies through increased cellular invasion. In the T-lymphoblast cell line HSB-2 and T-leukaemia cell line Jurkat, increase in both mutant DPP4 lacking enzyme activity and wt DPP4 expression through siRNA transfection enhanced stromal-cell-derived factor-1-α (SDF-1/CXCL12) mediated invasion activity *in vitro* (Havre et al., 2009). This increase in invasive activity was regulated by phosphoinositide 3-kinase (PI-3K) and mitogen-activated protein kinase 1 (MAP2K1) pathways. Indicated by increased phosphorylation of key intracellular signalling molecules p44/42 MAP kinase and Akt known to be involved in cell growth, proliferation, differentiation, motility, survival and intracellular trafficking (Caunt et al., 2015; Havre et al., 2009; Yang et al., 2019). Increase in DPP4 expression is also shown to induce secretion of matrix metalloproteinase-9 (MMP-9) an endopeptidase involved in activation of cytokines and chemokines required for degradation of ECM proteins and regulation of tissue remodelling (Havre et al., 2009; Yabluchanskiy et al., 2013). In addition, inhibition of tyrosine phosphatase CD45 in T-lymphoblast and T-leukaemia cells expressing high levels of DPP4 decreased the invasive activity, indicating that DPP4 plays a role in cellular invasion through association with the CD45 (Fernandis et al., 2003; Havre et al., 2009).

As seen in both colon cancer and mesothelioma, DPP4/CD26 is similarly described as a specific marker of leukemic stem cells in chronic myeloid leukemia (CML). Furthermore, in cell samples taken from patients with CML, 100% of DPP4/CD26 +ve leukemic stem cells were shown to express oncoprotein BCR/ABL1 which is considered essential for CML development, whereas DPP4/CD26 -ve leukemic stem cells from the same patients were all shown to be BCR/ABL1 negative (Herrmann et al., 2014). In addition, CML patients who were shown to be BCR/ABL1 positive but were receiving gliptin treatment for uncontrolled diabetes, BCR/ABL1 transcript levels decreased during treatment with either saxagliptin or sitagliptin (Herrmann et al., 2014). In migration assays performed using the monocytic cell line U937 and primary CML leukemic stem cells, incubation of SDF-1/CXCL12 with soluble recombinant DPP4 prior to assay was shown to disrupt the SDF-1/CXCL12-CXCR4-axis and reduce migration through cleavage and inactivation of SDF-1/CXCL12 (Château et al., 1996;

Herrmann et al., 2014). The enzyme activity of DPP4 was essential for the reduction in SDF-1/CXCL12 facilitated migration, as addition of sitagliptin or vildagliptin with recombinant DPP4 before incubation with SDF-1/CXCL12 increased SDF-1/CXCL12 facilitated migration. Additionally, treatment of primary CML cells with vildagliptin prior to injection into immunodeficient NOD SCID gamma mice (NSG mice) reduced engraftment of leukemic cells *in vivo* (Herrmann et al., 2014).

DPP4 plays a known role in immune regulation and T cell activation through co-stimulation and association with adenosine deaminase (ADA) (Herrera et al., 2001; Ishii et al., 2001). In addition to these actions, DPP4 facilitates the metabolism of adenosine to inosine thru its interaction with ADA. DPP4 binds ADA retaining its presence at the cell surface thereby controlling the presence of adenosine an inhibitor of T-cell proliferation. The downregulation of DPP4 would result in increased adenosine within the cell local environment resulting in immune suppression and enhance tumour progression through inhibition of T-cell proliferation (Blay et al., 1997; Montesinos et al., 2002; Mujoomdar et al., 2004). Although this regulation of adenosine through the interaction of DPP4 and ADA is highlighted as tumour suppressive, in haematological malignancies DPP4 expression is shown to be a marker of aggressive cancer progression and poor survival prognosis, and is associated with the protumorigenic increase in cellular adhesion to the extracellular matrix again highlighting that DPP4 plays an adaptable role in the tumour state.

1.4.2.4 Ewing's sarcoma

Ewing's sarcoma are a family of malignant bone tumours but are known to also involve the surrounding soft tissue (Lahl et al., 2008). Molecular targets identified as being upregulated in Ewing's sarcoma family of tumours (ESFT) are the known DPP4 substrate and neurotransmitter, neuropeptide Y (NPY) and its receptors Y1 and Y5. NPY is shown to promote cell death in ESFT through activation of the Y1 and Y5 receptors (Kitlinska et al., 2005). When cleaved by DPP4, NPY can no longer bind to the Y1 receptor and overexpression of DPP4 in Ewing's sarcoma cells is related to prevention of NYP induced cell death through reduced binding of the Y1 receptor. Thus, DPP4 is a key cell survival factor in Ewing's sarcoma tumours (Lu et al., 2011). Hypoxic non-perfused areas within Ewing's sarcoma tumours are shown to have increased expression of the Y2 NPY receptor as well as increased numbers of cancer stem cells and increased DPP4 activity. Under these conditions the DPP4 truncated form of NPY acts as a Y2 and Y5 receptor agonist preferentially stimulating cellular proliferation and migration. Therefore, DPP4 appears to be a promotor of Ewing's sarcoma cell angiogenesis through decreased cell death and increased proliferation and migration (Tilan et al., 2013). The tumour promotive actions of

DPP4 in other cancer types associates altered DPP4 expression with regulation of cellular proliferation, growth, differentiation and migration through pathways that are as yet undefined. In comparison decreased cell death, increased proliferation and migration in Ewing's sarcoma is correlated with DPP4 enzyme activity truncating NPY and altering its receptor specificity. This is a pathway that is specifically related to Ewing's sarcoma but may relate to results seen in other cancer types and indicate that the truncation of specific DPP4 substrates is involved in the alteration of cellular proliferation, growth, differentiation and migration and thus its action as a tumour promoter or suppressor, if enzyme dependent, is determined by the substrates involved with controlling tumour properties.

1.4.3 DPP4 targeted cancer therapy

The multifaceted nature of DPP4 may represent a hypothetical advantage for targeted therapeutic design as the non-enzymatic functions of the protein would remain in action when using specific inhibitors to block enzymatic function. DPP4 is identified as a promising target for cancer related therapy and treatment with DPP4/CD26 monoclonal antibody both *in vitro* and *in vivo* improved survival through reduced tumour growth in malignant mesothelioma (Inamoto et al., 2007, 2006; Ohnuma et al., 2002). DPP4 inhibitors have also proven effective in cancer targeted therapy, patients with chronic myeloid leukemia were shown to have increased survival and decreased levels of oncoprotein BCR/ABL1 with DPP4 inhibitor treatment, while DPP4 inhibitor vildagliptin reduced engraftment of leukemic cells *in vivo* and is also highlighted as a potential therapeutic treatment in lung metastases derived from colorectal cancer (Herrmann et al., 2014; Jang et al., 2019). DPP4 inhibitors are also shown to regulate cellular migration, invasion, adhesion and metastasis in cancer cells highlighting the potential clinical use of both inhibitor and monoclonal antibody based treatments in cancers where DPP4 acts as a tumour promoter (Beckenkamp et al., 2015; Sun et al., 2008). Additionally, DPP4 expression in some cancers is associated with increased chemotherapeutic sensitivity which is attributed to the action of DPP4 in stimulation of cellular proliferation as highly proliferative cells are more sensitive to the effects of chemotherapy (Aoe et al., 2012).

1.5 Fibroblast Activation Protein

Fibroblast activation protein (FAP; also called seprase) is the closest enzyme family member to DPP4. FAP resides in close proximity to DPP4 on chromosome 2 and is believed to arise from gene duplication. FAP is a 170 kDa homodimer that consists of two 97 kDa subunits, it is only active enzymatically as a homodimer but can also form enzyme active heterodimers with DPP4 (Ghersi et al., 2006). The FAP protein, like DPP4 it is a type II integral membrane

protein consisting of a large C-terminal extracellular domain and short N-terminal region located in the cytoplasm (O'Brien and O'Connor, 2008). A soluble form of FAP shed from the cellular membrane has also been identified in bovine serum and human plasma (Brennen et al., 2012; Collins et al., 2004; K. N. Lee et al., 2006). Sequence analysis identifies FAP as having an overall 48% amino acid sequence identity with DPP4 and a 68% amino acid sequence identity with the DPP4 carboxyl terminus region (Liu et al., 2012; Yazbeck et al., 2009). FAP in addition to its exopeptidase activity, also has endopeptidase activity and is able to degrade gelatin and type I collagen (Liu et al., 2012; Yazbeck et al., 2009).

Like DPP4, each subunit of FAP has a distinct β-propeller and α/β-hydrolase domain with the catalytic triad located at the interface (O'Brien and O'Connor, 2008). FAP has an eight bladed β-propeller where substrates of FAP can gain access to the catalytic site via two openings, the cavity formed between the β-propellers, and at the interface of the hydrolase and β-propeller domains (O'Brien and O'Connor, 2008). The catalytic site of FAP has the crucial Glu motif associated with all enzymes of the DPP4 protein family, in FAP these vital amino acids are identified as Glu203-Glu204, FAP and DPP4 also share a similar structure and specificity in the S2–S2′ substrate subsites (Aertgeerts et al., 2005).

1.5.1 FAP mRNA expression and protein presence

FAP is not ubiquitously expressed and is mostly found at sites of tissue remodelling and wound healing. Increased FAP protein expression is seen at regions of active tissue remodelling during mouse embryogenesis but is absent in healthy adult tissue (Garin-Chesa et al., 1990; Niedermeyer et al., 2001). In human tissue, *in silico* northern blot analysis of FAP mRNA expression reflects results seen in mice with normal tissue generally lacking FAP mRNA with the exception of the endometrium (Dolznig et al., 2005). FAP protein expression is considered to be induced by normal growth factors required for wound healing that are also up-regulated during malignant transformation (Kelly et al., 2012; Puré and Blomberg, 2018; Rettig et al., 1988). FAP protein is detected via immune-based assays in activated fibroblasts in areas of wound healing such as remodelling sites in the liver, as well as in the reactive stroma of epithelial cancers and some sarcomas (Garin-Chesa et al., 1990; Lay et al., 2019; Puré and Blomberg, 2018; Rettig et al., 1993, 1988). Increased FAP protein expression is seen in diseases associated with activated stroma, including cirrhosis, pulmonary fibrosis, rheumatoid arthritis and osteoarthritis (Bauer et al., 2006; Lay et al., 2019; Mathew et al., 1995; Milner et al., 2006; Sinnathurai et al., 2018; Xin et al., 2008). FAP is also found formed in a complex with DPP4 at invadopodia of migratory fibroblasts (Wagner et al., 2016). In addition to its absence in normal adult tissue, FAP is generally
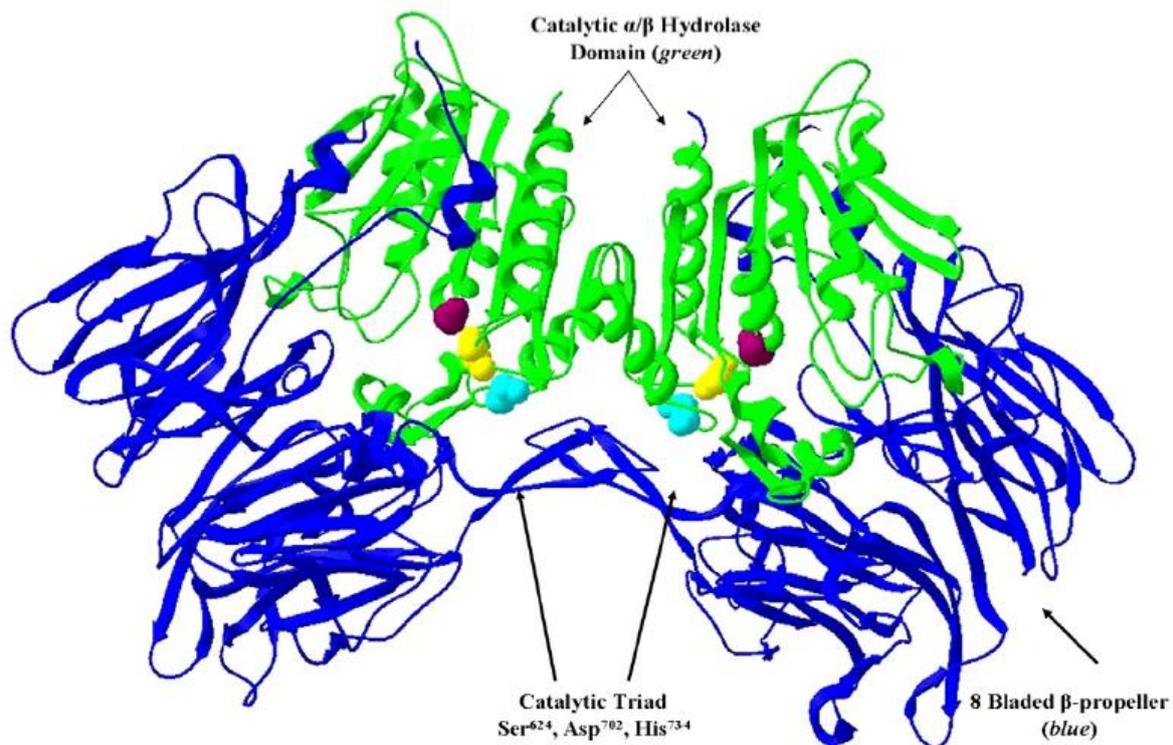
Figure 1.2. Ribbon diagram of FAP illustrating the extracellular domains. The eight bladed β-propeller domains are shown in blue and the α/β hydrolase domains are shown in green. The catalytic residues are shown in space filling form in purple, cyan and yellow representing serine, aspartic acid and histidine respectively. Image adapted from, O'Brien and O'Conner, 2008, (pdb accession code 1Z68), reprinted with permission from Elsevier.

absent from the stroma of benign epithelial tumours (Rettig et al., 1993; Rosenblum and Kozarich, 2003).

1.5.2 FAP inhibitor targeted therapy

Inhibitors or antibodies to FAP have been acknowledged as possible therapeutics for cancer and cirrhosis (Rosenblum and Kozarich, 2003). The non-specific dipeptidyl peptidase inhibitor L-valinyl-L-boroproline (VbP) has been shown to promote hematopoietic progenitor cell growth *in vivo*, and to also accelerate neutrophil and erythrocyte regeneration in mouse models of neutropenia and acute anaemia. The molecular targets of VbP promoting the cellular growth in this study were indicated to be FAP and DPP4 and the neutrophil recovery in response to VbP was shown to occur in Dpp4-/- mice. In this work Jones et al., (2003) suggests FAP is the possible hematopoietic target in the absence of DPP4 but VbP is a very nonselective dipeptidyl peptidase inhibitor so the claim that FAP is functioning in the neutrophil regeneration pathway is not proven. Future work with more specific dipeptidyl peptidase targeted inhibitors would need to be undertaken to define any possible role FAP may play in the neutrophil recovery response (Jones et al., 2003).

1.6 FAP and cancer

Because FAP is found commonly at sites of tissue remodelling and wound healing much of the research targeted at this protein is associated with its possible roles in tumorigenesis, angiogenesis and metastasis. Early research into FAP and its association with primary and metastatic carcinomas identified that FAP is selectively expressed by cancer-associated fibroblasts (CAFs) and pericytes rather than direct expression in tumour cells, increased FAP expression is seen in greater than 90% of human epithelial malignancies including colorectal, breast, ovarian, bladder, and lung carcinomas (Cohen et al., 1986; Rettig et al., 1993, 1988). This early research also investigated dermal incision wounds and found that FAP was strongly induced during scar formation. These studies provided a picture of FAP as being associated with specialised fibroblast functions involved in pro-tumorigenic actions such as inflammation and the increased cellular growth required for wound healing (Garin-Chesa et al., 1990; Rettig et al., 1993).

Dolznig et al., (2005) used *in silico* database mining of the BioExpress database containing Affymetrix U133 GeneChip expression transcriptional profiles of thousands of tissues samples, to analyse FAP mRNA expression. Dolznig et al., (2005) termed this process, *in silico* electronic Northern blot (eNorthern), and used it to compare FAP mRNA expression in both normal tissue and cancerous tissue types. While this analysis showed that normal

tissues generally lack FAP mRNA signals, of the 3200 separate human tissue samples used more than 1700 were from human cancer specimens. In this work FAP mRNA expression was detectable in association with lung, colorectal, pancreas and breast carcinomas, as well as squamous cell carcinomas of the head and neck in varying expression levels. FAP mRNA expression was identified in some normal uterus, cervix, skin, and breast tissue but it was not indicated if this association was related to any non-cancerous disease states such as fibrosis or inflammation. Although the data base mining used in this research associated FAP mRNA expression with these normal tissue types, there has been no FAP protein presence detected with these cell types in previous work. This may indicate that there is expression of FAP mRNA in these cells, but further regulation of protein expression is imparted at the translational level, possibly by miRNAs, and may be a point of interest for future investigations (Dolznig et al., 2005).

As with DPP4 there are conflicting results presented in the research identifying FAP with actions leading to both promotion and suppression of tumorigenesis. Consistent with the contradictory tumour suppressor or promoter properties, FAP expression is significantly reduced or lost in some tumours, while clearly up-regulated in other cancer types with this upregulation related to specific areas within the tumour environment such as the tumour centre. These findings are not yet linked to the specific biological properties of FAP which may provide some explanation as to why this protease shows variable actions in cancer. What is interesting in terms of FAP is like DPP4, its actions in cancer, result in biological activities that can contribute to both tumour progression or suppression depending on the type of cancer and tumour microenvironment.

1.6.1 FAP as a tumour suppressor

Although many of the research outcomes to date identify a tumour promotive role for FAP in cancer, there are some studies in melanoma, cervical and breast cancer which suggest that like DPP4, FAP also has a tumour suppressive role that may be independent of its enzymatic activity. Work in cervical and breast cancer shows contradictory results, with elevated expression of FAP related to both the promotion or suppression of tumour growth depending on the model or system investigated (Liu et al., 2012; O'Brien and O'Connor, 2008). It may be that FAP like DPP4 shows differing actions during tumorigenesis, executing its biological functions in a cell specific manner through its dual actions as both a protease and a binding molecule.

1.6.1.1 Melanoma

In melanoma, FAP is indicated as playing a tumour suppressive role, immunohistochemical analysis of human melanoma lesions showed that FAP is present in benign melanocytic nevi but is absent from primary and metastasising melanoma lesions (Ramirez-Montagut et al., 2004). Furthermore, in human melanocytes FAP expression is eliminated during malignant transformation and this absence is aligned to increased tumorigenesis and growth factor independence, indicating that FAP expression is involved in the suppression of tumorigenicity in melanoma (Rettig et al., 1993). In a mouse model where mice were challenged intradermally with the mouse melanoma cell line B78H1 transfected with wt or enzyme inactive FAP. Mice challenged with wt FAP or enzyme inactive FAP showed no tumour growth or significantly decreased tumour growth and delayed tumour progression when compared to vector transfected controls indicating that the enzyme activity of FAP was not required for its tumour suppressive actions (Ramirez-Montagut et al., 2004).

1.6.1.2 Cervical cancer

Invasion of cervical cancers is facilitated through degradation of the basement membrane and remodelling of the interstitial stroma. This is a process that requires a decrease of fibronectin and collagens and partial replacement by a laminin-rich matrix. When fibroblasts were taken from normal cervix, and from cervical cancers, and then grown in co-culture with cervical cancer cell line CSCC7, cancer-associated fibroblasts (CAFs) increased the invasive potential of CSCC7 cells through increase in laminin-1 while normal fibroblasts supported cell proliferation but not invasion (Fullár et al., 2015). To identify genes involved in the control of tumorigenic progression, Tsujimoto et al., (1999) performed differential expression analysis of the non-tumorigenic and tumorigenic HeLa fibroblast hybrid cells (Tsujimoto et al., 1999). In this work FAP was identified as one of the eight genes that were differentially expressed, showing increased expression in the non-tumorigenic hybrid cells when compared to the tumorigenic hybrid cells derived from long term cell culture (Tsujimoto et al., 1999). This is consistent with the identified role for FAP in suppressing the tumorigenic phenotype but is contradictory to more recent work conducted on patient derived cervical cancer sections which showed that all fully invasive cervical carcinomas have FAP immunoreactivity (Jin et al., 2003). These contradictory results may be related to the difference in biological functions and protease activity in a cell culture context compared to an *in situ* derived carcinoma (Liu et al., 2012).

1.6.1.3 Breast cancer

Immunohistochemical analysis of FAP expression in 112 cases of invasive ductal carcinoma associated increased expression of FAP in stromal fibroblasts adjacent to the tumour with longer overall and disease-free survival rates (Ariga et al., 2001). Additionally, patients with lymph node metastasis and increased FAP expression in stromal fibroblasts, showed better survival rates that patients without FAP stromal expression (Ariga et al., 2001). These results indicate that FAP expression may serve as a vital prognostic factor that in patients with invasive ductal carcinoma but as with cervical cancer is in contradiction to work conducted in infiltrating ductal carcinomas and breast phyllodes tumours described above. Kimoto., (1998) suggested that the gelatinolytic actions of FAP in cancer stroma may also be related to the tissue remodelling actions of the protein providing protection for the host through the inhibition of cancer cell growth by collagen deposition, a mechanism which is similar to the encapsulation process (Kimoto, 1998).

The stromal compartment plays a pivotal role in tumorigenesis and cellular invasion, FAPs involvement in cancer is largely related to its expression by CAFs, which is a principal component of the cancer stoma. Since its discovery most of the research into FAP and cancer has focussed on localization and expression of this protease in relation to differing cancer states. A defined role for FAP in tumour growth and invasion, as well as the mechanisms this enzyme utilises in its tumour promotive and suppressive actions remain unknown. Although current findings show that the association between FAP and cancer is significant, there may still be novel functions provided by this protein that have not been identified. Future work focused on the role of FAP in tumour growth and invasion will provide an essential step towards the development of targeted anticancer therapy.

1.6.2 FAP as a tumour promoter

FAP is reported to correlate to higher tumour grade and worse overall survival across a wide range of human cancers. Meta-analysis across a range of immunohistochemical based studies in various tumour types, reported a consistent association between high FAP expression, increased lymph node metastasis and poor overall survival (Liu et al., 2015). This association between FAP and tumour progression is reflected in results from work conducted in ovarian and cervical cancer, breast, colorectal and pancreatic cancer.

1.6.2.1 Ovarian and cervical cancer

Addition of FAP to cell culture medium is reported to increase invasion, proliferation and migration in the ovarian cancer cell line HO-8910PM (Chen et al., 2009). While in cervical

cancer study of *in situ* precursor lesions known as dysplasia as well as cervical intraepithelial neoplasms have shown that micro-invasive and fully invasive carcinomas have FAP immunoreactivity (Jin et al., 2003). There is also an established direct correlation between gelatinase expression and a malignant phenotype in cervical cancer. This gelatinase activity can be associated with invasive tumour growth and indicates that FAP expression may be utilized as a possible early marker of negative tumour progression (Jin et al., 2003).

1.6.2.2 Breast cancer

In breast cancer FAP protein expression is seen in high levels in infiltrating ductal carcinomas of the breast as well as in the human breast cancer cell lines MDA-MB-435 and MDA-MB-436 (Goodman et al., 2003). Suppression of FAP expression in MDA-MB-435 and MDA-MB-436 cells through expression of antisense cDNA rendered the cells sensitive to serum starvation, with control transfectants expressing high levels of FAP showing strong growth even in the absence of serum. The ability to circumvent normal growth regulation is a key characteristic in malignant transformation that distinguishes cancer cells from normal cells. These findings suggest a role for FAP in breast cancer tumorigenesis through reduced dependence on exogenous growth factors and promotion of aberrant growth of the cancer cells (Goodman et al., 2003).

Breast phyllodes tumours are large, fast growing benign tumours with frequent local relapse that have an unpredictable shift to malignancy and distant metastasis. In recurrent phyllodes tumour progression toward the more malignant phenotype is associated with the acquisition of new genetic changes within the tumour-associated fibroblasts (Jones et al., 2008). Work by Gong et al., (2014) examined miRNA expression in tumour-associated fibroblasts by *in situ* hybridisation on paraffin-embedded sections taken from breast phyllodes tumours (Gong et al., 2014). This group demonstrated the expression of FAP is progressively increased in the malignant progression of phyllodes tumours indicating a role for FAP in development of the malignant phenotype (Gong et al., 2014).

1.6.2.3 Colorectal cancer

High FAP expression is correlated with worse overall survival in colorectal cancer. In an immunohistochemical study of 449 samples from patients with colorectal cancer, FAP expression was seen in the fibroblasts of 85–90 % of the tumours examined. Additionally, high FAP expression in the tumour centre was correlated with overall poor prognosis when compared to no or low FAP expression, while FAP expression at the tumour front was not associated as a prognostic factor (Wikberg et al., 2013).

FAP is selectively expressed in tumour-associated fibroblasts which are the principal component of the stoma in most cancer types required for maintenance of the tumour microenvironment. This role for FAP in tumour microenvironment makes it a viable therapeutic target for cancer immunotherapy which has been investigated in a murine xenograft model using human colon cancer cells. In this work mice injected subcutaneously with CT26 colon cancer cells transfected with wt FAP developed larger tumour volumes than mice injected with cells carrying a vector only control (Wen et al., 2010). Further to these findings, mice vaccinated using a DNA vaccine directed against FAP had reduced primary tumour size as well as decreased instance of metastasis through increased CD8^{+}T-cell-mediated anti-tumour immune response (Wen et al., 2010).

In an alternate xenograft study using SCID mice subcutaneously injected with HEK293 colon cancer cells transfected to express murine wt FAP. Mice injected with wt FAP expressing cells were 2–4 times more likely to develop tumours and showed a 10- to 40-fold enhancement of tumour growth compared with mice injected with vector only transfected cells (Cheng et al., 2002). In addition to these findings Cheng et al., (2002) developed a recombinant murine polyclonal anti-FAP antibody derived from FAP-immunized rabbit sera that significantly inhibited murine FAP activity *in vitro*. Treatment of the HEK293 xenografts with this inhibitory anti-FAP antisera attenuated tumour growth when compared with tumours treated with preimmunization rabbit antisera (Cheng et al., 2002).

1.6.2.4 Pancreatic cancer

FAP is highly expressed in the tumour stroma of pancreatic adenocarcinoma and associated with overall worse clinical outcomes. In an immunohistochemical study of 70 paraffin-embedded human pancreatic adenocarcinoma sections, FAP protein expression was significantly increased in tumour-associated myofibroblasts immediately adjacent to the tumour when compared to tumour-associated myofibroblasts in surrounding tissue (Cohen et al., 2008). Increased FAP expression in surrounding tumour-associated myofibroblasts also correlated in all patients with an increase in metastasis to the lymph nodes, a higher risk of postoperative tumour recurrence and mortality (Cohen et al., 2008).

1.6.2.5 FAP and cancer-associated fibroblasts

The tumour microenvironment (TME) is a complex multicellular system that involves reciprocal interactions between cancer cells and the extracellular matrix (ECM). These interactions also involve various cell types including immune cells, endothelial cells, pericytes, and fibroblasts (Monteran and Erez, 2019; Quail and Joyce, 2013). The

components of the TME that are vital to non-cancerous cell maintenance are also central to tumour initiation, progression and metastasis, within this environment fibroblasts are important custodians of tissue integrity (Quail and Joyce, 2013; Servais and Erez, 2013). Fibroblasts can initiate a response to tissue damage signals by differentiating to myofibroblasts which enables orchestration of tissue repair and wound healing, this action is mediated by ECM synthesis and remodelling as well as interaction between fibroblasts and innate immune cells (Barnes and Gorin, 2011; LeBleu and Kalluri, 2018). Cancer-associated fibroblasts (CAFs) are a dominant cell type in solid tumour lesions and are found in direct contact with neoplastic cells, CAFs produce cytokines, chemokines, metabolites, enzymes and EMC growth factors that control the growth of cancer cells and are that are critical to tumorigenesis and angiogenesis (Kalluri, 2016).

FAP is a common marker for CAFs and FAP+ fibroblasts are shown to suppress the anti-tumour immune response. In mice with melanoma, depletion of FAP+ CAFs reduces immunosuppressive cell activity and improves the antitumor activity of CD8^{+} tumour-infiltrating T cells (Zhang and Hildegund, 2016). FAP+ CAFs are also associated with reduced T cell infiltration in pancreatic and lung cancer bearing mice through the CXCL12-CXCR4 axis (Feig et al., 2013). In human breast and ovarian cancers, a CAFs subtype characterised by elevated FAP expression generates an immunosuppressive tumour microenvironment by accumulating CD4^{+}CD25^{+} T cells and enhancing their differentiation to T regs (Costa et al., 2018; Givel et al., 2018). In addition to the impact on infiltration of immune cells in to the tumour microenvironment, FAP+ CAFs may also play a role in ECM remodelling through the production of TGF-β, VEGF, and multiple matrix processing enzymes which indirectly disrupts infiltration of cytotoxic T cells to the tumour site (Kobayashi et al., 2019; Ziani et al., 2018). FAP+ CAFs are a source of distinct chemokines and cytokines that drive tumour promotive immunosuppressive actions within the tumour microenvironment, indicating that FAP targeted therapy may prove effective in slowing tumour growth through reversal of these immunosuppressive actions.

1.7 Conclusion

The link between the closely related genes, DPP4 and FAP, and carcinogenesis is now well established. The actions of both proteins in relation to tumour initiation and progression appears to depend on the initiating cell type, localisation and tumour microenvironment. Both DPP4 and FAP show variable expression in differing types of cancer and can act as both a tumour suppressor and a tumour promotor, dependent on tumour type.

FAP expression is associated with cancer-associated fibroblasts a predominant component of the cancer stoma that plays a key role in tumorigenesis and invasion. The biological function of FAP, like DPP4 includes both protease activity and its ability to form complexes with other cell-surface molecules, which is a contributor to the ability of FAP to act as a tumour promotor and tumour suppressor in a cell-context dependent manner. FAP is shown to play a role in malignant cell invasion and metastasis through deposition and remodelling of ECM as well as deregulation of antitumor immune responses. Given the strong presence of FAP within the tumour stroma, the role it plays in cancer progression may also be determined by the signalling molecules that are available for interaction with FAP on the cell. However, a definitive role played by FAP in tumour growth and invasion remains largely unknown, future studies on the contribution of FAP to tumorigenesis will constitute an essential step toward stroma-targeted anticancer therapy.

In this review the role of DPP4 in tumour progression has been related to its actions as an ECM binding molecule able to bind ECM proteins, DPP4 is also shown to play a role in cell adhesion through involvement with the cellular adhesion proteins, integrin β1, β-catenin, E-cadherin, versican, periostin, and CD44 (Havre et al., 2013; Kajiyama et al., 2003; Komiya et al., 2014; Sato et al., 2005). Additionally, DPP4 expression is correlated with increased expression of known markers of invasive metastasis, Twist1, matrix metalloproteinases and tissue inhibitors of matrix metalloproteinases, although a direct role for DPP4 in the regulation of these proteins is yet to be defined (Kajiyama et al., 2003; Komiya et al., 2014).

The enzymatic activity of DPP4 is established as playing a role in regulation of the tumour microenvironment through the control of SDF-1/CXCL12 mediated cellular invasion. In the absence of DPP4, SDF-1/CXCL12 promotes tumorigenesis through activation of the CXCR4 receptor simulating cellular proliferation, migration and invasion. When DPP4 is absent in endometrial carcinoma, prostate cancer, and neuroblastoma cell lines, SDF-1/CXCL12 binding to its receptor is unchecked however this malignant phenotype can be reverted when DPP4 expression is induced and is then able to cleave SDF-1/CXCL12 and alter CXCR4 receptor binding (Arscott et al., 2009; Mizokami et al., 2004; Sun et al., 2008).

The work outlined in this review does highlight DPP4's usefulness as a tumour biomarker. Decreased DPP4 expression within the tumour is associated with diseased progression in melanoma, ovarian cancer, general lung cancer, endometrial cancer and neuroblastoma identifying DPP4 as a marker of tumorigenesis. Alternately, increased DPP4 expression is noted as a marker of tumour aggression, invasion and metastasis in colorectal cancer, malignant mesothelioma and haematological malignancies and increased DPP4 expression is associated with higher incidence of postoperative reoccurrence and overall poor survival

prognosis in gastric cancers (Yamaguchi et al., 2008). DPP4 is also identified as an important diagnostic and prognostic biomarker for identification of CSCs in mesothelioma as well as colorectal cancer where DPP4 positive CSCs were also linked to enhanced chemoresistance and increased incidence of tumour regrowth post treatment. Although comparison of work using cell cultures to work conducted on patient samples does in some instances produce conflicting results, DPP4 enzymatic activity within the tumour has been highlighted as a potential diagnostic tool and may provide an inexpensive and minimally invasive method for prediction of disease state, metastatic potential and overall survival prognosis when measured in patient plasma/serum (Yazbeck et al., 2018). Given the multifaceted actions of DPP4 and the variable role it has been shown to play in cancer biology to date, further studies are required to define its actions in terms of cancer initiation and progression with results that may target this multifunctional protein as a possible diagnostic and therapeutic target for the treatment of cancer.

1.8 Summary

DPP4 plays a long-established but complex role in cancer biology which changes depending on cancer and tissue type. DPP4 expression can be upregulated or down-regulated in cancer depending on the cell type and it is touted as both a suppressor and a promoter of tumour adhesion, proliferation and metastasis. DPP4 is shown to play a role in the regulation of growth factors, apoptosis, angiogenesis, tissue invasion and metastasis. The multifunctional actions of DPP4 allow it to act as a protease regulating bioactive peptides through enzymatic cleavage as well as a binding protein involved in cellular adhesion through binding of extracellular matrix proteins like fibronectin and collagen. Mounting evidence suggests that some of the influence DPP4 has on tumour growth is conveyed through non-enzymatic regulation of cellular processes or modification of alternate signalling pathways rather than its more recognized enzymatic function.

DPP4 is a therapeutic target for treatment of T2DM, a chronic disease that is increasing in Australia and worldwide. A recently emerged therapy for T2DM is sitagliptin, also known by the brand name Januvia, a targeted inhibitor of DPP4 that results in higher levels of active GLP-1, a gut hormone, which increases insulin secretion and lowers blood glucose. Sitagliptin is one of the most readily available DPP4 inhibitors in Australia. In the 2019/20 financial year 1.5 million pharmaceutical scripts for sitagliptin were claimed in Australia amassing a total cost of $82 million dollars. The increasing use of this DPP4 targeted therapy has raised some warranted concerns within the research and medical community that long-term use of DPP4 inhibitors may increase the risk of colorectal and other cancers.

DPP4 has two domains, an alpha/beta hydrolase domain that is responsible for its enzyme activity, which DPP4 inhibitors bind to, and an eight bladed propeller domain that can mediate protein-protein interactions that may be involved in tumorigenesis. Thus, we hypothesise that the inhibition of DPP4 enzyme activity will be protective while removal of the protein binding domain will be harmful, this body of work is designed to specifically further the investigation of this hypothesis.

1.9 Aims

The aims of this work are:

1. There is an increased interest in cancer metabolism as a therapeutic target, recent research has highlighted that control of the insatiable metabolic needs of cancer cells by T2DM therapeutics that are nontoxic to normal cells can offer selective inhibition of cancer cell growth. Chapter two aims to determine the role DPP4 inhibitors play in the regulation of cellular metabolism and compare the effects of sitagliptin with that of metformin a T2DM treatment currently under investigation for its anti-tumorigenic effects.

2. The aim of chapter three is to develop the azoxymethane (AOM) chemical model of sporadic CRC for use with DPP4 and FAP knockout mice (Dpp4-/- and Fap-/- mice).

3. The aim of chapter four was to use the AOM model of CRC, to examine the role of DPP4 and FAP in CRC progression.

Chapter 2

Sitagliptin a dipeptidyl peptidase 4 inhibitor attenuates mitochondrial bioenergetic function in lymphocytic cancer cell lines

2.1 Introduction

Diabetes and cancer are two diseases with significant impact on worldwide health that share many mutual risk factors and biological links (Giovannucci et al., 2010). Epidemiological studies indicate that patients with diabetes have a significantly higher risk of developing certain types of cancer. When compared to non-diabetic patients, diabetics are two-fold more likely to develop cancers of the liver, pancreas, and endometrium, and 1.5-fold more likely to develop cancers of the colon, breast, and bladder (Vigneri et al., 2009). The mechanism underlying the relationship between diabetes and cancer is yet to be identified but both disease states involve significant metabolic change as well as activation of inflammatory and stress-related pathways (Joshi et al., 2015; Tudzarova and Osman, 2015)

Recent observational studies suggest that some medications used to treat hyperglycaemia and T2DM are associated with a reduced risk of cancer. Interest in the potential of T2DM treatments as effective anticancer agents has centred on the commonly used biguanide treatment for T2DM, metformin (Quinn et al., 2013). Metformin has been associated with a reduced cancer burden in diabetic patients taking the medication with the reduction in tumorigenesis linked to AMPK activation (DeCensi et al., 2010; Quinn et al., 2013; Singh et al., 2017). Sitagliptin is a selective dipeptidyl peptidase-4 (DPP4) inhibitor also used for the treatment of T2DM. The insulinotropic action of sitagliptin involves the increase of nutrient-stimulated insulin release through inhibition of DPP4 enzymatic degradation of the active form of incretins, particularly glucose-dependent insulinotropic peptide (GIP) and glucagon-like peptide-1 (GLP-1) (Drucker, 2003; Herman et al., 2006). Recent research has indicated that sitagliptin and other DPP4 inhibitors, linagliptin and gemigliptin, like metformin are linked to AMPK activation indicating that the *in vivo* action of this DPP4 inhibitor may be associated with decreased cancer risk, positioning it as a potential anticancer agent (Herman et al., 2006; Hwang et al., 2015b; Kornelius et al., 2015; Quinn et al., 2013; Wu et al., 2017; Zeng et al., 2014).

Despite there being a wide diversity in the cellular origin of all cancers, this heterogenous disease presents with a common metabolic phenotype where accumulation of metabolic mutations allows tumour cells to sustain their cellular growth pathways, activate uncontrolled proliferation and evade cell death. Otto Warburg was the first to observe that even in the presence of oxygen, cancer cells have an altered metabolic state that enables them to drive energy production primarily through glycolysis (Warburg, 1956). This aerobic glycolysis commonly referred to as 'The Warburg Effect' is also associated with rapidly dividing embryonic tissue and is postulated to provide the cancerous cell a proliferative advantage as

glycolytic intermediates are required for the formulation of nucleosides and amino acids that feed into the development of macromolecules and organelles required for formation of new cells (Hanahan and Weinberg, 2011; Vander Heiden et al., 2009; Warburg, 1956). The Warburg effect has been associated with multiple tumour types and is now commonly used as a diagnostic tool to detect tumours by fluorodeoxyglucose positron emission tomography (FDG-PET) (Yizhak et al., 2014).

There is an increased interest in cancer metabolism as a therapeutic target, recent research has highlighted that control of the insatiable metabolic needs of cancer cells by drugs such as metformin that are nontoxic to normal cells can offer selective inhibition of cancer cell growth, delay tumour progression and provide increased sensitivity to chemotherapeutic treatment (Cheong et al., 2011; Shafaee et al., 2015; Zhang and Guo, 2016). In this chapter I aim to determine the role the DPP4 inhibitor sitagliptin plays in the regulation of cellular metabolism and the AMPK signalling pathway and to compare theses effects on cellular metabolism with that of metformin a well characterised AMPK activator.

2.2 Materials and Methods

Unless stated otherwise, all reagents used in this chapter were sourced from Sigma Aldrich, New South Wales, Australia. All water used was triple distilled and filtered using Millipore Q Gard®1 (Australia, Cat#QGARD00L1).

2.2.1 Cell Culture

Two mammalian cell lines were used throughout this work. Jurkat, an immortalized line of human T lymphocyte cells obtained from a previously frozen in-lab culture, and THP-1, human acute monocytic leukemia cells, obtained as a generous gift from the Flinders Flow Cytometry Facility (Flinders Medical Centre).

Cell were maintained in RPMI 1640 media (cat no. R5886, Sigma-Aldrich, NSW, Australia). Culture media was made in 50 mL stock aliquots containing, 44 mL RPMI 1640 sterile-filtered liquid with 25 mM HEPES and sodium bicarbonate added, 0.5 mL of sterile-filtered penicillin 10 000 U/mL (100 units/mL final concentration) with streptomycin 10 mg/mL (100 μg/mL final concentration), 5 mL (10% v/v) sterile filtered fetal bovine serum (FBS) (Bovogen, Vic, Australia) and 0.5 mL 200 mM sterile-filtered L-glutamine solution (2mM final concentration) and stored at 4^0C until required. Cell cultures were maintained in 25 mL media in 75 cm^2 cell culture flasks and grown in standard conditions, incubated at 37^0C with 5% CO_2. Cells were passaged every three to four days when growth had reached 70 to 90%

confluence. Cell concentration for replating was between 5 x 10^4 and 1 x 10^5 cells/mL (12.5 x 10^5 and 2.5 x 10^6 cells in total).

To ensure successive retrieval and continuation of culturing, cell cultures were periodically frozen in liquid nitrogen. Cells were counted using trypan blue exclusion, as described in section 2.2.2, and pelleted by centrifugation. Cells were then re-suspended in a final concentration of 10% DMSO and 50% FBS in appropriate media at a maximum concentration of 1 x 10^6 cells/mL. One mL of this cell suspension was then added to a cryo-vial and stored at -80°C for a minimum of 24 hr. After 24 hr at -80^0C, cells were transferred to liquid nitrogen storage until required.

Cells to be thawed were removed from liquid nitrogen storage and transferred immediately to a 37°C water bath for rapid thaw. The cell suspension was transferred to 9 mL of culture media in a sterile container and pelleted by centrifugation at 1500 rpm for 5 min. After centrifugation the supernatant was removed, and the subsequent cell pellet resuspended in 5 mL of media ready for cell culture.

2.2.2 Cell counting and viability by trypan blue exclusion

Cells to be counted were diluted 1:2 or 1:4 as required in 0.4% w/v trypan blue in Dubelcco's PBS. After mixing, the cells in trypan blue were added to a Neubauer chamber haemocytometer. The number of unstained (viable) cells was then counted in eight 1 mm^2 areas (both sides of haemocytometer). The total combined number of viable cells in all eight 1 mm^2 areas was then divided by eight to provide the average number of cells per 1 mm^2. The number of cells per mL was then calculated using $c = n \times d \times 10^4$, where c = concentration of cells/mL, d = dilution and n = average number of cells/mm^2.

2.2.3 Cell treatment with sitagliptin and metformin

The DPP4 specific inhibitor sitagliptin and the biguanide oral hypoglycaemic agent metformin were sourced from Sigma and dissolved in PBS to a working concentration of 10 mM with 1 mL aliquots stored at -20^0C until required. From the 10 mM storage solution both sitagliptin and metformin were diluted to required working concentrations in PBS immediately prior to use.

For treatment with sitagliptin and metformin prior to resazurin cell viability assay or XF Extracellular Flux analysis, cell cultures were plated into 96 well cell treatment plates in 190 µL of appropriate media at required concentration between 1 x 10^5 to 4 x 10^5 cells/mL (1.9 x 10^4 to 7.6 x 10^4 cells per well). For cells designated to be treated with either sitagliptin or

metformin, 10 µL of 0.8 µM sitagliptin to achieve a final concentration of 0.04 µM, or 10 µL of 10 mM metformin to achieve a final concentration of 0.5 mM, was added to each well with addition of treatment timed to be at four and six hr prior to commencement of resazurin cell viability assay or XF Extracellular Flux analysis respectively. Wells designated as cells only without treatment had 10 µL of PBS added at the start of the treatment period.

For treatment with sitagliptin and metformin prior to enzyme assay, HPLC analysis and western blotting cells were passaged into 10 mL of RPMI media with additives as described above in 25 cm^2 culture flasks at 1 x 10^5 cells/mL (1 x 10^6 cells in total). For cells designated to be treated with either sitagliptin or metformin, 500 µL of 0.8 µM sitagliptin to achieve a final concentration of 0.04 µM, or 10 mM metformin to achieve a final concentration of 0.5 mM, was added to each culture flask 24 hrs after time of passage with addition of treatment timed to be at four and six hr prior to use. Culture flasks designated as cells only without treatment had 500 µL of sterile PBS added at the start of the treatment period.

2.2.4 Resazurin reduction assay for cell viability

Resazurin, also known as Alamar Blue is a cell permeable redox indicator that allows for quantification of viable cell number without the need to lyse cells as required when utilizing tetrazolium compounds (Riss et al., 2004). Assays for determination of cell viability and proliferation were set up in 96 well plates (Corning Costar, cat no. CLS3595, Sigma-Aldrich, NSW, Australia). Cell treatment plates had 100 µL of cell culture in appropriate media at a concentration of 2 x 10^5 to 4 x 10^5 cells/mL (2 x 10^4 to 4 x 10^4 cells in total) added to all wells with the exception of wells in the very first and last rows which had 100 µL of PBS added to minimise any plate edge effects. Standard curves for determination of cell growth/decline were set up as described below.

Resazurin was dissolved to 0.15 mg/mL in PBS and adjusted to pH 7.4 prior to being filter-sterilized through a 0.2 µM filter (Corning syringe filter, cat no. CLS431229-50EA, Sigma-Aldrich, NSW, Australia) into a sterile, light protected container. To perform the assay 20 µL of resazurin pre-warmed to 37^{0}C was added to all plate wells including medium only wells for background subtraction and instrument gain adjustment. Plates were shaken on a plate shaker for 1 min and then incubated at 37^{0}C for 1 hr in the dark. Measurement of fluorescence was taken using a 560 nm excitation / 590 nm emission filter at ambient temperature using a FLUOstar Omega Microplate Reader (BMG LABTECH). Each treatment was performed in triplicate per assay with each assay also performed in triplicate.

Standard curves were set up alongside all resazurin cell viability assays to determine final cell growth/decline. One hundred µL of cell culture was added to each well in a concentration gradient of 0, 2.5, 5, 7.5, 10, 15, 20, 30, 40, 60 and 80 (x 10^3) cells/well with each concentration plated into six replicate wells of the 96 well plate. Addition of resazurin was carried out as outlined above and plates were processed and read at time zero, one hr after addition of resazurin. Standard curve plates were also read at time of experimental plate treatment and time of experimental plate reading to give a comparison of normal cell growth over the experimental period for differing starting cell numbers.

2.2.5 Extracellular flux analysis

The Seahorse XF Extracellular Flux Analyser provides the ability to simultaneously quantify the cellular oxygen consumption rate (OCR) as a measure of oxidative phosphorylation and the extracellular acidification rate (ECAR) as a measure of glycolytic metabolism (Kalyanaraman et al., 2018). Oxygen consumption rate (OCR) refers to picomoles of oxygen consumed per min per microgram of protein and is a measure of the amount of oxygen consumed as a terminal electron acceptor in the production of ATP via the mitochondrial electron transport chain. The extracellular acidification rate (ECAR) refers to the change in media mpH per min per microgram of protein as a result of increased hydrogen cation concentration as a by-product of glycolytic conversion of pyruvate to lactate (Divakaruni et al., 2014; Pelletier et al., 2014; Teslaa and Teitell, 2014). A detailed outline of bioenergetic analysis using the XF Extracellular Flux is provided in the appendix, section A.1.

The XFe96 Extracellular Flux Analyser (Seahorse Bioscience, Billerica, MA) is a 96-well instrument able to measure the uptake and excretion of cellular metabolic end products in real time. The XFe96 FluxPak contains a disposable sensor cartridge which is embedded with 96 pairs of fluorescent biosensors that measure the excitation wavelengths of oxygen (532 nm) and extracellular acidification (pH, 470 nm) and transmit a fluorescent signal to a set of highly sensitive photodetectors. The instrument supports simultaneous measurement of both oxygen and pH and each sensor cartridge is equipped with reagent delivery chambers able to deliver up to four agents into the wells during the assay, for this work the reagent delivery chambers were used to sequentially deliver electron transport chain (ETC) modulators into the cell population.

In this work two different immune cell lines were used in conjunction with the Seahorse XF Extracellular Flux Analyser to study the effects of DPP4 inhibitors on their bioenergetic metabolism. The similarity between the inflammatory milieu and the tumour microenvironment produces equivalences in the metabolic actions of immortalised immune

and malignant cells that is relevant for this type of analysis (Pelletier et al., 2014). Immune cells reflect the metabolic behaviour of malignant cells where their metabolic processes are not subject to external energy demand as fast metabolic response is required to adapt to changing microenvironmental conditions (Jacobs et al., 2008; Rathmell et al., 2003). This similarity in metabolic actions and the ability to produce the large cell numbers required for extracellular flux analysis resulted in the selection of immortalised immune cell lines Jurkat and THP-1 for this bioenergetic analysis.

Prior to the start of the XFe assay, 200 μL of calibrant (included in the XFe96 FluxPak) was added into each well of the microplate, the probes of the sensor cartridge were then immersed in calibrant for 12 to 18 hr at 37°C in a non-CO_2 incubator to hydrate all probes. The biosensors were independently calibrated prior to the assay using a pre-programmed automated routine that establishes unique sensor gain via measurement of a calibration medium of known pH and oxygen concentration. Twenty μl Cell-Tak (Corning, New York, USA) was added to each well of the XFe96-well cell culture plate to help Jurkat and THP-1 cells to adhere to the plate. Cell-Tak is required to enable non-adherent cells to form a consistent monolayer at the bottom of the cell well for reliable XFe results. Plates were incubated with Cell-Tak for 1 to 2 hr prior to aspiration and washed with MilliQ H_2O. Cell-Tak preparation was performed the day before the assay with Cell-Tak covered plates stored overnight at 4^0C and brought to RT prior to assay set up.

Cells were set up in 96 well plates for sitagliptin and metformin treatment prior to XFe analysis as outlined in section 2.2.3. To prepare for bioenergetic analysis the 96 well plate containing prepared cell culture was centrifuged at 1200 rpm for 5 min at room temperature, cell culture medium was removed and the cell pellet was resuspended in 180 μL XF media prior to being transferred to XFe96-well cell culture plate with addition of 10 μL of, 0.8 μM sitagliptin, 10 mM metformin, or PBS. Cells adhered to Cell-Tak through centrifugation with the centrifuge brought up to 450 rpm without braking and stopped as soon as 450 rpm was reached, plate orientation was then reversed, and the centrifugation step repeated up to 650 rpm. Plates were then incubated for 30 to 60 min at 37^0C in a non-CO_2 incubator and then visually inspected under a microscope to verify that a monolayer of cells was present in all groups with no cells dislodged. Two point eight mL stock solutions of ETC modulators (included in XF Assay Kit) in XF media were produced, the stock solutions were added directly into three of the four drug delivery ports on top of the sensor cartridge, 20 μL of 10 μM oligomycin A was added to port A to produce a final concentration of 1 μM once delivered into the well, 20 μL of 22 μM FCCP (carbonyl cyanide-4-(trifluoromethoxy)phenylhydrazone) was added to port B to produce a final concentration of

2 μM, and 10 μL of 12 μM rotenone and 10 μL of 12 μM antimycin A were both added to port C to give a final working concentration of 1 μM for each. The cartridge was then incubated at 37^0C in a non-CO_2 incubator while the XFe analyser was set up. Analysis was completed using the standard protocol for the XFe analyser, assays were run using five replicates per plate over three individual plates.

Taking the 1×10^5 cell density as the starting point a mitochondrial stress test optimisation was run using Jurkat cells at a density of 1×10^5 cells per well (Figure 2.1), 1.5×10^5 cells per well (Figure 2.2) and 2×10^5 cells per well (Figure 2.3), these cell densities were then each run using three different concentrations of oligomycin A, 0.5, 1.0 and 2.0 μM and four different concentrations of FCCP, 0.2, 0.4, 0.8 and 1.2 μM. FCCP optimisation in Jurkat cells was undertaken at a concentration of 0.2, 0.4, 0.8 and 1.2 μM. Optimisation of FCCP with THP-1 cells was undertaken using concentrations of 0.8, 1.2 and 2.0 μM, at the optimal cell density of 1×10^5 cells per well (Figure 2.4),

2.2.6 DPP enzyme activity assay

Methods for the detection of DPP enzyme activity in cells were adapted from Sulda, M.L. 2009, and originally provided by Professor Mark Gorrell, Centenary Institute, Sydney, Australia (Sulda, 2009).

To prepare cell lysate for DPP enzyme activity assays 1×10^6 cells pre-treated for four or six hr with 0.8 μM sitagliptin, 10 mM metformin, or PBS as described in section 2.2.3 were washed twice in 1 mL PBS and then pelleted in a 1.5 mL microcentrifuge tube with centrifugation at 2000 rpm for 5 min at each step. The cell pellet was then resuspended in 1 mL of PBS with 0.2% Tween-20 added to facilitate cell membrane permeability with addition of 50 μL of, 0.8 μM sitagliptin, 10 mM metformin, or PBS. As the cell pelleting and resuspension would result in removal of the inhibitor from the cell culture, re-addition of inhibitor was undertaken after cell pelleting and resuspension was to ensure enzyme activity was conducted in the presence of the inhibitor.

To detect DPP activity, enzyme activity assays were performed using the DPP substrate H-Ala-Pro-pNA.HCl (Bachem, CA, USA). Once cleaved by the target enzyme, H-Ala-Pro-pNA emits colorimetric changes that are detectable with absorbances at 690 nm subtracted from absorbances at 405 nm to increase the specificity of measurements (Abbott et al., 1999). Assays were carried out in triplicate in 96 well plates. The H-Ala-Pro-pNA substrate was dissolved in 10 μL methanol prior to being diluted to a final concentration of 2 mM in 0.1 M sodium phosphate buffer at pH 7.6 with 0.2% Tween-20 to permeabilize the cells. DPP

cleavage of H-Ala-Pro-pNA was measured using 1×10^3 cells and 40 μL of 0.1 M sodium phosphate buffer. Fifty μL of 2 mM substrate was added just prior to enzyme activity reading to achieve a final substrate concentration of 1 mM.

Total activity for the DPP enzyme assay was calculated using the Beer-Lambert law (A=%LC) where A is the optical density (OD), L is the optical path length in cm and C is the concentration. An extinction coefficient of 9.45 $mM^{-1}.cm^{-1}$ was used for pNA and a path length of 0.26 cm for a 100 μL volume in a 96 well plate was used for all reactions. Pathlengths were taken from Sulda, 2009 and were originally determined by comparing the absorbance of BSA (Bovine Serum Albumin) standards in 96-well plate format and standard 1 cm cuvettes (Sulda, 2009). Specific activity was determined by dividing the total activity by the protein concentration of the sample (in mg) measured via Pierce BCA (Thermo Scientific, Melbourne, Australia) using BSA (Bovine Serum Albumin) to create a standard curve (O'callaghan, 2018).

2.2.7 Determination of ATP, ADP and AMP concentrations by HPLC

High performance liquid chromatography (HPLC) was used to determine levels of adenosine triphosphate (ATP), adenosine diphosphate (ADP) and adenosine monophosphate (AMP) in Jurkat and THP-1 cells treated with sitagliptin and metformin and AMP to ATP ratio was determined. Methods for HPLC determination of ATP, ADP and AMP were adapted from Liu et al., (2006) (Liu et al., 2006).

Cells were lysed using 0.6 M perchloric acid solution, 8.57 mL of 70% (w/w) solution perchloric acid added to 91.43 mL deionised water. Cells were treated as outlined in section 2.2.3 and then pelleted via centrifugation at 1500 g for five min and washed twice with ice cold PBS with centrifugation at 1500 g for 5 min after each wash. The cell pellet was resuspended in 0.5 mL of ice-cold 0.6 M perchloric acid, vortexed briefly and then incubated on ice for 10 min prior to centrifugation at 1500 g for 10 min at 4^0C. Three hundred μL of supernatant was added to 300 μL of 8 mM potassium phosphate buffer (pH 7.0) and centrifuged at 1500 g for 10 min at 4^0C, the resulting supernatant was used for HPLC analysis.

ATP, ADP and AMP standards (1 mg) were dissolved in 10 mL of deionized water to a concentration of 100 mg/mL. To produce a standard curve for HPLC analysis, dilutions of 0, 0.2, 0.5, 1, 2 and 4 mg/mL were created using deionized water.

Two mobile phases were used for analysis, mobile phase A (A) consisted of 0.06 mol/L dipotassium hydrogen phosphate (K_2HPO_4) and 0.04 mol/L potassium dihydrogen

phosphate (KH$_2$PO$_4$) dissolved in deionized water and adjusted to pH 7.0 with 0.1 mol/L potassium hydroxide, and mobile phase B (B) which consisted of 100% acetonitrile. Air bubbles in both mobile phase solutions were removed prior to use via sonication for 20 min in an ultrasonic bath sonicator.

HPLC analysis was conducted at Flinders Analytic by Dr Daniel Jardine using a C18 250 x 4.60 mm column with peaks detected at 254 nm. HPLC separation was completed using continuous gradient elution: 0 min 100% A, 0% B; 2 min 95% A, 5% B; 4 min 80% A, 20% B; 5.3 min 75% A, 25% B and 6 min 100% A, 0% B. The flow rate for the mobile phase was 1.2 mL/min and total retention time was approximately five min. The retention time of ATP, ADP and AMP standards were used to identify their corresponding peaks within the samples. The total concentration of ATP, ADP and AMP was determined using a standard curve of the know concentration dilutions. Replicate sets of three were repeated in three individual analysis.

2.2.8 Western blotting for determination of protein levels

Protein samples (25 µg) were mixed with three x sample buffer (93 mM Tris-HCl pH 6.8, 3% (w/v) SDS, 7.5% 2-ß mercaptoethanol, 0.015% bromophenol blue, and 37.5% glycerol) and boiled at 100ºC for 5 min in a dry block heater (Thermoline, Australia). Samples as well as protein marker were loaded on to 10% SDS-PAGE gel (1.5 mM Tris pH 8.8, 30% (w/v) Polyacrylamide, 3.3% 29:1 Acrylamide:N,N´-Methylene-bis Acrylamide (Bio-Rad Laboratories, NSW, Australia), 10% (w/v) SDS, 0.5% (v/v) Tetramethylethylenediamine (TEMED) and 10% (w/v) Ammonium Persulphate). The gel was immersed in running buffer (192 mM glycine, 25 mM Tris, and 0.1% SDS pH 8.3) and run using a Mini-Protean® II electrophoresis system (Bio-Rad Laboratories, NSW, Australia) at 170 V, 400 mA for 60 min.

The separated proteins were transferred from the SDS-PAGE gel to Hybond-P PVDF membrane (GE Healthcare, Buckinghamshire, UK) using a semidry transfer method. Prior to transfer the PVDF membrane was soaked in 100% methanol for five min, rinsed briefly with water and equilibrated in transfer buffer (25 mM Tris and 192 mM Glycine and 10% (v/v) methanol) along with three pieces of 3 mm Whatmann chromatography filter paper. The wetted filter paper was placed on the tray of the transfer apparatus followed by PVDF membrane, the SDS-PAGE gel, and three more pieces of filter paper on the top. The sandwich transfer was run in a Trans-Blot®Turbo™ transfer system from Bio-Rad at 25 V, 1 A for 30 min. The membrane was the incubated in blocking buffer (25 mM Tris, 0.1% (v/v) Tween-20 and 5% (w/v) skim milk powder) for 60 min at RT with shaking using an orbital shaker.

Table 2.1. Primary and secondary antibodies used for Western blotting

Antibody	Source	Dilution
Primary antibodies		
AMPKα (Rabbit polyclonal anti human)	Cell Signalling Technology (Danver, MA, USA)	1:2,000
Phospho-AMPK (Thr172) (Rabbit polyclonal anti human)	Cell Signalling Technology (Danver, MA, USA)	1:1,000
DPP4 (Mouse polyclonal)	AbD Serotec (Raleigh, NC, USA)	1:500
RP1- DPP8 (Rabbit polyclonal anti human)	Triple Point Biologics Inc (Forest Grove, OR, USA)	1:5,000
RP1-DPP9 (Rabbit polyclonal anti human)	Triple Point Biologics (Forest Grove, OR, USA)	1:5,000
ß-Actin (Mouse monoclonal anti human)	Sigma-Aldrich (NSW, Australia).	1:10,000
Secondary antibodies		
Donkey anti goat IgG HRP	Santa Cruz Biotechnology (Dallas, TX, USA)	1:10,000
Swine anti rabbit IgG HRP	Dako|Agilent (Santa Clara, CA, UAS)	1:10,000

Once blocked the membrane was rinsed with washing buffer (25 mM Tris and 0.1% (v/v) Tween-20) and then incubated with diluted primary antibody in blocking buffer, primary antibodies and dilutions used are outlined in Table 2.1. Incubation was performed overnight at 4ºC with shaking. Unbound antibody was removed using washing buffer with three washes of 10 min conducted at RT with shaking. To detect the antigen-antibody binding complex, the membrane was incubated for 60 min at RT with secondary antibody chosen based on the host of primary, secondary antibodies and dilutions used are outlined in Table 2.1. As with the primary antibody, unbound secondary antibody was removed with three washes of washing buffer for 10 min with shaking. The washed membrane was then exposed to the substrate solution (Amersham ECL Western blotting detection reagent from GE Healthcare) for five min at RT with shaking. After five min any excess substrate solution not bound to the HRP, was removed by tapping on tissue paper. The ChemiDoc™ imaging system (Biorad) was used to image signals resulting from enzymatic reaction between protein targets and their antibodies. Exposure time began at one second up to 1200 seconds and the resulting image of protein bands was quantified using the Image lab™ software package program from Bio-Rad. Image quantification was presented in volume pixel

intensity per mm^2 area and bands were normalised to β-Actin at dilutions outlined in Table 2.1.

2.3 Results

In this study we used immune cells in conjunction with the Seahorse XF Extracellular Flux Analyser to study the bioenergetic metabolism of cultured cells. The similarity between the inflammatory milieu and the tumour microenvironment produces equivalences in the metabolic actions of immortalised immune and malignant cells that is relevant for this type of analysis (Pelletier et al., 2014). Immune cells reflect the metabolic behaviour of malignant cells where their metabolic processes are not subject to external energy demand as fast metabolic response is required to adapt to changing microenvironmental conditions (Jacobs et al., 2008; Rathmell et al., 2003). This similarity in metabolic actions and the ability to produce the large cell numbers required for extracellular flux analysis resulted in the selection of immortalised immune cell lines Jurkat and THP-1 for this bioenergetic analysis.

2.3.1 Optimisation for XF Extracellular Flux bioenergetic analysis

2.3.1.1 Jurkat optimisation

For this work optimisation was undertaken prior to performing bioenergetic analysis using the Extracellular Flux Analyzer. This included titration of cell seeding density and ETC modulators to determine optimal nontoxic experimental conditions for accurate analysis. Optimal seeding density varies dependent on cell type, a general guide of cell density of 1 x 10^5 cells per well for Jurkat cells is reported by Agilent as part of a detailed protocol for this assay (Agilent Technologies, 2019a).

Comparison of the differing cell densities in Jurkat cells indicated that 1 x 10^5 cells per well is the optimal density for XFe analysis. A cell density of 1 x 10^5 cells per well (Figure 2.1) gave the lowest basal OCR reading of all three densities that was less than the overall maximal capacity at the higher FCCP concentration, visual analysis of the cells at this density also confirmed that the cells gave a healthy and consistent monolayer and were evenly distributed in the Cell-Tak without evidence of overcrowding after incubation time had elapsed (Plitzko and Loesgen, 2018). A cell density of 1.5 x 10^5 cells per well (Figure 2.2) showed a similar basal to maximal OCR comparison as 1 x 10^5 cells per well, but visual analysis indicated the presence of overcrowding after the incubation time had elapsed which may provide inconsistent results. A cell density of 2 x 10^5 cells per well (Figure 2.3) presented with extremely high basal OCR that showed negative or no comparable difference
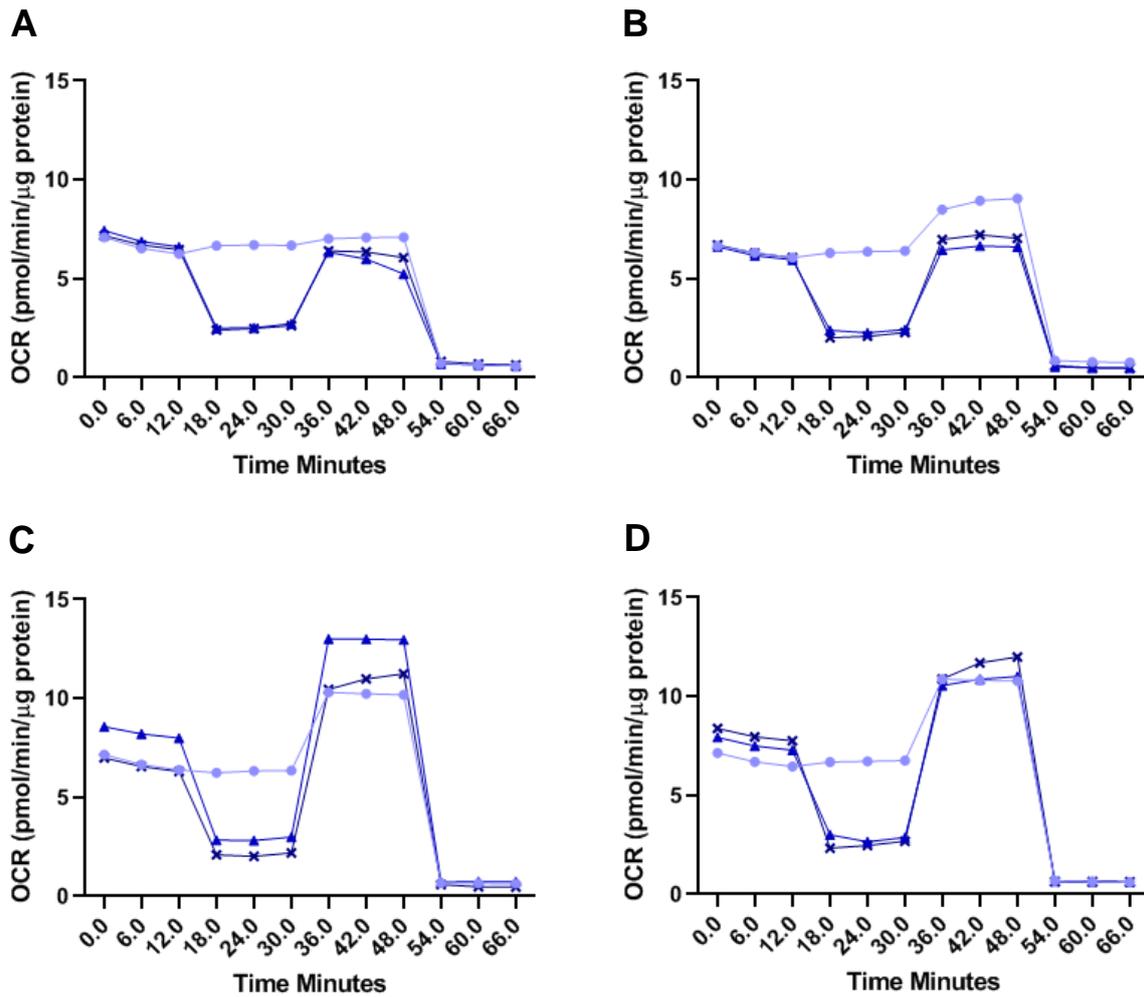
Figure 2.1. Jurkat cell optimisation for mitochondrial stress test with 1×10^5 cells per well. XFe assay run using concentrations of ●─0.5, ▲─1.0 and ✳─2.0 μM oligomycin A, with A) 0.2 μM, B) 0.4 μM, C) 0.8 μM, and D) 1.2 μM FCCP. Results taken from five replicates across two independent experiments (n=2).
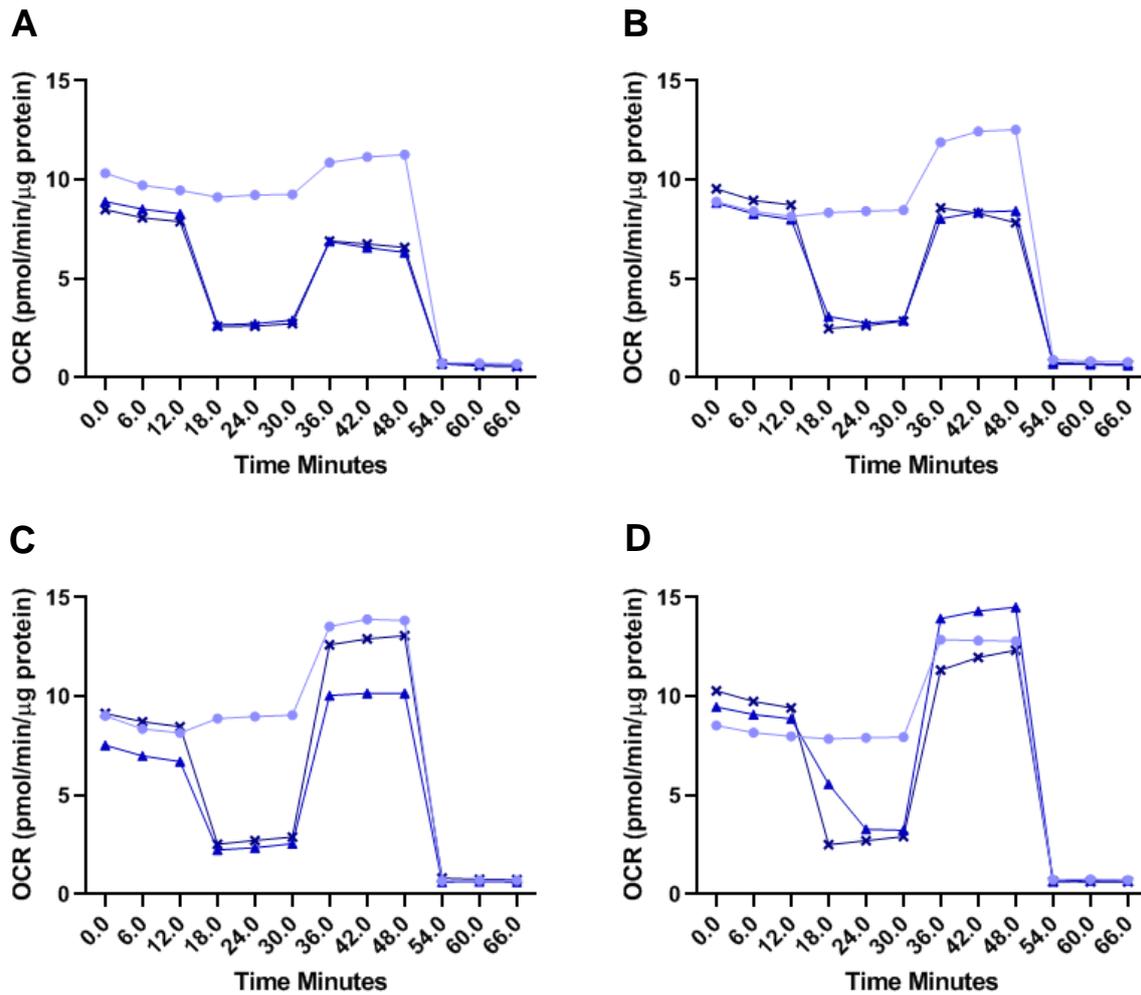
Figure 2.2. Jurkat cell optimisation for mitochondrial stress test with 1.5 x 10^5 cells per well. XFe assay run using concentrations of ●0.5, ▲1.0 and ✱2.0 µM oligomycin A, with A) 0.2 µM, B) 0.4 µM, C) 0.8 µM, and D) 1.2 µM FCCP. Results taken from five replicates across two independent experiments (n=2).
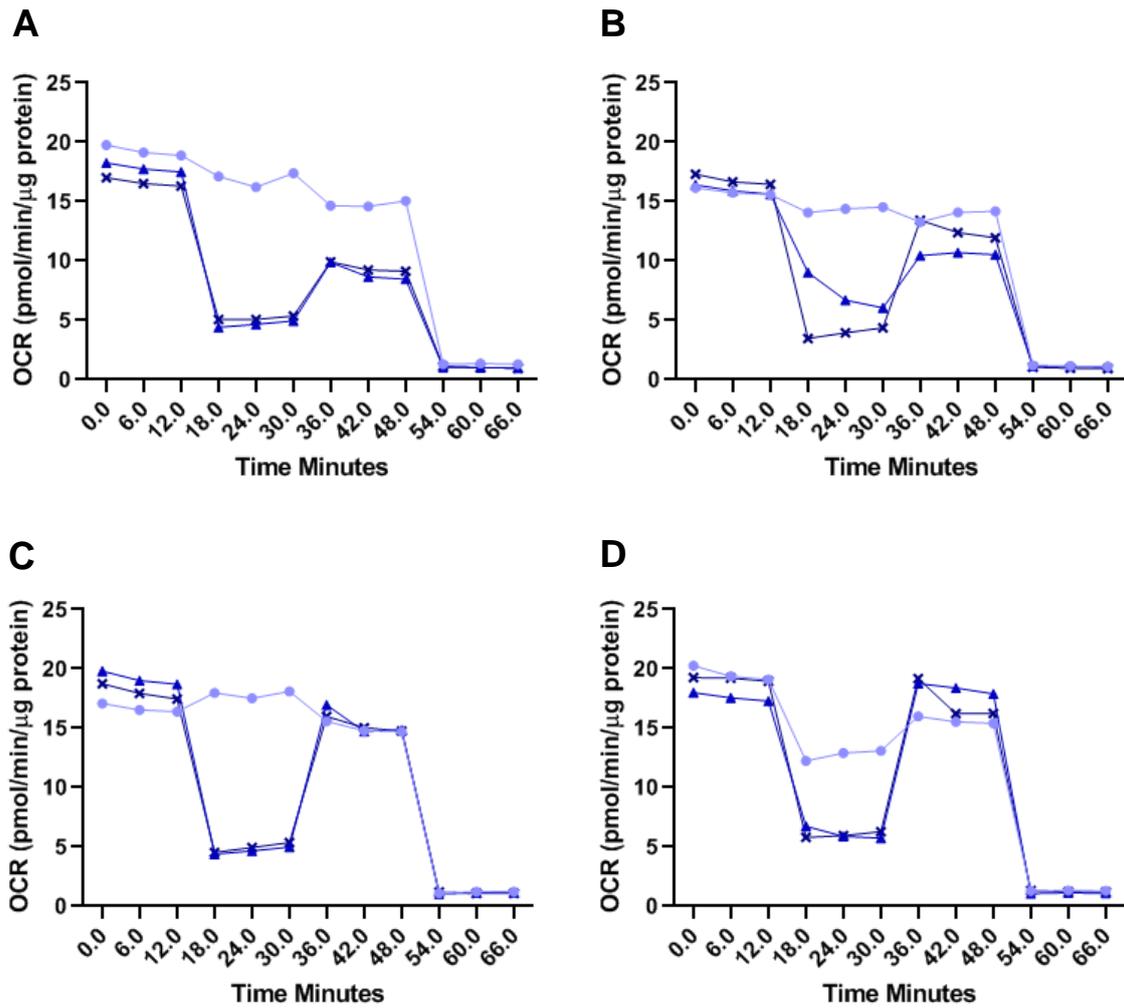
Figure 2.3. Jurkat cell optimisation for mitochondrial stress test with 2 x 10^5 cells per well. XFe assay run using concentrations of ●0.5, ▲1.0 and ✕2.0 μM oligomycin A, with A) 0.2 μM, B) 0.4 μM, C) 0.8 μM, and D) 1.2 μM FCCP. Results taken from five replicates across two independent experiments (n=2).
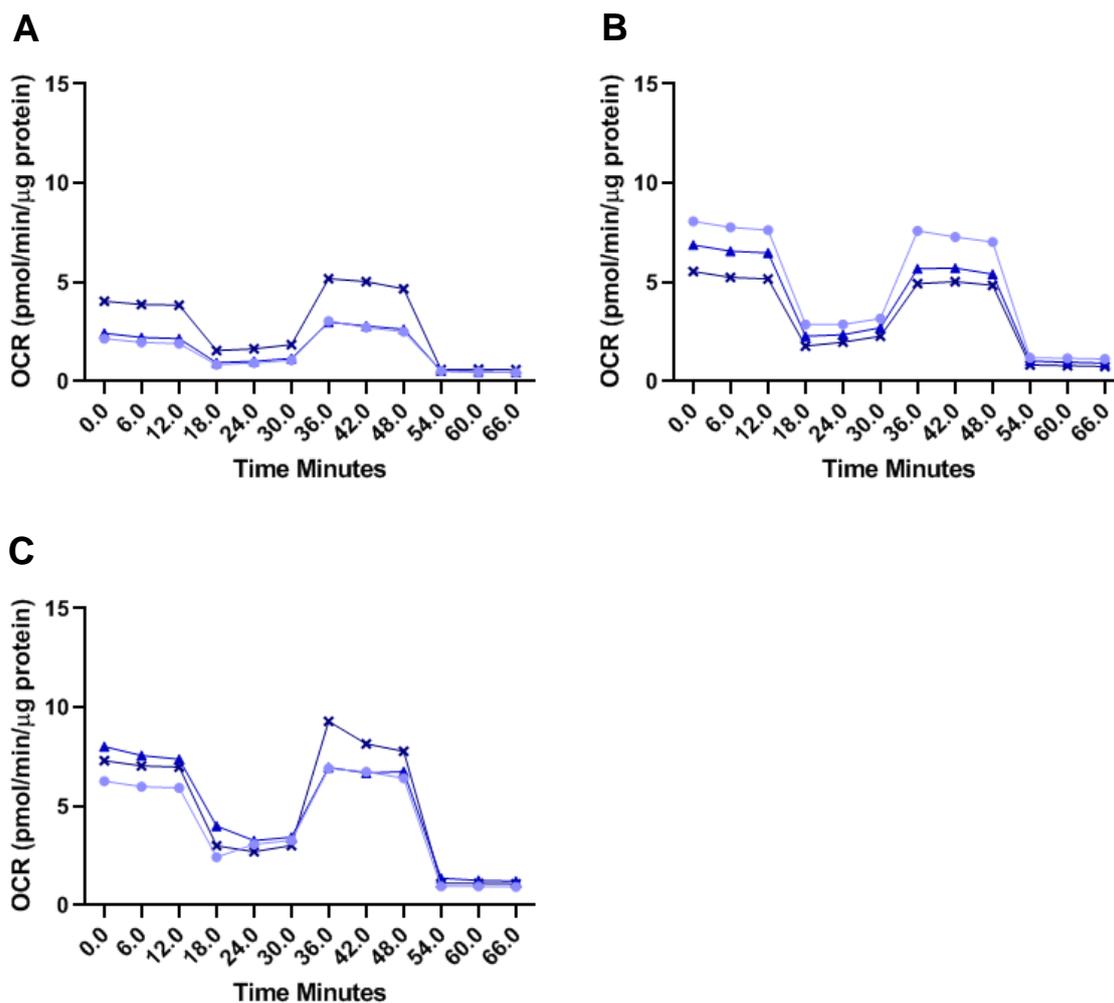
Figure 2.4. THP-1 cell optimisation assays for mitochondrial stress test. XFe assay run using, 1.0 μM oligomycin A, with, 0.8, 1.2 and 2.0 μM FCCP concentration, on A) 1×10^5, B) 1.5×10^5 and C) 2×10^5 cells per well. Results taken from five replicates across two independent experiments (n=2).

to the maximal respiration capacity of the cell. Based on these optimisation results a cell density of 1 x 10^5 Jurkat cells per well was chosen for further analysis.

Optimisation of oligomycin A showed that a concentration of 0.5 µM was too low to provide complete inhibition of the ETC complex V, while basal OCR was comparable to OCR in the presence of oligomycin A at this concentration meaning quantification of basal ATP production via oxidative phosphorylation could not be determined (Figure 2.1). An oligomycin A concentration of 1.0 µM gave consistent reduction of OCR comparable to complete inhibition of complex V which was confirmed by the results for 2.0 µM oligomycin A where the increase in inhibitor concentration did not produce any significant decrease in OCR (Figure 2.1). From the optimisation results 1.0 µM oligomycin A was chosen as the optimum concentration to provide complete inhibition of ETC complex V.

For Jurkat cells FCCP at 0.2 and 0.4 µM gave OCR levels that were comparable to basal OCR for all cell densities this indicates incomplete disruption of the proton gradient meaning the resulting OCR measurement at these lower FCCP concentrations will not be a true reflection of the maximal respiration capacity of the cells. While FCCP at a concentration of 0.8 and 1.2 µM provided maximal respiration OCR values that were above basal OCR indicating disruption of the mitochondrial proton gradient and a resulting increase in oxidative phosphorylation. The FCCP concentrations for optimisation were chosen based on information provided by Agilent (Agilent Technologies, 2019a), it was noted in work from other groups using the Seahorse XFe Extracellular Flux Analyser on lymphocytes that higher concentrations of FCCP were used (Berster and Göke, 2008; Pelletier *et al.*, 2014; van der Windt, Chang and Pearce, 2016). To determine if a 1.2 µM concentration of FCCP was the optimal to use for this analysis, concentrations were adjusted for THP-1 optimisation to include FCCP at 0.8, 1.2 and 2.0 µM.

2.3.1.2 THP-1 cell optimisation

Optimisation of THP-1 cell density (Figure 2.4) showed similar results to that seen for Jurkat cells, 1 x 10^5 cells per well gave the lowest basal OCR reading of all three densities and a basal OCR that was less than the overall maximal capacity at the higher FCCP concentration. Visual analysis of the cells confirmed that like Jurkat cells, THP-1 cells at this density have a healthy and consistent monolayer that was evenly distributed in the Cell-Tak without evidence of overcrowding after incubation time had elapsed (Plitzko and Loesgen, 2018). THP-1 cells at a density of 1.5 x 10^5 and 2 x 10^5 cells per well (Figure 2.4) gave extremely high basal OCR that showed negative or no comparable difference to the maximal

respiration capacity of the cell. Based on these optimisation results a cell density for THP-1 cells of 1 x 10^5 cell per well was chosen for further analysis.

Based on oligomycin A optimisation results that were consistent with both published Agilent protocols (www.agilent.com) and work from other groups using the Seahorse XF Extracellular Flux Analyser with lymphocytes, a working concentration of 1.0 µM oligomycin A was chosen for all subsequent mitochondrial stress test analysis, further optimisation of oligomycin A was not undertaken on THP-1 cells (Pelletier et al., 2014; van der Windt et al., 2016). The 0.8 and 1.2 µM FCCP concentrations gave a maximal respiration OCR reading that was slightly higher than basal OCR with no discernible difference in maximal respiration OCR seen between the two concentrations. FCCP at a concentration of 2.0 µM on THP-1 cells, gave a maximal respiration OCR that was well above basal OCR and provided the expected mitochondrial stress test profile (appendix Figure A.1). Based on these results FCCP at a concentration of 2.0 µM was determined to be the optimum concentration to be used for further analysis (Agilent Technologies, 2019b).

2.3.2 Enzyme inhibition and cellular proliferation analysis

For this work sitagliptin was used at a concentration of 0.04 µM, this concentration was chosen based on an approximate doubling of the reported IC50 for sitagliptin of 0.018 µM and is within range of plasma concentration seen following the usual dose range of 25 to100 mg in healthy adults (Kim et al., 2005; Merck Sharp & Dohme Corp., 2015; Thornberry and Weber, 2007). The concentration of metformin determined as optimum for this analysis was 500 µM, this is the concentration of metformin required for inhibition of the respiratory chain complex 1 and associated increase in AMPK activation (He and Wondisford, 2015).

Metformin and sitagliptin are both identified as potential AMPK activators (DeCensi et al., 2010; Quinn et al., 2013; Singh et al., 2017; Zeng et al., 2014). As AMPK activation is a modulator for cellular growth and survival the effect of 0.04 µM sitagliptin and 500 µM metformin on cellular proliferation was assessed in Jurkat cells over a six hr treatment timeline (Figure 2.5, A & B)(Zhang et al., 2019). This treatment timeline was chosen to mimic the timeline of a maximal plasma concentration after a single dose of sitagliptin (2-6 hr) and metformin (3 hr) and was also within the single dose half-life for sitagliptin (9-14 hr) (Herman et al., 2011; Robert et al., 2003). Sitagliptin at 0.04 µM showed a 1.2-fold decrease in cell number at the three hr time point. Cell number was static in this treatment group between the three and four hr time points with gradual recovery of cell number up to that seen for non-treated cells between the five and six hr time points (Figure 2.5, A). Metformin at 500 µM showed a 1.1-fold decrease in cell number at the two and three hr time points that

A

B

C
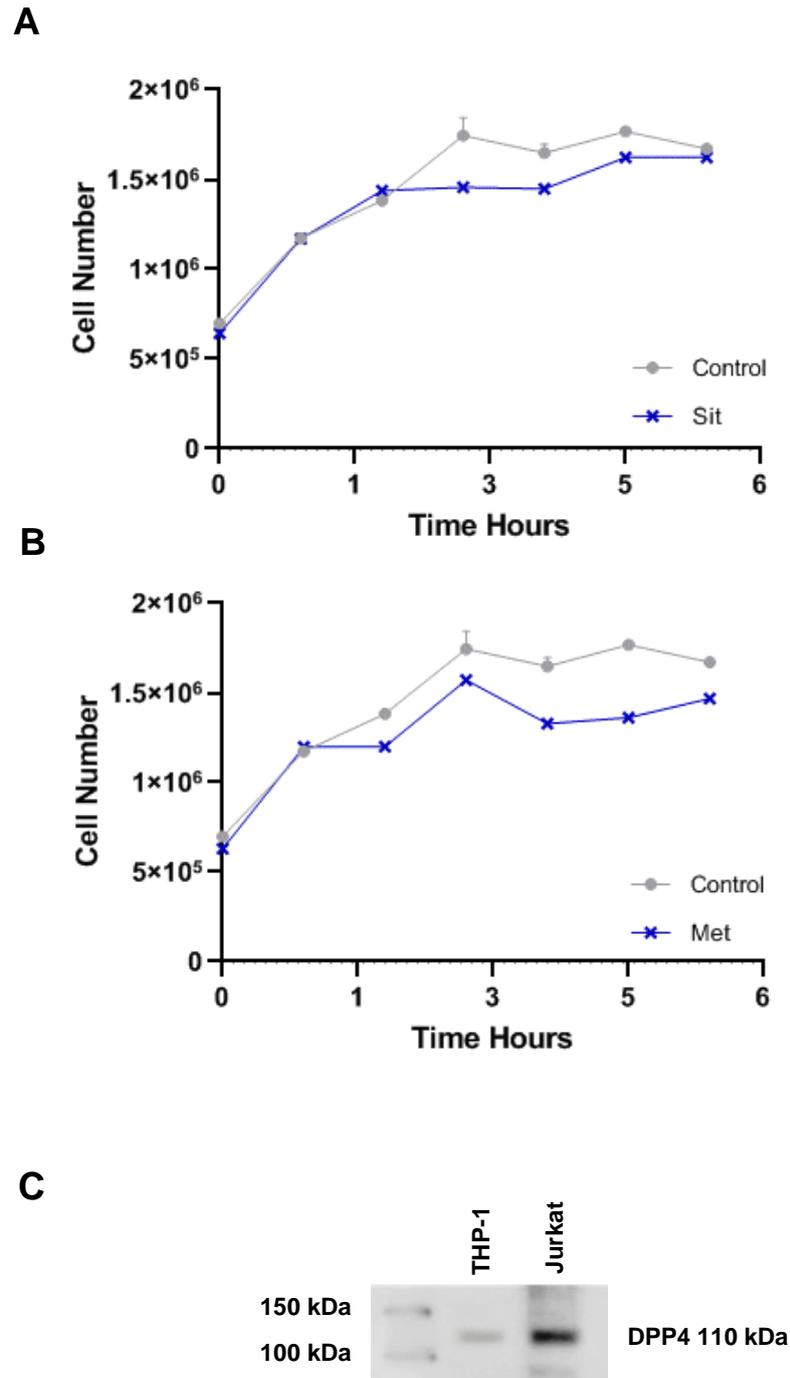
Figure 2.5. Jurkat cells treated with sitagliptin and metformin show reduced cellular proliferation. Cell number determined via resazurin reduction over 6 hr in Jurkat cells treated with, A) 0.04 µM sitagliptin and B) 500 µM metformin. Results taken as three replicates across three independent experiments (n=3). C) Western blot for DPP4 protein in THP-1 and Jurkat cells, DPP4 detected via DPP4 mouse polyclonal antibody (AbD Serotec).

increased to a 1.3-fold decrease in cell number by the five hr with gradual recovery of cell number towards that seen for non-treated cells between the five and six hr time points (Figure 2.5, B). Cellular proliferation analysis on Jurkat cells treated with sitagliptin and metformin confirms that both compounds are effectors of cellular growth with maximal effect on cell number seen after three to five hr of treatment and recovery of cell number after six hr. Based on these results a treatment timeline for bioenergetic analysis via the XFe analyser was determined with two treatment periods of four and six hr with either 0.04 µM sitagliptin or 500 µM metformin to be conducted on both cell populations. Western blot analysis of Jurkat and THP-1 cells was undertaken to confirm DPP4 protein was present for targeting by sitagliptin in these cell lines. Jurkat cells were identified as having a higher expression of a 110 kDa DPP4 monomer protein than THP-1 (Figure 2.5, C).

2.3.3 The bioenergetic profile of Jurkat cells

Analysis of the bioenergetic profiles of Jurkat cells indicates a high reliance on mitochondrial respiration for cellular energy as evident by the large mitochondrial spare capacity seen in untreated cells (Figure 2.6, F). Jurkat cells have a lower level of basal glycolysis signifying that the aerobic glycolysis model of cancer cell metabolism is not used by this cell type although a glycolytic spare capacity is evident in these cells (Figure 2.7, D), signifying an ability to use an increase in both glycolysis and oxidative phosphorylation to respond to heightened cellular energy demands.

2.3.3.1 Sitagliptin reduces mitochondrial respiration and glycolysis in Jurkat cells

Sitagliptin significantly reduces both oxidative phosphorylation and glycolysis in Jurkat cells after four hr treatment with some recovery of mitochondrial and glycolytic energy production seen after six hr treatment. Jurkat cells treated with 0.04 µM sitagliptin for four hr consume very little oxygen and have a low basal OCR of 0.7 ± 0.2 which is significantly lower than cells only ($p < 0.001$). This is equivalent to a 90% reduction in basal oxygen consumption when compared to untreated cells (Figure 2.6, A & C). Addition of oligomycin A reduced this low basal OCR to zero indicating that the basal oxygen consumption for these cells is associated solely with mitochondrial production of ATP (Figure 2.6, A). Subsequent addition of FCCP did not cause any increase in oxygen consumption, indicating an absence of spare capacity and an inability to increase mitochondrial energy production to address increased energy demands (Figure 2.6, F).

Reflective of the results seen with oxidative phosphorylation, treatment of Jurkat cells with sitagliptin reduces glycolysis and eliminates the glycolytic reserve. After four hr of treatment
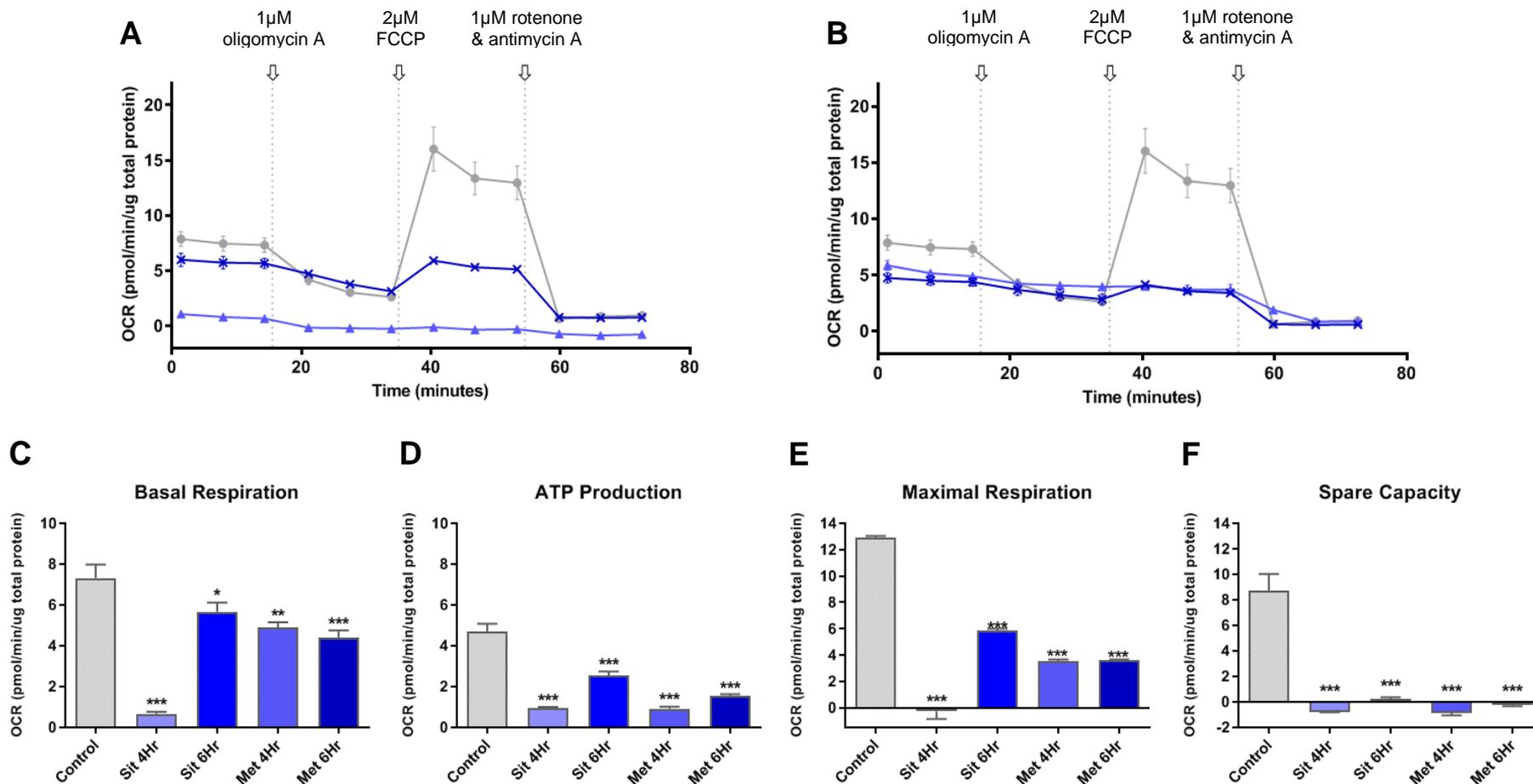
Figure 2.6. Sitagliptin and metformin reduce mitochondrial respiration in Jurkat cells. Oxygen consumption profiles determined using XFe analysis of Jurkat cells treated with, A) 0.04 µM sitagliptin, and B) 500 µM metoformin for ▲ four, ✖ six hr, and ● untreated controls. Individual mitochondrial respiratory parameters derived from XFe analysis including C) basal respiration, D) ATP production, E) maximal respiration and F) spare capacity. Results taken across three independent experiments (n=3), all treatment groups are compared to control by ANOVA: $P \leq 0.05$ (*), $P \leq 0.01$ (**) and $P \leq 0.005$ (***). Values represent means and error bars ± standard error (SEM).
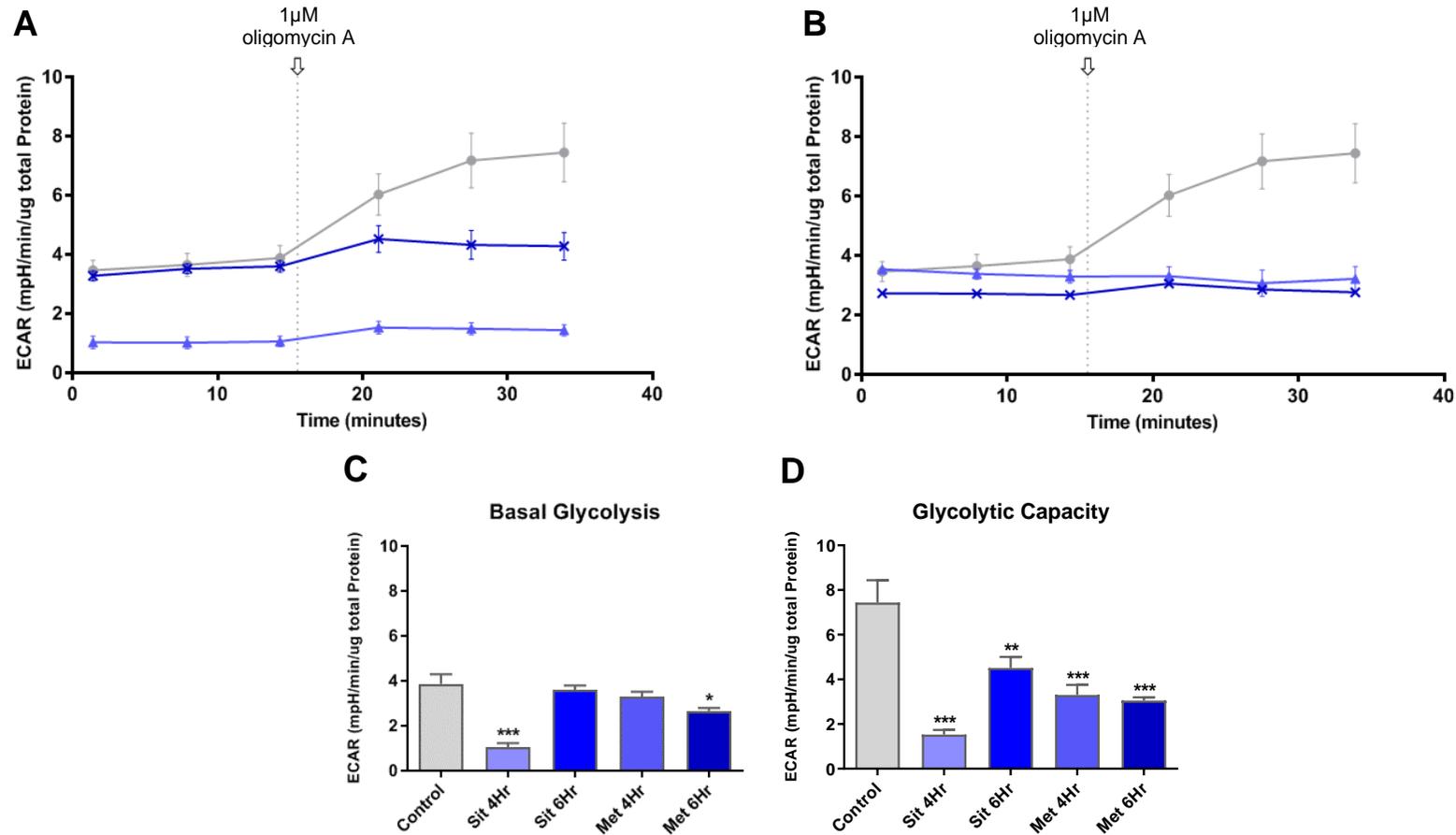
Figure 2.7. Sitagliptin and metformin reduce glycolysis in Jurkat cells. Glycolytic profiles determined using XFe analysis of Jurkat cells treated with A) 0.04 µM sitagliptin or B) 500 µM metformin for ▲four. ✕ six hr, and ● untreated controls. Individual glycolytic parameters derived from XFe analysis including, C) basal glycolytic activity and D) glycolytic capacity. Results taken across three independent experiments (n=3), all treatment groups are compared to control by ANOVA: $P \leq 0.05$ (*), $P \leq 0.01$ (**) and $P \leq 0.005$ (***). Values represent means and error bars ± standard error (SEM).

with 0.04 µM sitagliptin, Jurkat cells had a significant (p<0.001), 70% reduction in glycolysis compared to untreated cells (Figure 2.7, A & C). Also notable at this treatment time point is the 78% reduction in glycolytic capacity when compared to untreated cells. The maximal glycolytic rate after four hr of sitagliptin treatment produces an ECAR of 1.5 ± 0.4 this is only, 0.5 mpH per min per microgram of protein, higher than the basal glycolytic rate at this treatment time point and is significantly (p<0.001) reduced from the maximal glycolytic ECAR of 7.4 ± 2.0 seen for untreated cells, indicating that in addition to lacking mitochondrial spare capacity, Jurkat cells also have an inability to increase glycolytic production to meet heightened energy demands after four hr of sitagliptin treatment (Figure 2.7, D).

After six hr of treatment with 0.04 µM sitagliptin, Jurkat cells show some recovery of both oxidative phosphorylation and glycolysis when compared to results from the four hr treatment time point. Basal OCR after six hr was 5.7 ± 0.9 (Figure 2.6, C), this was much higher than the OCR of 0.7 ± 0.2 seen after four hr of treatment but still showed a significant (p<0.05) 20% reduction of OCR when compared to untreated cells. Jurkat cells at this treatment time point also show an increased response to the addition of oligomycin A and FCCP but with a maximal respiration that is equivalent to basal oxygen consumption indicating the cells still have no spare capacity to address increased energy needs via oxidative phosphorylation (Figure 2.6, F). Reflective of results seen for oxidative phosphorylation, Jurkat cells after six hr of sitagliptin treatment show recovery of basal glycolysis and have a basal ECAR that is comparable to that seen in untreated cells (Figure 2.7, A & C). The glycolytic capacity of the cells is still significantly (p<0.01) reduced at this treatment time point when compared to untreated cells indicating that the cells have an impaired ability to rely on glycolysis for increased cellular energy (Figure 2.7, D). Six hr treatment Jurkat cells overcome the suppressive actions of sitagliptin on basal oxidative phosphorylation and glycolysis but do not recover the ability to increase cellular ATP production beyond that of the basal energy needs of the cell. These results correspond to those seen for cellular proliferation where after six hr treatment with sitagliptin cell numbers are shown to recover and begin to reflect cell numbers comparative to that seen in untreated cell culture (Figure 2.5, A).

2.3.3.2 Metformin reduces mitochondrial respiration and glycolysis in Jurkat cells

Commensurate of results seen with sitagliptin, metformin reduces both the oxidative phosphorylation and glycolytic energy pathways in Jurkat cells. After 500 µM metformin treatment for four hr, Jurkat cells showed a significant (p<0.01) 30% reduction in basal

oxygen consumption and a significant ($p<0.001$) 80% reduction in basal ATP production, with comparative results shown at the six hr treatment time point (Figure 2.6, B, C & D). Addition of oligomycin A after metformin treatment did not cause the expected drop in oxygen consumption and instead produced a slow decline in OCR over the three subsequent readings with a low OCR of 0.9 ± 1.9 attributed to ATP production after 4 hr treatment and 1.5 ± 0.2 after six hr of treatment, indicating that most of this basal OCR is not connected with mitochondrial energy production (Figure 2.6, B). In addition, the presence of the proton uncoupler FCCP did not cause any increase in oxygen consumption beyond basal OCR at both treatment time points indicating that the cells have no spare capacity or ability to increase mitochondrial energy production to address heightened energy demands (Figure 2.6, E).

Metformin in Jurkat cells only had minimal effect on basal glycolysis but produced a similar inhibitory effect on glycolytic capacity as sitagliptin treatment. No significant reduction in basal glycolytic rate was seen after four hr metformin treatment but a significant ($p<0.05$) 30% reduction was seen after six hr (Figure 2.7, B). Although the effect on basal glycolysis in Jurkat cells was minimal, glycolytic capacity was significantly ($p<0.001$) reduced by 60% at both treatment time points, this reduction in the maximal glycolytic rate was much greater than the overall reduction in basal glycolysis resulting in elimination of the glycolytic reserve (Figure 2.7, D). The overall profile for ECAR in Jurkat cells treated with metformin is quite similar at both the four and six hr treatment time point with the main difference being the greater reduction in basal glycolysis after six hr treatment, this indicates that the effect of metformin on glycolysis is not overcome by the cells and instead strengthens with treatment time up to six hr (Figure 2.7, D).

2.3.4 The bioenergetic profile of THP-1 cells

THP-1 cells present with a bioenergetic profile that is more metabolic than Jurkat cells with a high reliance on glycolysis for cellular energy demands. Untreated THP-1 cells show a low basal oxygen consumption rate and a very low maximal respiration that is only slightly increased from the basal OCR resulting in a low spare capacity indicating very little ability to use mitochondrial respiration to respond to increasing energy demands (Figure 2.6). THP-1 cells additionally show an increased reliance on glycolysis for cellular energy with a high basal ECAR and large maximal glycolytic capacity, this high glycolytic capacity coupled with the diminished mitochondrial respiration indicates the use of the aerobic glycolysis as the preferred energy pathway in this cell type (Figure 2.7).
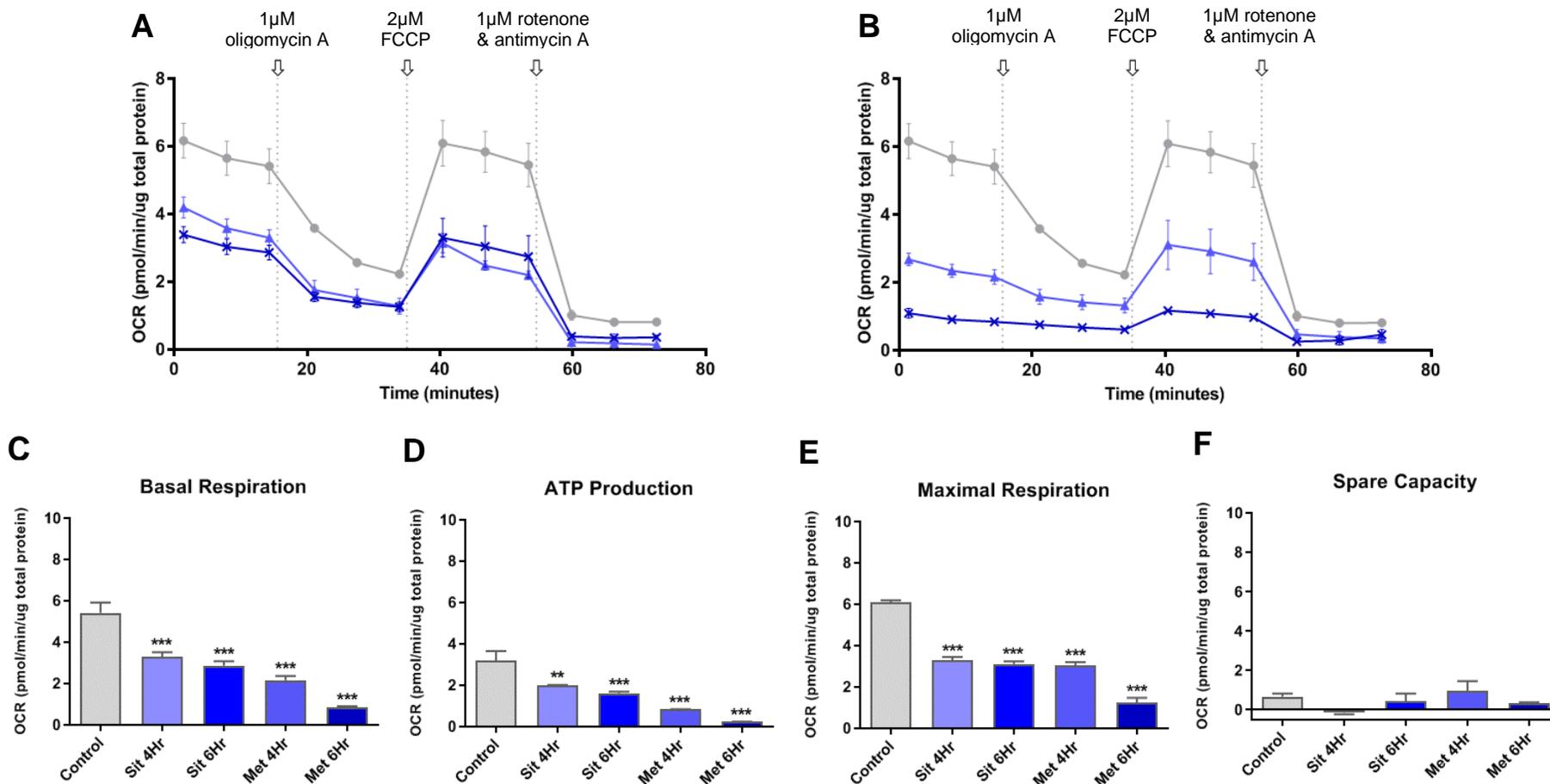
Figure 2.8. Sitagliptin and metformin reduce mitochondrial respiration in THP-1 cells. Oxygen consumption profiles determined using XFe analysis of THP-1 cells treated with, A) 0.04 µM sitagliptin, and B) 500 µM metformin for ▲ four, ✕ six hr, and ● untreated controls. Individual mitochondrial respiratory parameters derived from XFe analysis including C) basal respiration, D) ATP production, E) maximal respiration and F) spare capacity. Results taken across three independent experiments (n=3), all treatment groups are compared to control by ANOVA P ≤ 0.01 (**) and P ≤ 0.005 (***). Values represent means and error bars ± standard error (SEM).
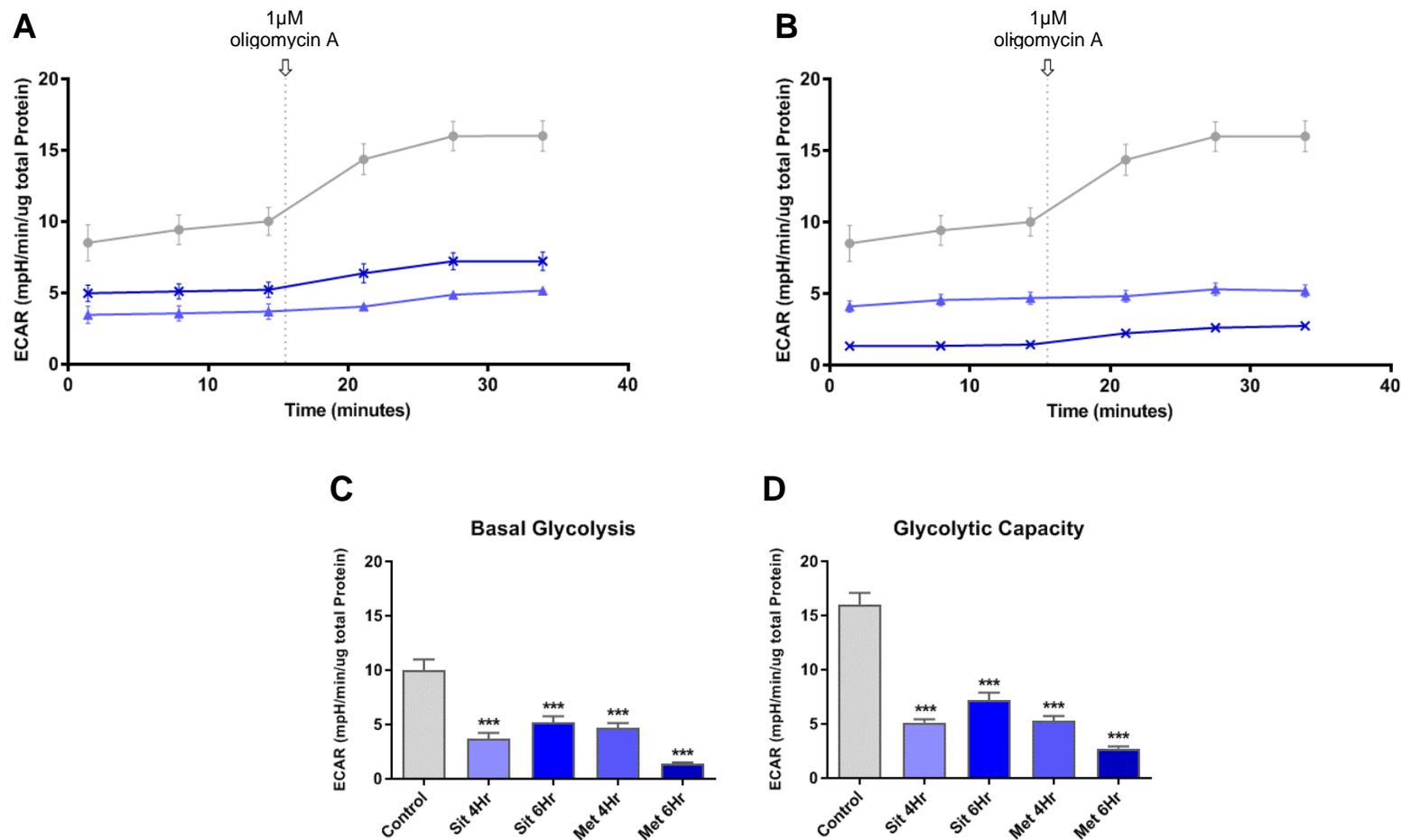
Figure 2.9. Sitagliptin and metformin reduce glycolysis in THP-1 cells. Glycolytic profiles determined using XFe analysis of THP-1 cells treated with A) 0.04 µM sitagliptin or B) 500 µM metformin for ▲ four, ✳ six hr and ● untreated controls. Individual glycolytic parameters derived from XFe analysis including, C) basal glycolytic activity and D) glycolytic capacity. Results taken across three independent experiments (n=3), all treatment groups are compared to control by ANOVA $P \leq 0.005$ (***). Values represent means and error bars ± standard error (SEM).

2.3.4.1 Sitagliptin reduces mitochondrial respiration and glycolysis in THP-1 cells

Sitagliptin is shown to significantly reduce oxidative phosphorylation and glycolysis in THP-1 cells. Treatment of THP-1 cells with 0.04 µM sitagliptin for four hr resulted in a significant 40% decrease in basal OCR ($p<0.001$), basal ATP production ($p<0.01$) and maximal respiration ($p<0.001$) when compared to untreated cells, with a similar 50% ($p<0.001$) reduction in these measurable parameters seen after six hr treatment (Figure 2.8, A, C, D & E). Untreated THP-1 cells show a very minimal spare capacity and an associated inability to increase ATP production via oxidative phosphorylation. After sitagliptin treatment for four and six hr, the reduction in maximal respiration reflected the reduction in basal oxygen consumption resulting in no significant improvement or reduction to the small spare respiratory capacity shown in untreated THP-1 cells (Figure 2.8, D).

Sitagliptin reduced basal glycolysis and abolished the large glycolytic reserve seen in untreated THP-1 cells. Treatment with 0.04 µM sitagliptin resulted in a significant ($p<0.001$) 65% reduction in basal glycolysis and maximal glycolytic rate after four hr and a significant ($p<0.001$) 50% reduction in these parameters after six hr (Figure 2.9, A, C & D). Sitagliptin treatment at both time points also reduced the difference between the basal glycolytic rate and the maximal glycolytic capacity of the cells. Untreated THP-1 cells show a maximal glycolytic ECAR value that is 5.9 mpH per min per microgram of protein greater than the basal glycolytic rate, this gap was reduced to 1.5 after four hr of treatment and 2.0 after six hr of treatment (Figure 2.9, A). The reduction of glycolysis by sitagliptin is greater after four hr of treatment with this time point showing the larger reduction in basal glycolysis as well as minimal glycolytic reserve. After six hr of treatment THP-1 cells show a small recovery of basal glycolysis without recovery of the glycolytic reserve indicating that the cells have an ability to overcome some of the effects of sitagliptin on basal glycolysis by this treatment time point. The reduction in both basal glycolysis and the maximal glycolytic capacity indicates that treatment with sitagliptin reduces glycolytic energy production in THP-1 cells and removes the ability to rely on glycolysis for increased cellular energy demands reverting the highly glycolytic THP-1 cells to a lowered metabolic state.

2.3.4.2 Metformin reduces mitochondrial respiration and glycolysis in THP-1 cells

In THP-1 cells metformin treatment showed a similar effect on oxidative phosphorylation as seen with sitagliptin. THP-1 cells treated with 500 µM metformin for four hr show a significant ($p<0.001$) 60% reduction in basal oxygen consumption and a 50% reduction in maximal respiration when compared to untreated cells (Figure 2.8, B, C & E). Additionally, cells at this

treatment time point had a very low OCR of 0.8 ± 0.0 attributed to basal ATP production, indicating a very limited ability to use oxidative phosphorylation for energy production (Figure 2.8, D), no significant change to spare capacity (Figure 2.8, B & F), and an inability to respond to increased energy demands via oxidative phosphorylation. The oxygen consumption profile at the four hr treatment time point shows that oxidative phosphorylation is reduced at all measurable points but still reflects the overall profile seen for untreated cells (Figure 2.8, B). These results indicate that metformin reduces the ability of THP-1 cells to use oxidative phosphorylation for energy production, but all components of the electron transport chain are still fully functional.

After six hr metformin treatment THP-1 cells have very minimal oxygen consumption and an impaired ability to use oxidative phosphorylation for ATP production. Cells at this treatment time point show a significant ($p<0.001$) 85% reduction in basal OCR when compared to untreated cells (Figure 2.8, B & C), addition of oligomycin A at this time point had no effect on oxygen consumption suggesting that this small basal OCR seen is not associated with mitochondrial ATP production (Figure 2.8, D). Cells did respond to addition of FCCP after 6 hr treatment but this response is minimal and shows a significant ($p<0.001$) 80% reduction in maximal respiration when compared to untreated cells (Figure 2.8, E) and a spare capacity close to zero which is reflective of results seen in untreated cells and at the four hr time point (Figure 2.8, F). Comparative to results seen in Jurkat cells, the oxygen consumption profile of THP-1 cells after six hr treatment has a plateaued profile after addition of oligomycin A and shows only minimal increase after addition of FCCP (Figure 2.8, B). This indicates that ATP production via oxidative phosphorylation has ceased after six hr of exposure to metformin and there is only minimal ability for the cells to increase ATP production to address increased energy demand. This response is more pronounced at the six hr treatment time point when compared to the four hr results suggesting that the inhibitory actions of metformin on oxidative phosphorylation are increased after six hr.

Reflective of results seen with sitagliptin, THP-1 cells treated with 500 μM metformin showed reduced glycolysis and elimination of the large glycolytic reserve. Metformin treatment for four hr resulted in a significant ($p<0.001$) 50% reduction in basal glycolysis and 70% reduction in maximal glycolytic rate when compared to untreated cells (Figure 2.9, B, C & D). These effects increased after six hr treatment to a significant ($p<0.001$) 80% reduction in both basal glycolysis and maximal glycolytic capacity (Figure 2.9, B, C & D). Commensurate to results seen with sitagliptin, metformin treatment at both time points reduced not only the basal glycolytic rate, but also reduced the difference between basal glycolysis and the maximal glycolytic capacity of the cells. This reduced the large glycolytic capacity of 5.9 mpH
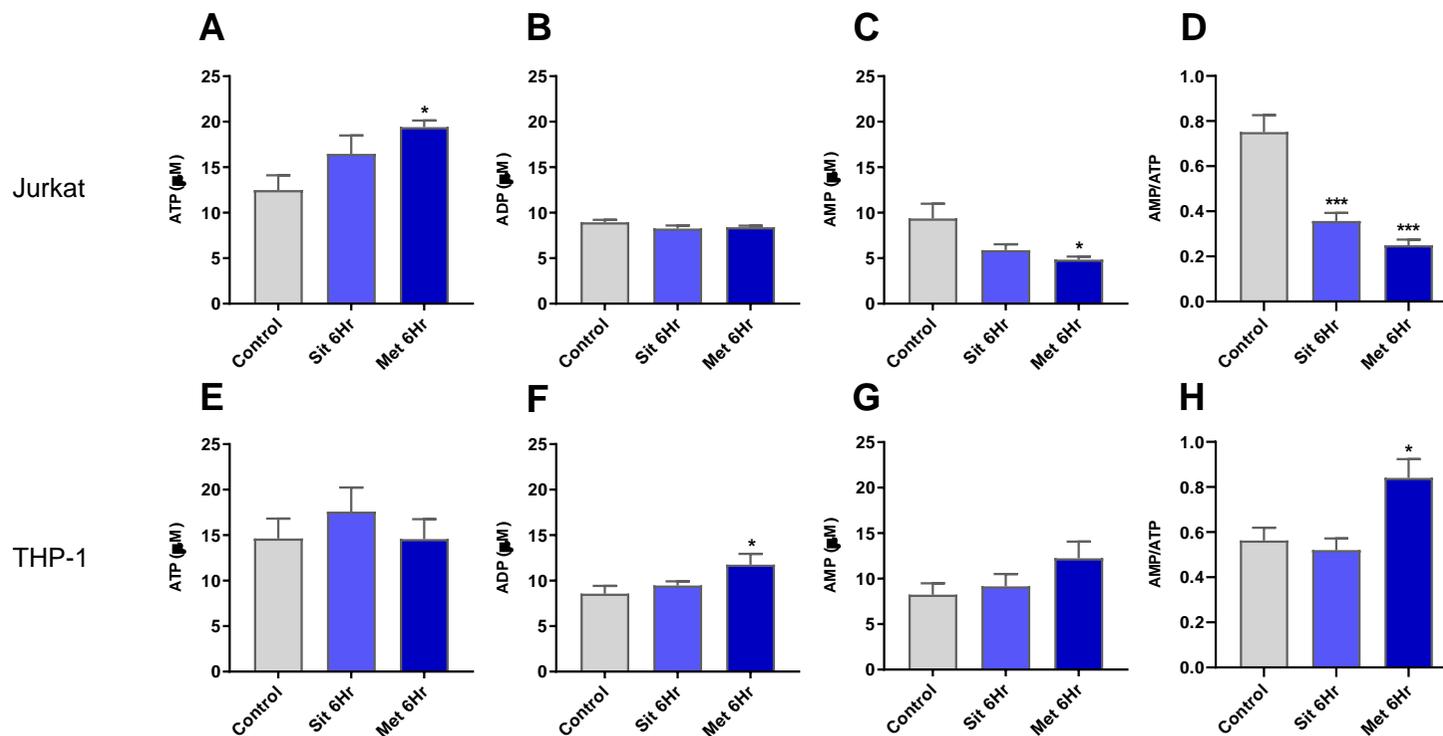
Figure 2.10. Sitagliptin and metformin alter energy balance within the nucleotide pool in Jurkat and THP-1 cells. ATP (A & E), ADP (B & F) and AMP (C & G) concentration as well as the AMP to ATP ratio (D & H) determined via HPLC analysis of cell lysate from 1 x 10^7 Jurkat cells (top row), and, THP-1 cells (bottom row) treated with either 0.04 µM sitagliptin or 500 µM metformin for six hr. Results taken across three independent experiments (n=3), all treatment groups are compared to control by ANOVA: P ≤ 0.05 (*) and P ≤ 0.005 (***). Values represent means and error bars ± standard error (SEM).

per min per microgram of protein seen in untreated cells to 0.6 after four hr and 1.3 after six hr of treatment (Figure 2.9, B & D). These results show that like sitagliptin, metformin reduces glycolytic energy production as well as eliminating the ability of the cells to rely on glycolysis for increased cellular energy demands reverting the highly glycolytic THP-1 cells to a lowered metabolic state.

2.3.5 Sitagliptin and metformin alter energy balance within the nucleotide pool

As both metformin and sitagliptin are associated with altered cellular metabolism, their effect on adenine nucleotide levels in cell lysate was determined using HPLC. In addition to ATP, ADP and AMP concentration the AMP to ATP ratio was also assessed as it is shown to be a responsive indicator of cellular energy status (Hardie et al., 2003; Liu et al., 2006). When compared to untreated cells, 0.04 µM sitagliptin treatment for six hr resulted in no significant shift in ATP, ADP or AMP levels in Jurkat cells but a significant decrease in the AMP to ADP ratio is seen driven by a non-significant increase in ATP and decrease in AMP levels (Figure 2.10, A, B, C & D). In THP-1 cells no shift in ATP, ADP or AMP levels or the AMP to ATP ratio was seen with sitagliptin treatment (Figure 2.10, E, F, G & H). Jurkat cells treated with 500 µM metformin for six hr showed a significant increase in ATP and corresponding decrease in AMP driving an overall reduction in the AMP to ATP ratio (Figure 2.10, A, B, C & D). While THP-1 cells treated with metformin showed no difference in ATP levels, they had a small significant ($p<0.05$) increase in ADP levels, and a small non-significant increase in AMP levels which was a driver for a significant ($p<0.05$) increase in the AMP to ATP ratio (Figure 2.10, E, F, G & H).

2.3.6 Sitagliptin and metformin increase AMPK and phosphorylated AMPK protein levels

AMP-activated protein kinase (AMPK) has a pivotal role in control of cellular metabolism through the regulation of glucose, protein, and fatty acid metabolism, its activation is also shown to support catabolism by inactivating growth-inducing pathways and promoting the oxidation of fatty acids to supply energy needs (van der Windt and Pearce, 2012; Wong et al., 2009). Metformin is associated with activation of AMPK through the AMP mediated phosphorylation of the key regulatory site (Thr-172) of its catalytic (α) subunit creating phosphorylated AMPK (pAMPK) (Hawley et al., 2002). Given sitagliptin has a similar effect on cellular metabolism to that seen for metformin, AMPK and pAMPK protein levels were determined in Jurkat and THP-1 cells treated with sitagliptin or metformin (Figure 2.11).
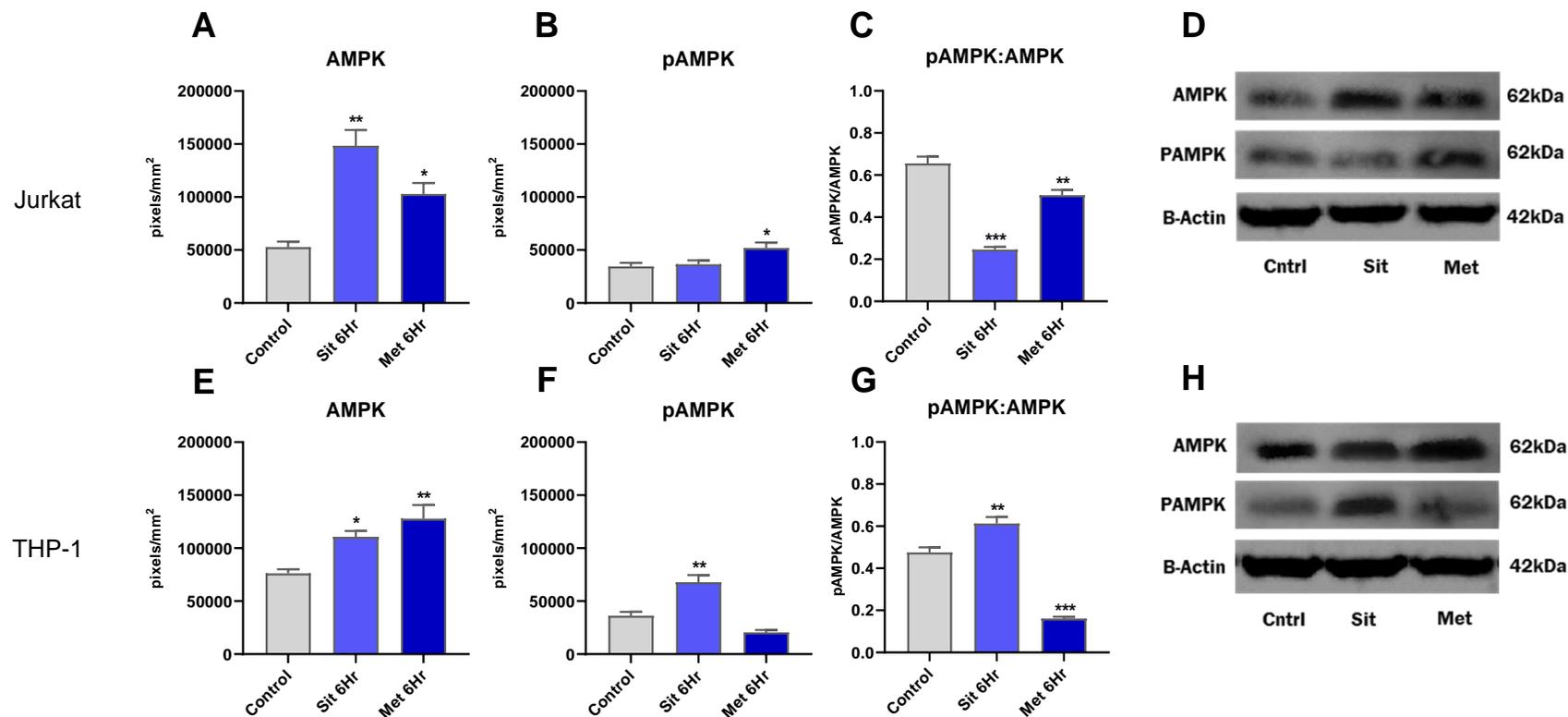
Figure 2.11. Sitagliptin and metformin increase total AMPK and phosphorylated AMPK (pAMPK) protein levels in Jurkat and THP-1 cells. AMPK (A & D) and pAMPK (B & E) total protein as well as pAMPK to AMPK ratio (C & G) determined by western blot analysis in Jurkat cells (top row) and THP-1 cells (bottom row) treated with 0.04 µM sitagliptin or 500 µM metformin for six hr. Image of western blot results (C & F), protein levels were normalised to β-actin protein levels and quantified using BioRad Image Doc analysis, using 25 µg of protein loaded on to 10% SDS-PAGE gel. Results taken across three independent experiments (n=3), all treatment groups are compared to control by ANOVA: P ≤ 0.05 (*) and P ≤ 0.01 (**). Values represent means and error bars ± standard error (SEM).
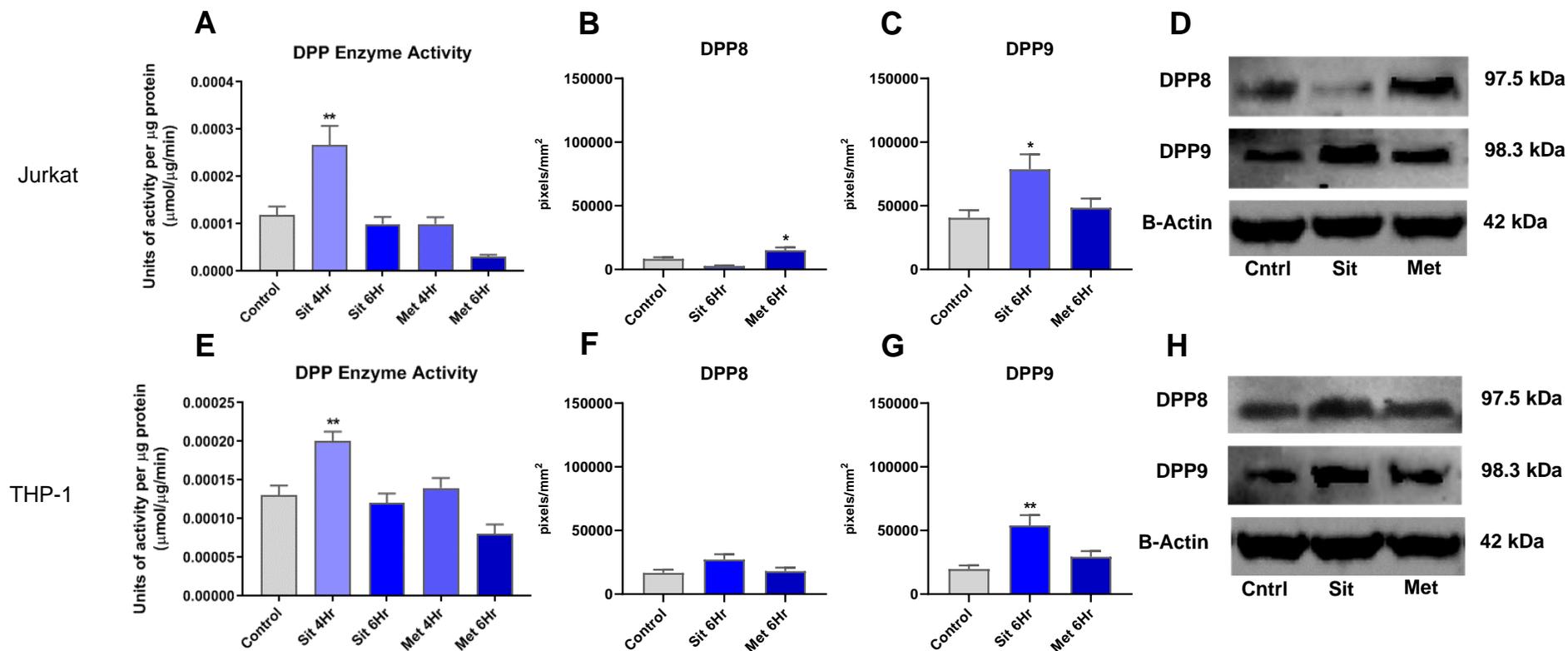
Figure 2.12. Sitagliptin increases DP enzyme activity associated with increased DPP9 protein presence. DP enzyme activity determined via H-Ala-Pro-pNa cleavage assay (A & E) as well as DPP9 (B & F), and DPP8 (C & G) total protein determined by western blot analysis in Jurkat cells (top row) and THP-1 cells (bottom row) with 0.04 μM sitagliptin or 500 μM metformin added to cell culture four or six hr prior and at time of enzyme assay and six hr prior to western blot. Image of western blot results (D & H), protein levels were normalised to β-actin protein levels and quantified using BioRad Image Doc analysis. Results taken across three independent experiments (n=3), all treatment groups are compared to control by ANOVA: $P \leq 0.05$ (*) and $P \leq 0.01$ (**). Values represent means and error bars ± standard error (SEM).
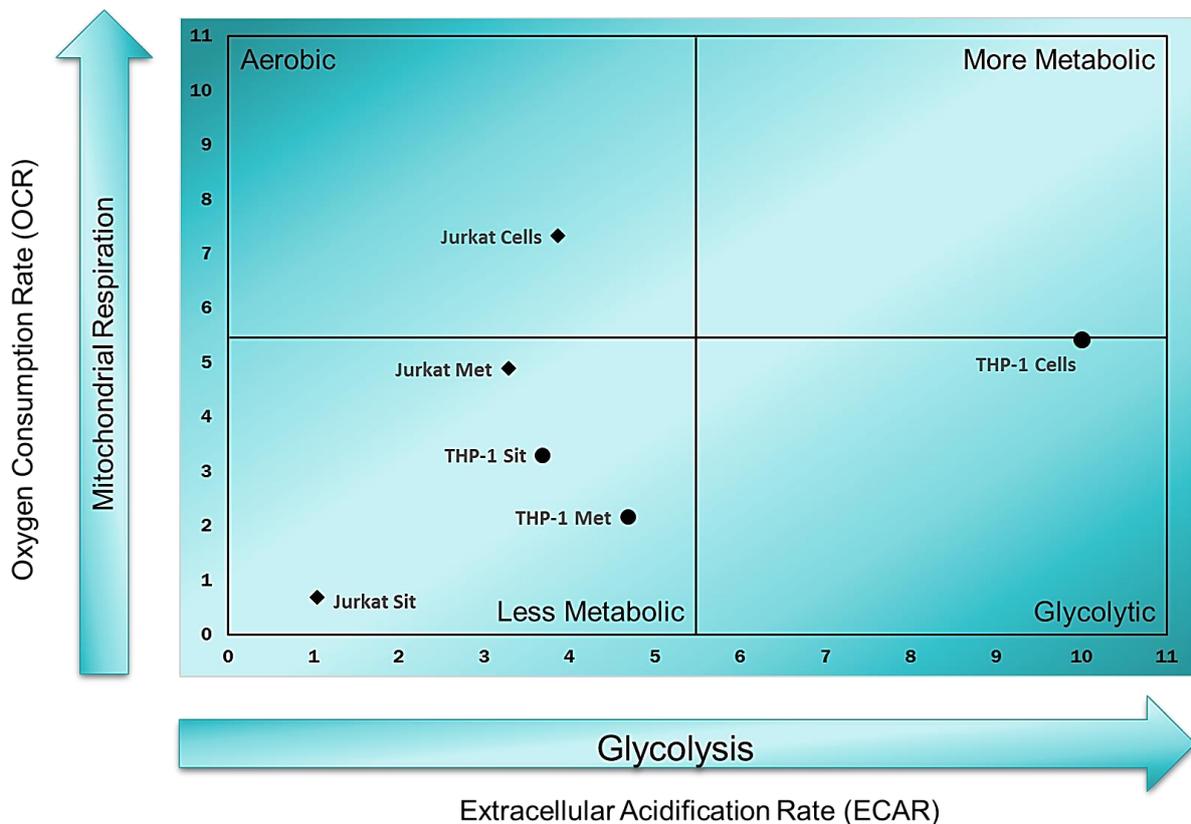
Figure 2.13. Overview of the effect sitagliptin and metformin treatment have on the metabolic profile of ◆ Jurkat and ● THP-1 cells. Untreated Jurkat cells are more aerobic with a high reliance on mitochondrial respiration for cellular energy production while THP-1 cells are more metabolic have a high reliance on glycolysis for cellular energy production. Both sitagliptin and metformin move the highly aerobic Jurkat cells and the highly glycolytic THP-1 cells into a lowered metabolic state with reduced ability to use either glycolysis or mitochondrial respiration for ATP production.

AMPK protein levels are significantly increased in both Jurkat (p<0.01) and THP-1 (p<0.05) cells after six hr 0.04 µM sitagliptin treatment (Figure 2.11, A & E), additionally, THP-1 cells treated with sitagliptin show a significant (p<0.01) increase in activated pAMPK which is reflected in a significant increase in the pAMPK to AMPK ratio (Figure 2.11, G), although pAMPK is not increased in Jurkat cells at this treatment time point and the pAMPK to AMPK ratio is significantly reduced (Figure 2.11, B, C & D). In Jurkat cells 500 µM metformin treatment for six hr significantly (p<0.05) increased both AMPK and pAMPK protein levels, in THP-1 cells metformin treatment significantly (p<0.01) increased AMPK levels but did not affect pAMPK and the pAMPK to AMPK ration was significantly reduced with metformin treatment in both cell types (Figure 2.11). The increase in AMPK in both cell types and increase in pAMPK in Jurkat cells after treatment with metformin is indicative of the known association between metformin and AMPK, although given the association between metformin and AMPK phosphorylation, the nil affect metformin treatment has on pAMPK protein levels in THP-1 cells is surprising (Hawley et al., 2002; Rena et al., 2017).

2.3.7 Sitagliptin increases dipeptidyl peptidase enzyme activity

The two DPP4 family members dipeptidyl peptidase 8 (DPP8) and dipeptidyl peptidase 9 (DPP9) share similarities in substrate specificity with DPP4 and have been identified as able to cleave many known DPP4 substrates, additionally the activities of DPP8 and DPP9 have been associated with control of the immune response and cancer biology (Waumans et al., 2015; Wilson et al., 2013). H-ala-pro-pNA is a substrate of DPP4, DPP8 and DPP9 so but in the presence of a DPP4 inhibitor such as sitagliptin can be used to determine DPP8 and DPP9 enzyme activity (Dubois et al., 2009). DPP enzyme activity was significantly (p<0.01) increased after four hr sitagliptin treatment in both Jurkat and THP-1 cells, although this increase in DPP activity is not seen after six hr (Figure 2.12, A & E). Quantification of DPP8 and DPP9 protein levels in cells treated with sitagliptin show a significant increase in DPP9 protein levels in both Jurkat (p<0.05) and THP-1 (p<0.01) cells but no increase in DPP8 protein (Figure 2.12, B, C, F & G). The increase in DPP enzyme activity seen after four hr sitagliptin treatment was not seen after six hr treatment in either Jurkat or THP-1 cells (Figure 2.12, A & E).

Metformin treatment had no significant effect on DP activity in Jurkat and THP-1 cells at either the four or six hr treatment time point which was an expected result as metformin is not defined as a DPP inhibitor (Figure 2.12, A & E). However, metformin did produce a significant (p<0.05) increase in DPP8 protein levels after six hr treatment which may indicate a compensatory increase in DPP8 after prolonged exposure to metformin (Figure 2.12, C).

2.4 Discussion

The work in chapter two clearly illustrates for the first time in immune cells that sitagliptin like metformin reduces the metabolic state of both T cell derived Jurkat cells and monocytic THP-1 cells with the greatest effect seen on the preferred energy pathway of each cell type. Metabolic reprogramming by sitagliptin was associated with increased AMPK and activated AMPK presence, indicating that DPP4 imparts control over cellular metabolism through AMPK associated actions. Additionally, treatment with sitagliptin in Jurkat and THP-1 cells results in a significant increase in DPP9 protein levels which may play a role in driving the reduced metabolic state.

In this work the analysis of the metabolic state of untreated cells identified distinction in the preferred energy pathway of each cell type. The T-lymphocyte cell line Jurkat, established from a human male with T cell leukemia (Abraham and Weiss, 2004), showed a high reliance on oxidative phosphorylation with a large mitochondrial spare capacity for increased cellular energy, a lowered reliance on glycolysis but presence of a glycolytic spare capacity indicating an ability to increase ATP production via glycolysis if required. In contrast, the monocytic cell line THP-1, derived from a human male with acute monocytic leukemia which develops a macrophage like phenotype when stimulated (Starr et al., 2018; Tsuchiya et al., 1980), showed a higher reliance on glycolysis for basal energy production with a large glycolytic spare capacity able to address heightened cellular energy demands, and a lowered reliance on oxidative phosphorylation with no mitochondrial spare capacity (Bosshart and Heinzelmann, 2016). While both cell types are utilizing a differing bioenergetic pathway it is not unusual for immune cells to undergo metabolic reprogramming to change the use of bioenergetic pathways to modulate their functional characteristics (O'Neill et al., 2016; Vijayan et al., 2019). Furthermore, many immune cell types including T-cells, monocytes and macrophages are shown to undergo metabolic reprogramming in response to stimulation and shift from utilising oxidative phosphorylation to the use of fatty acid oxidation or aerobic glycolysis depending on environmental factors including culture conditions (Smokelin et al., 2020; Vijayan et al., 2019). It is this highly dynamic and fluid process that enables change in cellular functions in quick response to environmental cues that plays a key role in the adaptive immune response (Fernández-Ramos et al., 2017).

The difference in utilized energy pathway between Jurkat and THP-1 cells in chapter two provided a comparative metabolic model of cancer cells with THP-1 cells presenting with a metabolic profile as defined by Warburg with a high reliance on glycolysis even in the presence of oxygen, while Jurkat cells show a more hybrid metabolic profile with the ability

to use either oxidative phosphorylation or glycolysis for increased energy needs (Warburg, 1956). While the reliance on aerobic glycolysis in normoxic environments is a hallmark of cancer metabolism, recent evidence has identified the ability of cancer cells to use a hybrid metabolic pathway where either glycolysis or oxidative phosphorylation can be called on for increased energy production, additionally, this metabolic flexibility is now marked as a defining characteristic of cancer stem cells (Cavalli et al., 1997; Hayashi et al., 1992; Morais et al., 1994; Snyder et al., 2018; Yu et al., 2017). The use of Jurkat and THP-1 cells in chapter two allowed for determination of the effect of sitagliptin on the aerobic glycolysis model of cancer cell metabolism while also determining its effect on a hybrid metabolic model using both the glycolytic and mitochondrial pathways.

Importantly this chapter has demonstrated that both sitagliptin and metformin reduces mitochondrial respiration and glycolysis in the T cell derived Jurkat cells and monocytic THP-1 cells. In Jurkat cells, sitagliptin significantly reduced oxidative phosphorylation with complete cessation of mitochondrial function seen after four hr with no response to the addition of ETC modulators. Additionally, sitagliptin was shown to significantly reduce basal glycolysis and remove the glycolytic reserve capacity after four hr. After six hr treatment recovery of basal glycolysis was observed but there was no recovery of the glycolytic reserve. The results seen for sitagliptin in Jurkat cells is comparable to that seen for metformin. Four hr treatment with metformin significantly reduced basal oxidative phosphorylation and impaired mitochondrial function. In addition, treated cells were unable to respond to ETC modulators and had no spare capacity for increasing ATP production. Basal glycolysis was only reduced after six hr metformin treatment in Jurkat cells, but glycolytic spare capacity was significantly reduced at both treatment time points.

In THP-1 cells, sitagliptin significantly reduced oxidative phosphorylation although this was not associated with an impaired mitochondrial function as reaction to ETC modulators was still evident after both treatment time points. Sitagliptin also significantly reduced basal glycolysis and removed the glycolytic reserve in THP-1 cells, eliminating their ability to rely on glycolysis for increased ATP production. This was comparable to metformin treatment in THP-1 cells which significantly reduced oxidative phosphorylation although complete mitochondrial function was still evident after four hr as noted by response to ETC modulators, after six hr no basal oxidative phosphorylation was observed and only a very minimal response to addition of proton uncoupler FCCP was seen, indicating a very small spare capacity for increased ATP production. Metformin treatment also significantly reduced basal glycolysis and removed the glycolytic reserve in THP-1 cells.

The difference in results between Jurkat and THP-1 cells show that sitagliptin imparts the greatest effect on the preferred energy production pathway of the cells and may indicate its involvement in modulation of cellular metabolic stasis ensuring a basal metabolic state is maintained to support ongoing cell maintenance rather than direct impact on glycolytic or oxidative phosphorylation processes (Fernandez-De-Cossio-DIaz and Vazquez, 2018; Sarkar et al., 2017; Yang et al., 2017). This reduction in energy metabolism was also associated with a reduction in cellular proliferation in Jurkat cells, with recovery of cell numbers after six hr sitagliptin treatment correlating with a recovery in mitochondrial and glycolytic function. While DPP4 protein is more highly expressed in Jurkat compared to THP-1 cells, the effects of sitagliptin on energy metabolism are occurring via its inhibition of DPP4 activity. The timeline observed is in line with pharmacokinetic characteristics of sitagliptin where maximal plasma concentration and DPP4 activity inhibition occurred two to six hr after a single dose of five to 400 mg sitagliptin with a terminal half-life seen at nine to 14 hr (Herman et al., 2011). DPP4 has a known association with control of cellular proliferation, overexpression of DPP4 in endometrial carcinoma cell lines has been shown to increase cellular proliferation, tumour cell adhesion and metastasis, as well as increase the tumorgenicity of cells when injected into nude mice (Yang et al., 2017). DPP4 overexpression has also been shown to increase cellular proliferation in human vascular smooth muscle cells (hVSMCs), while its effects on proliferation in hVSMCs, or tumorgenicity in endometrial cancer cells, could be reversed by DPP4 inhibition (Wronkowitz et al., 2014; Yang et al., 2017). Additionally, DPP4 has been associated with cell cycle regulation, with inhibition of DPP4 activity shown to induce G1-S cell cycle arrest and increase apoptosis (Inamoto et al., 2007, 2006; Sarkar et al., 2017; Yang et al., 2017). The reduction in cell numbers seen with sitagliptin treatment in Jurkat cells indicates that these cells may be subject to cell cycle arrest induced by the absence of DPP4 activity. While a significant impact on immune cell metabolism is seen *in vitro*, it is noted that patients taking DPP4 inhibitors do show reduced T-cell proliferation and a direct effect of DPP4 inhibitors on innate immunity has been established *in vivo* (Yazbeck et al., 2021). On the other hand, although an impact on immune cell function is noted in patients taking DPP4 inhibitors no significant differences in the rates of infections is seen between patients taking DPP4 inhibitors compared to placebo which indicates that the reduction in metabolism and proliferation associated with DPP4 inhibition in immune cells does not affect overall function (Yazbeck et al., 2021).

The reduction in cellular proliferation seen with sitagliptin again reflects that seen with metformin. Metformin treatment in Jurkat cells reduced cellular proliferation after two hr but only partial recovery of cell number was seen after six hr metformin treatment. The treatment

timeline in metformin is however longer than sitagliptin as only partial recovery of cell number is seen after six hr which correlated with a small recovery of mitochondrial function but did not correlate with recovery of glycolytic function. As with sitagliptin this timeline is in line with pharmacokinetic characteristics of metformin where maximal plasma concentration and action is seen three hr after a single 850 mg dose with the longer recover period reflecting the longer half-life of 23 hr which is reported for metformin (Robert et al., 2003). The growth inhibition seen with metformin treatment was an expected result as metformin has been previously associated with antineoplastic actions via AMPK-dependent growth inhibition and cell cycle arrest (Dowling et al., 2007; Jones et al., 2005; Li et al., 2018; Zakikhani et al., 2006). These results reflect those seen in patients where treatment with metformin suppresses immune responses through direct effect on immune cell function, results which have let to metformin being investigated as a potential treatment for immune mediated inflammatory diseases (Schuiveling et al., 2018).

Inhibition of DPP4 by sitagliptin resulted in an increase in AMPK, but no change in pAMPK and an overall reduction in the pAMPK to AMPK ratio in Jurkat cells and an increase in both AMPK and pAMPK with an overall increase in the pAMPK to AMPK ratio in THP-1 cells. The lack of change in pAMPK in Jurkat cells may be associated with the treatment time point used and the ability of the cells to overcome the actions of sitagliptin with the reduction in activated AMPK signifying the initiation of anabolism upon recovery from the low energy state induced by sitagliptin treatment (van der Windt and Pearce, 2012). This work shows that the augmentation of cellular energy metabolism by sitagliptin is associated with regulation of the AMPK signalling pathways. Although not defined in control of cellular metabolism, the association between sitagliptin and AMPK has been previously identified in atherosclerosis where sitagliptin was shown to reduce atherosclerotic lesions through the regulation of AMPK (Zeng et al., 2014).

The increase in AMPK and pAMPK with sitagliptin treatment was notably not associated with a corresponding increase in the AMP to ATP ratio in either cell type. AMPK is a known regulator of cellular metabolism and during energy stress is shown to directly modulate intermediates of key regulatory pathways to restore energy balance through inhibition of anabolism and corresponding stimulation of catabolism (Herzig and Shaw, 2018; Sanli et al., 2014). AMPK activation has been correlated with increased presence of cyclin-dependent kinase inhibitor p27/kip1 (p27) known to play a role in cell cycle regulation through direct inhibition of cyclin-dependent kinase complexes resulting in cell cycle arrest in G1 (Lloyd et al., 1999; Short et al., 2010). In conjunction with an associated increase in G1 cell cycle arrest, inhibition of DPP4 by sitagliptin has also been associated with increased expression

of p27 in breast cancer cells (Sarkar et al., 2017; Yang et al., 2017). The increase in AMPK and phosphorylated AMPK as well as the reduction in cellular proliferation associated with sitagliptin in this work may indicate that inhibition of DPP4 allows increased presence and activation of AMPK which induces catabolism and G1 cell cycle arrest through increased expression of p27.

AMPK is shown to play a key role in mitochondrial homeostasis, in the absence of mitochondrial damage AMPK activation is shown to induce mitochondrial fragmentation and fission an action that allows consolidation of the functional elements of the mitochondria in nutrient-limited conditions (Herzig and Shaw, 2018; Toyama et al., 2016). AMPK is also activated by increased intracellular levels of AMP so may conversely be activated by decreased mitochondrial function as is the postulated action of metformin via inhibition of the mitochondrial ETC complex 1 (Batandier et al., 2006; Toyama et al., 2016). The work in chapter two indicates that sitagliptin treatment results in decreased mitochondrial function and an increase in both AMPK and activated AMPK without increase in the AMP to ATP ratio. Experimental evidence suggests that AMPK has a localised presence both within the cytosol and as part of a mitochondrial pool and that it is the mitochondrial AMPK that is involved in regulation of ATP levels independent of cytosolic AMPK (Liang et al., 2015; Miyamoto et al., 2015). Inhibition of DPP4 by sitagliptin may be imparting its inhibitory effect on oxidative phosphorylation through direct activation of cytosolic AMPK as opposed to increase in AMP through inhibition of mitochondrial function. In addition to its mitochondrial targeted actions, AMPK activation has also been associated with inhibition of glycolysis in primary T cell acute lymphoblastic leukemia (T-ALL) cells where removal of the major AMPKα subunit in T-ALL cells resulted in an increased ECAR that was associated with increased mTORC1 activity (Kishton et al., 2016). Additionally in T-ALL cells, AMPK activation is shown to protect from metabolic stress by reducing energy demand through catabolic metabolism and is associated with reduction in both oxidative phosphorylation and glycolysis as well as reduction in cellular proliferation through increased G1 cell cycle arrest (Kishton et al., 2016).

This work demonstrated that DPP4 inhibition by sitagliptin reduces cellular proliferation, oxidative phosphorylation and glycolysis, and is associated with increased AMPK presence and activation indicating sitagliptin is involved in metabolic reprogramming through activation of AMPK. This ties in with work from Hwang et al., (2015), who demonstrate that in human hepatocellular carcinoma cell line HepG2, a significant dose dependent increase in AMPK phosphorylation is seen with the DPP4 inhibitor gemigliptin. Hwang et al., (2015) demonstrated that gemigliptin was shown to reduce hallmarks of non-alcoholic fatty liver

disease (NAFLD) including TNFα-induced mTOR phosphorylation and lipid accumulation via AMPK phosphorylation. Furthermore, the reduction in fatty liver hallmarks seen with DPP4 inhibition by gemigliptin were significantly attenuated by compound C, an AMPK-specific inhibitor (Hwang et al., 2015b). In further work by the same group, inhibition of DPP4 via gemigliptin induced phosphorylation of AMPK in human umbilical vascular endothelial cells (HUVECs) and THP-1 cells, and AMPK phosphorylation by gemigliptin was related to a dose dependent increase in phosphorylated Akt (Hwang et al., 2015a). AMPK is an essential regulator of Akt and AMPK activation of Akt has known involvement in a variety of cellular functions including proliferation, metabolism, cell survival, and migration. The relationship between DPP4 inhibition and Akt activation is also seen in cardiomyocyte H9c2 cells where DPP4 inhibition with gemigliptin increases Akt phosphorylation and protects H9c2 cells from tunicamycin-mediated cell death. While gemigliptin treatment resulted in a dose dependent increase in phosphorylated Akt, treatment with an Akt inhibitor was able to decrease the anti-apoptotic effect (Hwang et al., 2014). The body of work relating DPP4 inhibition to AMPK activation is largely tied into altering inflammatory disease states including NAFLD and atherosclerosis with reduction in the expression of inflammatory cytokines seen with DPP4 inhibition and AMPK activation in cardiomyocytes and HUVECs (Hwang et al., 2015a, 2014). This chapter ties into this wider body of work relating DPP4 inhibition with control of cell metabolism and immune cell viability through increase in AMPK activation. Furthermore, this study has provided further evidence for a role of DPP4 in control of cellular metabolism as well as immune and cancer cell proliferation, positioning sitagliptin as a potential antitumorigenic therapeutic target.

The effects of Metformin were slightly different on Jurkat and THP-1 cells. An overall decrease in the AMP to ATP ratio was associated with metformin treatment in Jurkat cells, while an increase in the AMP to ADP ratio was seen with metformin treatment in THP-1 cells. The decrease in the AMP to ATP ratio in Jurkat cells treated with metformin was driven by a significant increase in ATP and decrease in AMP, this is an unexpected result. While the increase in the AMP to ATP ratio in THP-1 cells seen with metformin treatment is in line with the reported actions of metformin as a known inhibitor of ETC complex 1 which supresses ATP production driving an increase in the AMP to ATP ratio (El-Mir et al., 2000).

The decrease in the AMP to ATP ratio in Jurkat cells treated with metformin for six hr may correspond to the results seen with sitagliptin as well as those reported for Jurkat cells treated with AMP where the increase in ATP is correlated to activation of compensatory mechanisms to counteract the energetic distress caused by ATP depletion in the cell (Fernández-Ramos et al., 2017). As with sitagliptin Jurkat cells may be overcoming the

inhibitory effect of metformin on ATP production. This would also tie in with the recovery of cellular proliferative activity which is seen after six hr metformin treatment in Jurkat cells and commensurate with sitagliptin results, indicating the ability of the cells to overcome the antiproliferative effect of metformin after six hr.

On the other hand, the increase in the AMP to ATP ratio seen in THP-1 cells treated with metformin was not associated with a significant decrease in ATP. Given the tight regulation of ATP, ADP and AMP levels by the cell, the non-significant increase in AMP driving a significant increase in the AMP to ATP ratio is expected as only a small increase in AMP is required to effect a change in the functional activity within the cell (De La Fuente et al., 2014; Rena et al., 2017). As with results seen with sitagliptin treatment in THP-1 cells the increase in the AMP to ATP ratio may be reflective of the slower growth rate in THP-1 cells. On comparison with the four hr treatment results, THP-1 cells show an overall reduction in basal respiration, ATP production, maximal respiration and basal glycolysis after six hr metformin treatment. The lack of shift in ATP, ADP and AMP levels in THP-1 cells after six hr metformin treatment may reflect the results seen with sitagliptin treatment, THP-1 cells may remain in a quiescent state for a longer period in the presence of metformin where low metabolic requirements enable maintenance of the adenylate energy charge via the reduced glycolytic and mitochondrial function (De La Fuente et al., 2014; MacIver et al., 2013). This delay in recovery from the inhibitory effects of metformin may also be related to slower growth rate in THP-1 cells which are reported to have a doubling time of 30 hr compared to Jurkat cells which are reported to have a much shorter doubling time of 16 hr (Schoene and Kamara, 1999; Tsuchiya et al., 1986).

In summary of the results presented in chapter two, changes in the AMP to ATP ratio were not directly correlated to an increase in activated AMPK (pAMPK). Sitagliptin treatment in Jurkat cells resulted in a significant reduction in the AMP to ATP ratio and a significant increase in AMPK but not pAMPK. In THP-1 cells sitagliptin treatment resulted in no change to the AMP to ATP ratio but a significant increase in both AMPK and pAMPK was seen. It may be that the impact of sitagliptin treatment on AMPK is not directly related to the AMP to ATP ratio but may be as a result of increased DPP9 presence.

Both Jurkat and THP-1 cells treated with sitagliptin show a significant increase in DPP9 protein levels. This increase in DPP9 protein is associated with increased DPP activity and may be a compensatory action by the cell to overcome inhibition of DPP4 indicating a potential overlap of functionality between DPP4 and DPP9. On the other hand, DPP4 may act as a regulator of DPP9 expression and activity, as it was observed in this study that inhibition of DPP4 resulted in increased DPP9 protein expression. This inverse relationship

between DPP4 and DPP9 expression has been previously identified in breast cancer cells where DPP4 is shown to play a potential role in the post-transcriptional regulation of DPP9 (Wilson and Abbott, 2012). Using a proteomics approach Wilson et al., (2013) identified AK2 as a natural substrate of DPP8 and 9 (Wilson et al., 2013). Recently this role was confirmed by Finger et al., (2020) who showed that DPP9 and to a lesser extent DPP8, played a role in controlling mitochondrial biogenesis but most prominently in control of the mitochondrial import and cytosolic degradation of adenylate kinase 2 (AK2) (Finger et al., 2020). AK2 is formed in the cytosol but is transported to the mitochondrial intermembrane space (IMS) where it regulates intracellular ATP levels by catalysing the reversible transfer of a phosphate group in the reaction ATP+AMP $\leftrightarrow$ 2 ADP (Noma, 2005). AK2 also controls high-energy phosphoryl exchange between mitochondria and cytosol and through regulation of AMP controls metabolic signalling and maintains energy homeostasis in the cell (Dzeja and Terzic, 2009; Six et al., 2015). Finger et al., (2020) have demonstrated that in HEK293 cells DPP9 cleaves the N-terminal dipeptide from AK2 and this proteolytic processing targets AK2 for proteasomal degradation within the cytosol before it is transported to the IMS. While siRNA mediated depletion of DPP9 as well as inhibition by DPP8/9 inhibitor IG244, stabilised AK2 reducing degradation which increased endogenous levels within the cytosol. This stabilisation of AK2 was increased further with double depletion of both DPP8 and DPP9 but depletion of just DPP8 did not affect AK2 stability indicating that DPP9 is the main processing enzyme with DPP8 acting as a backup (Finger et al., 2020).

Six et al., (2015) investigated the role of AK2 in lymphoid T-cell differentiation, knock down of AK2 expression in CD34+ progenitors from cord blood inhibited cellular proliferation as well as T-cell differentiation (Six et al., 2015). In addition to the effects in primary cells, AK2 knockdown in the HL60 cell line inhibited cellular proliferation and significantly decreased oxidative phosphorylation through impaired respiratory chain activity (Six et al., 2015). While activation of AMPK is regulated via changes in cellular AMP levels, the primary activator of AMPK is identified as adenylate kinase as it controls the balance of cellular ATP, ADP and AMP, affecting AMPK activation through control of AMP levels (Klepinin et al., 2020). The significantly increased DPP9 protein levels seen with DPP4 inhibition in Jurkat and THP-1 cells may result in a decrease of AK2 within the IMS through increased DPP9 driven degradation of AK2 in the cytosol before it is able to be transported into the IMS. The reduction in AK2 in the IMS would diminish phosphoryl exchange between mitochondria and cytosol and disrupt cellular proliferation and mitochondrial function through reduced intracellular ATP levels. Sitagliptin may be disrupting cellular metabolism through increase in DPP9 protein and associated proteolytic degradation of AK2.

Metformin treatment in Jurkat cells resulted in a significant decrease in the AMP to ATP ratio as well as a significant increase in both AMPK and pAMPK, while a significant increase in the AMP to ATP ratio is seen in THP-1 cells treated with metformin, but only AMPK is significantly increased not pAMPK. Zhou et al., (2001) were one of the first groups to report that metformin activates AMPK in hepatocytes but found that total ATP concentrations were not affected by 500 to 2000 µM metformin-treatment. Zhou et al., (2001) instead proposed that metformin treatment results in a subtle decrease in the free ATP/ADP and ATP/AMP ratios or cause a localised change in nucleotide concentrations resulting in a stimulus for AMPK activation (Zhou et al., 2001). Since then, metformin has been associated with increased cellular levels of AMP through suppression of complex I of the mitochondrial electron transport chain, it is this elevation of AMP concentration that is proposed as the driver for metformin mediated activation of AMPK (Batandier et al., 2006). In THP-1 cells the expected increase in the AMP to ATP ratio with metformin treatment is seen although a corresponding increase in pAMPK is not. In Jurkat cells the expected increase in pAMPK is seen but this is not correlated to an increase in the AMP to ATP ratio. In summary the increase in the AMP to ATP ratio in THP-1 cells was driven by a small non-significant increase in AMP but no corresponding decrease in ATP. ATP and AMP competitively bind to two exchangeable sites on the γ subunits of AMPK and both sites must bind AMP for phosphorylation and activation to occur, as the process is antagonized by high concentrations of ATP this activation requires an increase in AMP coupled with an associated decrease in ATP (Hawley et al., 2010). The non-significant increase in AMP seen in THP-1 cells treated with metformin was not associated with the required decrease in ATP for AMPK activation which may be a factor in the reduced pAMPK levels seen in the cells.

The non-consistent relationship between metformin treatment, AMP levels, and increased presence of pAMPK may indicate that the effect metformin has on mitochondrial oxidative phosphorylation and glycolysis may be via an AMPK independent action. Metformin has been associated with inhibition of mitochondrial respiratory capacity and cellular growth through direct inhibition of protein kinase mechanistic target of rapamycin complex 1 (mTORC1) which is involved in regulation of cellular energetics and plays a central role in regulating cell growth, proliferation and survival (Kalender et al., 2010; Schmelzle and Hall, 2000). Metformin is shown to inhibit mTORC1 by restraining the nuclear pore transport of GTP-binding protein (Rag) GTPase. Metformin driven reduction in mitochondrial function through inhibition of complex I of the ETC is shown to trigger the exclusion of Rag-GTPases from the nuclear pore complex (NPC) inhibiting mTORC1 through this restrained nuclear transport (Sancak et al., 2008; Wu et al., 2016). Furthermore, it is identified that it is the effect of metformin on nuclear pore transport and not the drop in ATP levels that has the

greatest effect on cellular proliferation and is likely to be involved in the anti-tumorigenic actions of the drug (Li et al., 2018; Wu et al., 2016). Additionally, concentration may play a part in the route of action of metformin, at low doses of 200 µM in rat hepatocytes metformin has been associated with mTORC1 inhibition through AMPK activation, this action is shown to occur through AMPK independent mechanisms at higher doses of 500 µM, reflective of those used in this work (Howell et al., 2017; Li et al., 2018).

2.5 Conclusion

The work described here in chapter two has demonstrated that sitagliptin alters the bioenergetic profile of both Jurkat and THP-1 cells, reducing both oxidative phosphorylation and glycolysis with results congruent to those seen for the well-established regulator of these pathways metformin. Metabolic reprogramming by sitagliptin was associated with increased AMPK and activated AMPK presence, indicating that DPP4 imparts control over cellular metabolism through AMPK associated actions. Additionally, inhibition of DPP4 resulted in a significant increase in DPP9 protein levels which may be involved in the metabolic reprogramming seen with sitagliptin treatment through control of the mitochondrial import and cytosolic degradation of AK2. Results taken from this work indicate that sitagliptin like metformin may provide a novel therapeutic approach for targeted metabolic reprogramming of cancer cells.

Chapter 3

Refinement of the AOM murine model of
colon carcinogenesis for use with knockout
mice lacking DPP4 or FAP

3.1 Introduction

In the work outlined in chapter two, DPP4 inhibition was shown to impart control over cellular metabolism that is correlated with AMPK activation, results that link the actions of DPP4 with targeted metabolic reprogramming of cancer cells. Cancer is a major contributor to disease related deaths, in 2018, 9.6 million deaths worldwide were attributed to cancer, while colorectal cancer (CRC) is the second leading cause of cancer related mortality (Bray et al., 2018). DPP4 and its related protein family member fibroblast activation protein (FAP) are both implicated in tumorigenesis, and both proteins are identified as biomarkers and potential treatment targets in colorectal cancer.

Both genetic and epigenetic alterations are established as the basis for the adenoma to carcinoma progression within the colon, with accumulation of these genetic alterations transforming normal colon epithelium from early adenomas through to invasive metastatic carcinoma (Armaghany et al., 2012). The metabolic processes involved in the initiation and progression of colonic tumorigenesis however are still largely undefined. DPP4 and FAP are peptidases with known biological functions that are potentially involved in neoplastic transformation within the colon. DPP4 is known to alter the activity of bioactive peptides including cytokines, chemokines and neuropeptides, it is involved in extracellular matrix interactions through collagen and fibronectin, as well as in cell to cell adhesion and the secretion of matrix metalloproteases (Havre et al., 2008; Larrinaga et al., 2015). FAP is a membrane-bound serine protease that exhibits both dipeptidyl peptidase and prolyl-endopeptidase activity. FAP is expressed transiently in tissues associated with wound healing and in chronic inflammation and has gelatinase and collagenase activity suggesting a role in extracellular matrix remodelling (Ghersi et al., 2002; Levy et al., 2002; Xin et al., 2008; Yu et al., 2010). DPP4 and FAP have demonstrated roles in the control of neoplastic transformation through regulation of tumour cell behaviour and function (Enz et al., 2019; Puré and Blomberg, 2018).

In the study of human disease such as colon cancer, animal models are consistently used to cultivate deeper understanding of the disease state. Genomic sequencing has established that of the ~30,000 genes identified in mice and humans there are just 300 or 1% are distinctive to either species (Waterston et al., 2002). Thus, genetic, and physiological similarities between mice and humans make rodents an excellent target for modelling human diseases. Azoxymethane (AOM) the downstream metabolite of 1,2-dimethylhydrazine (DMH) was identified in the 1960s as a chemical carcinogen able to drive the development of colon cancer in rodents when it was shown that feeding rats untreated flour from nuts of the *Cycas*

circinalis L. containing the DMH carcinogenic agent, produced a variety of gastrointestinal tumours (Laqueur et al., 1963).

The azoxymethane (AOM) induced colorectal cancer model has been used extensively to study potential targets for disease prevention and treatment. In rodents AOM is a potent carcinogen that leads to the formation of tumours in the distal colon that emulate the pathogenesis of human sporadic CRC (Lijinsky et al., 1985). Following intra-peritoneal treatment with AOM the colon epithelial cells undergo transformation forming epithelial legions known as aberrant crypt foci (ACF), adenomas and malignant adenocarcinomas (Chen and Huang, 2009; Takahashi and Wakabayashi, 2004). *In vivo* AOM itself is not a carcinogenic metabolite, it must undergo metabolism and activation initiated by cytochrome P450. Hydroxylation of AOM forms methylazoxymethanol (MAM), further metabolism via factors of the colonic flora form a highly reactive alkylating species, most likely methyldiazonium, which then causes alkylation of DNA guanine to O6-MEG and O4-methylthymine. Tumorigenesis is then initiated through several key components of the MAPK and Wnt signalling pathways including K-ras, β-catenin and TGFβ (Chen and Huang, 2009; Neufert et al., 2007; Takahashi and Wakabayashi, 2004). Since this initial study AOM has been used in rodents to provide a highly reproducible model of human CRC, with several thousand studies now published using this model (Rosenberg et al., 2009). The AOM model of CRC has been historically used in rats, however it is now more commonly used in mice due to the availability of recombinant inbred strains, associated genetic information and the ability to create transgenic knockin and knockout genetic models (Rosenberg et al., 2009).

Although the AOM mouse model has been used comprehensively to examine the pathology of CRC, there is currently reported a broad variation in treatment methods and results which make it difficult to conduct cross study comparisons (Bissahoyo et al., 2012). While the genetic manipulation obtainable in mouse models is an excellent tool for investigating the pathology of CRC there are a range of modifiers that need to be considered when using AOM to drive tumorigenesis. Several factors may affect susceptibility to AOM induced CRC, genetic background is the most notable modifier of tumorigenesis in the AOM model with susceptibility to AOM driven tumorigenesis reported to vary considerably between differing inbred strains (Bissahoyo et al., 2012; Chen and Huang, 2009; Neufert et al., 2007). In addition to these genetic effects, environmental effects such as variances in housing, enrichment, diet and the intestinal microflora in animals bred at differing animal facilities have all been shown to play a role in altering tumour development (Bissahoyo et al., 2012; Chen and Huang, 2009; Neufert et al., 2007).

Targeted inactivation of DPP4 and FAP is shown to produce healthy mice that are fertile with no explicit developmental defects (Keane et al., 2012; Marguet et al., 2000; Niedermeyer et al., 2000). DPP4 knockout mice (Dpp4-/-) have been beneficial in delineating the mechanism of action of DPP4 *in vivo*. DPP4 knockout animal models have been used to define the role of DPP4 in incretin degradation and glucose homeostasis and have been useful in identifying peptide substrates of DPP4 through quantification of peptide profiles following genetic ablation (Marguet et al., 2000). Dpp4-/- mice are protected from obesity when fed a high fat diet, are resistant to the development of glucose intolerance, and have a diminished cytokine response to antigenic stimulation, highlighting a role for DPP4 in the regulation, development, and migration of CD4+ T, NK and NKT cells (Coburn et al., 1994; Conarello et al., 2003; Yan et al., 2003). Although Dpp4-/- mice themselves do not present with major defects in lymphocyte activation or immune function. FAP knockout mice (Fap-/-), like Dpp4-/- mice are resistant to diet induced obesity; and remain lean, glucose tolerant and insulin sensitive when maintained on a high fat diet (Gorrell et al., 2010). Similar results are also seen with administration of targeted FAP inhibitors in mice indicating that as seen with DPP4, targeted inhibition of FAP may also have a role in metabolic regulation (Ryabtsova et al., 2012; Sánchez-Garrido et al., 2016).

The use of the AOM model in conjunction with Dpp4-/- and Fap-/- genetic models will allow targeted investigation of how the Dpp4-/- and Fap-/- genetic background influences the extent of CRC. Although Dpp4-/- and Fap-/- mice have been studied for over a decade they have not been previously reported in conjunction with the AOM model of CRC and an AOM driven tumour susceptibility profile has not been established in these mice. The Dpp4-/- and Fap-/- mice used in this work were bred on a C57Bl/6 background. In the AOM model tumours are expected to occur in wildtype C57Bl/6 mice at 30 weeks after the sixth 10mg/kg AOM injection (Neufert et al., 2007). Surprisingly in previous work conducted using this AOM murine model to study early neoplastic changes six weeks after the sixth AOM injection, in addition to observing the expected large aberrant crypt foci in the distal colon, small tumours were also observed in control mice (Rudd et al., 2019). This indicated under our experimental conditions this model led to more aggressive tumour progression than previously reported in the literature. In addition, analysis of the liver weight to body weight ratio of the 64 mice used in this study showed a defined subset of mice presenting with low adult body weight of less than 24 grams and small livers weighing less than 0.5 grams. Visual examination of the mice presenting with low liver weights showed that this subset of mice had small livers that were light in colour with a hardened contracted appearance indicating heightened levels of liver damage and potential liver fibrosis.

Building on the results described above the aims of work in chapter three were in the C57Bl/6 background to :1) To refine the AOM model to identify mice with AOM driven liver damage early for removal from the experiment. Metabolism plays a role in the development of CRC, removal of mice presenting with liver damage would reduce cofounding variable influence on results due to reduced liver function altering the phenotype, while also reducing animal distress. 2) To confirm the number of weeks required to develop tumours in wildtype, Dpp4-/- and Fap-/- mice under our diet and environmental conditions. Previous results from our group suggested tumour development had already occurred six weeks after the sixth AOM injection in wildtype mice, so we needed to check this result was reproducible. 3) Determine the efficacy of the use of the AOM model on Dpp4-/- and Fap-/- mice by monitoring the overall health and condition of the mice over the experimental period. It is possible that the knockout of these genes, may lead to an exacerbation or protection against disease symptoms in these mouse strains.

3.2 Materials and Methods

3.2.1 AOM model of colorectal cancer (CRC)

The experimental design for this work was adapted from an established AOM model of induced carcinogenesis (Fu and Lawrance, 2015). All animal work was conducted according to the Australian Code of Practice for the Care and Use of Animals for Scientific Purposes under the Flinders University Animal Ethic Committee approval notice 828-12. A pilot study consisting of five mice from each treatment group was undertaken as a starting point for this work as recommended by the Animal Ethics Committee. For the pilot study mice were acclimatised to the new housing facility for one to two weeks, at eight weeks of age genotoxic damage was induced in wildtype (WT), Dpp4-/- or Fap-/- mice by six weekly intraperitoneal injections of AOM at a dosage of 10 mg/kg bodyweight, with controls administered comparable intraperitoneal injections of saline. For the pilot study the timeline was planned to monitor mice for 24 weeks after the final AOM dosage with sacrifice at 30 weeks as the end point for tissue collection. Results from the pilot study which are discussed in section 3.3.1 showed formation of multiple large tumours in Dpp4-/- and large singular tumours in WT mice at 14 weeks post AOM treatment. Based on these results the AOM model was reduced from a 30 week model with mice being sacrificed 24 weeks after six weeks of AOM treatment, to a 20 week model with mice being sacrificed 14 weeks after treatment (Figure 3.3).

For all work conducted after the completion of the pilot study, mice were acclimatised to the new housing facility for one to two weeks prior to six weekly intraperitoneal injections of

AOM at a dosage of 10mg/kg bodyweight, with controls administered comparable intraperitoneal injections of saline. Mice were then monitored daily for 14 weeks prior to sacrifice and tissue collection (Figure 3.3).

3.2.2 *In vivo* murine model

A total of 80, eight-week-old wild-type C57Bl/6 male mice at an average weight of 23 grams were obtained from the Animal Research Centre (Perth, Australia). The generation of Dpp4-/- and Fap-/- mice has been previously described, mice for this work were inbred on C57Bl/6 background (Marguet et al., 2000; Niedermeyer et al., 2000). Eighty Dpp4-/- and 60 Fap-/- male mice on a C57Bl/6 genetic background were obtained from Professor Mark Gorrell, Centenary Institute, Sydney, Australia in batches. Dpp4-/- and Fap-/- mice were received at six to eight weeks with Dpp4-/- mice weighing an average of 20 grams and Fap-/- mice weighing an average of 23 grams. Mice were acclimatised to the new animal facility for one to two weeks before commencing the first of six weekly intraperitoneal injections of 10 mg/kg AOM for treatment animals and controls were administered saline only. This adjustment period allowed for recovery from any weight loss due to travel stress and was also used to ensure all Dpp4-/- mice were 20 grams in weight or more before commencing AOM treatment. Due to the lean body type of Dpp4-/- mice, the average weight was between 20 to 22 grams at eight weeks of age compared to WT and Fap-/- mice which had an average weight of 23 grams. A minimum of 30 replicate mice were used in each treatment and control group. During experimental conditions Dpp4-/- and WT mice were kept at a maximum cage density of five mice per cage, but due to overtly aggressive behaviour observed in the Fap-/- mice and the resulting injuries which is covered in detail in the results section 3.3.1, Fap-/- mice were housed at a consistent cage density of two animals per cage which was proven to eliminate instances of aggression.

Mice were housed within a quarantine room in individually ventilated cages with High Efficiency-Particulate Air (HEPA) filtering to remove AOM metabolites from the cage and were maintained at 22 ± 2°C on a 12-hr light/dark cycle. Personal respirators with HEPA filters were used by staff during the six-week AOM experimental period, when injecting mice, monitoring, and when cage cleaning was performed to reduce exposure to vaporized AOM as it is carcinogenic and hepatotoxic for humans (Hori et al., 2011). Cages were cleaned twice a week as well as 72 h after AOM injection to remove AOM particulate waste. All cage components, water and food receptacles, bedding and enrichment, were replaced, with housing and all other cage components sterilised by autoclave at 121^0C for 20 min. Mice were given food and water ad libitum and were fed a high protein and high energy diet consisting of Gordons rat and mouse premium breeder diet, 23% protein and 6% fat with a

metabolizable energy (ME) content of 13 mj/Kg. This food is noted as providing sufficient protein, fat and energy to support maximal growth in male mice consuming a purified and sterilized diet (National Research Council, 1995), a complete breakdown of the diet composition is included in the appendix (section A.2). All food was sterilised before use via autoclave at 121^0C for 20 min. To assess general health parameters mice were weighed three times a week, or daily if showing signs of weight loss, and monitored daily for signs of ill health. Mice showing a continual weight loss of more than 15% initially (10% later in the study) from maximum body weight, or, continual signs of ill health including, lethargy and lack of motility, dehydration, noted by recovery when pinching the skin over the shoulder blades, extreme hair loss, laboured breathing, sunken or cloudy eyes, or large amount of blood in their stools for three continuous days, were eliminated from the study.

3.2.3 Blood and Liver Collection

Fourteen weeks after the final dose of AOM, deep terminal anaesthesia was induced by placing the mice for two to three minutes in an induction chamber filled with three to five percent volume-to-volume (v/v[1]) isoflurane (Forane, 1-chloro-2,2,2-trifluoroethyldifluoromethyl ether) (Constantinides et al., 2011). Once anesthetised mice were moved from the induction chamber and placed in a ventilator face mask administering a continual dose of three to five percent isoflurane, blood samples were then obtained via cardiac puncture prior to cervical dislocation (Morton et al., 2001; Szczesny et al., 2004). Blood was collected into sample coded sodium heparinised-EDTA vials (BD Microtainer®), with 10 individual blood samples from each treatment group sent to Gribbles Pathology, South Australia, to test blood biochemistry and haematology parameters. In addition, six blood samples from different mice in each treatment group were collected and sent to the Australian Proteome Analysis Facility (APAF) for quantification of metabolic hormones and cytokines involved in inflammatory and immune response. Methods and results for APAF samples are described in further detail in chapter four. After blood collection and cervical dislocation mice were dissected immediately for removal of colons as described in chapter four.

3.2.4 Statistical analysis

Statistical analysis was performed using GraphPad Prism version 6.0.0 for Windows, GraphPad Software, San Diego, California USA (www.graphpad.com, California, USA). A one-way ANOVA test was performed to compare the treatment groups to the control group with a Tukey's multiple comparison test applied to determine significant differences between

the means of individual groups. For analysis of results a probability level of $p \leq 0.05$ against control was considered as statistically significant.

3.3 Results

3.3.1 Preliminary evidence of liver damage in AOM treated mice

Previous work conducted by our group used a 14-week AOM model on C57BL/6 mice sourced from the Animal Research Centre in Perth. In this model, mice were administered a potential chemo-preventative indole, 6-bromoisatin or oil control. Two weeks after the first dose of 6-bromoisatin mice received six weekly intraperitoneal injections of AOM at a dosage of 10 mg/kg bodyweight. The end point of this model for euthanasia and tissue collection was six weeks post final AOM treatment. The shorter time point was used to measure pre-cancerous ACF formation. Analysis of the liver weight to body weight ratio of the 64 mice used in Rudd et al, 2019, showed two defined subsets within the group.

A larger group of 47 mice with liver weights within the average reported for C57BL/6 male mice between 1 and 1.5 grams and body weights 25 grams and over was observed. In addition a second smaller group of 17 mice with liver weights 0.5 grams or less which was well below the average reported for C57BL/6 male mice and body weights under 24 grams (Figure 3.1). Visual examination of the livers that were low in weight showed these livers were lighter in colour, with a harder contracted appearance indicating potential liver fibrosis. This work indicates that AOM leads to permanent liver damage in a subset of C57BL/6 male mice which would be a confounder in any CRC studies using this model. Thus, it was clear that the model needed further refinement to remove this confounding variable, but more importantly to reduce stress and suffering that may occur in mice with this extent of liver damage, but not evident in the parameters that we were monitoring.

3.3.2 Pilot study of AOM model in Dpp4-/- and Fap-/- mice

This new study commenced with a pilot study consisting of five mice from each treatment group as recommended by our Animal Ethics Committee. The first most prominent finding identified during the pilot study was that Fap-/- mice displayed compulsive repetitive behaviours such as overgrooming and were also overtly aggressive sustaining severe injuries from in cage fighting. Several Fap-/- mice had to be euthanised due to excessive injury at the beginning of the pilot study prior to AOM treatment. To combat this aggression the cage density for Fap-/- mice was reduced from five to two mice per cage, this reduced the instances of aggression while allowing socialisation, preventing adverse effects from social isolation stress (Chen et al., 2016). Aggression in Fap-/- mice was also noted to be
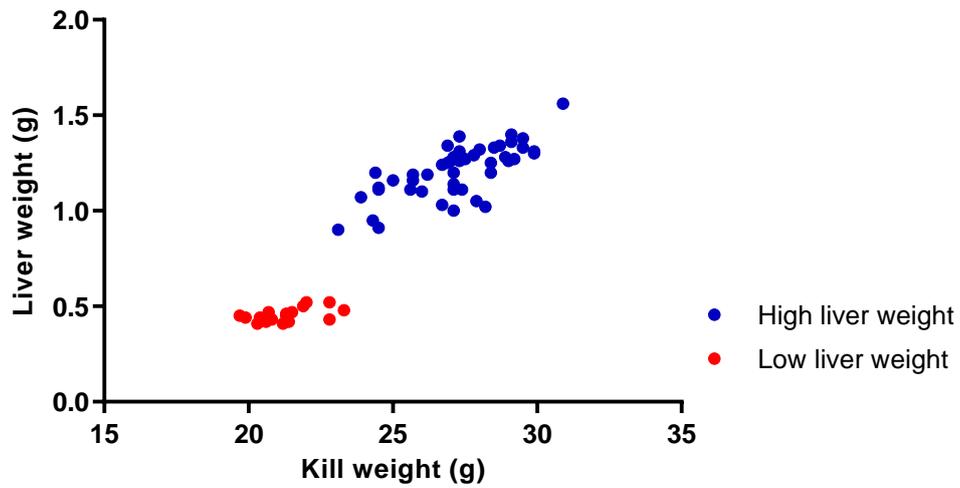
Figure 3.1. A subset of C57Bl/6 mice at six weeks post AOM treatment present with low liver and total body weight. Mice were administered six weekly intraperitoneal injections of 10mg/kg AOM and at six weeks post AOM treatment mice they were euthanised and their kill weight and liver weight recorded (Rudd et al., 2019).

Figure 3.2. Example of enrichment used in all mouse cages. Enrichment was sterilised by autoclave at 121^0C for 20 min and was replaced when cages were cleaned twice a week as well as 72 hr after AOM injection.

worse directly after transport to the Flinders University animal house facility. To reduce this post transport aggression, bedding from the transport cage was included in the new cage housing for the first few days after arrival. This was shown to eliminate all post transport aggression. In addition to the reduced cage density, enrichment in the form of housing and hides made from small cardboard boxes and tubes was included in all cages throughout the study (Figure 3.2.) This provided all mice in the study, areas where they could hide from view which is essential to their well-being, but also helped to reduce repetitive behaviours, aggression and in cage fighting in Fap-/- mice (Bailoo et al., 2018).

In the pilot study Dpp4-/- and Fap-/- mice were able to tolerate AOM at 10mg/kg over six weekly doses without adverse effects directly after dosage or during the treatment period. In addition to these findings one AOM treated Dpp4-/- mouse had to be eliminated at four weeks, during AOM treatment, and four WT AOM treatment mice had to be eliminated at 18 weeks, 12 weeks after the last AOM injection, from the pilot study early due to excessive weight loss of greater than 15% of their total max body weight as per approved ethics conditions. Examination of these mice highlighted that they all had small livers weighing less than a gram that on comparison with livers from saline treated mice appeared lighter in colour with a harder contracted appearance. These results tied into those seen with our earlier work identifying a subset of mice treated with AOM that present with potential liver damage and associated weight loss and identified an area for refinement where these mice if identified correctly could be removed from the study early.

3.3.3 Refinement of weight loss cut off point

Analysis of the mice eliminated from the pilot study for greater than 15% weight loss showed that each mouse took time to reach this point. The mice sometimes displayed small weight gains and losses over a prolonged period but with an overall weekly weight gain that was greatly reduced compared to littermates. Due to breeding cycles and availability of Dpp4-/- and Fap-/- mice our work was conducted in batches over a greater than 12-month period. Initially weight data for the first three batches of mice which included 15 WT, 7 Dpp4-/- and 10 Fap-/- AOM treated mice and 15 WT, 7 Dpp4-/- and 10 Fap-/- saline treated controls was analysed. It was identified that in some instances overall weight loss in AOM treated mice never reached the 15% from max point although mice failed to make any significant gain in weight over the entire length of the trial. Study of the thrice weekly weight monitoring for these mice showed that all mice eliminated for excessive weight loss consistently showed a greater than 10% weight loss from max weight by the end of the AOM treatment period while no other mice in the treatment group dropped to this 10% from max point.
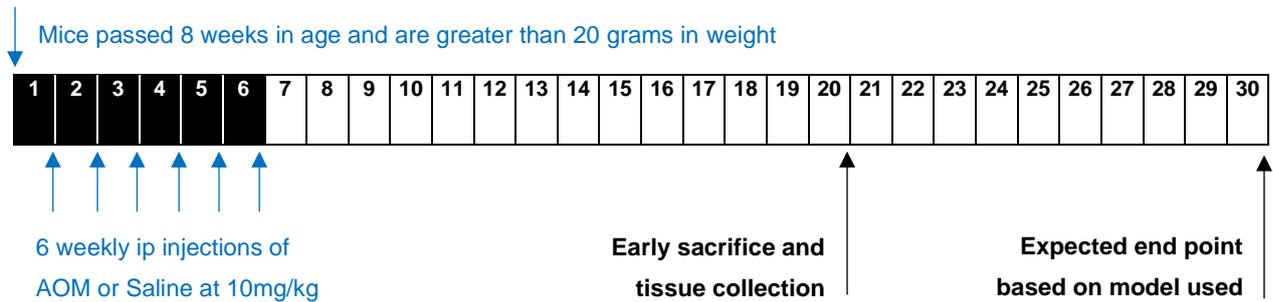
Figure 3.3. Outline of AOM murine model of CRC development. Mice are eight weeks in age and at least 20 grams in weight at entry to the model then receive six weekly intraperitoneal injections of either saline or AOM at a dose 10 mg/kg. DPP-/- mice presented with rectal bleeding and colonic prolapses related to tumour load, thus were sacrificed for tissue and blood collection 14 weeks after final AOM or saline treatment. This timepoint was ten weeks earlier than the expected sacrifice point of 24 weeks post treatment.

To further investigate the 10% weight loss cut off point, weight analysis of the first 15 mice from each treatment group was undertaken after the trial end point was reached for these mice (Figure 3.4, Figure 3.5, Figure 3.6). This analysis showed that all AOM treated WT (Figure 3.4) and Dpp4-/- mice (Figure 3.5) presented with small livers with liver weights well below the average of 1.44g for male C57Bl/6 mice also showed weight loss greater than 10% from their max weight during or shortly after AOM treatment with a plateaued weight profile after this point. The outcomes of this analysis also confirmed that moving the weight loss cut off from 15% from max weight to 10% would allow elimination of these mice earlier from the work reducing distress and suffering as well as ensuring end point analysis was not skewed by the potential presence of liver damage. It was also confirmed that moving the weight loss cut off point to 10% would not result in early elimination of mice with livers greater than one gram. Mice removed early for weight loss were not included in the end point results for this work (chapter four). Prior to refinement of the weight loss cut off point some mice with small livers completed the 20-week trial, these mice often did not lose enough weight to be eliminated under the 15% cut off parameter. Any mice who presented with livers weighing less that one gram at the trial end point were not included in the end point results of this work presented in chapter four.

At the timepoint used to conduct this weight analysis AOM treated Fap-/- mice did not show any signs of excessive weight loss (Figure 3.6) and at the end of the study only two mice out of the 30 used in the Fap-/- AOM treatment group were seen to have smaller livers weighing less than one gram, although these livers were only just under a gram weighing approximately 0.9g. Saline treated WT, Dpp4-/- and Fap-/- mice for this analysis had expected weekly weight increases with no mice in these groups losing more than 10% from their max weight and all had healthy liver weights over one gram at completion of the trial (Figure 3.4 C, Figure 3.5 C).

3.3.4 Adjustment of timeline due to early tumour development

During the pilot study four WT mice were eliminated at 12 weeks post treatment for weight loss in excess of 15% from max body weight, examination of the colons of these mice showed formation of large singular tumours. One Dpp4-/- mouse was eliminated at four weeks for weight loss and the four remaining Dpp4-/- mice had to be sacrificed at 14 weeks post AOM treatment due to excessive rectal bleeding. Due to the large tumours seen in the WT mice eliminated early for weight loss the final WT remaining in the pilot study was also sacrificed at 14 weeks. Examination of the colons of the mice at 14 weeks post treatment showed formation of multiple large tumours in Dpp4-/- and large singular tumours in WT mice. This was an unexpected result as advanced tumour presence in the AOM model used
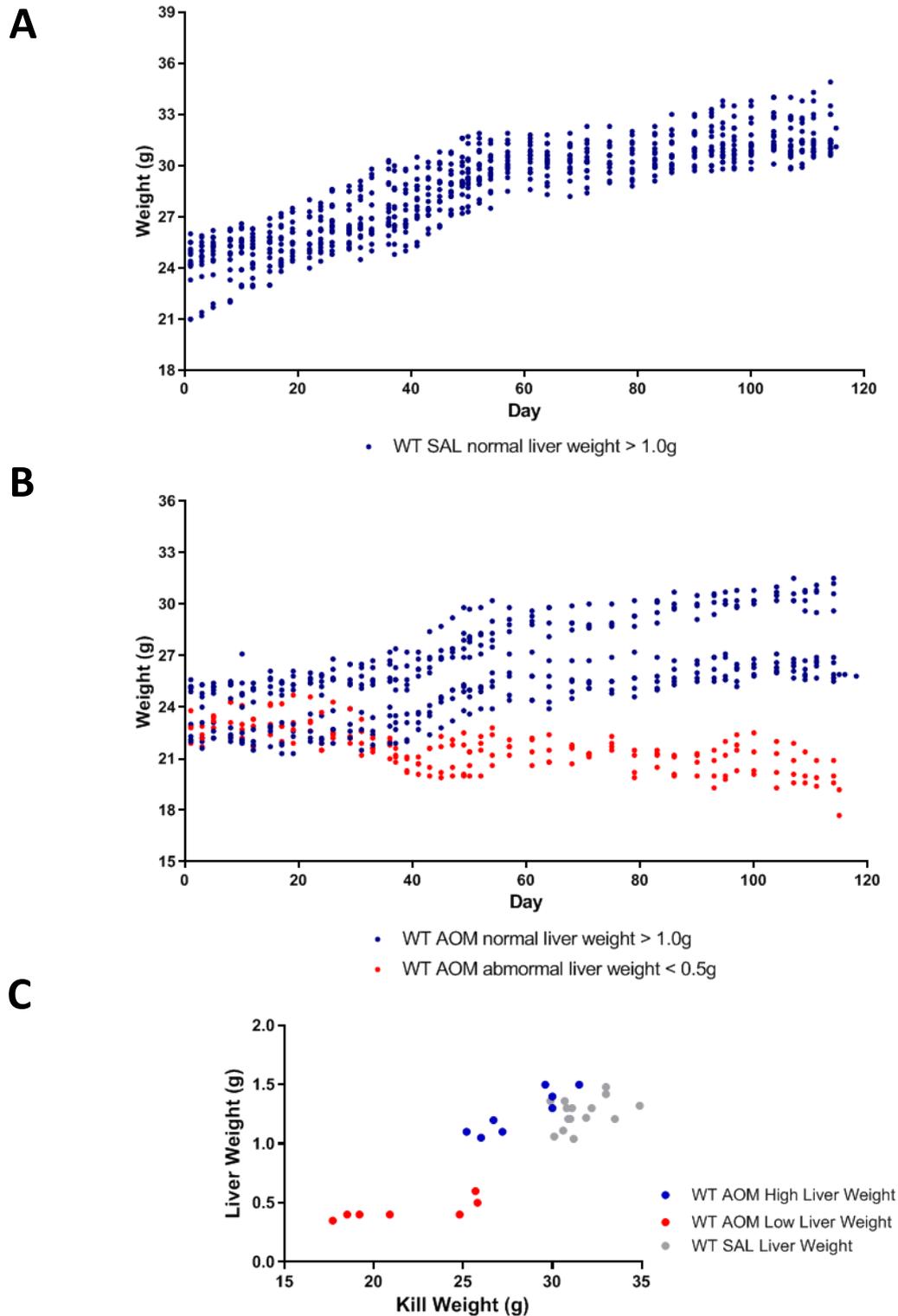
Figure 3.4. Analysis of AOM treated WT mice identifies a population subset with low liver and body weight. Measurement of body weight of male WT C57Bl/6 mice taken every three days for 120 days for A) saline treated WT mice (n=15), B) Six x 10 mg/kg AOM treated WT mice (n=15), C) comparison of mean kill weight (g) and liver weight (g) at 14 weeks post saline (n=15) and AOM treatment (n=15) for WT mice.

A

B

C
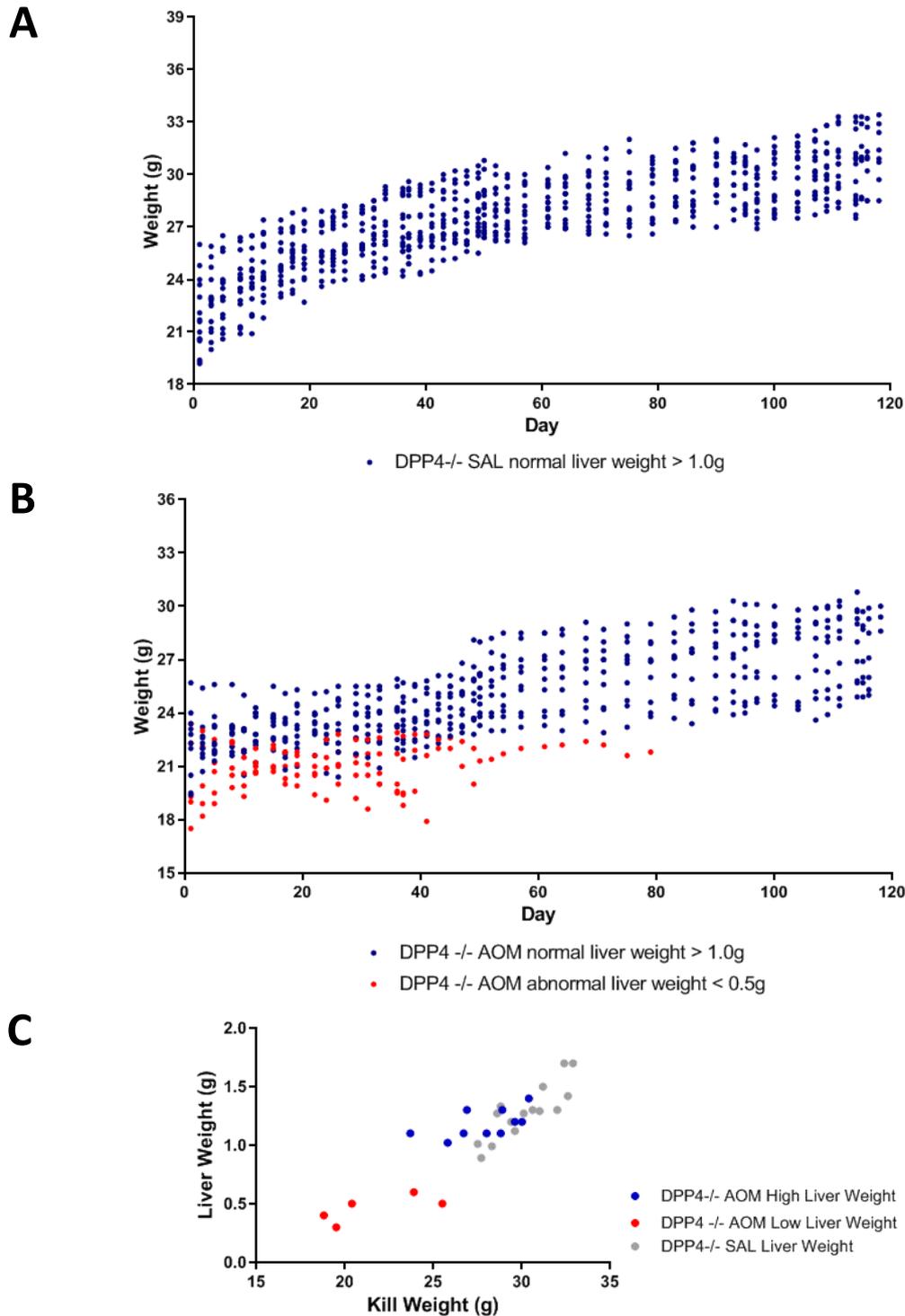
Figure 3.5. Analysis of AOM treated Dpp4-/- mice identifies a population subset with low liver and body weight. Measurement of body weight of male Dpp4-/- C57Bl/6 mice taken every three days for 120 days for A) saline treated Dpp4-/- mice (n=15), B) Six x 10 mg/kg AOM treated Dpp4-/- mice (n=15), C) comparison of mean kill weight and liver weight at 14 weeks post saline (n=15) and AOM treatment (n=15) for Dpp4-/- mice.
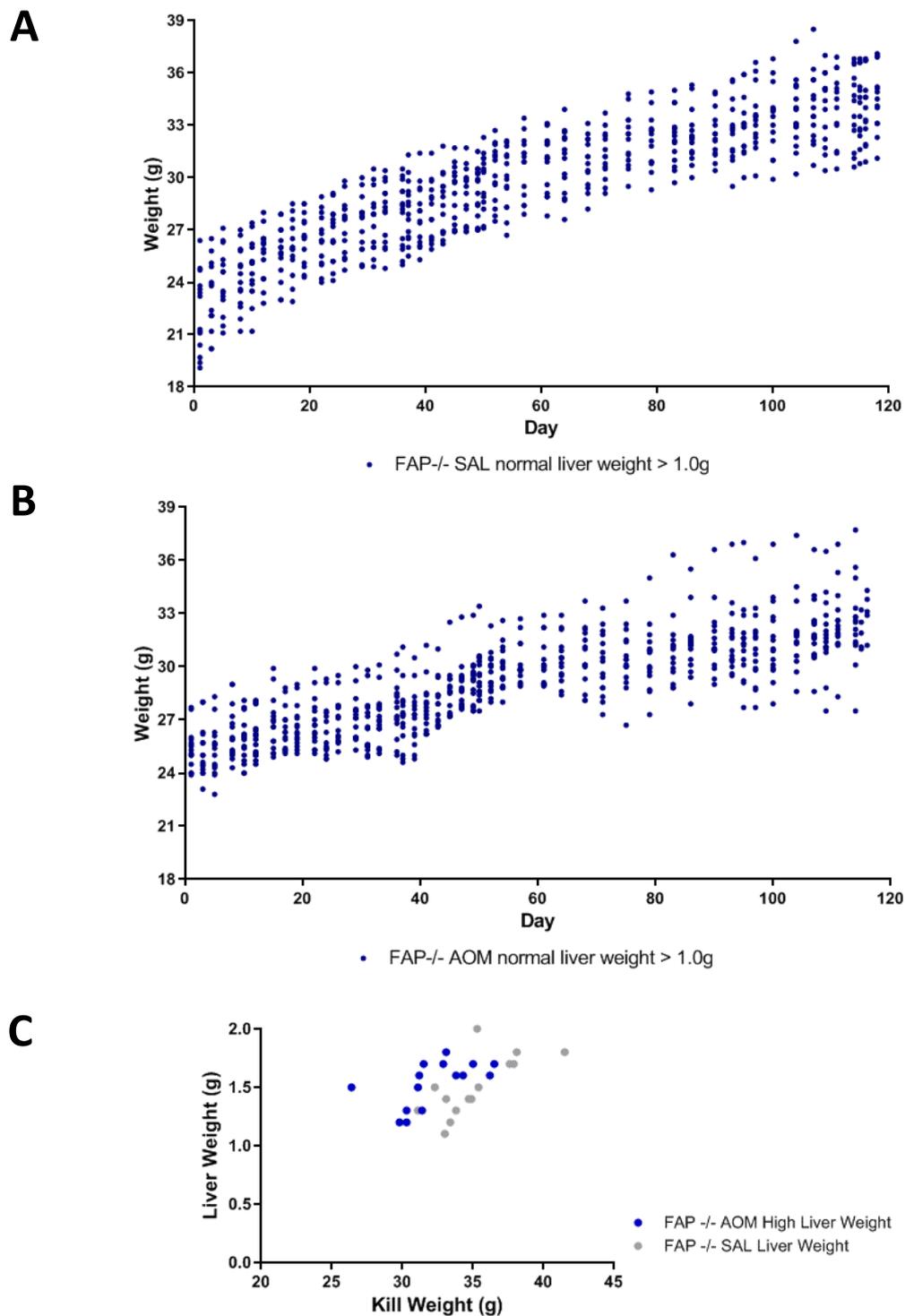
**Figure 3.6.** Analysis of AOM treated Fap-/- mice identifies no population subset with low liver and body weight. Measurement of body weight of male Fap-/- C57Bl/6 mice taken every three days for 120 days for A) saline treated Fap-/- mice (n=15), B) Six x 10 mg/kg AOM treated Fap-/- mice (n=15), C) comparison of mean kill weight and liver weight at 14 weeks post saline (n=15) and AOM treatments (n=15) for Fap-/- mice.

was not expected to occur until 24 weeks posttreatment (Neufert et al., 2007; Rosenberg et al., 2009). In previous work from our group mice developed large pre-cancerous ACF, and small tumours were observed in the distal colon at six weeks post treatment (Rudd et al., 2019). However, no symptoms of CRC such as rectal bleeding, bowel prolapse, or weight loss were observed six weeks post AOM. Based on the results from this pilot study, particularly the results for Dpp4-/- mice where large tumour load was causing undue discomfort (observed as rectal bleeding and prolapse), the timeframe of this model was refined. The AOM model was reduced from a 30 week model with mice being sacrificed 24 weeks after six weeks of AOM treatment, to a 20 week model with mice being sacrificed 14 weeks after treatment (Figure 3.3) (Hu et al., 2005). Results relating to ACF and tumour formation in these mice are presented and discussed in chapter four.

3.3.5 Body weight disparity between WT, Dpp4-/- and Fap-/- mice

Both during and at completion of the trial there was body weight disparity between WT, Dpp4-/- and Fap-/- mice. Saline and AOM treated Dpp4-/- mice had an average body weight increase per week, as well as an end point total body weight, that was below the average for male C57Bl/6 mice (Figure 3.7 A, B, D, Figure 3.8 A), while average weights for Fap-/- mice were comparable to the average weight increase and adult weight reported for C57Bl/6 male mice (Figure 3.7 A, C, Figure 3.8 A). In analysis of saline treated mice at 14 weeks post AOM treatment, Dpp4-/- mice showed a total body weight and an average weekly body weight increase over 20 weeks that was significantly lower when compared to WT mice ($p < 0.001$ and $p < 0.05$ respectively) and Fap-/- mice ($p < 0.001$) (Figure 3.7 A, Figure 3.8 A). Fap-/- mice also showed a significant increase in total body weight at 14 weeks post AOM treatment when compared to saline treated WT mice ($p < 0.05$) (Figure 3.8, A).

In comparison between AOM and saline treated mice, AOM treated Dpp4-/- mice show no significant difference in their average weekly body weight increase and final body weight when compared to saline treated controls (Figure 3.7, A, Figure 3.8, A), while AOM treated Fap-/- mice have a significantly lower average weekly body weight increase ($p < 0.05$) and final total body weight ($p < 0.01$) when compared to saline treated Fap-/- mice (Figure 3.7, A, Figure 3.8, A). Average weekly body weight increase and final body weight was significantly lower in AOM treated WT mice compared to saline treated WT mice ($p < 0.001$) (Figure 3.7, A, Figure 3.8, A).
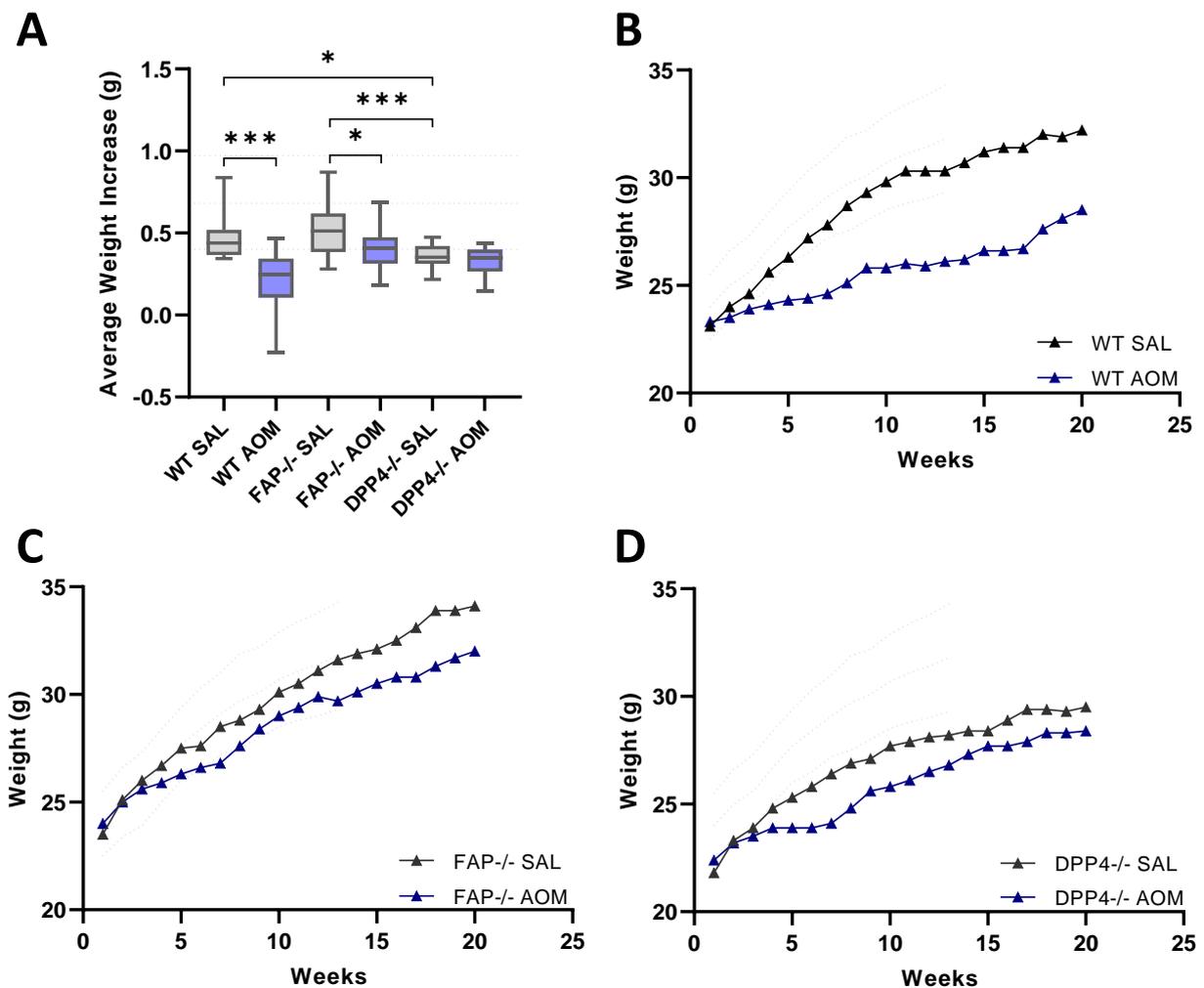
Figure 3.7. Average weekly weight increase in Dpp4-/- mice is not significantly impacted by AOM treatment. Comparison of body weight increase in saline treated WT (n=30) and AOM treated WT (n=44), saline treated Fap-/- (n=30) and AOM treated Fap-/- (n=28), saline treated Dpp4-/- (n=30) and AOM treated Dpp4-/- (n=36) mice over 20 weeks. A) Comparison of average body weight increase per week over 20 weeks in each treatment group; body weight increase comparison for AOM and saline treated B) WT mice, C) Fap-/- mice, D) Dpp4-/- mice. Light grey dashed lines indicate average, upper and lower 95 percentile range in healthy male C57Bl/6 mice as reported by The Jackson Laboratory (The Jackson Laboratory, 2019), asterisk denotes significance at the * <0.05 and *** <0.001 probability level between groups. Values represent means and error bars ± standard error (SEM).
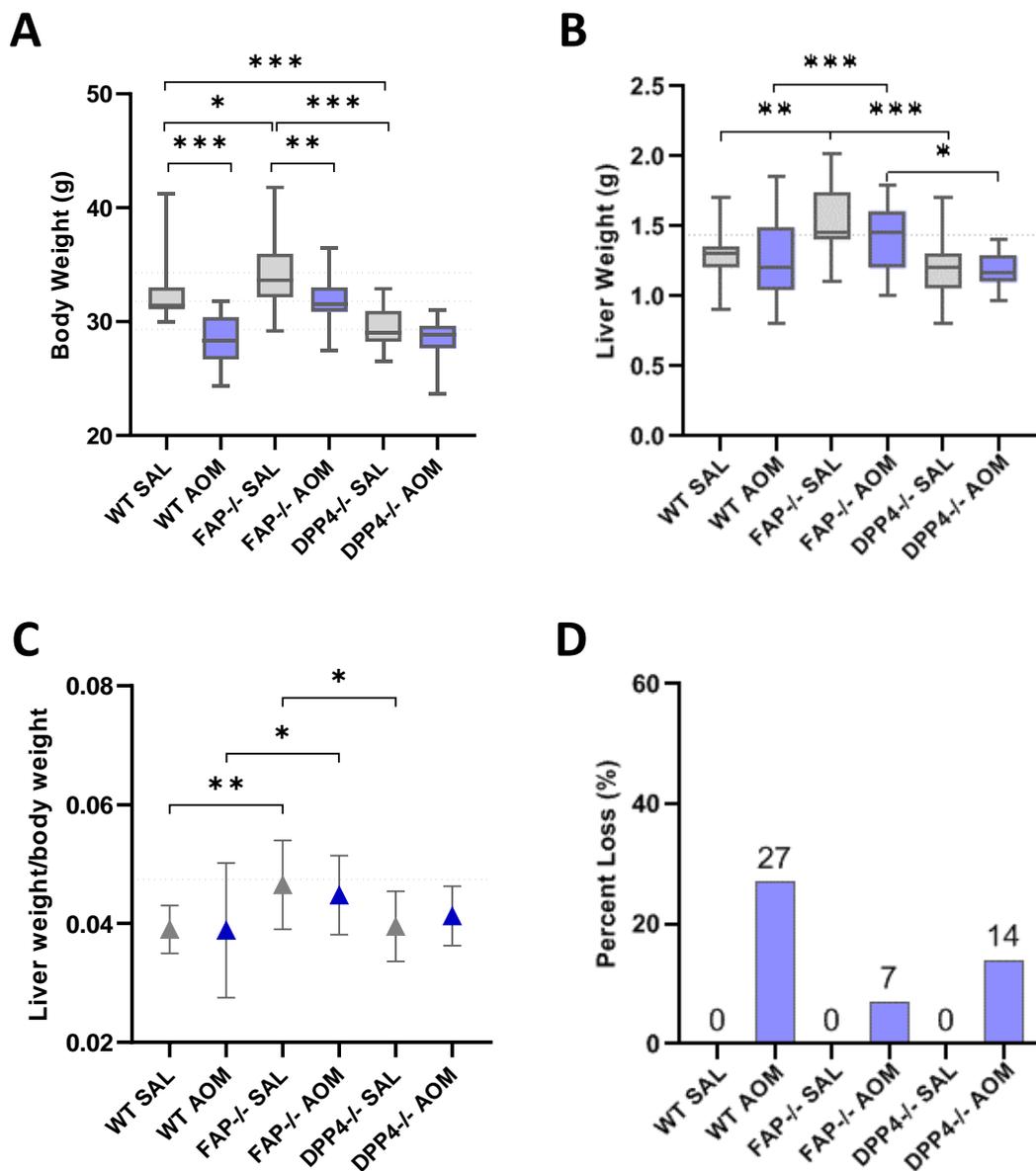
Figure 3.8. Dpp4-/- mice have reduced while Fap-/- mice have increased, body and liver weight on comparison with WT mice. Body and liver weight differences between saline treated WT (n=30) and AOM treated WT (n=44), saline treated Fap-/- (n=30) and AOM treated Fap-/- (n=28), saline treated Dpp4-/- (n=30) and AOM treated Dpp4-/- (n=36) mice 14 weeks post AOM treatment. A) Average kill body weight, B) average kill liver weight, C) liver weight to body weight ratio, D) number of mice lost as a percentage of total due to weight losses greater than 15% and then 10% stemming from AOM driven liver damage. Light grey dashed lines indicate average, upper and lower 95 percentile range in healthy male C57Bl/6 mice as reported by The Jackson Laboratory (The Jackson Laboratory, 2007, 2019), asterisk denotes significance at the * <0.05, ** <0.01 and *** <0.001 probability level between groups. Values represent means and error bars ± standard error (SEM).
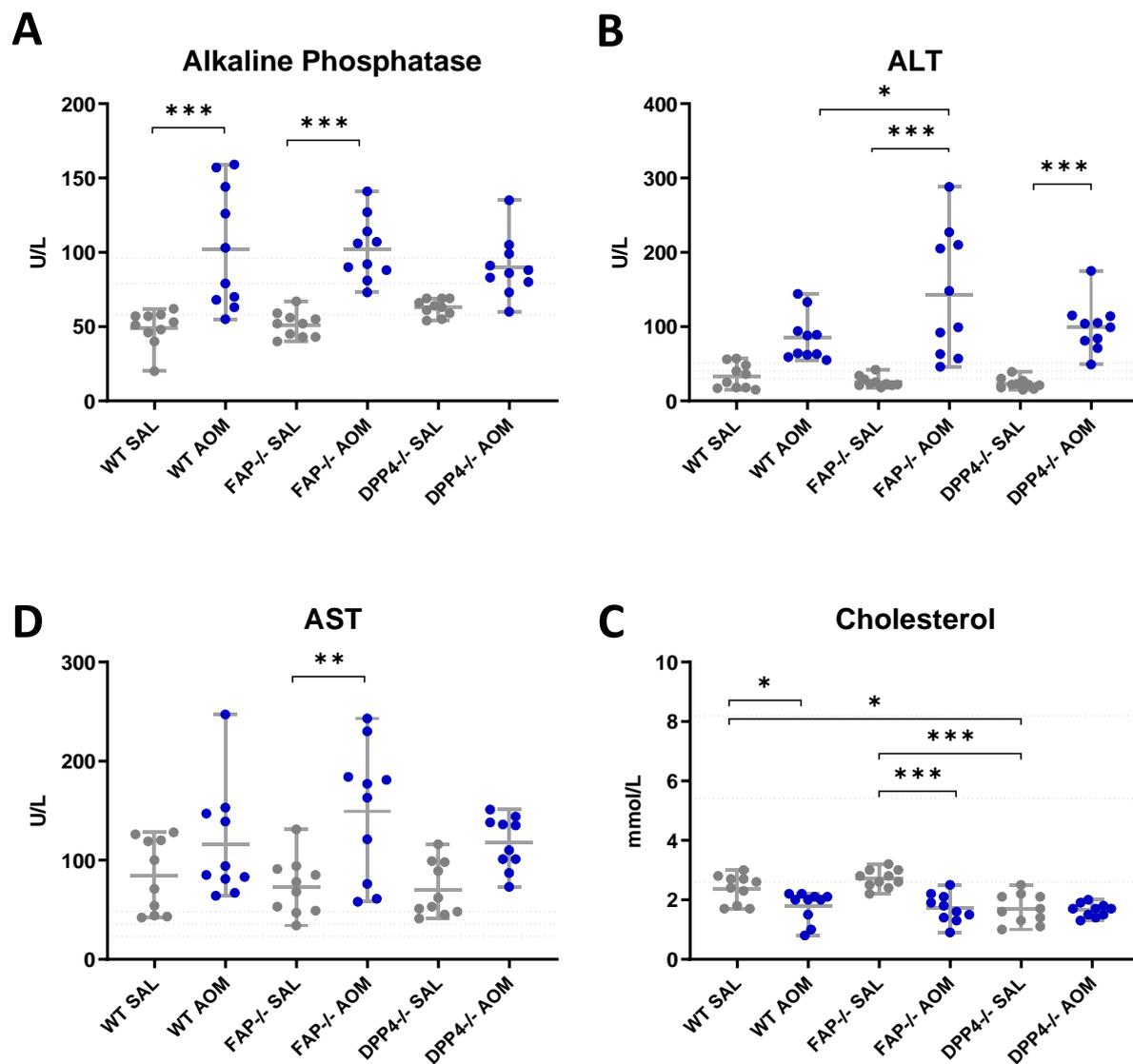
Figure 3.9. AOM treated mice show elevated levels of hepatic damage markers and lower cholesterol levels. Plasma concentrations of A) alkaline phosphatase, B) alanine aminotransferase (ALT), C) aspartate aminotransferase (AST), D) cholesterol, in AOM and saline treated WT, Dpp4-/- and Fap-/- mice at 14 weeks post AOM treatment. Blood pathology determined by Gribbles Pathology on n=10 mice for each treatment group. Light grey dashed lines indicate average, upper and lower 95 percentile range in healthy male C57Bl/6 mice as reported by Jensen, Schnell and The Jackson Laboratory (Schnell et al., 2002; The Jackson Laboratory, 2007; Jensen et al., 2013), asterisk denotes significance at the * <0.05, ** <0.01 and *** <0.001 probability level between groups.
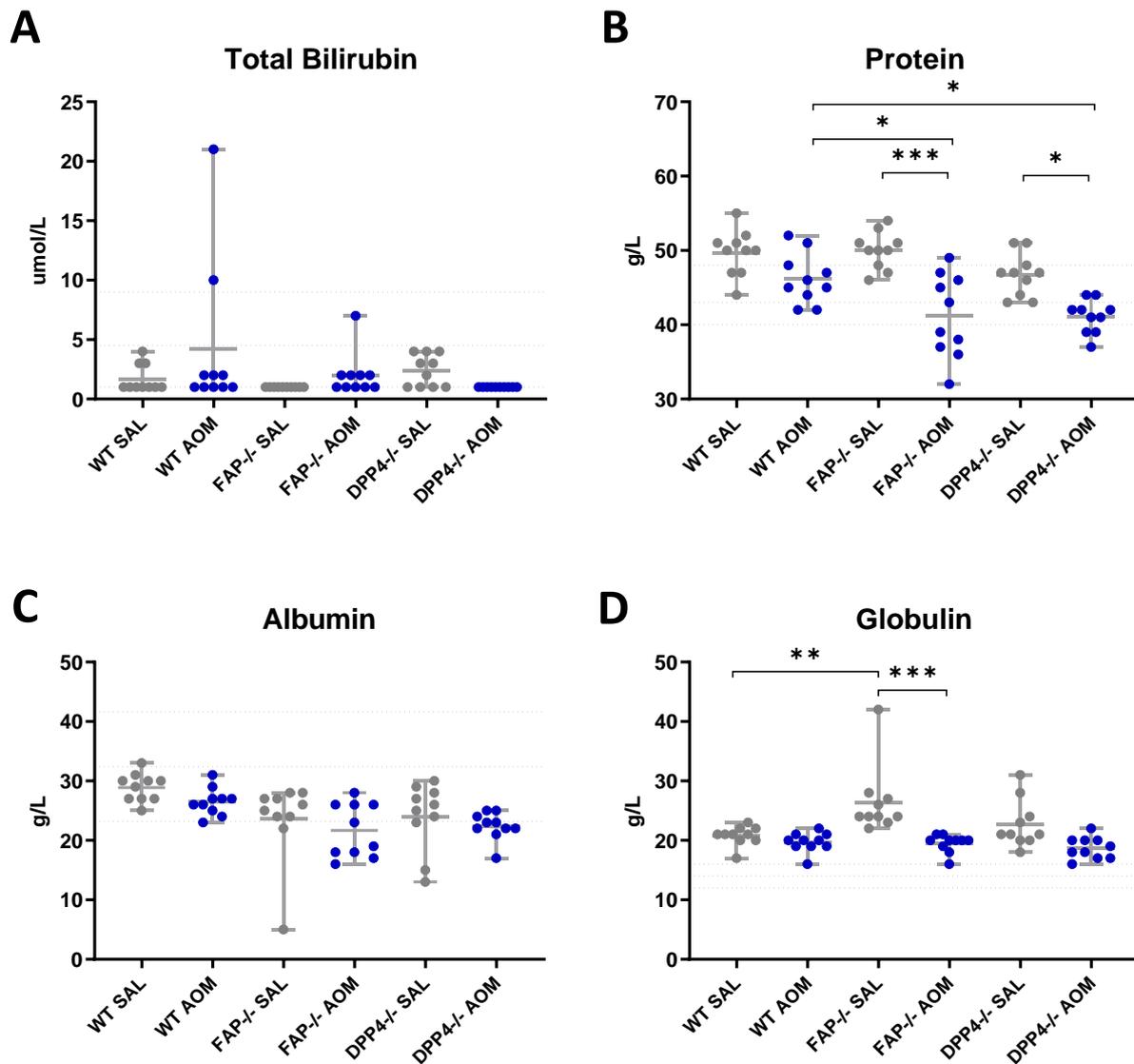
Figure 3.10. AOM treated Dpp4-/- and Fap-/- mice show significantly reduced total protein. Plasma concentrations of A) total bilirubin, B) total protein, C) albumin and D) globulin, in AOM and saline treated WT, Dpp4-/- and Fap-/- mice at 14 weeks post treatment. Blood pathology determined by Gribbles Pathology on n=10 mice for each treatment group. Light grey dashed lines indicate average, upper and lower 95 percentile range in healthy male C57Bl/6 mice as reported by Jensen, Schnell and The Jackson Laboratory (Schnell et al., 2002; The Jackson Laboratory, 2007; Jensen et al., 2013), asterisk denotes significance at the * <0.05, ** <0.01 and *** <0.001 probability level between group

3.3.6 Comparison of liver weight and liver function in WT, Dpp4-/- and Fap-/- mice

Comparison of liver weight between groups reflected the results seen for body weight comparison. Saline treated WT and Dpp4-/- mice had comparable liver weight to body weight ratio while AOM treated WT and Dpp4-/- mice showed no significant reduction in liver weight to body weight ratio when compared to saline treated controls (Figure 3.8, B, C). Saline treated Fap-/- mice showed a significantly increased liver weight at 14 weeks post AOM treatment when compared to WT ($p < 0.01$) and Dpp4-/- ($p < 0.001$) mice (Figure 3.8, B), this correlated to liver weight to body weight ratio where saline treated Fap-/- mice showed a significant increase compared to both WT ($p < 0.01$) and Dpp4-/- mice ($p < 0.05$) (Figure 3.8, C).

On comparison with adult male C57Bl/6 liver weights reported by The Jackson Laboratory (The Jackson Laboratory, 2007) WT and Dpp4-/- mice had liver weights below the average and Fap-/- mice showed liver weights comparable to the average (Figure 3.8, C). Over the course of the first trial and subsequent study, 27% (16/60) of AOM treated WT mice, 14% (6/42) of AOM treated Dpp4-/- mice and 7% (2/30) of AOM treated Fap-/- mice were removed from the final experimental results due to weight loss in excess of ethics approved parameters. All saline treated mice completed the trial with a weekly steady weight increase in all groups (Figure 3.8, D).

In determination of liver function through blood pathology (Figure 3.9), AOM treated WT, Dpp4-/- and Fap-/- mice all showed increased circulating liver enzymes which is an indicator of liver damage. On comparison with reported averaged data for C57Bl/6 mice, saline treated WT mice had alkaline phosphatase levels that were below average, alanine aminotransferase (ALT) levels in the normal range and aspartate aminotransferase (AST) levels above average (Figure 3.9) (Schnell et al., 2002). The alkaline phosphatase, ALT and AST levels were all seen to increase in AOM treated WT mice with a significant increase in alkaline phosphatase ($p < 0.001$) and a non-significant increase in ALT and AST when compared to saline treated controls (Figure 3.9). Saline treated WT mice also had total blood cholesterol levels that were below average for C57Bl/6 mice (The Jackson Laboratory, 2007) and AOM treated WT mice had significantly reduced ($p < 0.05$) cholesterol levels compared to saline treated controls (Figure 3.9). Total bilirubin was below the C57Bl/6 average in both saline and AOM treated WT mice indicating no presence of jaundice (Figure 3.10, A) (The Jackson Laboratory, 2007). As all major blood proteins are synthesized in the liver a measure of total protein as well as individual albumin and globulin levels was undertaken as a marker of liver function. A decrease in total protein and albumin would indicate loss of liver

function while an increase in globulin would indicate dehydration or chronic inflammation (Busher, 1990). Saline treated WT mice had total protein and globulin levels above the average and albumin levels just below the average for C57Bl/6 mice. AOM treatment in WT mice did not have a significant impact on protein levels (Schnell et al., 2002). However, AOM treated WT mice did show significantly higher protein levels when compared to AOM treated Dpp4-/- ($p<0.05$) and Fap-/- ($p<0.05$) mice (Figure 3.10).

Saline treated Dpp4-/- mice showed similar liver enzyme levels to that seen in saline treated WT mice indicating that both phenotypes have comparable liver function (Figure 3.9). Against the reported average for C57Bl/6 mice, saline treated Dpp4-/- mice had alkaline phosphatase levels and ALT levels that were below average, and AST levels above the average (Figure 3.9) (Schnell et al., 2002). AOM treated Dpp4-/- mice showed a significant increase in ALT ($p<0.001$) and a non-significant increase in alkaline phosphatase and AST when compared to saline treated controls indicating liver damage (Figure 3.9). Saline treated Dpp4-/- mice had total blood cholesterol levels below the average for C57Bl/6 mice (The Jackson Laboratory, 2007) that was also significantly lower than that seen for both saline treated WT ($p<0.05$) and Fap-/- mice ($p<0.001$). Dpp4-/- cholesterol levels were not affected by AOM treatment (Figure 3.9). Like WT mice, Dpp4-/- mice showed no presence of jaundice with total bilirubin levels just below the C57Bl/6 average (Figure 3.10, A) (The Jackson Laboratory, 2007). Dpp4-/- mice had total protein levels comparable to WT mice with total protein and globulin levels above the average, and albumin levels just below average for C57Bl/6 mice (Figure 3.10) (Schnell et al., 2002). AOM treated Dpp4-/- mice showed a significant decrease in total protein ($p<0.05$) and a small non-significant decrease in albumin and globulin compared to saline treated controls (Figure 3.10).

Fap-/- mice have alkaline phosphatase and ALT levels below the average, and AST levels above the average for C57Bl/6 mice (Figure 3.9) (Schnell et al., 2002). AOM treatment in Fap-/- mice resulted in a significant increase in alkaline phosphatase ($p<0.001$), ALT ($p<0.001$) and AST ($p<0.01$) when compared to saline treated controls indicating the presence of liver damage (Figure 3.9). Saline treated FAP mice had total blood cholesterol levels that were below the average for C57Bl/6 mice (The Jackson Laboratory, 2007) and AOM treatment significantly reduced ($p<0.001$) cholesterol levels compared to saline treated controls (Figure 3.9). Like WT and Dpp4-/- mice, Fap-/- mice had total bilirubin levels below the C57Bl/6 average (The Jackson Laboratory, 2007) indicating no presence of jaundice (Figure 3.10, A) and total protein and globulin levels above the average and albumin levels just below average (Figure 3.10). AOM treated Fap-/- mice also had significantly reduced total protein ($p<0.001$) and globulin ($p>0.001$), and a slight non-significant reduction in albumin compared to saline treated controls (Figure 3.10) (Schnell et al., 2002).
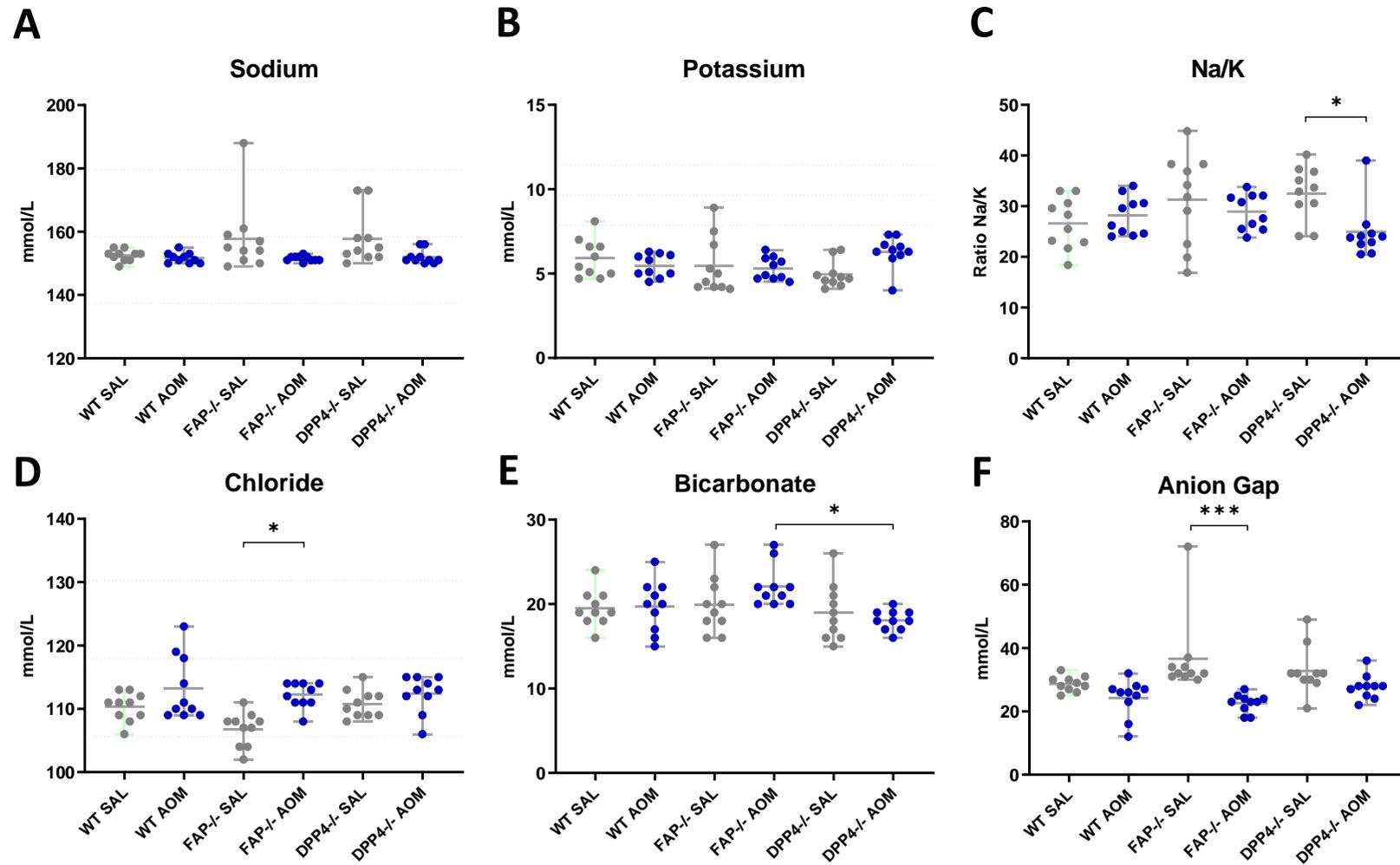
Figure 3.11. Blood biochemistry measurements from AOM and saline treated WT, Dpp4-/- and Fap-/- mice, panel 1. Plasma concentrations of A) sodium, B) potassium, C) ratio of sodium to potassium, D) chloride, E) bicarbonate, and F) anion gap in AOM and saline treated WT, Dpp4-/- and Fap-/- mice at 14 weeks post AOM treatment. Blood pathology determined by Gribbles Pathology on n=10 mice for each treatment group. Light grey dashed lines indicate average, upper, and lower 95 percentile range in healthy male C57Bl/6 mice as reported by The Jackson Laboratory (The Jackson Laboratory, 2021), asterisk denotes significance at the * <0.05 and *** <0.001 probability level between groups.
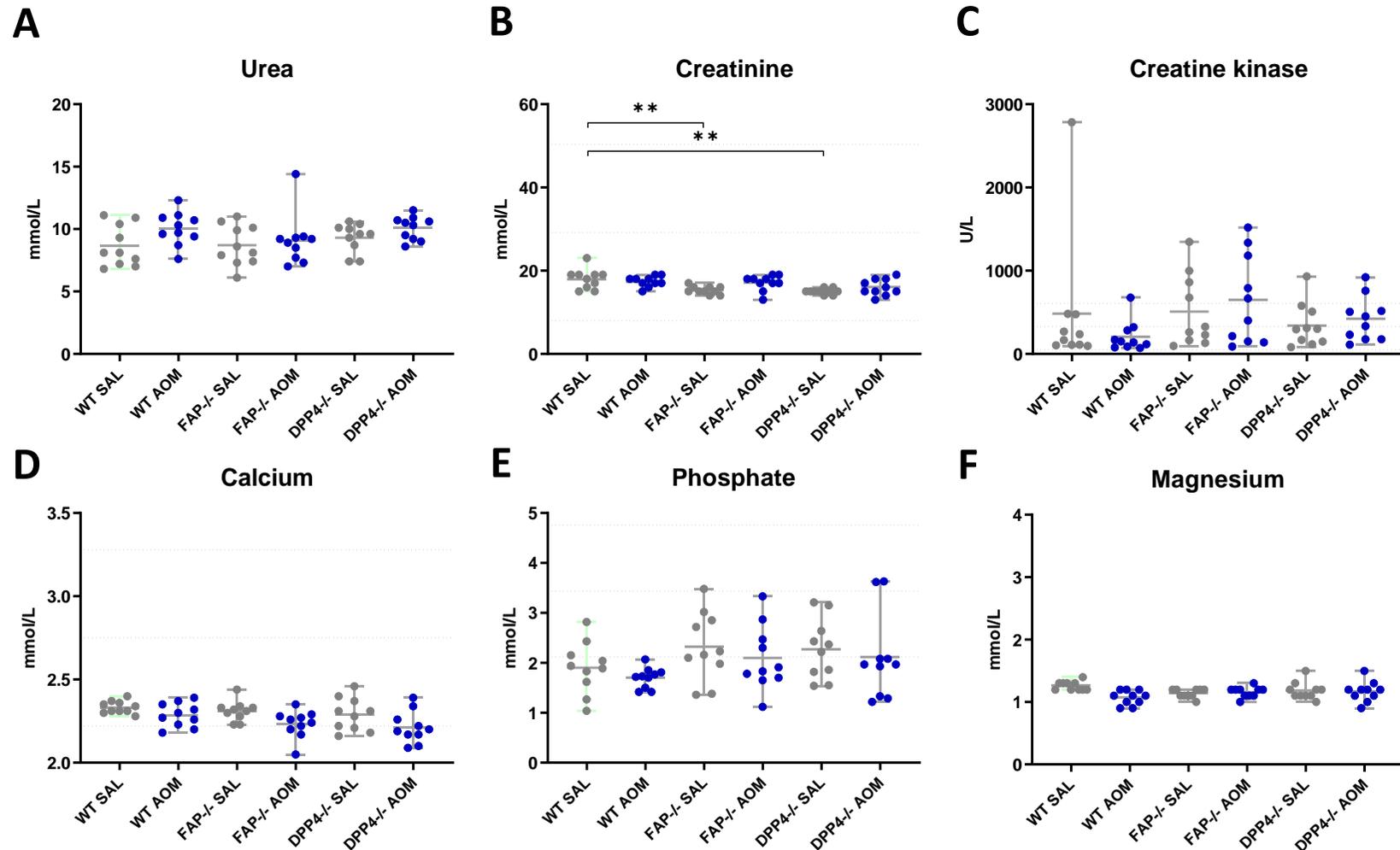
Figure 3.12. Blood biochemistry measurements from AOM and saline treated WT, Dpp4-/- and Fap-/- mice, panel 2. Plasma concentrations of A) urea B), creatinine C), creatine kinase D), calcium, E) phosphate, and F) magnesium in AOM and saline treated WT, Dpp4-/- and Fap-/- mice at 14 weeks post AOM treatment. Blood pathology determined by Gribbles Pathology on n=10 mice for each treatment group. Light grey dashed lines indicate average, upper, and lower 95 percentile range in healthy male C57Bl/6 mice as reported by The Jackson Laboratory (The Jackson Laboratory, 2021), asterisk denotes significance at the ** <0.01 probability level between groups.

3.3.7 Quantification of general blood biochemistry

General animal health was examined by measuring blood biochemistry markers in mice plasma 14 weeks post AOM treatment and in saline controls (Figure 3.11). All three phenotypes had sodium levels within the reported normal range for C57Bl/6 mice and comparable potassium levels below average, and no significant difference between groups was observed for sodium or potassium (Figure 3.11). AOM treated Dpp4-/- mice showed a significantly lower sodium to potassium ratio compared to saline treated controls ($p < 0.05$) and this increase in the sodium to potassium ratio is associated with a non-significant increase in total serum potassium (Figure 3.11). No significant difference in sodium to potassium ratio was seen between AOM and saline treated WT and Fap-/- mice (Figure 3.11). AOM treated Fap-/- mice had significantly higher blood chloride levels compared to saline treated controls ($p < 0.05$) as well as a significantly lower anion gap (< 0.001) (Figure 3.11). As anion gap is the measured difference between the primary cations, sodium and potassium, and the primary anions, chloride and bicarbonate, the decrease in anion gap seen in AOM treated Fap-/- mice is probably due to the increase in serum chloride levels (Lee et al., 2006). AOM treated Fap-/- mice also had significantly increased levels of bicarbonate compared to AOM treated Dpp4-/- mice ($p < 0.05$) (Figure 3.11). No significant difference in chloride, bicarbonate or anion gap was seen between AOM and saline treated WT and Dpp4-/- mice (Figure 3.11). Saline treated wildtype mice showed significantly increased levels of creatinine compared to saline treated Fap-/- ($p < 0.01$) and Dpp4-/- ($p < 0.05$) mice (Figure 3.12). No significant difference between groups was seen for urea, creatine kinase, calcium phosphate or magnesium (Figure 3.12).

3.4 Discussion

Chapter three is the first study to utilise the AOM model of colorectal cancer in Dpp4-/- and Fap-/- mice and establishes that this model of colorectal cancer is suitable for use with these genetic knockouts. In chapter three a monitoring refinement was established that led to improvements in animal welfare when using the AOM model of CRC in C57Bl/6 mice. This work determined that reducing the weight loss cut off point for euthanasia from 15 to 10% weight loss from maximum weight can identify a subset of treated mice where AOM treatment has led to severe liver damage allowing elimination of these mice early from the study. This modification reduces animal distress and suffering tying into the refinement alternative of the three R's principal of animal experimentation which outlines the guiding principles that support the humane use of animals in scientific research (Fenwick et al., 2009). Refinement of the experimental procedures to eliminate mice suffering from potential liver damage early, minimises their pain and distress, enhancing the welfare of experimental

animals as well as ensuring end point analysis is not impacted by cofounding variable influence associated with a secondary disease state (e.g. liver injury). Additionally, chapter three identifies AOM exposure in the CRC model leads to varying levels of liver damage with all AOM treated WT, Dpp4-/- and Fap-/- mice presenting with elevated enzyme markers, alkaline phosphatase, alanine aminotransferase and aspartate aminotransferase 14 weeks after exposure indicating low levels of liver injury. Additionally, in this chapter it was demonstrated that Dpp4-/- and Fap-/- mice appear to be protected from liver injury as less instances of severe AOM driven liver injury where observed in Dpp4-/- and Fap-/- mice. Subsequently less mice in these groups were removed during the trial due to meeting the 10% weight loss cut-off for euthanasia.

Previous work conducted using Dpp4-/- and Fap-/- mice on C57Bl/6 backgrounds show that both phenotypes have no anatomical abnormalities through all stages of development from neonates to adulthood and show no sign of disease (Conarello et al., 2003; Niedermeyer et al., 2000). Dpp4-/- mice are reported to weigh less, have reduced food intake and increased energy expenditure when compared to wildtype littermates, and are shown to have increased metabolic control and resistance to development of obesity and hyperinsulinemia when maintained on a high fat diet (Conarello et al., 2003). Fap-/- mice are reported to be comparable in size and anatomy to their wildtype littermates and like Dpp4-/- mice are shown to be resistant to diet induced obesity and remain lean, glucose tolerant and insulin sensitive when fed on a high fat diet (Gorrell et al., 2010; Niedermeyer et al., 2000).

In our hands Dpp4-/- mice show the expected lean body type with an average weekly weight increase and final adult body weight that is significantly lower than WT controls in this study and the average reported for male C57Bl/6 mice (The Jackson Laboratory, 2021, 2019). In contrast to previously reported findings taken from Gorrell et al's patent targeting FAP inhibitors for treatment of abnormal glucose metabolism, Fap-/- mice have a weekly weight increase and final adult body weight that was significantly higher than WT controls (Gorrell et al., 2010). The higher body weight seen for Fap-/- mice in this work may be attributed to cage density. For this study WT and Dpp4-/- mice were housed at an average cage density of five animals per cage, but due to overtly aggressive behaviour observed in the Fap-/- mice and the resulting injuries, Fap-/- mice were housed at a consistent cage density of two animals per cage which was proven to eliminate instances of aggression. This disparity in average cage densities was a probable driver for the significantly greater body weights seen in Fap-/- mice as lower cage densities have been shown to drive increased food consumption and consistently higher body weight in male C57Bl/6 mice (Paigen et al., 2012).

This study is also the first to report on Dpp4-/- and Fap-/- mice in a 28 week model as most work to date has been with the use of shorter term eight week trial timelines (Keane et al., 2012; Marguet et al., 2000; Niedermeyer et al., 2000). Mice at 28 weeks of age, the end point used in this work, are considered mature adult mice (Hagan, 2019). Outside of body weight disparity, saline treated Dpp4-/- and Fap-/- control mice at 28 weeks of age are comparable to WT controls and do not display any gross abnormalities or unexpected disease states. There was however a notable difference in behaviour with Fap-/- mice displaying extremely aggressive behaviour leading to severe injuries as well as compulsive repetitive behaviours such as overgrooming that were not seen with the Dpp4-/- or WT mice. This overt aggression and compulsive behaviours have not been previously reported in Fap-/- mice and required both reduction in cage density as well as increased enrichment to eliminate. Future work using Fap-/- mice should take these findings into consideration and plan for lower cage density as well as increased enrichment when working with this phenotype. Further work to identify why the ablation of FAP results in behavioural change would also be beneficial as FAP inhibitors are currently under investigation for their efficacy as treatment in controlling blood glucose level through increased insulin secretion (Gorrell et al., 2010).

This study and work conducted by Rudd et al., (2019) identified a subset of mice treated with AOM that failed to thrive and presented with low liver weights (Rudd et al., 2019). Rudd et al., (2019) identified these mice six weeks post treatment at time of sacrifice, in our work refinement of the weight loss cut off point from 15 to 10% loss from maximum weight allowed this subset of mice to be identified early, during or shortly after AOM treatment, and removed from the trial before completion of the AOM treatment period. Necropsy confirmed that these mice had visible liver damage, presented with small fibrotic livers and had liver weight to body weight ratios that were 2-fold less than the average reported for their AOM treated phenotype matched littermates (Matkowskyj et al., 1999). Refinement of the weight loss cut off point allowed for identification and early removal of all mice with very low liver weights under 0.8 grams. However, in the remaining animals in our study some mice still ended the study with a liver weight just under 1 gram. These mice showed an expected pattern of weight gain across the trial and no other signs of ill health, their livers although small did not show other visual signs of liver damage such as the contracted fibrotic appearance and light colour so further individual analysis would need to be carried out to determine if the smaller liver weight was actually due to AOM driven liver damage. Although liver histology was outside of the scope of this thesis it should be considered as a future direction leading on from these results.

It was unexpected that the six low weekly doses of 10 mg/kg AOM used to induce colorectal cancer in this study resulted in liver injury as to our knowledge liver injury has not been reported in the literature when AOM is used to chemically induce CRC. Although six intraperitoneal injections of 10 mg/kg is commonly reported as optimal for formation of colon carcinomas in mice, doses of 20 mg/kg or more are used to model acute liver failure in C57Bl/6 mice and are reported to be fatal within 24 to 48 hrs of the injection (Bissahoyo et al., 2012; Matkowskyj et al., 1999; Neufert et al., 2007). Thus high dose AOM treatment is associated with liver injury in rodents and causes preneoplastic and neoplastic liver legions that are proportional to the dose and duration of exposure (Burlamaqui et al., 2013).

The lack of a reported association between the 10 mg/kg AOM treatment regime and liver injury may be correlated with diet modifications commonly used in conjunction with the AOM model and the nature of tissue collection for models of colorectal cancer. AOM is commonly used to determine the association between the consumption of certain foods or beverages and colon cancer (Chen and Huang, 2009; Hu et al., 2015). The diet used in our work was a rat and mouse premium breeder diet from Gordon's specialty feeds with a standard 6% total fat content while the tailored diets used in diet induced CRC studies generally have a higher fat content of 40% to effectively model the standard westernised diet (Benninghoff et al., 2020; Chen and Huang, 2009; Hu et al., 2015; Newmark et al., 2009). The use of tailored diets with higher calorie content from fats would minimise AOM associated liver injury as increased calorie intake is shown to improve liver function in patients suffering chronic liver disease (Silva et al., 2015).

The standard protocol for colon tissue collection in CRC animal models may also result in AOM associated liver injury not being reported for the six times 10 mg/kg dosage regime. As colonic tumour load is the commonly reported end point for AOM models, tissue collection is limited to dissection of the colon. This is achieved via incision into the lower abdomen and is a procedure that does not require visualisation or removal of the liver (Bissahoyo et al., 2012; Neufert et al., 2007). It may be that AOM associated liver injury is not widely reported in models of colon cancer because weight loss in mice suffering from liver injury is not great enough for them to be removed under standard animal ethics parameters (15-20% weight loss) and liver damage is not readily detected during standard tissue collection.

Models of colon cancer are often associated with alterations to metabolic stasis thus the inclusion of animals presenting with severe AOM driven liver injury in these studies would potentially skew results. As part of this work we performed a weight analysis of the first 15 mice from each treatment group to determine if the subset of mice presenting with severe AOM driven liver injury were easily identified via weight loss. Comparison of individual body

weight for AOM and saline treated mice over 120 days coupled with their liver weights at time of kill showed that AOM treated WT and Dpp4-/- mice presenting with small livers consistently had early weight losses greater than 10% of their maximum body weight, it was also noted via this analysis that mice presenting with minimal to no liver injury showed a plateau in body weigh during AOM treatment but then consistently resumed gradual increase in total body weight once treatment had ceased. At the time of this weight analysis AOM treated Fap-/- mice did not present with any instances of AOM associated liver injury. Prior to this analysis our animal ethics parameters required removal of an animal if they lost more than 15% of their total maximum body weight without recovery over three consecutive monitoring sessions (in one week). Based on results taken from the weight analysis of the first 15 mice it was identified that this 15% weight loss cut off point was not sufficient to identify the subset of mice presenting with small livers early as body weight in these mice was shown to plateau post treatment with small weight gains and losses seen over an extended period but many did not drop to the 15% from max loss required for removal from the study. Additionally, it was noted that all mice presenting with small livers and potential liver injury consistently had weigh loss of 10% from max weight during or shortly after AOM treatment. Based on these results we submitted a refinement to our animal ethics approval to allow any mouse presenting with a greater than 10% body weight decrease from their maximum weight to be removed immediately from the trial and euthanised. This modification to our animal ethics parameters allowed refinement of our procedures to remove animals suffering from liver injury early and ensured end point analysis was not skewed by the presence of liver injury. Overall, this refinement improved the consistency of our results while also reducing the pain or distress caused to the animals within the study and will be adopted for future work in our group utilising this model.

Although steps were taken during this work to ensure the early removal of animals presenting with more severe liver injury, results indicate that lower levels of AOM driven liver injury is present in all AOM treated Dpp4-/-, Fap-/-, and WT mice. Fourteen weeks after the final AOM injection mice presented with elevated plasma levels of alkaline phosphatase, alanine aminotransferase (ALT) and aspartate aminotransferase (AST) and decreased levels of cholesterol, total protein, albumin and globulin in all groups, which combined is clear evidence of liver damage (Chrostek et al., 2014; Gowda et al., 2009). Plasma alkaline phosphatase, ALT and AST levels in WT mice 14 weeks after AOM treatment were comparable to the levels seen in plasma six weeks after the sixth 10mg/kg injections of AOM to wildtype C57Bl/6 mice in previous work conducted by our group (Rudd et al., 2019). On comparison with saline treated WT mice, AOM treated WT mice show significantly increased levels of alkaline phosphatase with non-significant increases in ALT and AST as well as a

significant decrease in cholesterol, confirming the presence of general inflammation of liver cells (Ukpo et al., 2012). No significant reduction in total protein, albumin or globulin between saline and AOM treated WT mice is seen which indicates that the liver inflammation evident by the increased levels of alkaline phosphatase has not progressed to the point of impacting liver function in terms of blood protein development (Busher, 1990). Bilirubin is also not elevated in AOM treated WT mice when compared to saline treated controls indicating that liver injury has not impacted liver function in terms of blood protein breakdown.

Comparison of saline treated Dpp4-/-mice with AOM treated Dpp4-/- mice shows that AOM treated mice have significantly increased ALT and non-significant increases in alkaline phosphatase and AST as well as significantly lowered total protein levels, the increase in ALT but not AST in Dpp4-/- mice coupled with reduced total protein indicates the presence of chronic hepatocellular injury that has been present for a period longer than 48 hrs but has not progressed to cirrhosis (Kim et al., 2008). AOM treated WT and Dpp4-/- mice also have significantly increased levels of IL-6 when compared to saline treated phenotype matched controls (chapter four, Table 4.4) which is an additional marker of liver injury and associated inflammation as serum levels of IL-6 have been shown to be elevated in rodent models of hepatic inflammation (Perla et al., 2017). These results indicate that while AOM driven liver injury is present in both WT and Dpp4-/- mice, the progression of liver damage is greater in the Dpp4-/- phenotype. This is an interesting result as inhibition of DPP4 has been associated with improved liver function and reduced levels of ALT and AST in T2DM patients with non-alcoholic fatty liver disease (NAFLD) (Kanazawa et al., 2014). Given this positive association between inhibition of DPP4 and improved liver function, the AOM driven injury seen in Dpp4-/- mice may indicate that reduction of DPP4 enzyme activity is beneficial for the metabolic dysregulation driven liver injury seen in obese patients with T2DM. However, liver cells lacking in DPP4 may be less effective in repair of liver damage associated with the AOM, a chemical carcinogen (Burlamaqui et al., 2013; Kanazawa et al., 2014; Perla et al., 2017).

When compared to saline treated phenotype matched controls AOM treated Fap-/- mice show significant increase in alkaline phosphatase, ALT and AST as well as a significant decrease in cholesterol, total protein, and globulin. The significant increase in both ALT and AST in Fap-/- mice with AST levels above ALT indicate that liver injury in Fap-/- mice is more representative of the liver damage associated with cirrhosis (Kim et al., 2008). Both saline and AOM treated Fap-/- mice also showed a non-significant increase in IL-6 when compared to treatment matched WT and Dpp4-/- mice (chapter four, Table 4.4). These results indicate that when compared to AOM treated WT and Dpp4-/- mice, Fap-/- mice have a greater level of AOM driven liver injury. FAP has a defined association with sites of liver injury, it is known

to be expressed at the tissue remodelling interface in cirrhotic livers, FAP blood plasma levels are elevated in cases of severe fibrosis, and increased FAP expression is correlated with increase in severity of the fibrotic disease state (Gorrell, 2005; Gorrell and Park, 2013; Keane et al., 2014; Williams et al., 2015). In a mouse model of high fat diet induced obesity using a diet consisting of 23% total fat, the ablation of the FAP protein in Fap-/- mice has been shown to impart protection against liver injury (Chowdhury et al., 2018). Given the positive association between FAP and disease progression in the liver in human patients, coupled with the reduced liver injury seen in Fap-/- animals on high fat diets, the results seen in this work where Fap-/- mice show greater levels of AOM driven liver injury when compared to WT and Dpp4-/- mice is unexpected. It may be that the much higher fat content used in the Chowdhury et al., (2018) study is protective against liver injury. However, as with DPP4, the contradictory results seen in AOM treated Fap-/- mice may be due to the nature of the AOM driven liver injury where the ablation of FAP is beneficial for the metabolic dysregulation driven liver injury associated with obesity but is less effective in repair of legions associated with AOM, a chemical carcinogen, driving liver damage (Burlamaqui et al., 2013; Chowdhury et al., 2018; Perla et al., 2017). Both DPP4 and FAP are identified as biomarkers of inflammation, while a systemic inflammatory response is shown to play a role in the pathophysiology of fulminant liver failure and is associated with a more aggressive disease state (Baggio et al., 2020; Hori et al., 2011; Waldele et al., 2015). In chapter four Dpp4-/- and Fap-/- mice both present with a significant decrease in IP-10 (CXCL10) which acts as a chemoattractant for a variety of immune cells, this would reduce the inflammatory immune response in Dpp4-/- and Fap-/- mice which would reduce the progression of hepatic necrosis in response to AOM driven liver injury (Vazirinejad et al., 2014).

Although AOM associated liver injury in Dpp4-/- mice is seen at greater levels than WT mice and liver injury in AOM treated Fap-/- mice is seen at greater levels than both Dpp4-/- and WT mice, the number of mice sacrificed for excessive weight loss (10% from maximum weight) was lower in both Dpp4-/- and Fap-/- compared to WT mice. While AOM treated WT, Dpp4-/- and Fap-/- mice all showed varying signs of liver damage via abnormal blood pathology 14 weeks after the last AOM dose, the number of mice requiring early sacrifice due to liver injury and associated excessive weight loss was 27% (16/60) in AOM treated WT mice, this was consistent with results seen in our previous work, this number was only 14% (6/42) in Dpp4-/- mice and 7% (2/30) in Fap-/- mice. The smaller number of AOM treated Dpp4-/- and Fap-/- mice removed from the study for weight loss above 15% initially and 10% later in the study was an unexpected result as the blood pathology from both AOM treated Dpp4-/- and Fap-/- mice showed the presence of greater levels of liver injury than that seen in treatment matched WT mice. In addition to the resistance to weight loss, AOM

treated Fap-/- mice also showed significantly higher liver weights and greater liver weight to body weight ratios than that seen for both Dpp4-/- and WT mice. Average weekly weight increases in AOM treated Dpp4-/- and Fap-/- mice is also closer to that seen for saline treated phenotype matched mice than for AOM and saline treated WT mice where AOM treatment significantly ($p<0.001$) reduced the weekly body weight increase. These results indicate that Dpp4-/- and Fap-/- mice are not resistant to AOM driven liver damage but do have the ability to resist the weight loss associated with this disease state which may indicate that they have greater metabolic control in regard to disease driven weight loss. Although metabolic control and resistance to high fat diet driven obesity has been observed in both Dpp4-/- and Fap-/- mice, metabolic control in resistance to disease driven weight loss has not been previously reported and is an association that requires further investigation (Chowdhury et al., 2018; Conarello et al., 2003; Gorrell et al., 2010).

Elevated levels of circulating aminotransferases as markers of hepatic damage have been previously reported in conjunction with low level AOM exposure (Moawad Mahmoud et al., 2014; Ward, 1975), although refinement of our animal ethics parameters allowed for identification and early removal of mice suffering with more severe liver injury, all mice exposed to the AOM treatment regime presented with elevated aminotransferases indicating varying levels of liver damage dependent on phenotype. Although the timepoint at which markers of liver damage were measured was 14 weeks after exposure to AOM, the presence of liver damage is still evident to varying levels in all AOM treated mice. This may in part be due to the CRC disease state limiting resources required to repair the liver and is an associated result that needs to be taken into consideration when using AOM to model the progression of colorectal cancer in rodents. The nature of the cellular damage associated with AOM exposure may also be modelling a more progressed cancer development than a single site colonic tumour model. Exposure to AOM and metabolism through the liver with the resulting liver damage identified through elevation in aminotransferases may be modelling a more advanced CRC disease progression that includes liver metastasis formation which is the preferred site for metastasis in CRC patients (Heijstek et al., 2005). The presence of AOM driven liver injury does not invalidate the results taken from this model in terms of colon cancer progression but does indicate that all results need to be interpreted in terms of the more advanced cancer model being represented.

Measurement of general plasma biochemical markers in AOM treated Dpp4-/- and Fap-/- mice showed both groups also had low level signs of kidney damage. When compared to saline treated phenotype matched controls, AOM treated Dpp4-/- mice showed a significant decrease in their sodium to potassium ratio and AOM treated Fap-/- mice showed a significant decrease in anion gap associated with increased levels of serum chloride.

Increases in serum levels of potassium and chloride are indicators of renal damage which would be an expected result in AOM treated Dpp4-/- and Fap-/- mice as AOM has been previously associated with nephrotoxicity in mice although the results indicate only low levels of renal damage that are noted as not being severe enough to skew overall end point results (Moawad Mahmoud et al., 2014; Nakhoul et al., 2015; Pfortmueller et al., 2018). The kidneys contain the highest levels of DPP4, emerging evidence suggests that DPP4 may have nephroprotective effects while the DPP4 inhibitor linagliptin is reno-protective in animal models of kidney disease (Kanasaki, 2018). The elevated markers of kidney damage seen in Dpp4-/- mice but not WT mice provides further evidence that the presence of the DPP4 protein in the kidney is reno-protective. FAP results reflect that seen for DPP4 which may indicate that FAP also imparts nephroprotective effects. No significant difference in sodium, potassium, chloride, or bicarbonate was seen between saline and AOM treated WT mice indicating no presence of AOM associated kidney damage in this phenotype. Saline treated WT mice have significantly increased creatinine when compared to saline treated Dpp4-/- and Fap-/- mice, as no other markers of kidney function indicate the presence of kidney damage in saline treated WT, Dpp4-/- or Fap-/- mice this difference in creatinine levels could be attributed to difference in lean muscle mass, creatinine is created as a by-product of muscle function and when kidney function is normal it can be correlated as an indicator of lean muscle mass (Baxmann et al., 2008; Thongprayoon et al., 2016). This is an expected result for Dpp4-/- mice due to their noted lean body type when compared to wildtype mice but appears to be unusual result for Fap-/- mice in this study as they have average body weights greater than treatment matched WT mice. As creatinine is a measure of lean muscle mass and not total body mass the lowered serum level of creatinine in saline treated Fap-/- mice may indicate reduced muscle mass but not reduced total body weight, this is an expected result in Fap-/- mice as FAP has been previously associated with skeletal muscle maintenance and its ablation has been positively associated with overall loss of muscle mass (Baxmann et al., 2008; Roberts et al., 2013; Thongprayoon et al., 2016).

3.5 Conclusion

Findings from chapter three have identified a refinement for the monitoring and ethics parameters associated with the AOM model of CRC in addition to establishing the efficacy of the use of the AOM model of colorectal cancer in DPP4 and FAP genetic knockout mice. This study is also the first to report on Dpp4-/- and Fap-/- mice in a 28-week model with mice at full adult maturity presenting as phenotypically normal with no gross abnormalities or unexpected disease states. Our results have associated AOM exposure with varying levels of liver damage with all AOM treated mice presenting with elevated enzyme markers 14 weeks after exposure. Although out of scope for the work in chapter three future work on

liver histology in this model would validate the extent of AOM driven liver injury. Additionally, DPP4 and FAP ablation in this work is identified as protective in instances of severe AOM driven liver injury with less Dpp4-/- and Fap-/- mice requiring removal from the trial due to weight loss in excess of ethics parameters. Despite the low level liver damage in all groups observed this model is still useful to look at the role of genes or treatments for CRC however the increase in AOM driven liver injury may be modelling a more advanced disease progression and should be considered during experimental design.

Chapter 4

Ablation of dipeptidyl peptidase 4 or fibroblast activation protein leads to increased tumorigenesis in the azoxymethane colorectal model

4.1 Introduction

Colorectal cancer (CRC) is the worldwide second leading cause of cancer related deaths, with approximately 1,800,000 identified cases accounting for 881,000 deaths in 2018 (Australian Institute of Health and Welfare, 2020; Gandomani et al., 2017; Mulsow, 1953; Rawla et al., 2019). Increased prevalence of colorectal cancer is associated with western diet and lifestyle factors such as high calorie intake, low physical activity and excess abdominal fat, factors linked with a predisposition to type 2 diabetes mellitus (T2DM) and increased insulin resistance (Bruce et al., 2000; Giovannucci et al., 2010). Moreover, epidemiologic evidence suggests that obesity and T2DM increase incidence of several cancer types including pancreatic, breast and colon cancer (Giovannucci et al., 2010). Given this association, there is a growing interest in determining whether T2DM treatments have a positive or negative effect on the initiation and progression of different cancers.

In the search for novel therapies to combat cancer, the dipeptidyl peptidase 4 (DPP4) enzyme family have been identified as potential diagnostic and therapeutic targets. DPP4 inhibitors are now in use as treatment for T2DM, with inhibition of DPP4 reducing degradation of the incretin hormone GLP-1 prolonging its insulinotropic actions (Lovshin and Drucker, 2009). In addition to its regulation of GLP-1, the enzymatic activity of DPP4 is shown to cleave bioactive peptides, including cytokines, chemokines and neuropeptides, resulting in their inactivation or targeted degradation and its actions are shown to be involved in a diverse range of biological processes involved in neoplastic transformation including cell differentiation and adhesion, immune modulation and apoptosis (Havre et al., 2008; Larrinaga et al., 2015). In cancer biology DPP4 has been identified as both a promotor and inhibitor of tumour progression, DPP4 expression and enzyme activity is shown to be significantly altered in solid tumour tissue and changes in activity and expression levels are seen, dependent on tumour type and stage of development (Havre et al., 2008; Larrinaga et al., 2015; Pitman, 2009).

In relation to colon cancer, increased DPP4 serum levels are identified as a predictive marker for diagnosis, while higher DPP4 immunohistochemical expression in CRC tissue is linked to increased metastasis and overall poor prognosis (Lam et al., 2014; Larrinaga et al., 2015). Although there is an established link between DPP4 and CRC the impact of long term use of DPP4 inhibitors in respect to incidence and progression of colon cancer has only been explored in a small body of research that has produced conflicting results (Femia et al., 2013; Kissow et al., 2012; Koehler et al., 2011). The incretin targets of DPP4 inhibition are also associated with intestinal actions that are pro-tumorigenic and anti-tumorigenic. The

primary target of DPP4 inhibition for T2DM treatment, GLP-1, has been associated with inhibition of cell growth and increased apoptosis in colon cancer cells indicating that DPP4 inhibitors may act as a suppressor in this cancer type (Koehler et al., 2011). On the other hand, GLP-1 analogues have been associated with increased intestinal proliferation, a pro-carcinogenic action that may indicate that prolonged action of GLP-1 through DPP4 inhibition has a promotive effect on the colonic epithelial growth related to CRC (Kissow et al., 2012). DPP4 is also shown to degrade and inactivate GLP-2 which is involved in colonic mucosal stimulation and expansion (Rowland and Brubaker, 2011). These findings indicate that DPP4 inhibition may play a promotive role in respect to CRC. Where DPP4 inhibition prolongs the actions of GLP-1 increasing the insulin response, its will likewise increase the actions of GLP-2 which has an association with increased carcinogenesis in murine models of colorectal cancer (Iakoubov et al., 2009; Rowland and Brubaker, 2011; Thulesen et al., 2004).

The DPP4 peptidase family member fibroblast activation protein (FAP) shares 48% amino acid sequence identity with DPP4 (Liu et al., 2012). FAP is expressed by tumour-associated fibroblasts but is only transiently expressed in normal fibroblasts in association with wound healing or chronic inflammatory conditions such as cirrhosis (Ghersi et al., 2002; Levy et al., 2002). The proteolytic activity of FAP is also associated with remodelling of the extracellular matrix through gelatinase and collagenase activity (Javidroozi et al., 2012; Keane et al., 2012). While FAP is not shown to be expressed in epithelial carcinoma cells, induction of FAP positive stromal fibroblasts are detected in greater than 90% of malignant breast, colorectal, skin, and pancreatic tumours (Cohen et al., 1986; Garin-Chesa et al., 1990; Rettig et al., 1993). Additionally, stromal cells associated with benign epithelial breast fibroadenomas or colorectal adenomas are FAP negative, suggesting that FAP induction is positively correlated with malignancy (Cheng et al., 2005). In a xenograft tumour model, tumours initiated via HT-29 colon adenocarcinoma cells have attenuated growth when treated with inhibitory anti-FAP antisera, while transfection of enzymatically active FAP increased growth and enhanced tumorigenicity in in a xenograft model using HEK293 embryonic kidney cells (Cheng et al., 2005, 2002). In CRC, high expression of stromal FAP in resected primary human colon cancer tissue is correlated with aggressive disease progression and increased metastases (Henry et al., 2007). While FAP expression at the CRC tumour centre is associated with poor overall prognosis on comparison with tumours presenting with low or no tumour centre expression (Wikberg et al., 2013). Similar results are seen for patients with rectal cancers where high stromal FAP expression after preoperative chemoradiotherapy is associated with increased reoccurrence and poor probability towards overall survival (Saigusa et al., 2011). These findings indicate a negative prognostic role for

FAP in respect to CRC with heightened FAP expression noted as a prerequisite for the invasive phenotype.

Work targeted at the relationship between DPP4, FAP and colon carcinogenesis has identified both DPP4 and FAP as potential CRC treatment targets, but conflicting results are seen to date regarding the exact role these peptides play in tumorigenesis. In chapter four the azoxymethane (AOM) murine model of CRC development is utilised in wildtype (WT), DPP4 knockout (Dpp4-/-) and FAP knockout (Fap-/-) mice to examine the role of DPP4 and FAP in CRC progression. This work demonstrates that both DPP4 and FAP play a role in tumour incidence and development and that DPP4 plays a significant role in tumour prevalence.

4.2 Materials and Methods

Unless stated otherwise, all reagents used in this chapter were sourced from Sigma Aldrich, New South Wales, Australia.

4.2.1 *In vivo* murine model

All methods describing the *in vivo* murine model used for chapter four are outlined in chapter three (section 3.2.1).

4.2.2 Blood and Colon Collection

Fourteen weeks after the final dose of AOM deep terminal anaesthesia was induced by isoflurane inhalation, blood samples were obtained via cardiac puncture prior to cervical dislocation (Morton et al., 2001; Szczesny et al., 2004). Blood was collected into sodium heparinised-EDTA vials (BD Microtainer®, Melbourne, Australia), sample coded and sent to a pathology clinic (Gribbles Pathology, South Australia) to test blood biochemistry and haematology parameters (reported in chapter three). Blood was also collected from additional mice (n=10, per group) for the multiplex plasma assay and this is described in section 4.2.5 below. Mice were dissected immediately post kill for removal of colons. To remove colons an incision was made in the lower abdominal wall exposing the internal organs, the pelvic bones were spread apart, and the reproductive organs were removed to expose the gastrointestinal tract. The colon was cut at the anus, carefully lifted out of the abdomen and excised below the ileo-caecal valve (McGinley et al., 2010). Once excised the colons were straightened and cleaned to remove any faecal matter, opened longitudinally, flattered on Hibond C paper (NL1011; GE Healthcare) and fixed for 24 hrs in 10%

paraformaldehyde and then transferred to 70% ethanol for histologic processing (Bissahoyo et al., 2012). Livers were also removed and weighed this data is reported in chapter three.

4.2.3 Aberrant Crypt Foci and tumour scoring

Aberrant Crypt Foci (ACF), which are regard as early neoplastic lesions in colorectal cancer progression, as well as tumours were quantified in fixed colons 14 weeks after final AOM treatment (Orlando et al., 2008). For ACF and tumour visualisation fixed colons were rinsed in deionized water and stained in 0.05% methylene blue for three min (McGinley et al., 2010). Stained colons were rinsed in deionized water to remove excess methylene blue stain, a count of the number of ACFs and tumours present was then conducted, and images taken, using a dissecting Carl Zeiss Stemi 2000 C microscope and Axio cam imager at 40X magnification. ACFs were differentiated from normal crypts by their larger size, elevation from surrounding mucosa, darker staining and luminal polymorphism of the crypt opening creating slit like and oval openings (Di Gregorio et al., 1997). The ACF count was based on the number of crypts present per individual lesion with ACFs grouped as having less than three, three to four, and greater than four crypts. Tumours were identified by pedunculate protrusion, dark staining and dysplasia, small adenomas were distinguished from large ACFs by the level of dysplasia (lack of defined crypt openings) and larger size. Tumours were scored by number and size, in mm diameter, via blinded count and were equated according to size, <1mm, 1-2mm, 2-4mm, 4-6mm and >6mm.

4.2.4 Histologic evaluation of tumours

To classify tumours as adenoma or adenocarcinoma, colon sections were dissected at the tumour site, embedded in paraffin, and stained using hematoxylin and eosin for histopathologic evaluation on a subset of colons. Sectioning and staining of colon tissue was undertaken by Julian Di Ubaldo and histopathological evaluation of stained sections was completed by Dr Ying Hu. Cold paraffin embedded colon segments were sectioned at four-five µM thin and fixed on Superfrost Plus™ slides (Thermo Scientific, Melbourne, Australia). Slides were placed flat onto a slide rack and allowed to dry for two hours, then incubated at 60^0C for 20 min and then returned to room temperature overnight. Paraffin sections mounted on slides were then rehydrated via an ethanol gradient consisting of two x two min washes in Histoclear followed by two x two-min washes in 100%, 90%, 70% and 50% ethanol solutions. Slides were then rinsed briefly in tap water prior to incubation in hematoxylin solution for two min with removal of excess hematoxylin by rinsing under running tap water until the water ran clear. Slides were then dipped in 3% acid ethanol (92 mL ethanol, 3 mL hydrochloric acid, 5 mL H_2O) three times and blotted on a paper towel to remove excess

ethanol before being dipped in 0.2% ammonia water (2 mL concentrated ammonium hydroxide, 1000 mL H_2O) three times, rinsed in tap water, and then dipped in 90% ethanol 10 times. Slides were finally incubated in eosin solution for 45 sec and washed under running tap water until the water ran clear prior to dehydration using the ethanol gradient in the reverse order of the rehydration process. Slides were left at room temperature to dry completely prior to mounting of coverslips using DPX mounting solution (Esmaeelian et al., 2014).

All tumours were examined histologically using a Motic BA300 light microscope at 400X magnification and evaluated by an independent experienced observer, Dr Ying Hu, based on the following criteria. Adenoma, or benign epithelial tumours, were classified by cellular dysplasia, enlargement of the mucosa layer, decrease in goblet cell number, loss of mucosal architecture by glandular growth and absence of invasion through the basement membrane. Adenocarcinoma, or malignant tumour growth, was characterised through typical cytological change, pronounced cellular atypia, loss of cell polarity, evident distortion of glandular architecture and invasion (Hu et al., 2005).

4.2.5 Milliplex Immunoassay

Metabolic hormones and cytokines involved in inflammatory and immune response were quantified by the Australian Proteome Analysis Facility, (APAF, Macquarie University, Sydney, Australia). Blood for multiplex plasma assay was collected into sodium heparinised-EDTA vials (BD Microtainer®, Melbourne, Australia) with 1mM DPP4 inhibitor diprotin A added. To isolate plasma, samples were centrifuged for 10 min at 1000xg, plasma was removed immediately, addition of 1mM diprotin A again and stored at -80^{0}C until shipment to APAF. The plasma concentrations of Amylin (active), C-peptide 2, Ghrelin (active), GIP (total), GLP-1 (active), Glucagon, IL-6, Insulin, Leptin, MCP-1, PP, PYY (total), Resistin, and TNFα, were quantified using the MILLIPLEX MAP Mouse Metabolic Hormone Magnetic Bead Panel (Millipore, cat. no. MMHMAG-44 K), and the plasma concentrations of Eotaxin, VEGF, RANTES, MIP-1α, GM-CSF, LIX, IP-10, IL-17, IL-13, IL-10, IL-4, IL-2, IL-1β, IL-1α, IFN-γ, were evaluated using MILLIPLEX MAP Mouse Cytokine/Chemokine Magnetic Bead Panel (Millipore, cat. no. MCYTMAG70PMX32BK). For immunoassay plasma samples were prepared, and assays performed, as per the manufacturer's instructions at APAF (Breen et al., 2016).

4.2.6 Fasting Glucose

For determination of fasting glucose a subset of saline treated mice, WT (n=15), Fap-/- (n=24), Dpp4-/- (n=20), and AOM treated mice, WT (n=18), Fap-/- (n=16) and Dpp4-/- (n=20), were fasted for five hrs and given a glucose bolus of 2g/kg via oral gavage 30 min prior to cardiac puncture (Andrikopoulos et al., 2008). Fasting blood sugar levels were determined using an Accu-Chek Performa Blood Glucose Meter and Accu-Chek test strips (Roche Diabetes Care, Sydney, Australia).

4.2.7 DPP enzyme activity assay

Methods for the detection of DPP enzyme activity in cells were adapted from Sulda, M.L. 2009, and originally provided by Professor Mark Gorrell, Centenary Institute, Sydney, Australia. (Sulda, 2009).

To detect DPP activity in plasma samples, enzyme activity assays were performed using the substrate H-Ala-Pro-pNA.HCl (Bachem, CA, USA). As H-Ala-Pro-pNA.HCl is cleaved by DPP4 as well as FAP, DPP8 and 9, the DPP4 specific inhibitor sitagliptin was used at a final concentration of 10 µM to determine residual DPP plasma activity, this concentration is greater than double the IC50 against DPP4 but below the concentration that will inhibit FAP, DPP8 or 9 (Kim et al., 2005; Waumans et al., 2015). Assays were carried out in 96 well plates with a 1 mM final substrate concentration. The H-Ala-Pro-pNA substrate was dissolved in 10 µL methanol prior to being solvated to a final concentration of 2 mM in 0.1 M sodium phosphate buffer at pH 7.6. DPP cleavage of H-Ala-Pro-pNA was measured in triplicate using 10 µL of plasma and 40 µL of 0.1 M sodium phosphate buffer and 50 µL of 2 mM substrate was added just prior to enzyme activity reading to achieve a final substrate concentration of 1 mM. The production of p-nitroanilide (pNA) was measured via absorbance at 690 nm subtracted from 405 nm and taken every five min for 60 min at 37°C using a FLUOstar Omega Microplate Reader (BMG LABTECH).

Total activity for the DPP enzyme assay was calculated as outlined in chapter two (section 2.2.6).

4.2.8 Statistical analysis

Statistical analysis was performed using GraphPad Prism version 6.0.0 for Windows, GraphPad Software, San Diego, California USA (www.graphpad.com). One-way ANOVA test was performed to compare the treatment groups to the control group with a Tukey's multiple comparison test applied to determine significant differences between the means of

individual groups. A probability level of $p \leq 0.05$ against control was considered as statistically significant.

4.3 Results

4.3.1 AOM model timeline for tumour development adjusted for Dpp4-/- mice

In the AOM model, tumours are expected to occur in WT C57Bl/6 mice at 20 weeks after the sixth 10mg/kg AOM injection. Previous work conducted by our group targeted at early stage tumour formation using the AOM murine model confirmed that mice presented with 1, 2-4 and >4 crypt ACF and <1mm tumours 6 weeks after the sixth AOM injection (Rudd et al., 2019). In this current model Dpp4-/- mice developed aggressive tumours within 14 weeks of their sixth AOM injection. In response to this aggressive tumour growth the endpoint of the trial was shortened from 20 weeks post AOM treatment to 14 weeks (Figure 4.1). Tumour penetrance at 14 weeks post AOM treatment was 100% in Dpp4-/- mice and 80% in Fap-/- mice compared to 63% in WT mice (Figure 4.2). No tumours were present in Dpp4-/-, Fap-/- or WT saline controls at 14 weeks post treatment.

4.3.2 Aberrant crypt foci (ACF) numbers in Dpp4-/- and Fap-/- mice

Given the shortened timepoint used in this model at 14 weeks post AOM treatment aberrant crypt foci (ACF) were also observed in the colons of mice examined. A significant reduction in this early marker of neoplastic changes in the colon was observed in Dpp4-/- mice compared to WT (Table 4.2). ACF were principally located in the distal and middle colon in all AOM treated mice, Dpp4-/- treated mice had significantly ($p<0.05$) less small ACF with less than three crypt openings and large ACF with more than four crypt openings and both Dpp4-/- ($P<0.001$) and Fap-/- ($p<0.05$) had significantly less ACF with three-four crypt openings (Table 4.2). On comparison with Dpp4-/-, WT and Fap-/- mice had an average 1.5-fold increase in both large ACF with more than four crypt openings and small ACF with less than three crypt openings (Table 4.2). ACF presence was not observed in the colons of WT, Dpp4-/- or Fap-/- saline controls.
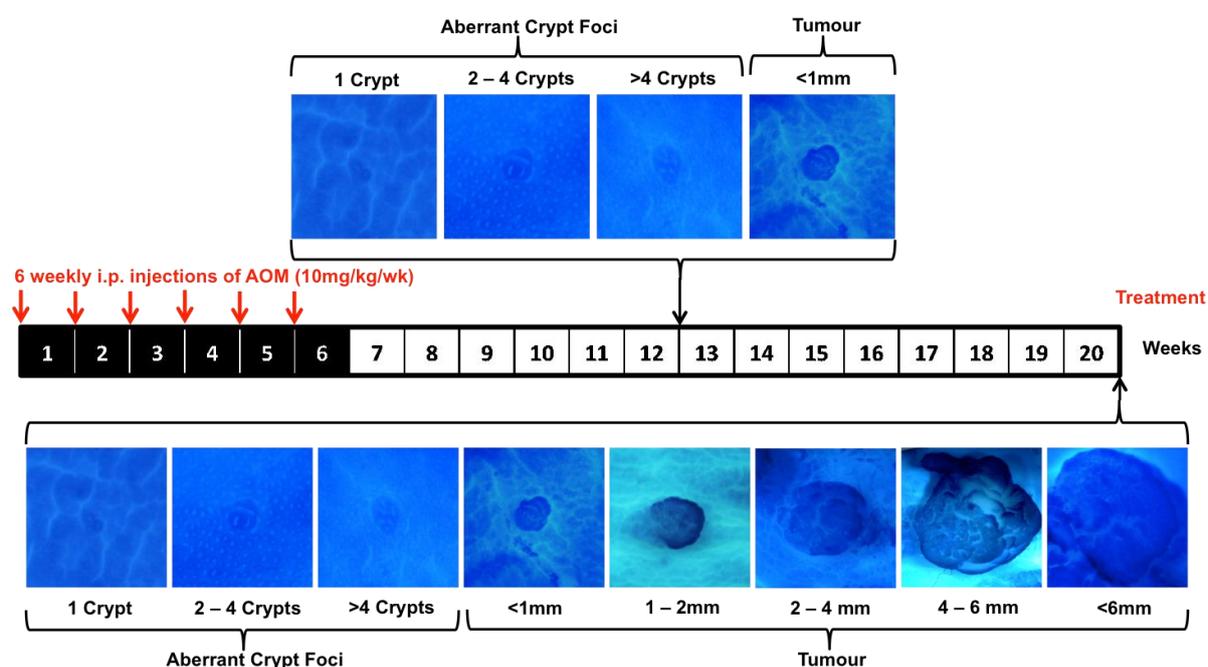
Figure 4.1. Timeline for ACF and tumour development in the AOM murine model of CRC. Genotoxic damage was induced in eight-week-old mice via six weekly intraperitoneal injections of AOM at a dosage of 10 mg/kg bodyweight. Illustrative example of results taken from Rudd et al., and chapter four. In results from Rudd et al., (2019) mice present with 1, 2-4 and >4 crypt ACF and <1mm tumour development six weeks after the sixth AOM injection (top panel). In results taken from chapter four mice present with 1, 2-4 and >4 crypt ACF and <1, 1-2, 2-4, 4-6 and >6mm tumour development at 14 weeks after the sixth AOM injection (bottom panel).

A

B
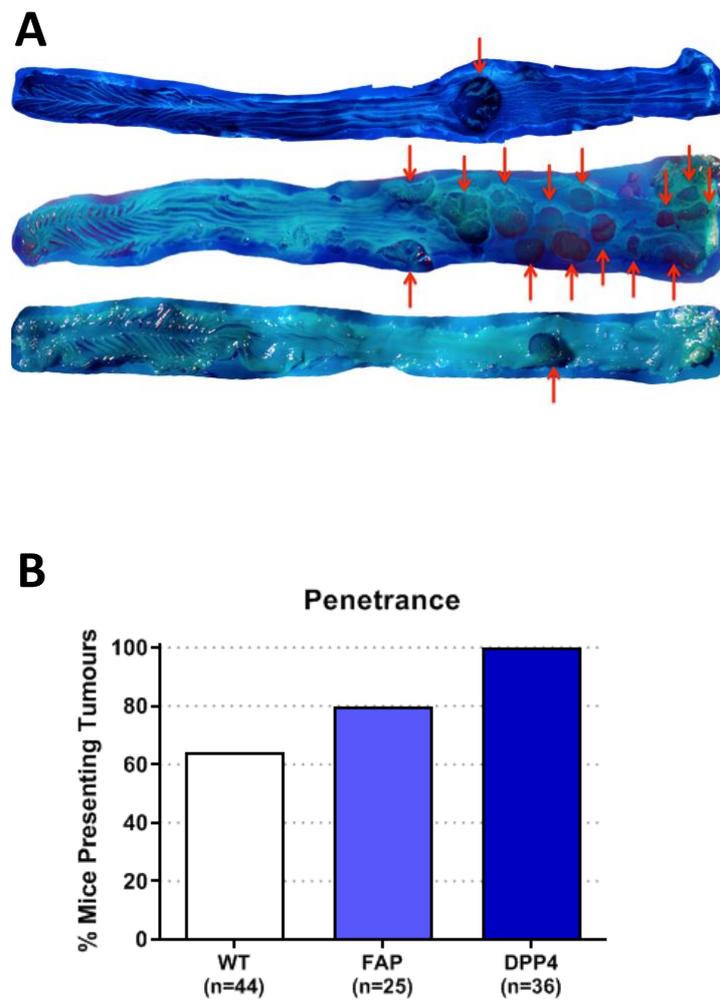
Figure 4.2. Dpp4-/- mice present with increased tumorigenesis compared to Fap-/- mice and WT controls 14 weeks after sixth AOM injection of 10 mg/kg. A) Tumour presence in WT (bottom), Dpp4-/- (middle) and Fap-/- (top) colons. Colons are opened longitudinally, flattened on Hybond C paper, fixed for 24 hours in 10% paraformaldehyde, and stained with 0.05% methylene blue. Red arrows indicate tumour localisation B) Tumour penetrance in AOM treated WT (n=44), Fap-/- (n=25) mice and Dpp4-/- (n=36) mice.

Table 4.1. Dpp4-/- mice have reduced numbers of aberrant crypt foci (ACF), pre-cancerous legions, in an AOM model of colorectal cancer. Total ACF number determined via direct visualisation of fixed colons stained in 0.05% methylene blue. ACF number in distal, middle and proximal colon, and ACF count by size designated as ACF with <3, 3-4, and >4 crypts in Dpp4-/- and Fap-/- compared to WT mice 14 weeks after sixth AOM injection of 10 mg/kg. ACFs were not present in the colons of saline treated WT, Dpp4-/- or Fap-/- mice. Asterisk denotes significance at the * <0.05, ** <0.01 and *** <0.001 probability level against WT control. Values represent means and ± standard error (SEM).

	WT n=44	Dpp4-/- n=36	Fap-/- n=25
Total	20.82 ± 2.46	11.61 ± 1.82 **	18.32 ± 1.64
Distal	14.32 ± 1.79	7.33 ± 1.39 **	13.48 ± 1.24
Middle	6.36 ± 0.98	4.28 ± 0.67 *	4.84 ± 0.74
Proximal	0.00 ± 0.00	0.00 ± 0.00	0.00 ± 0.00
<3 Crypts	14.32 ± 1.83	8.92 ± 1.47 *	13.76 ± 1.51
3-4 Crypts	5.77 ± 0.64	2.42 ± 0.51 ***	3.84 ± 0.69 *
>4 Crypts	0.73 ± 0.15	0.28 ± 0.09 *	0.72 ± 0.19

Table 4.2. Dpp4-/- mice have increased tumorigenesis in an AOM model of colorectal cancer. Tumour count determined via direct visualisation of fixed colons stained in 0.05% methylene blue, tumour count in distal, middle and proximal colon, and number of tumours <1, 1-2, 2-4, 4-6 and >6mm in size in Dpp4-/- and Fap-/- compared to WT mice 14 weeks after sixth AOM injection of 10 mg/kg. Tumours were not present in the colons of saline treated WT, Dpp4-/- or Fap-/- mice. Asterisk denotes significance at the * <0.05 and *** <0.001 probability level against WT control. Values represent means and ± standard error (SEM).

	WT n=28	Dpp4-/- n=36	Fap-/- n=20
Total	3.50 ± 0.66	8.06 ± 0.82 ***	3.55 ± 0.53
Distal	2.61 ± 0.41	6.17 ± 0.59 ***	2.85 ± 0.39
Middle	0.86 ± 0.32	1.89 ± 0.38 *	0.65 ± 0.23
Proximal	0.04 ± 0.04	0.00 ± 0.00	0.05 ± 0.05
<1mm	1.61 ± 0.31	2.14 ± 0.26	1.30 ± 0.24
1-2mm	1.07 ± 0.30	1.44 ± 0.20	0.65 ± 0.20
2-4mm	0.50 ± 0.17	1.64 ± 0.24 ***	0.85 ± 0.26
4-6mm	0.32 ± 0.12	2.47 ± 0.45 ***	0.70 ± 0.16 *
>6mm	0.00 ± 0.00	0.36 ± 0.08 ***	0.05 ± 0.05

4.3.3 Increased tumour growth and development in Dpp4-/- and Fap-/- mice

A significant 2.3-fold increase in tumour number was observed in AOM treated Dpp4-/- mice compared to WT mice, while AOM treated Fap-/- mice showed no significant difference in tumour number compared to WT (Table 4.1). In addition to the increased number of tumours, Dpp4-/- mice presented with larger tumours and on comparison with WT mice had significantly ($p < 0.001$) more tumours of 2-4, 4-6 and >6 mm in diameter. Fap-/- mice had significantly more ($p < 0.05$) 4-6 mm tumours and Dpp4-/- and Fap-/- mice both presented with very large >6 mm tumours which were not seen in WT mice (Table 4.1). Tumours were primarily located in the distal colon in Dpp4-/-, Fap-/- and WT mice but Dpp4-/- mice did have a significant ($p < 0.05$) increase in the number of tumours localised to the middle colon compared to WT mice. In Fap-/- mice tumour localisation reflected closely that seen in WT mice (Table 4.1). Histologic evaluation of tumours confirmed the presence of both adenomas and adenocarcinomas in WT, Dpp4-/- and Fap-/- mice. Classification identified 67% of WT and Dpp4-/- tumours to be adenomas and 33% adenocarcinomas, while Fap-/- mice presented with 57% adenomas and 43% adenocarcinomas (Figure 4.3).

4.3.4 AOM treated Dpp4-/- and Fap-/- mice have lowered white and red blood cell numbers

Lymphocytes are recognised as playing a major role in the fight against tumour progression and increased lymphocyte recruitment can be a marker of resistance against tumour development (Ménétrier-Caux et al., 2019). Lymphocyte recruitment was lowered in Dpp4-/- mice, with AOM treated Dpp4-/- mice showing a significant ($p < 0.05$) reduction in white blood cell numbers in comparison to AOM treated WT mice that was directly related to lymphocyte number (Figure 4.4, A & B). Dpp4-/- saline controls also showed a small non-significant increase in lymphocyte cell numbers compared to both WT and Fap-/- saline controls (Figure 4.4, B). No significant difference was seen between groups in neutrophils, monocytes, or eosinophils but saline treated Dpp4-/- and Fap-/- mice did show a non-significant reduction in neutrophils and increase in eosinophils when compared to saline treated WT controls (Figure 4.4, C & E). In addition to lowered lymphocyte numbers, AOM treated Dpp4-/- and Fap-/- mice show signs of anaemia with significantly reduced ($p < 0.01$) red blood cell numbers when compared to saline treated phenotype matched controls (Figure 4.5, A). In addition to the reduction in red blood cell numbers, a significant ($p < 0.01$) reduction in haematocrit, or the volume percentage of red blood cells within the whole blood, was seen in AOM treated Dpp4-/- and Fap-/- mice when compared to phenotype matched
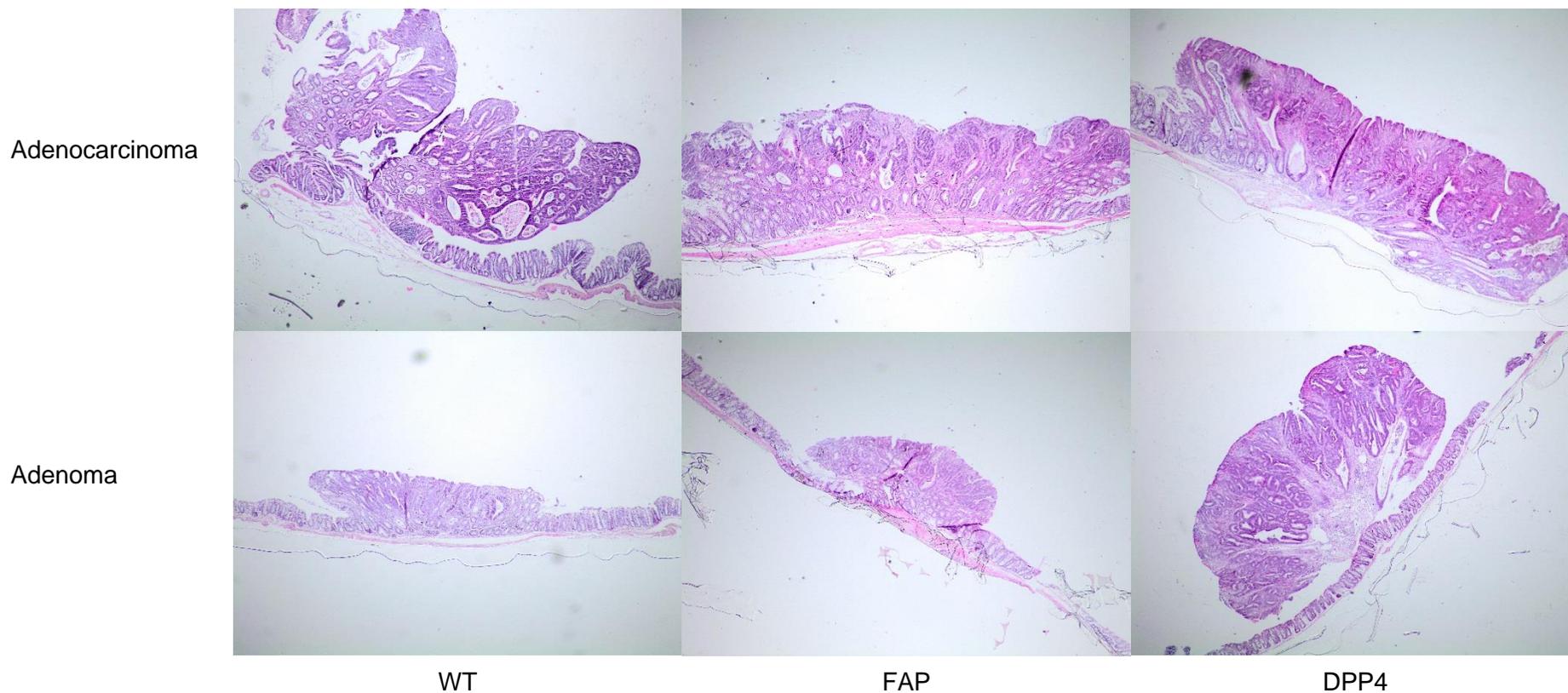
Figure 4.3. Representative sections of adenocarcinomas and adenomas from AOM treated WT, Fap-/- and Dpp4-/- mice. Colon sections from a subset of mice taken at 14 weeks post AOM treatment were dissected at the tumour site, embedded in paraffin, and stained using hematoxylin and eosin for histopathologic evaluation. Tumours were examined histologically using a Motic BA300 light microscope at 400X magnification, evaluated by an independent observer and classified as adenoma or adenocarcinoma.
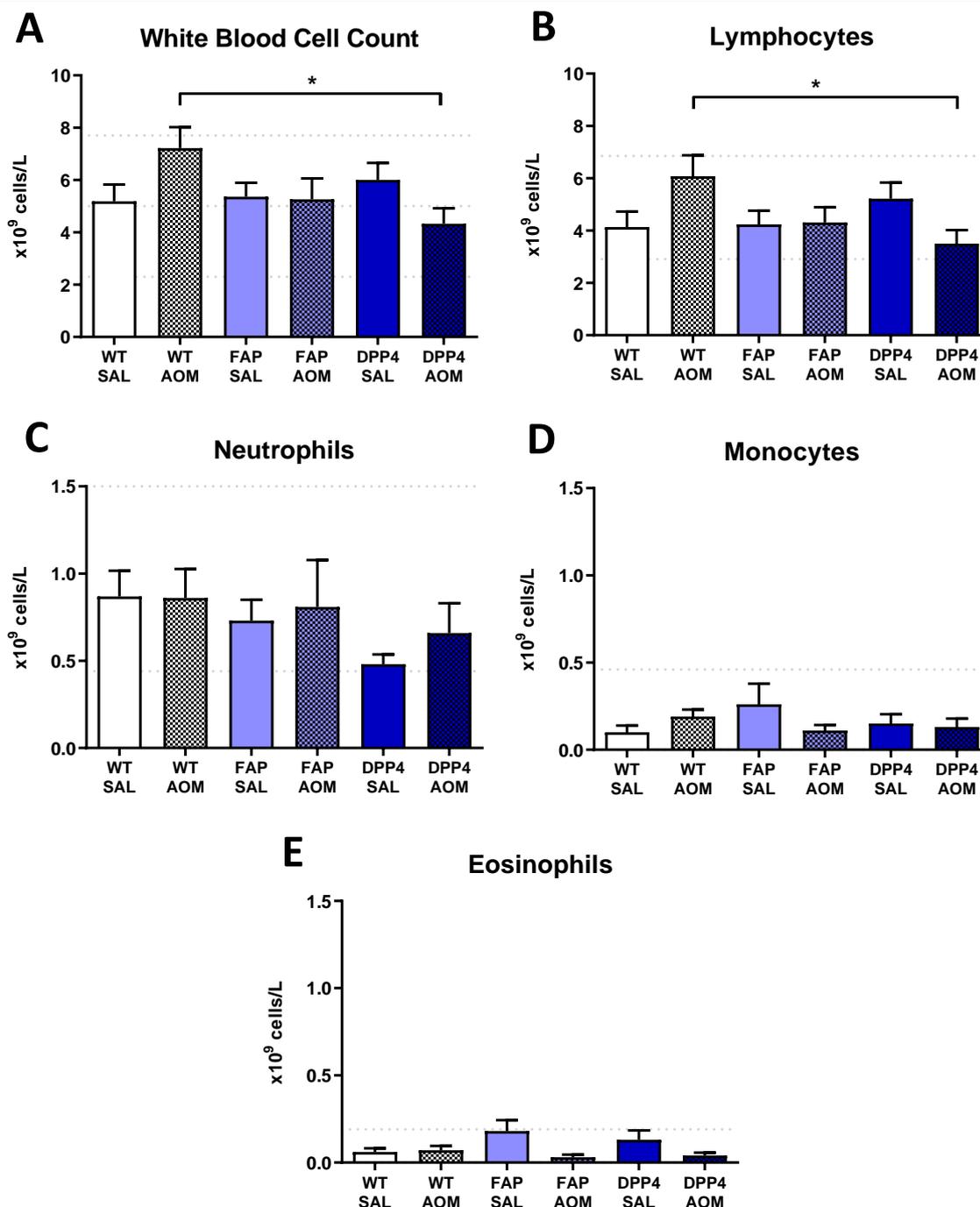
Figure 4.4. AOM treated Dpp4-/- mice show reduced white blood cell count and lymphocyte numbers. Blood counts were determined on blood collected via cardiac puncture into heparinised tubes from mice (n=10 per group), 14 weeks after sixth AOM injection of 10 mg/kg. The analysis was conducted by Gribbles veterinary pathology SA. Total count per litre of whole blood for A) white blood cells, B) lymphocytes, C) neutrophils, D) monocytes, E) eosinophils. Asterisk (*) denotes significance at the <0.05 probability level between groups. Values represent means and error bars ± standard error (SEM). Light grey dashed lines indicate average, upper and lower 95 percentile in healthy male C57BL/6 mice as reported by Jensen, Schnell and The Jackson Laboratory (Jensen et al., 2013; Schnell et al., 2002; The Jackson Laboratory, 2007).
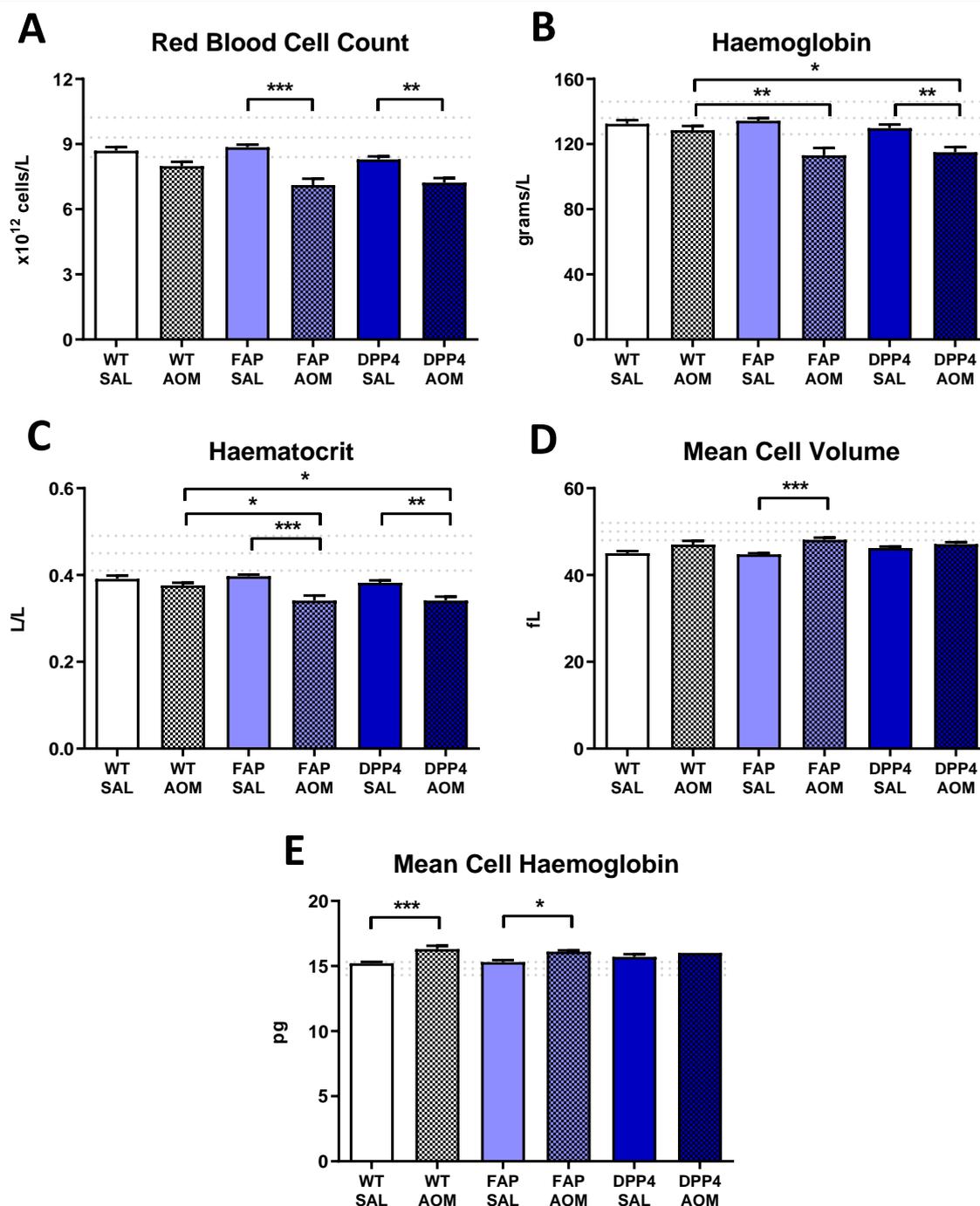
Figure 4.5. AOM treated Dpp4-/- and Fap-/- mice show reduced red blood cell count in plasma. Blood counts were determined on blood collected via cardiac puncture into heparinised tubes from mice (n=10 per group), 14 weeks after sixth AOM injection of 10 mg/kg. The analysis was conducted by Gribbles veterinary pathology SA. Total count per litre of whole blood for A) red blood cells, as well as total volume of B) haemoglobin, C) haematocrit, D) mean corpuscular volume, E) mean corpuscular haemoglobin. Asterisk denotes significance at the * <0.05, ** <0.01 and *** <0.001 probability level between groups. Values represent means and error bars ± standard error (SEM). Light grey dashed lines indicate average, upper and lower 95 percentile in healthy male C57BL/6 mice as reported by Jensen, Schnell and The Jackson Laboratory (Jensen et al., 2013; Schnell et al., 2002; The Jackson Laboratory, 2007).

controls as well as a significant (p<0.05) reduction in both haematocrit and haemoglobin when compared to AOM treated WT mice (Figure 4.5, B & C).

4.3.5 Dpp4-/- and Fap-/- mice have reduced immune and inflammatory responses

Quantification of 15 cytokines involved in immune and inflammatory response indicates that both Dpp4-/- and Fap-/- mice have a reduced plasma concentration of key chemokines required for chemoattraction of immune cells. Saline treated Dpp4-/- mice have significantly (1226.9 pg/mL) (p<0.05) reduced IP-10 (CXCL10) compared to saline treated WT controls (1827.9 pg/mL). Although a significant increase in the level of IP-10 (CXCL10) was observed in AOM treated WT (3077.7 pg/mL) (p<0.001), Dpp4-/- (1914.4 pg/mL) (p<0.01) and Fap-/- (1980.8 pg/mL) (p<0.01) mice when compared to saline treated phenotype matched controls, AOM treated Dpp4-/- and Fap-/- mice showed a significant (p<0.001) decrease in IP-10 (CXCL10) when compared to AOM treated WT mice (Table 4.3). A significant decrease in RANTES (CCL5) is seen in saline treated Dpp4-/- (p<0.05) and Fap-/- (p<0.01) mice when compared to WT controls. In addition, Fap-/- saline mice show a significant increase in IL-1b (p<0.01) and VEGF (p<0.001). AOM treated Fap-/- mice have significantly (19590.9 pg/mL) (p<0.001) reduced eotaxin (CCL11) compared to saline treated FAP mice (24969.7 pg/mL) and significantly reduced (p<0.01) IL-10 compared to AOM treated WT mice (Table 4.3). No significant difference was seen between groups in GM-CSF (Granulocyte-macrophage colony-stimulating factor), IFN-γ (interferon gamma), IL-1a (interleukin 1 alpha), IL-2 (interleukin-2), IL-4 (interleukin 4), IL-13 (interleukin 13), LIX (C-X-C motif chemokine 5 or CXCL5), IL-17 (interleukin 17) and MIP-1a (macrophage inflammatory protein 1α).

4.3.6 Dpp4-/- and Fap-/- mice show increased levels of incretin hormones

Elevated levels of metabolic hormones has been identified as a factor in increased incidence of CRC (Ahmed et al., 2006). In the quantification of 14 metabolic hormones saline treated Dpp4-/- mice show the expected shift in incretin hormones with significantly increased levels of glucagon-like peptide 1 (GLP-1) (p<0.001) and resulting reduction in glucagon (p<0.01) compared to saline treated WT mice (Table 4.4). AOM treated Dpp4-/- mice had significantly increased levels of GLP-1 (p<0.05) and PYY (p<0.05) and significantly reduced levels of leptin (p<0.05) compared to AOM treated WT mice and also had significantly increased levels of GIP (p<0.001), IL-6 (p<0.05), glucagon (p<0.05), PYY (p<0.01) and resistin (p<0.01) when compared to saline treated Dpp4-/- mice (Table 4.4). Fap-/- mice also showed a similar shift in incretin hormones with saline treated Fap-/- mice showing

Table 4.3. Quantification of cytokines involved in inflammatory and immune responses. Plasma collected via cardiac bleed at 14 weeks post treatment from saline and AOM treated WT, Dpp4-/- and Fap-/-mice (n=6 per group) was evaluated for concentration of Eotaxin, VEGF, RANTES (Regulated upon Activation, Normal T Cell Expressed and Presumably Secreted), MIP-1α (macrophage inflammatory protein 1 alpha), GM-CSF, LIX, IP-10, IL-17, IL-13, IL-10, IL-4, IL-2, IL-1β, IL-1α, IFN-γ, using MILLIPLEX MAP Mouse Cytokine/Chemokine Magnetic Bead Panel (Millipore, cat. no. MCYTMAG70PMX32BK) with output reported as average fluorescent intensity plus or minus the SEM, asterisk denotes significance at the * <0.05, ** <0.01 and *** <0.001 probability level against WT control, cross denotes significance at the † <0.05, †† <0.01 and ††† <0.001 probability level against the phenotype matched saline controls.

	Saline			AOM		
	WT	**Dpp4-/-**	**Fap-/-**	**WT**	**Dpp4-/-**	**Fap-/-**
Eotaxin (CCL11)	10709.0 ± 972.2	10377.1 ± 544.0	10827.5 ± 379.3	9829.6 ± 541.6	8908.3 ± 660.8	8472.0 ± 512.5 †††
MIP-1a (CCL3)	30.7 ± 2.4	30.2 ± 2.1	32.8 ± 1.9	39.4 ± 13.6	29.0 ± 1.4	31.4 ± 3.5
IP-10 (CXCL10)	1754.9 ± 129.6	1215.6 ± 206.2 *	1507.8 ± 94.3	3027.6 ± 163.4 †††	2025.5 ± 174.4 *** ††	2032.9 ± 143.5 *** ††
RANTES (CCL5)	63.2 ± 5.0	44.5 ± 6.6 *	45.0 ± 4.2 **	60.6 ± 7.3	62.3 ± 8.8	116.1 ± 67.9
LIX	329.5 ± 114.7	521.6 ± 210.0	337.2 ± 104.3	268.9 ± 65.8	192.2 ± 50.4	339.9 ± 56.8
GM-CSF	21.5 ± 1.4	21.5 ± 0.8	20.8 ± 0.9	23.2 ± 5.5	22.9 ± 1.3	18.9 ± 1.0
IFN-g	46.5 ± 3.6	49.9 ± 4.0	49.0 ± 7.9	48.5 ± 12.6	45.9 ± 3.9	45.7 ± 3.2
IL-1a	34.5 ± 2.4	38.8 ± 4.6	38.9 ± 3.7	39.9 ± 3.7	46.5 ± 10.1	62.3 ± 22.8
IL-1b	20.5 ± 0.9	19.6 ± 0.9	27.3 ± 2.4 **	20.5 ± 0.9	20.6 ± 1.2	24.2 ± 3.2
IL-2	22.0 ± 1.0	26.4 ± 2.8	30.0 ± 3.9	36.3 ± 11.8	28.6 ± 1.4	31.4 ± 7.7
IL-4	26.0 ± 4.8	19.9 ± 1.6	24.5 ± 3.1	26.7 ± 3.1	23.0 ± 3.0	21.2 ± 1.7
IL-10	25.0 ± 1.9	34.8 ± 7.5	25.0 ± 1.4	34.0 ± 3.4 †	31.7 ± 2.1	23.7 ± 1.3 **
IL-13	39.8 ± 1.8	37.8 ± 2.9	40.3 ± 2.4	48.0 ± 12.2	41.4 ± 3.2	37.0 ± 2.2
IL-17	48.0 ± 2.5	53.6 ± 3.1	53.1 ± 3.4	56.3 ± 4.1	66.0 ± 7.8	70.0 ± 8.8
VEGF	31.9 ± 1.5	36.8 ± 3.0	45.2 ± 4.4 ***	37.0 ± 4.8	34.0 ± 2.2	38.5 ± 6.1

Table 4.4. Quantification of mouse metabolic hormones. Plasma collected via cardiac bleed at 14 weeks post treatment from saline and AOM treated WT, Dpp4-/- and Fap-/-mice (n=6 per group) was evaluated for concentration of Amylin (active), C-peptide 2, Ghrelin (active), GIP (total), GLP-1 (active), Glucagon, IL-6, Insulin, Leptin, MCP-1, PP, PYY (total), Resistin, and TNFα, were quantified using MILLIPLEX MAP Mouse Metabolic Hormone Magnetic Bead Panel (Millipore, cat. no. MMHMAG-44 K) with output reported as average fluorescent intensity plus or minus the SEM, asterisk denotes significance at the * <0.05, ** <0.01 and *** <0.001 probability level against WT control, cross denotes significance at the † <0.05, †† <0.01 and ††† <0.001 probability level against the phenotype matched saline controls.

	Saline			AOM		
	WT	**Dpp4-/-**	**Fap-/-**	**WT**	**Dpp4-/-**	**Fap-/-**
Amylin	73.1 ± 18.4	80.9 ± 14.3	140.1 ± 36.3	103.9 ± 35.4	94.6 ± 19.1	60.4 ± 9.1 †
C-peptide	532.2 ± 76.4	425.0 ± 30.7	967.3 ± 181.0	324.1 ± 76.6	456.5 ± 81.9	300.2 ± 50.1 †††
Ghrelin	44.4 ± 15.6	70.7 ± 16.2	45.0 ± 6.5	45.4 ± 5.8	50.8 ± 6.3	57.2 ± 10.0
GIP	641.0 ± 133.5	510.6 ± 90.8	2338.3 ± 352.7 ***	832.3 ± 256.7	1213.0 ± 179.8 †††	855.3 ± 181.2 †††
GLP-1	23.6 ± 1.6	33.3 ± 2.6 ***	37.9 ± 4.9 ***	23.8 ± 3.5	34.0 ± 3.8 *	48.3 ± 7.9 ***
Glucagon	42.0 ± 6.4	24.3 ± 1.5 **	38.5 ± 4.8	36.4 ± 4.7	32.6 ± 3.2 †	26.8 ± 3.3 †
IL-6	45.5 ± 7.4	33.3 ± 5.2	62.6 ± 14.8	76.6 ± 14.4 †	60.4 ± 12.0 †	87.0 ± 25.4
Insulin	239.0 ± 44.8	367.7 ± 78.5	843.8 ± 339.2	347.7 ± 66.8	416.6 ± 82.0	206.6 ± 34.9
Leptin	1485.3 ± 237.8	1404.2 ± 255.1	3446.5 ± 478.8 ***	2101.3 ± 441.7	1028.7 ± 197.2 *	1802.6 ± 220.7 ††
MCP-1	45.0 ± 6.9	49.9 ± 6.9	142.4 ± 53.1	90.2 ± 24.9	72.8 ± 17.9	97.6 ± 18.6
PP	147.0 ± 10.9	156.5 ± 5.6	150.1 ± 7.8	167.0 ± 10.4	168.0 ± 4.4	168.3 ± 20.5
PYY	118.5 ± 14.4	130.4 ± 15.1	590.8 ± 115.6 ***	203.5 ± 24.4 ††	350.8 ± 64.7 * ††	876.3 ± 255.3 **
Resistin	5411.5 ± 287.4	5495.8 ± 218.4	6253.4 ± 343.9	5741.0 ± 309.5	6643.9 ± 382.5 ††	5021.1 ± 319.2 ††
TNFα	31.2 ± 10.0	27.0 ± 5.4	113.2 ± 47.0 ***	40.8 ± 10.9	30.6 ± 5.8	55.9 ± 17.4
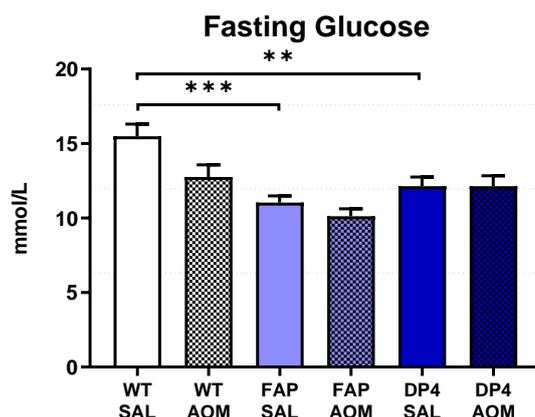
Figure 4.6. 28-week-old Dpp4-/- and Fap-/- mice have reduced fasting glucose. Fasting glucose in AOM and saline treated WT, Dpp4-/- and Fap-/- mice at 14 weeks post treatment. Mice were fasted for five hours and given a glucose bolus of 2g/kg via oral gavage 30 min prior to cardiac puncture with fasting blood sugar levels determined using an Accu-Chek Performa blood glucose meter. Bars are average glucose measurements in saline treated mice, WT (n=15), Fap-/- (n=24), Dpp4-/- (n=20), and in AOM treated mice, WT (n=18), Fap-/- (n=16) and Dpp4-/- (n=20). Asterisk denotes significance at the ** <0.01 and *** <0.001 probability level between groups. Values represent means and error bars ± standard error (SEM). Light grey dashed lines indicate average, upper and lower 95th percentile in healthy male C57BL/6 mice as reported by Jensen, Schnell and The Jackson Laboratory (Jensen et al., 2013; Schnell et al., 2002; The Jackson Laboratory, 2007).

significantly increased levels of gastric inhibitory polypeptide (GIP) ($p < 0.001$), GLP-1 ($p < 0.001$), as well as increases in leptin ($p < 0.001$), peptide tyrosine tyrosine (PYY) ($p < 0.001$) and tumour necrosis factor alpha (TNF-α) ($p < 0.001$) compared to saline treated WT mice (Table 4.4). AOM treated Fap-/- mice had significantly reduced levels of C-peptide ($p < 0.001$), GIP ($p < 0.001$), glucagon ($p < 0.05$), leptin ($p < 0.01$), resistin ($p < 0.01$) and amylin ($p < 0.05$) compared to saline treated Fap-/- mice, and had significantly increased levels of GLP-1 ($p < 0.001$) and PYY ($p < 0.01$) compared to AOM treated WT mice. AOM treated WT mice had significantly increased levels of IL-6 ($p < 0.05$) and PYY ($p < 0.01$) compared to saline treated WT mice (Table 4.4). No significant difference was seen between groups in ghrelin, insulin, MCP-1 (monocyte chemoattractant protein-1) and PP (pancreatic polypeptide hormone) levels.

4.3.7 Dpp4-/- and Fap-/- mice have reduced fasting glucose

Fasting blood glucose measurement was taken after a five hr fast and a glucose bolus 30 min prior to cardiac bleed as an indicator of metabolic control. Compared with average fasting blood glucose for C57BL/6 (Jensen et al., 2013) saline treated WT mice showed fasting glucose just above average and Fap-/- and Dpp4-/- mice showed fasting glucose comparable to the average (Figure 4.6). Fasting blood glucose in saline treated WT mice was significantly higher when compared to both saline treated Dpp4-/- ($p < 0.01$) and saline treated Fap-/- mice ($p < 0.001$), although lowered fasting blood glucose in Dpp4-/- and Fap-/- mice is not in the range indicative of hypoglycaemia. AOM treatment had no significant effect on fasting blood glucose in all three phenotypes (Figure 4.6).

4.3.8 Dpp4-/- and Fap-/- mice have altered dipeptidyl peptidase plasma activity

DPP plasma enzyme activity was increased in AOM treated WT and Fap-/- mice with both groups showing a non-statistical increase in total DPP activity compared to saline controls (Figure 4.7, A). Dpp4-/- mice showed a small amount of DPP enzymatic activity which is attributed to low level Ala-Pro-pNA cleavage by other S9B family enzymes. When compared to AOM and saline treated Fap-/- and WT mice, AOM and saline treated Dpp4-/- mice had significantly ($p < 0.001$) lower levels of residual DPP activity measured in the presence of the DPP4 specific inhibitor sitagliptin (Figure 4.7, A & B). WT mice showed no change in residual DPP activity between AOM and saline treated mice. Fap-/- saline treated mice have significantly ($p < 0.001$) decreased residual DPP activity compared with WT mice, and AOM treated Fap-/- mice showed a significant ($p < 0.01$) increase in residual DPP enzyme activity compared to Fap-/- saline controls (Figure 4.7, B).
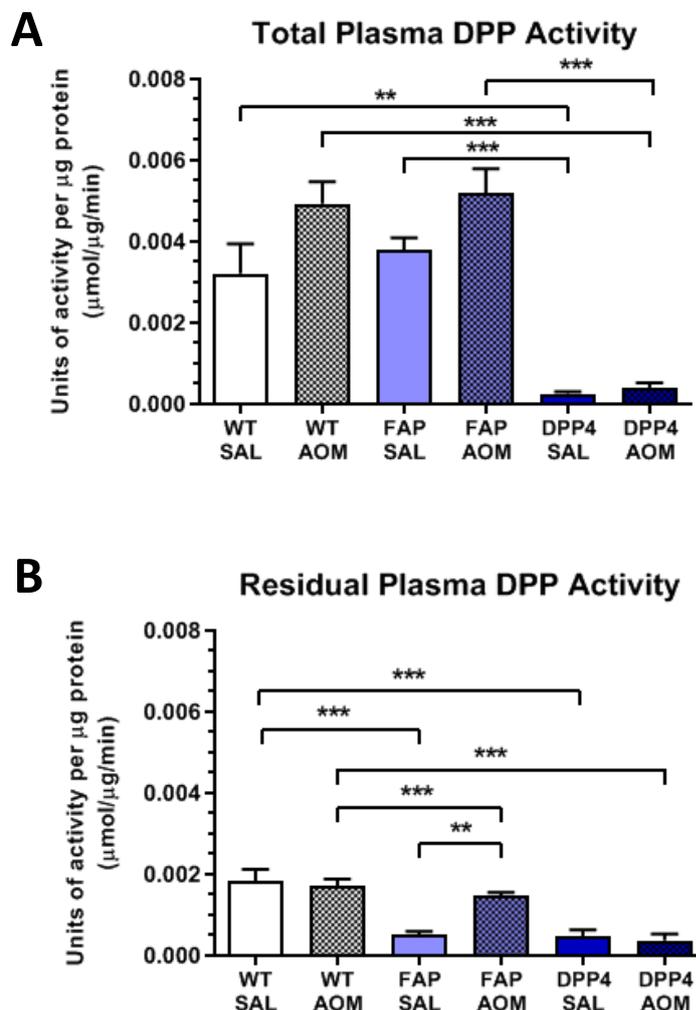
Figure 4.7. Total and residual plasma DPP enzyme activity. Plasma collected via cardiac bleed at 14 weeks post treatment. Plasma from saline and AOM treated WT, Dpp4-/- and Fap-/-mice was evaluated for A) total DPP enzyme activity, and B) residual DPP enzyme activity, determined using 10 μM sitagliptin to inhibit DPP4 activity with enzyme activity assays performed using the substrate H-Ala-Pro-pNA.HCl. Bars are averages from six individual plasma samples (n=6) for saline treated Fap-/- and AOM treated WT, Fap-/- and Dpp4-/- mice, and five individual plasma samples (n=5) for saline treated WT and Dpp4-/- mice. Asterisk denotes significance at the, ** <0.01 and *** <0.001 probability level between groups. Values represent means and error bars ± standard error (SEM).

4.4 Discussion

DPP4 and FAP have been identified as both promotors and inhibitors of tumour progression, while altered expression of DPP4 and FAP is seen in colorectal cancers and both have been recognised as potential diagnostic and therapeutic targets in CRC. The main finding of chapter four is it associates DPP4 and FAP expression with tumour suppressive actions in CRC. Mice lacking DPP4 develop a significantly increased number and increased size of adenomas and adenocarcinomas compared to wild type controls in the AOM CRC model. While mice lacking FAP did not develop more tumours than wild type controls in the AOM CRC model, tumour growth and penetrance in this phenotype was significantly increased. In addition, AOM treated Dpp4-/- mice showed a significant reduction in total numbers of aberrant crypt foci (ACF) compared to AOM treated WT controls. This is most likely related to the increased tumorigenesis observed in Dpp4-/- mince as ACF are characterised as pre-cancerous colonic lesions, and in the Dpp4-/- mice early lesions progressed quickly to forming tumours (Bird, 1995). When compared to AOM treated WT mice, AOM treated Dpp4-/- mice have a significant reduction in white blood cell numbers that is directly related to lymphocyte number. Additionally, both Dpp4-/- and Fap-/- mice treated with AOM have reduced plasma concentration of IP-10 (CXCL10) a key cytokine required for chemoattraction of immune cells which may be contributing to the differences observed in adenoma number and size between Dpp4-/- and WT mice and difference in adenoma size between Fap-/- and WT mice.

Chapter four is the first study to use this chemically induced carcinogenesis model with Dpp4-/- and Fap-/- mice and is also the first model to monitor these phenotypes over a 20 week period with mice reaching 28 weeks of age, full adult maturity at completion of the trial. In addition to the general observations from these phenotypes reported in chapter three, saline treated Dpp4-/- and Fap-/- mice show significantly reduced fasting blood glucose levels when compared to saline treated WT mice. Additionally, saline treated Dpp4-/- and Fap-/- mice show the expected increase in incretin hormones observed by others (Conarello et al., 2003; Gorrell et al., 2010). In this study saline treated Dpp4-/- mice have increased levels of circulating glucagon-like peptide 1 (GLP-1) and decreased levels of glucagon. This increase in circulating GLP-1 and increased ability to control blood glucose was also demonstrated by Conarello et al., (2003) in an obesity model at 24 weeks of age (Conarello et al., 2003). Moreover, in our study Fap-/- mice have increased levels of GLP-1 and glucose-dependent insulinotropic polypeptide (GIP). The patent application by Gorrell et al., (2010) targeting FAP inhibition for treatment of abnormal glucose metabolism, also showed an increase in circulating GLP-1 levels in Fap-/- mice comparable to that seen for Dpp4-/- mice (Gorrell et al., 2010). In addition to the significant increase in circulating GLP-1, Fap-/-

mice had a greater than 3-fold increase in GIP levels which is not seen in Dpp4-/- mice. GIP is shown to stimulate GLP-1 secretion (Janssen et al., 2013), the dramatic increase in GIP may indicate that Fap-/- mice overcome inactivation of GLP-1 via DPP4 enzyme activity through GIP driven increase in circulating GLP-1.

The increased tumour number and size in Dpp4-/- mice and increased size of tumours in Fap-/- mice is unusual given that both phenotypes show improved blood glucose control. In the AOM model of CRC it has been demonstrated that diet induced obesity enhances tumorigenesis while calorie restriction suppresses it, additionally, alterations in several biological pathways, including inflammation and other metabolic markers are associated with these effects (Olivo-Marston et al., 2014). Many known DPP4 substrates are involved in regulating these processes including GLP-1 and GIP which are associated with metabolic actions, as well as substrates associated with regulating the immune system such as stromal cell-derived factor (SDF or CXCL12) and RANTES (regulated on activation, normal T cell expressed and secreted or CCL5) (Yazbeck et al., 2009). Previous work using both Dpp4-/- and Fap-/- mice has shown that these phenotypes are protected against obesity and insulin resistance when fed a high fat diet (Conarello et al., 2003; Gorrell et al., 2010). Dpp4-/- mice produce less leptin, an adipocyte-derived cytokine shown to be elevated in obesity with involvement in cancer development, so DPP4 deficiency clearly effects metabolism in mice (Barone et al., 2012; Conarello et al., 2003). Given the lean body type reported in chapter three for Dpp4-/- mice in conjunction with improved glucose control and expected increase in incretin hormones seen in both Dpp4-/- and Fap-/- mice it would be expected that these phenotypes may confer a protection from tumour development. DPP4 and FAP both have multiple biological functions, although the increased metabolic control seen with DPP4 and FAP ablation may confer protection against tumour development, the increased tumour number and size seen in these mice may be related to alternate actions of each protein.

Given the multifaceted actions of DPP4 it is likewise possible that inhibiting DPP4 enzyme activity will be protective while removal of the protein binding domain will be harmful. DPP4 is known to initiate intracellular signalling and is shown to play a multitude of roles in maintaining cellular homeostasis (Gorrell, 2005; Mulvihill and Drucker, 2014). In normal tissue, DPP4 is constitutively expressed by an array of differing cell types, but primarily on epithelial and endothelial cells of the small intestine, liver and the kidney. In the immune system DPP4 is known as CD26 and is constitutively expressed on the surface of mature thymocytes, activated T-cells, B- cells, natural killer cells and macrophages (Gorrell et al., 2001). The protein structure of DPP4 comprises two distinct subdomains, an N-terminal domain which forms an eight- bladed propeller and a C-terminal domain that forms an α/β hydrolase domain which contains the three catalytic residues responsible for its serine

protease activity (Gorrell, 2005). DPP4 inhibitors such as sitagliptin bind to the catalytic site and block DPP4 enzyme activity. The propeller domain is a protein binding domain that binds multiple proteins including, adenosine deaminase (ADA), caveolin-1, fibronectin, plasminogen 2 and streptokinase, Na(+)-H(+) exchanger isoform NHE3, CD45 (protein tyrosine phosphatase), CARMA1 and glypican-3 (De Meester et al., 1999; Gorrell, 2005; Lambeir et al., 2003). These DPP4 binding partners are involved in a multitude of processes in different tissues where DPP4 is expressed but particularly in regulating extracellular matrix interactions involved in cell homeostasis and pathogenesis (Mulvihill and Drucker, 2014). Given that DPP4 acts as a protease as well as a binding protein able to bind extracellular matrix proteins like fibronectin and collagen, it is these independent functions that are likely to be involved in the actions of DPP4 in tumour suppression or promotion (Sulda et al., 2006).

DPP4 shows highly variable expression in human CRC which is dependent on the stage of cancer development although very little is known about the underlying mechanisms behind this variability (Cordero et al., 2000; De La Haba-Rodríguez et al., 2002). In patients with CRC high DPP4 expression in the tumour cells is correlated to overall worse survival rate and a higher rate of CRC recurrence suggesting that DPP4 is acting as tumour promoter in CRC (Lam et al., 2014). Further evidence of DPP4 being a tumour promoter in CRC is found in an animal study by Femia et al., (2013) where rats fed on a high fat diet were injected with the colon carcinogen, 1,2-dimethylhydrazine (DMH). In this work the DPP4 inhibitor sitagliptin was included in the diet of rats at an estimated dosage of 10 mg/kg body weight for 12 weeks, beginning one week after the last DMH injection and a reduction in the number of precancerous lesions was observed via counting mucin-depleted foci (MDF) (Femia et al., 2013). This work clearly provides evidence that inhibition of DPP4 enzyme activity may be protective during the early initiation stages of carcinogenesis. In contrast, Kissow et al., (2012) found that inhibition of DPP4 via oral gavage of sitagliptin at 400 mg/kg body weight twice per day did not impact the number of ACF, MDF or adenomas compared with control groups (Kissow et al., 2012). Kissow et al., (2012) used mice instead of rats and began six weeks of sitagliptin treatment 16 weeks after carcinogen induction. Maximal ACF formation is shown to occur by seven weeks after the final carcinogen injection with some adenomas already established at this timepoint (Rudd et al., 2019). In this 16 week timeline most adenomas will have formed so results from this study would only measure the effect of DPP4 inhibition on adenoma growth or progression, parameters which were not directly measured in end point analysis by Kissow et al., (2012). Additionally, the six week treatment timeline may not be enough for the anti-cancer effects of sitagliptin to be measurable. Based on the results taken from these two studies with Sitagliptin, it appears that inhibition of DPP4

enzyme activity may be protective during the early stages of carcinogenesis but may have no effect on adenoma growth once tumours are established. These results should be reflective of results presented in chapter four as removal of the DPP4 protein removes the enzyme activity the same as inhibition. Results in chapter four however demonstrate that Dpp4-/- mice treated with AOM have significantly higher numbers of adenomas that are larger in size when compared to WT mice treated with AOM. At the same time point, Dpp4-/- mice have significantly less ACF than WT mice. ACF are identified as the earliest histopathological manifestations of colon cancer with increased numbers of ACF correlated with increased risk of developing CRC although not all ACFs develop into CRCs (Femia et al., 2008; Wargovich et al., 2010). This contrasts with the animal work conducted by Femia et al, (2008) where DPP4 inhibition by sitagliptin reduced the number of pre-cancerous legions. It may be that when DPP4 is inhibited a reduction in cancer initiation is seen but when the DPP4 protein is completely absent tumour progression is occurring at a faster rate and thus more ACFs have fully developed into adenomas.

AOM treated Dpp4-/- and Fap-/- mice show signs of anaemia with significantly reduced red blood cell numbers as well as reduced haematocrit and haemoglobin compared to saline treated controls and AOM treated WT mice. Anaemia is a common extraintestinal complication seen with advanced CRC in humans dependent on tumour location and size so the reduction in red cell numbers seen in both Dpp4-/- and Fap-/- mice may be due to the more advanced tumour progression seen in these phenotypes (Mizoguchi et al., 2011; Muñoz et al., 2014). Dpp4-/- mice as well as mice receiving DPP4 inhibitor treatment have been shown to have increased haematopoiesis after radiation or chemotherapy (Aono and Sato, 2016). Hematopoietic stimulation is also associated with FAP with similar increase in haematopoiesis seen with inhibition of FAP in the absence of DPP4 that is related to increased G-CSF and erythropoietin activity (Jones et al., 2003). As the inhibition of DPP4 and FAP is associated with increased haematopoiesis, the increased propensity towards anaemia in the AOM model with Dpp4-/- and Fap-/- mice is unexpected. It is also noted that the related white blood cell growth factor, granulocyte-macrophage colony-stimulating factor (GM-CSF), which is also inactivated by DPP4 and FAP, was quantified as part of the mouse cytokine and chemokine magnetic bead panel and did not show any difference in plasma concentration between treatment groups. As DPP4 and FAP show overlapping function in the inactivation of these hematopoietic cytokines (Jones et al., 2003; Keane et al., 2011; O'Leary et al., 2013), a compensatory pathway may be in place in each knockout mouse strain resulting in continued inactivation of G-CSF and erythropoietin and an inability to compensate for CRC related blood loss.

The absence of the DPP4 protein may result in increased tumour numbers through loss of DPP4 binding to the extracellular matrix (ECM) which may lead to tumour cells migrating and thus an increase in metastasis. DPP4 is known to bind to a major component of the ECM, fibronectin, an association identified as a suppressor of metastasis in solid tumours as it allows tumour cells to be restrained at the primary tumour site (Cheng et al., 2003; Piazza et al., 1989; Tan et al., 2004). DPP4 expression is shown to be significantly altered in solid tumour tissue and reduction in DPP4 expression in melanoma, as well as lung, prostrate and colorectal cancer has been associated with increased tumorigenesis and invasive metastasis, while its re-expression in melanoma, prostrate and lung cancer leads to increased growth factor dependence and reversal of the malignant phenotype (Bogenrieder et al., 1997; Morrison et al., 1993; Tan et al., 2004; Wesley et al., 2004, 1999). The increase in tumorigenesis observed in Dpp4-/- mice may be due to loss of DPP4 mediated binding of the tumour cells to the ECM via fibronectin, which would result in reduced adhesion of tumour cells at their primary site and increased metastasis (Tan et al., 2004; Wesley et al., 1999).

Due to the marker limitations in the metabolic hormone immunoassay, plasma concentrations of the known DPP4 substrate glucagon-like peptide-2 (GLP-2) was not included in the results. Although inhibition of DPP4 enzyme activity after tumour initiation is protective against tumorigenesis, ablation of the protein and resulting long term increase in the active form of it's known substrate GLP-2 may result in increased tumour numbers in the colon. GLP-1 and GLP-2 are released from the enteroendocrine L-cells of the intestinal epithelium after nutrient stimulation (Holst, 2007). In similar form to the insulinotropic action of GLP-1, GLP-2 has been shown to play an intestinotrophic role, promoting proliferation and inhibiting apoptosis in the intestinal mucosa and has been associated with increased rates of colonic neoplasia in carcinogen-treated mice (Ghatei et al., 2001; Thulesen et al., 2004). The tumour promoting effect of GLP-2 in the colon and its regulation by DPP4 has been previously established where Gly2-GLP-2 a stable long acting analogue of GLP-2 resistant to N-terminal processing by DPP4 significantly increased the incidence of colonic neoplasms in chemically induced murine CRC models using 1,2-dimethylhydrazine (DMH) and its metabolite azoxymethane (AOM) in mice, and 2-Amino-1-methyl-6-phenylimidazo[4,5-b]pyridine (PhIP) in rats (Iakoubov et al., 2009; Thulesen et al., 2004; Trivedi et al., 2012). Administration of active GLP-2 is also associated with increased activity of the canonical (c) Wnt pathway within intestinal crypt cells, the main control point for proliferation and maintenance of intestinal stem cells (Dubé et al., 2008; Novellasdemunt et al., 2015; Trivedi et al., 2012). The Wnt pathway is additionally one of the main signalling pathways associated with the development of human colorectal cancer (Ashton-Rickardt et al., 1989;

Ichii et al., 1993; Sparks et al., 1998). Endogenous bioactive GLP-2(1-33) has an active half-life of approximately seven minutes due to N-terminal truncation by DPP4 activity which produces the inactive metabolite GLP-2 (3–33) that has been shown to have no effect on mucosal growth (Drucker et al., 1997; Hartmann et al., 2000b, 2000a). As an increase in bioactive GLP-2 is linked to the three major factors for CRC development, control of mucosal proliferation and maintenance, colonic inflammation, and Wnt signalling, and, ablation of DPP4 would result in increased levels of active GLP-2(1-33) within the colon, the increased tumour load seen in Dpp4-/- mice treated with AOM may be directly related to prolonged activity of GLP-2.

In this study Fap-/- mice treated with AOM developed the same number of tumours as AOM treated wild type controls, however tumour growth and penetrance in Fap-/- mice was significantly greater with Fap-/- mice presenting with significantly more ($p<0.05$) 4-6mm tumours as well as very large >6mm tumours which were not seen in WT mice. FAP is not expressed in normal tissue but is known to be induced in activated fibroblasts and epithelial cells in response to wound healing as well as in areas of tissue damage such as inflammation and cancer (Rettig et al., 1988; Dunn, 2012). FAP is shown to be expressed in the stroma of human colorectal tumours and FAP expression and activity has been closely linked to tumour advantage where its overexpression is shown to promote tumour growth, while genetic deletion and enzymatic inhibition of FAP reduces tumorigenesis (Garin-Chesa, Old and Rettig, 1990; Cheng et al., 2002; Santos et al., 2009). In epithelial tumours such as CRC, FAP presence is associated with cancer associated fibroblasts (CAF). CAFs are vital factors in tumorigenesis as they supply the tumour with growth factors and enzymes involved in the degradation of the extracellular matrix (Teichgräber et al., 2015). FAP presence in CAFs is shown to promote malignant and invasive behaviour in epithelial cancer so it is unexpected that its absence is resulting in increased tumorigenesis in chapter four. As described with DPP4, FAP is a multifunctional protein with both enzymatic and non-enzymatic actions. Additionally, FAP enzyme activity is identified as a necessary factor correlated with the tumour promotive actions of FAP. Results taken from Cheng at al., (2005) using a murine xenograft model of HEK293 cells transfected with both wt and enzyme mutant FAP showed that overexpression of wt FAP significantly enhanced tumorigenicity when compared to enzyme mutant FAP (Cheng et al., 2005). As discussed in relation to DPP4, removal of the FAP protein in Fap-/- mice would result in the removal of both the enzyme activity and protein binding interactions. While removal of FAP enzyme activity may be tumour suppressive, removal of the extra-enzymatic modes of action may be tumour promotive (Yu et al., 2010).

This increase in tumour size seen in both Dpp4-/- and Fap-/- mice may be as a result of the observed decrease in IP-10 (CXCL10) which acts as a chemoattractant for a variety of immune cells (Vazirinejad et al., 2014). Although the level of IP-10 is significantly increased with AOM treatment in all three phenotypes, AOM treated Dpp4-/- and Fap-/- mice show a significant decrease in IP-10 when compared to WT controls which may contribute to increased tumour growth. IP-10, also known as interferon-γ inducible protein 10 (CXCL10), is a chemokine that exerts biological effect through its binding to the CXCR3 receptor (Liu et al., 2011). The CXCL10/ CXCR3 association is involved in immunoregulation where CXCL10 acts as a chemoattractant recruiting CXCR3-positive cells, including activated T lymphocytes, natural killer (NK) cells, inflammatory dendritic cells, macrophages and B cells, towards sites of inflammation, infection and neoplasia (Loetscher et al., 1998; Qin et al., 1998; Sallusto et al., 1998). The immunomodulatory properties of CXCL10 have been shown to have a significant antitumor effect through recruitment of immature antigen-presenting, dendritic or early activated T cells into the tumour site (Fujita et al., 2009; Jiang et al., 2009; Lu et al., 2008). The significant reduction in CXCL10 levels in Dpp4-/- and Fap-/- mice compared to WT controls indicates that Dpp4-/- and Fap-/- mice have a diminished ability to effect immunoregulation through CXCL10, this may contribute to increased tumorigenesis through reduced immune response to the neoplastic lesions.

The timeline of the model of CRC used in chapter four was reduced due to early tumour development which is likely related to the influence of environmental factors. The expected timeline for the AOM model used was a 30-week model with adenomas expected to be induced 24 weeks after the sixth AOM injection in WT C57Bl/6 mice. In our hands using this model, Dpp4-/- mice, due to the number of adenomas present in their colon, often developed bowel prolapses and rectal bleeding and were killed 14 weeks after the final AOM injection due to animal welfare concerns, 10 weeks earlier than expected. This was reflective of previous work conducted by our group using the AOM murine model for early stage tumour formation, in this model mice presented with large ACF, as well as small tumours, six weeks after the sixth AOM injection which is an unexpected result as tumour development is not expected with the six week model (Rudd et al., 2019). These results indicate that in our hands the AOM model results in more aggressive tumour development than previously reported. CRC tumorigenesis in mice is largely impacted by the microenvironment from which the tumour arises. Interactions between the resident microbiota and CRC localised immune cells support a microenvironment capable of providing a swift respond to stimuli. Changes in the homeostasis of this microenvironment impacts the dynamic equilibrium of the epithelium within the colon and creates a proclivity for disease. There is now growing evidence that resident microbiota play a critical role in influencing the frequency of tumour

initiation and rate of progression within the colon (Leystra and Clapper, 2019). The influence of environment is a likely driver for changes in gut microbiota as it is shown that there is a high degree of facility-level individuality in animal handling, housing, and care that all contribute to heterogeneity in gut microbiota. This includes treatment to animal chow such as sterilisation by irradiation or autoclave, type of housing used such as ventilated versus non ventilated cages, the presence of differing mouse strains within a facility as well as difference in vendors suppling the mice which are all shown to alter bacterial species and their relative abundance (Rausch et al., 2016). Additionally, these environmental influences leading to differences in the microbiota within differing institutions impacts propensity towards disease when using the same mouse model in C57Bl/6 mice (Franklin and Ericsson, 2017). It is likely that the reduced timeline of tumour development seen in our work is related to the influence of institutional-specific microbiota on disease progression which allowed for refinement of the AOM model in our hands reducing the overall timeline from 30 weeks down to 20 weeks (Cheng et al., 2020).

General DPP enzyme activity was measured using H-Ala-Pro-pNA which is a substrate of DPP4, FAP, DPP8 and DPP9 at neutral pH (Dubois et al., 2009). In the presence of a DPP4 inhibitor such as sitagliptin H-Ala-Pro-pNA can be used to determine residual FAP, DPP8 and DPP9 enzyme activity (Dubois et al., 2009). Total DPP activity is greatly reduced in plasma from Dpp4-/- mice when compared to WT and Fap-/- mice which indicates that the majority of H-Ala-Pro-pNA cleavage is coming from DPP4 in plasma from WT and Fap-/- mice. Total DPP activity is increased in AOM treated WT, Fap-/- and Dpp4-/- mice when compared to phenotype matched saline controls. This may be due to increased DPP4 activity in WT and Fap-/- mice as increased DPP4 plasma activity is associated as a poor prognostic factor in CRC (De Chiara et al., 2014; Larrinaga et al., 2015). In Dpp4-/- mice this increase in total DPP activity may be as a result of a compensatory increase in DPP activity in the absence of DPP4 (Keane et al., 2014). In the presence of the DPP4 specific inhibitor sitagliptin at two times the IC50 concentration, comparative residual DPP activity is seen in saline treated Fap-/- and Dpp4-/- mice as well as AOM treated Dpp4-/- mice. The similarity in this activity between saline treated Dpp4-/- and Fap-/- mice and the lack of FAP in normal tissue indicates that this activity is likely from DPP8 and DPP9 activity (Dubois et al., 2009). Compared to saline treated Fap-/- and Dpp4-/- mice as well as AOM treated Dpp4-/- mice, AOM treated Fap-/- and WT mice and saline treated WT mice have increased amounts of residual DPP activity in the presence of DPP4 inhibitor sitagliptin, this may be due to increase in the presence of other DPP family members in response to AOM treatment in WT and Fap-/- mice. Inflammation is commonly associated with sporadic colon cancer which is the form of colon cancer modelled using AOM in mice (Terzić et al., 2010). This increase in

DPP activity in response to inflammation of the bowel has been previously identified where an increase in both DPP8 and DPP2 activity is seen in WT and Dpp4-/- mice with dextran sulfate sodium induced colitis (Yazbeck et al., 2010).

DPP4 inhibitors such as sitagliptin and vildagliptin have been in clinic for over eight years and are used worldwide to treat T2DM (Wu et al., 2014). While FAP specific inhibitors are currently under investigation as an alternate treatment for T2DM due to their comparative ability to reduce fasting blood glucose and increase glucose tolerance through increased insulin sensitivity (Gorrell et al., 2010). Given the multitude of biological roles played by DPP4 and FAP and what is known about the role of these proteins in cancer, the safety of long term inhibition of DPP4 and FAP in patients with T2DM is a warranted concern as it may increase their cancer risk (Lamont and Andrikopoulos, 2014; Vangoitsenhoven et al., 2012). In addition to these concerns, there is also considerable evidence that DPP4 and FAP inhibitors could be retargeted for other uses including cancer therapy. Results taken from chapter four are some of the first to use Dpp4-/- and Fap-/- mice with the AOM model of CRC and have shown that removal of DPP4 protein expression leads to a significantly increased number of adenomas, while removal of FAP protein significantly increases adenoma size. This is particularly concerning given the number of T2DM patients currently on DPP4 inhibitors and the potential use of FAP inhibitors as a newly emerging treatment for T2DM. However, this result was not observed when DPP4 inhibitors where utilised in other CRC models (Femia et al., 2013; Kissow et al., 2012). DPP4 and FAP are multifunctional proteins with both enzymatic and non-enzyme activities that play a role in cancer biology, the comparison between results seen with Femia et al., (2013) and Kissow et al., (2012) and the increased tumorigenesis seen in chapter four may be related to the protein binding actions of DPP4 and FAP which are shown to play a role in ECM interactions that control tumour growth and metastasis. Results taken from this work confirm that both DPP4 and FAP are involved in CRC tumour development and highlights the need for further work to identify the mechanisms behind the effects of their ablation and inhibition on different aspects of tumorigenesis.

4.5 Conclusion

Chapter four clearly demonstrates that both DPP4 and FAP play a role in tumour pathogenesis, with exposure to AOM, Dpp4-/- mice develop a significantly increased number of adenomas and adenocarcinomas while both Dpp4-/- and Fap-/- mice have significantly increased tumour growth and penetrance. Dpp4-/- mice also show a significant reduction in total numbers of ACF which indicates that when DPP4 protein is completely absent tumour progression is occurring at a faster rate and thus more ACFs have developed into

adenomas. Dpp4-/- and Fap-/- mice have reduced plasma levels of immune cell chemoattractant CXCL10 which has a known antitumor effect through recruitment of immune cells into the tumour site, additionally, Dpp4-/- mice have significantly reduced lymphocyte numbers indicating that an impaired immune response to tumorigenesis may be contributing to increased tumour growth in both phenotypes. Increase in tumorigenesis in Dpp4-/- mice may be related to the multiple actions of DPP4 in the colon where the absence of DPP4 enzyme activity leads to increased proliferation in intestinal mucosa through increase activity of GLP-2(1-33) and absence of the protein binding domains decreases fibronectin mediated tumour cell adhesion to the extracellular matrix increasing incidence of metastasis. In summary this work confirms that both DPP4 and FAP are involved in CRC tumour development and highlights the need for further work to identify the mechanisms through which ablation of DPP4 and FAP increases tumorigenesis. Given the continued interest in both DPP4 and FAP inhibitors as therapeutics, further work should be conducted to unpack whether the increased tumorigenesis described in this study is due to their enzyme activity or the ability of these multi-faceted proteases to bind and regulate ECM interactions.

Chapter 5

General discussion and conclusion

5.1 DPP4 and its multifaceted role in cancer

Dipeptidyl peptidase 4 (DPP4) is a multi-functional cell surface protein with a wide spectrum of actions. It is due to the diversity of actions associated with DPP4 that its role in initiation and progression of cancer is yet to be defined, with the current body of research indicating that it can act as both a tumour suppressor and tumour promoter. Results in chapter two show DPP4 inhibitors can reprogram the metabolic pathway of the cell through AMPK and non- AMPK related pathways. Chapter three establishes the AOM model of colorectal cancer in Dpp4-/- and Fap-/- mice which gave insights into the DPP4 and FAP phenotypes independent of the tumour model and identified areas for refinement that led to improvements in animal welfare. Finally, chapter four clearly demonstrates that in the absence of DPP4 and FAP an overall worse tumour progression is seen that could be due to reduced plasma levels of IP10 indicating a reduced immune response at the tumour site. This work is the first study to use this chemically induced carcinogenesis model with Dpp4-/- and Fap-/- mice and demonstrates that both DPP4 and FAP play a role in tumour incidence and development and that DPP4 plays a significant role in tumour prevalence. Despite this chapter two indicates that DPP4 inhibitors may provide a novel therapeutic approach for targeted metabolic reprogramming of cancer cells positioning them as potential anti-cancer agents for some specific tumour types.

The collective results taken from this work reflect the larger body of research into DPP4 and FAP and further highlights the multifunctional nature of these proteins. DPP4 and FAP can undertake different biological functions in tumorigenesis dependent on localisation and cells of origin, DPP4 is also a known effector of immune modulation and through its enzymatic activity which is able to degrade multiple chemokines, an action that will have varied effect on tumour growth dependent on the target substrate. As binding proteins DPP4 and FAP interact with extracellular matrix proteins and can influence adhesion, migration, and metastasis and both have a defined involvement in metabolism. The inhibition of DPP4 is correlated with AMPK activation which is shown to be tumour suppressive, although the correlation between the actions of DPP4 and AMPK may also be related to the dual role of DPP4 in cancer biology as AMPK is also shown to play a tumour promotive or suppressive role dependent on the stage of tumour development. The role that these proteins play in tumorigenesis is explored further below.

5.1.1 Inhibition of DPP4 enzyme activity is associated with the tumour suppressive actions of AMPK

In chapter two DPP4 inhibition by sitagliptin was shown to reduce cellular energy metabolism and proliferation, tumour suppressive actions that were associated with an increase in both AMPK and phosphorylated AMPK. AMPK has known tumour suppressive actions, it phosphorylates downstream targets that promote catabolic pathways while suppressing anabolic pathways, cell cycle progression, and other ATP-consuming processes. Through these actions, AMPK restricts cell growth and proliferation and promotes ATP synthesis to balance energy homeostasis and maintain cell viability (Vara-Ciruelos et al., 2019b). The relationship between DPP4 inhibition and AMPK activation has been previously established in hepatic steatosis where DPP4 inhibitor gemigliptin was shown to reduce the molecular hallmarks of fatty liver via AMPK phosphorylation (Hwang et al., 2015b), and, in atherosclerosis where sitagliptin was shown to reduce atherosclerotic lesions through the regulation of AMPK (Zeng et al., 2014). The results taken from chapter two indicate that inhibition of DPP4 enzyme activity will impart tumour suppressive actions through increased AMPK activation which are in direct contrast to the results taken from chapter four. These results indicate that the inhibition of DPP4 enzyme activity may be tumour suppressive while removal of the direct protein interactions is promotive. On the other hand, the actions of AMPK itself have been shown to be multifaceted in relation to tumour suppressive or promotive actions.

AMPK initiates its tumour suppressive actions when it is activated through the binding of AMP and displacement of ATP at a crucial site on the γ regulatory subunit, this causes a conformational change promoting net phosphorylation and subsequent activation of the catalytic subunit by upstream kinases (Hardie and Hawley, 2001). In this manner AMPK is activated during situations of cellular energy stress via depletion of ATP and resulting increase in AMP, AMPK is also activated via AMP independent mechanisms including increases in intracellular Ca^{2+} (Hawley et al., 2005; Woods et al., 2005), glucose starvation (Zhang et al., 2017) and by DNA damage (Vara-Ciruelos et al., 2018). Upon activation, AMPK is shown to phosphorylate a range of downstream proteins, with approximately 60 now established as targets including the mTORC1 pathway which is required to activate the translation of proteins required for cells to proliferate (Hardie et al., 2016; Wullschleger et al., 2006). Despite evidence associating the downstream effects of AMPK activation with tumour suppression, several studies have identified that AMPK may also protect tumour cells and promote tumour growth once the disease is established.

The impact of removal of AMPK on tumorigenesis has been studied in mouse models of lymphoma and leukaemia. A global knockout of the two isoforms of the AMPK catalytic subunits (α1 and α2) is embryonic lethal which has driven the use of tissue-specific knockouts, haematopoietic cells make an excellent target for this work as they only express the α1 subunit requiring only a single gene knock out (Rolf et al., 2013). In mouse models of B-cell and T-cell lymphoma, tissue specific knockout of the Prkaa1 gene encoding AMPK-α1 markedly accelerated lymphoma development and reduced tumour free survival with lymphoma development seen in all mice carrying the AMPK-α1 deletion. Knockdown of AMPK in tumour progenitor cells was also shown to increase the 'Warburg effect', enhancing glycolysis and glucose uptake even in normoxic conditions (Adams et al., 1985; Hagenbeek and Spits, 2008; Vara-Ciruelos et al., 2019a). The increase in glucose uptake with loss of AMPK in tumour cells using aerobic glycolysis or the "Warburg" metabolic model is reflective of results seen in chapter two where inhibition of DPP4 by sitagliptin reduced the metabolic output of THP-1 cells with a high reliance on glycolysis for cellular energy demands. Interestingly treatment with sitagliptin was associated with significant increase in the presence of both AMPK and activated AMPK in THP-1 cells, linking the inhibition of DPP4 with metabolic control through increased AMPK activation.

In an alternate model of T-cell lymphoma where murine haematopoietic stem cells carried a floxed AMPK-α1 gene and Cre recombinase driven by a tamoxifen-inducible promoter, treatment with tamoxifen to acutely delete AMPK-α1 once lymphoma was developed reduced recovery of lymphoma cells and enhanced survival (Kishton et al., 2016). In an another mouse model of acute myeloid leukaemia (AML) using irradiated mice lacking an active endogenous immune system and transplanted with haematopoietic progenitor cells lacking AMPK-α1, the loss of AMPK from leukaemia-initiating cells delayed the onset of disease and enhanced overall mouse survival (Saito et al., 2015).

The overall discrepancy in the actions of AMPK towards tumour promotion or suppression appears to be related to the point in time where AMPK is deleted. In work where loss of AMPK-α1 occurs early prior to formation of lymphoma AMPK appears to impart tumour suppressive actions, however, when AMPK deletion coincided with initiation of tumorigenesis or was brought on after initiation, AMPK appeared to be acting as a tumour promoter (Vara-Ciruelos et al., 2019b). Loss of AMPK prior to the onset of tumorigenesis would eliminate its downstream actions *in vivo*, including control over the mTORC1 pathway which would result in unregulated biosynthesis and heightened cell growth, creating a metabolic and proliferative state that is supportive of tumour formation (Wullschleger et al., 2006).

In the results reported in chapter two, the inhibition of DPP4 and correlated AMPK activation is shown to be tumour suppressive through decrease in cell metabolism and proliferation. The correlation between the actions of DPP4 and AMPK may in part explain the varied roles identified for DPP4 in terms of tumour promotive or suppressive actions as AMPK is also identified as playing a dual role in tumorigenesis dependent on stage of tumour development. To further investigate the relationship between DPP4, AMPK and tumorigenesis, additional work comparing the impact of DPP4 inhibition on AMPK activation in immune cells would be beneficial. Measurement of cellular bioenergetics using the XFe analyser could be conducted using a greater number of timepoints to identify the ongoing impact of DPP4 inhibition on cellular metabolism during the period where the greatest impact is seen, as well as after recovery from the effects of DPP4 inhibition. In addition to this, quantification of AMPK expression and activation via semi quantitative RT-PCR to measure mRNA level as well as western blot would provide a better understanding of the impact of DPP4 inhibition on AMPK protein expression, extending the timeline out to include measurements prior to addition of DPP4 inhibitor as well as after complete recovery from DPP4 inhibition would provide a better view of the impact on AMPK. In conjunction with this work the relationship between DPP4 inhibition, DPP9 expression and AK2 would also need to be investigated to be investigated as suggested in chapter two.

5.1.2 Removal of non-enzymatic actions of DPP4 is tumour promotive

In chapter four the absence of DPP4 in knockout mice was correlated with increased tumorigenesis. Loss of DPP4 is associated with promotion of cancer growth in multiple cell types including neuroblastoma (Arscott et al., 2009), glioma (Busek et al., 2012), ovarian cancer (Kikkawa et al., 2005) prostate cancer (U. V Wesley et al., 2005) as well as in colon cancer HT-29 cells (Lefort and Blay, 2010) with re-expression of DPP4 being shown to revert the malignant phenotype. Interestingly, reversion of malignancy appears to be independent of DPP4 enzyme activity as re-expression of enzyme negative DPP4 produces similar anti-tumorigenic results to wildtype DPP4 re-expression (Arscott et al., 2009; Busek et al., 2012; Kikkawa et al., 2005; Wesley et al., 2004). These combined results reflect those seen in chapter four where ablation of DPP4 resulted in a significant increase in colonic tumour number and size, but is incongruent with work from both Femia et al., (2013) who found that inhibition of DPP4 by sitagliptin was tumour suppressive, lowering the number of precancerous lesions in a rat model of CRC, and Bishnoi et al., (2019) who showed that patients with CRC or lung cancer who were treated with DPP4 inhibitors exhibited a statistically significant survival advantage (Bishnoi et al., 2019; Femia et al., 2013). Taken together these results indicate that down regulation or removal of the DPP4 protein is tumour

promoting while inhibition of DPP4 enzyme activity is tumour suppressive indicating that the increase in tumour load seen in chapter four may be related to the removal of the non-enzymatic actions of the protein.

Increased DPP4 expression is shown to suppress tumour metastasis and invasiveness in ovarian cancer cells through increased expression of E-cadherin as well as α- and β-catenin (Kajiyama et al., 2003). E-cadherin is a transmembrane glycoprotein involved in epithelial–mesenchymal transition (EMT) that mediates intercellular adhesion in epithelial cells through complexing with the actin cytoskeleton via cytoplasmic α- and β-catenin and is shown to play a pivotal role in tumour suppression, while reduction in expression of E-cadherin is noted as a key contributor to tumour progression and acquisition of an invasive phenotype (Luo et al., 1999; Takeichi, 1993). Increased DPP4 expression in ovarian cancer is also associated with a morphological change, with DPP4 expressing cells moving from fibroblastic scattered growth to an epithelioid cobblestoned growth pattern. DPP4, E-cadherin and β-catenin are also shown to be colocalised within the cell-cell adherens junctions (Kajiyama et al., 2003). The correlation of DPP4 expression with increase in expression of E-cadherin and β-catenin in addition to their colocalization within cell junctions indicates that DPP4 may play a tumour suppressive role through regulation of proteins involved in cellular adhesion. In chapter four measurement of any ECM proteins was out of scope, but follow on work should include immunostaining for E-cadherin and β-catenin in tumours and surrounding tissue for comparison in Dpp4-/- and WT mice to determine if removal of the DPP4 protein is driving increased tumorigenesis through a corresponding reduction in expression of E-cadherin and β-catenin.

The association between DPP4 and E-cadherin is not widely reported in cancer research but the linkage between their expression and control of cellular invasion is seen in human placentation. During the first trimester extra villous trophoblast cells adhere to the uterine wall, infiltrate the basal plate and invade the spiral arteries, a physiological process required to establish maternal–foetal circulation (Shih et al., 2002). In this action trophoblasts acquire an invasive phenotype to allow infiltration into decidual issue and maternal arteries and it is suggested that the trophoblast invasion of maternal tissue partly imitates that of tumorous growth. As the trophectoderm layer is the outer layer of the blastocyst, trophoblasts located in the proximal part of the cell column will have a non-invasive phenotype while trophoblasts migrating in the decidual tissue have an invasive phenotype. During placental development DPP4 expression is strongly detected via immunohistochemical staining in the non-invasive cells of the proximal region of the cell column while its presence is not detected in the invasive cells migrating into the decidual tissue, indicating that cells with positive DPP4

presence have a non-invasive phenotype (Sato et al., 2002). This change in expression pattern and localisation of DPP4 during early placental development is similar to that seen for E-cadherin suggesting that the change in the localisation and downregulation of both are involved in development of the invasive phenotype (Floridon et al., 2000; Kajiyama et al., 2003; Sato et al., 2002).

In addition to increased E-cadherin expression, increased expression of DPP4 and resulting reduction in tumorigenicity in ovarian cancer cells was also correlated with down-regulated expression of matrix metalloproteinase 2 (MMP-2) and membrane type 1 matrix metalloproteinase (MT1-MMP), as well as increased expression of tissue inhibitors of matrix metalloproteinases (TIMPs) (Kajiyama et al., 2003). Matrix metalloproteinases (MMPs) are involved in the proteolytic degradation of extracellular matrix inclusive of the basement membrane, a process that is essential for invasion and subsequent metastasis of tumour cells, while the action of MMPs is controlled through the binding of TIMPs to the MMP catalytic site. Through the control of MMPs, TIMPs inhibit tumour invasion, angiogenesis and metastasis, disruption in the balance between the expression of MMPs and TIMPs is shown to be an important factor driving tumour cell invasion and metastasis (Khokha et al., 1989; Kikkawa et al., 1997). Increased expression of DPP4 in ovarian cancer cells is associated with decreased tumorgenicity both *in vivo* and *in vitro*, this reduction in metastasis and invasion seen with increase in DPP4 expression is correlated with downregulation of MMP-2 and MT1-MMP and a related increase in TIMPs coupled with the increase in E-cadherin . These results link DPP4 with the upregulation of proteins involved in cellular adhesion, tumour suppressive actions that are not associated with DPP4 enzyme activity as the reduction in the evasive potential of ovarian cancer cells overexpressing DPP4 was not affected by the presence of DPP4 inhibitors (Kajiyama et al., 2003). The results reported in chapter four show that DPP4 knockout mice have significantly increased tumour number and size, these findings are in direct contrast to results from Fermia et al., (2013) where inhibition of DPP4 by sitagliptin was tumour suppressive and may indicate that removal of the DPP4 protein and its associated non-enzymatic actions is tumour promoting. Follow on work to target the non-enzymatic effects of DPP4 in the tumour microenvironment and comparing these to inhibition of DPP4 enzyme activity would help to define the impact of DPP4 non-enzymatic actions in cancer progression.

Chapter four relates the absence of DPP4 with increased tumorigenesis but does not compare removal of the protein with inhibition of enzyme activity. Follow on work could continue to use the chemical AOM model to compare selective DPP4 inhibition with complete ablation of DPP4. Employing three differently timed AOM-rodent models would

allow the ability to compare the effects of DPP4 inhibition with knockout during the three different stages of the tumorigenic process, initiation, promotion and progression. A six hour single dose AOM model could be used to determine the effect of DPP4 inhibition and knockout on the acute apoptotic response to genotoxic carcinogens, i.e. the first steps in the initiation of cancer. A 12 week model, utilising six doses of AOM could be used in conjunction with sitagliptin treatment to observe the effects of DPP4 inhibition or knockout on early ACF formation, i.e. tumour development, 6 weeks after treatment. Finally, the effect of DPP4 inhibition on CRC progression could be determined using the same 20 week model employed in chapter four but including a group of mice receiving sitagliptin treatment and would allow comparison between results seen for DPP4 knockout with DPP4 inhibition on tumour progression. This work could also incorporate quantification of metabolic hormones and inflammatory cytokines, immunostaining for E-cadherin and β-catenin and MMPs in tumours and surrounding tissue, and identification of MMP activity changes in intestinal mucosa could be identified via gelatine zymography. The use of the three experimental models would allow for identification of key insights into the individual roles of DPP4 enzyme activity and DPP4 protein binding in the three main stages of CRC, initiation, promotion and progression.

5.1.3 The tumour suppressive actions of DPP4 inhibition is associated with increased DPP9 expression

In chapter two DPP4 inhibition by sitagliptin was shown to increase DPP9 protein expression. It is this increase in DPP9 protein and subsequent increase in enzymatic processing of AK2 that may be a driver for the tumour suppressive reduction in cellular bioenergetics seen with DPP4 inhibition. A proteomic study performed by Wilson et al., (2013) demonstrated the ability of DPP8 and DPP9 to modify N terminus of AK2 *in vitro* and showed that DPP9 had a higher affinity for this substrate over DPP8 (Wilson et al., 2013). Finger et al., (2019) then demonstrated that DPP9 mediates the cytosolic N-terminal processing of AK2 *in vivo*, targeting it for degradation and that DPP9 assisted degradation competes with mitochondrial protein import (Finger et al., 2020). It is the extreme N terminus of AK2 that is shown to direct cytoplasmic AK2 for mitochondrial import, and N-terminal processing of AK2 by DPP9 reduces AK2 presence at its site of action in the mitochondrial intermembrane space (IMS) (Finger et al., 2020; Schricker et al., 2002). In yeast the bulk of mature AK2 protein is localised in the cytoplasm while only six to eight percent of mature AK2 is translocated into IMS while more than 30% of mature AK2 is found in the mitochondrial IMS of higher vertebrates (Angermayr et al., 2001; Schricker et al., 2002; Strobel et al., 2002; Watanabe and Kubo, 1982). Because AK2 protein is susceptible to

DPP9 driven protein degradation in the cytosol, it is not surprising that only a small amount of the translated protein reaches the IMS (Angermayr et al., 2001; Finger et al., 2020; Strobel et al., 2002). It is also likely that an increase in DPP9 expression and activity would result in a decrease in the AK2 activity in the IMS due to higher instance of N-terminal processing and degradation in the cytosol.

AK2 is vital for mitochondrial nucleotide exchange, phosphotransfer and export of ATP out of the IMS. While deficiency in AK2 disrupts cellular bioenergetics causing severe combined immunodeficiencies in humans, it is also embryonically lethal in mice, signifying the importance of phosphotransfer and mitochondria nucleotide exchange in maintaining biological function (Klepinin et al., 2020; Six et al., 2015). This is also reflective of the relationship between DPP9 and AK2 as the targeted inactivation of DPP9 enzyme activity through a serine to alanine point mutation in mice is shown to result in 100% lethality in neonates within 24 hours of birth (Gall et al., 2013). Furthermore, knockdown of AK2 in lung adenocarcinoma cells is shown to suppress cellular proliferation, migration, and invasion (Liu et al., 2019). While absence of AK2 in human T-cells reduces cellular proliferation and survival blocking differentiation and its absence alters mitochondrial function in neutrophilic HL60 cells compromising energy metabolism through a significant decrease in routine respiration that results in reduced neutrophil differentiation (Six et al., 2015). This association between decrease in AK2, reduced cellular respiration and decrease in cellular proliferation is also seen in results taken from chapter two where treatment of T-cells and monocytes with sitagliptin reduced both oxidative phosphorylation and glycolysis as well as cellular growth. Indicating that the effects of sitagliptin on cellular metabolism may be associated with an inhibition of AK2.

AK2 monitors fluctuation in AMP signals and regulates metabolic response by catalysing nucleotide exchange to elicit action from metabolic sensors. Reduction or increase in AK2 activity would result in distortion of AMP signals impacting AMP-generating reactions and could result in both positive and negative impacts on the actions of metabolic sensors including AMPK (Dzeja and Terzic, 2009). AMP signalling through AK2 plays a vital role in the control of cellular senescence. In fibroblasts the AMP to ATP ratio is seen to be several folds higher in senescent cells compared to young fibroblasts, and the increase in the AMP to ATP ratio is associated with significant increase in AMPK activity (Wang et al., 2003; Zwerschke et al., 2003). Suppression of AK2 phosphotransfer and balance of AMP in cancer cells could be a significant factor in the initiation of cancerous transformation, facilitating uncontrolled cell cycle and growth through increased AMPK activation (Dzeja and Terzic, 2009).

In breast and ovarian cancer cells, DPP4 expression has been shown to play a defined role in the post-transcriptional regulation of DPP9 (Wilson and Abbott, 2012). It seems likely that the impact inhibition of DPP4 has on cell bioenergetics may be as a result of regulation of AMPK through increased DPP9 expression decreasing AK2 presence in the IMS. However, the scope of this work did not include examination of AK2 expression and activity. In addition to the western blotting used to identify DPP9 protein presence in chapter two, semi quantitative RT-PCR could be used to better identify the relationship between DPP4 inhibition and DPP9 mRNA level. This could be done over a time course of treatment and in conjunction with quantification of bioenergetics via the XFe analyser to correlate the impact on cell metabolism with DPP9 protein expression. While measurement of AK2 kinetic profiles in both the cytoplasmic and mitochondria fractions of immune cells treated with DPP4 inhibitors as well as with DPP9 knock down would provide further evidence on the relationship between DPP4, DPP9 and AK2 activity in both the IMS and cytosol. Purification of cleaved and un-cleaved AK2 protein from cells treated with DPP4 inhibitors or DPP9 knockdown would confirm the relationship between DPP9 and AK2 N-terminal processing in immune cells.

The control of AMP signalling via AK2 is also an important mediator involved in insulin and metabolic protein kinase Akt signalling. The protein kinase Akt is involved in mediating the inhibitory effects of insulin on AMPK (Zwerschke et al., 2003). Direct de-phosphorylation of AMPK by Akt is not seen but changes in Akt activity in response to insulin is shown to negatively regulate AMPK through decrease in the AMP to ATP ratio (Hahn-Windgassen et al., 2005). Interestingly, Akt-mediated inhibition of AMPK in response to insulin levels can be
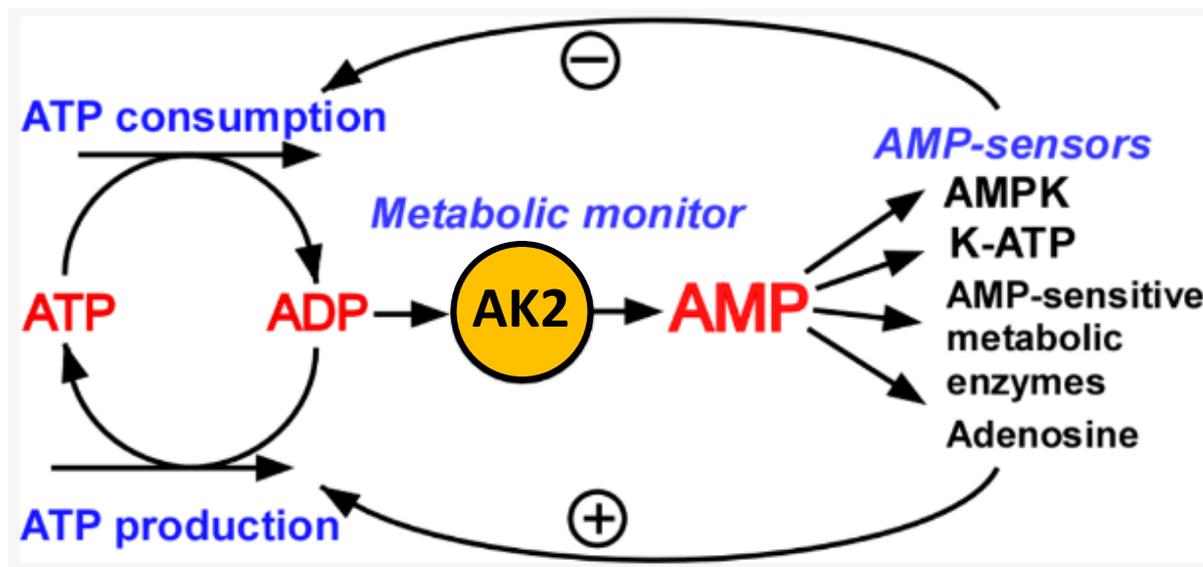
Figure 5.1. Metabolic monitoring by AK2 controls cellular energy state and communicates AMP signals to metabolic sensors. AK2 conveys information about the adenine nucleotide pool status controlling the overall energy balance. Metabolic sensors respond to AMP signalling via AK2 through adjustment of the ATP-consuming and ATP-generating pathways to control energy metabolism. Image is adapted from Dzeja and Terzic, 2009, reprinted with permission from MDPI (Basel, Switzerland).

overcome by metformin through increase in in AMP levels (Kovacic et al., 2003; Owen et al., 2000). Findings that are correlated to results seen in chapter two where treatment with both sitagliptin and metformin increased AMPK activation. The relationship between DPP4 and Akt phosphorylation has been previously reported in human hepatocellular carcinoma cell line HepG2 where treatment with gemigliptin suppressed the inhibitory effects of TNFα on Akt phosphorylation although a mechanism of action was not defined as part of this work (Hwang et al., 2015b). The results seen in chapter four where ablation of DPP4 resulted in increased tumorigenesis may be related to the removal of the DPP4 protein and the resulting increase in DPP9 expression leading to greater inactivation of Ak2 and impact on Akt signalling. A better understanding of the relationship between DPP4 inhibition, DPP9 and Akt activation would be another vital step in understanding the mechanism through which sitagliptin is exerting its effect on cell metabolism. Evaluation of changes in protein expression and function in the presence and absence of sitagliptin would provide valuable data to support the involvement of DPP4 inhibition and the potential impact on Akt.

5.1.4 The tumour promotive actions of DPP4 may be related to GLP-2

In chapter four increased tumorigenesis was seen with ablation of the DPP4 protein in knockout mice. While the removal of the DPP4 protein and associated protein binding has been identified as a probable driver for the increased tumour load observed, heightened tumorigenesis in the colon may also be correlated to unrestrained activity of glucagon-like peptide-2 (GLP-2) and associated gut hormone insulin-like growth factor 1 (IGF-1). The intestinotrophic hormone GLP-2 is an established DPP4 substrate responsible for inducing intestinal proliferation and is known to play a role in the development of CRC (Drucker et al., 1996; Kannen et al., 2013). GLP-2 promotion of intestinal cell growth is controlled indirectly through pathways that involve both IGF-1 and the intestinal-epithelial IGF-1 receptor (IE-IGF-1R) (Dong et al., 2014). IGF-1 is a growth hormone and member of a family of insulin related peptides, it is a mitogenic and antiapoptotic factor that is strongly connected with the development of human cancers including CRC (Laron, 2001; Palmqvist et al., 2002). Although the intestinotrophic activity of GLP-2 is known to be inactivated by N-terminal processing by DPP4 (Drucker et al., 1997), and the IGF-1 signalling axis is clearly a target in CRC (Leiphrakpam et al., 2014), it is not yet clear whether DPP4 cleavage plays a role in IGF-1 actions. An N-terminally truncated form of IGF-1 has been identified in the human brain which is missing three amino acids and has been called Des(1-3) IGF-1 and has strong anabolic effects in the gut (Ballard et al., 1996). Although N-terminal removal of three amino acids is not associated with the actions of DPP4, the N-truncated form of AK2 is missing three amino acids due to the removal of a methionine by methionine aminopeptidase prior to

DPP9 proteolytic actions (Finger et al., 2020), the removal of 3 amino acids in Des(1-3) IGF-1 may be as a result of the dual action of DPP4 working in conjunction with a second protease.

There is strong evidence linking GLP-2 signalling to IGF-1 synthesis in intestinal sub epithelial fibroblasts confirming that these peptides can work together to promote proliferation in the colon (Kannen et al., 2013). The increased tumour number and size seen in Dpp4-/- mice treated with AOM in chapter four may be related to the removal of DPP4 enzyme activity and resulting increase in endogenous active GLP-2 and IGF-1 with intact N-termini. Additionally, results taken from chapter four reflect those seen in an AOM mouse model comparing the effect of daily treatment with intact exogenous bioactive GLP-2(1-33) or N-terminally truncated GLP-2(3-33), treatment with GLP-2(1-33) for four weeks increased the number of ACF when given during the promotion stage while GLP-2(3-33) was shown to decrease ACF number when compared to PBS administered controls (Iakoubov et al., 2009). The presence of GLP-2(1-33) also impacted tumorigenesis during the progression stage with the development of adenocarcinomas seen in mice administered GLP-2(1-33) but not GLP-2(3-33) or PBS (Iakoubov et al., 2009). An increase in colon tumorigenesis is also seen with elevation of serum IGF-1 levels. Using a tumour transplant model with colon adenocarcinoma tissue fragments transplanted onto the cecum surface of IGF-1-deficient mice, intraperitoneal injection of recombinant human IGF-1 twice daily for six weeks resulted in a significant increase in tumour development on the cecum as well as increased metastasis to the liver (Wu et al., 2002). Moreover, in an AOM model of CRC, reduced circulating IGF-1 levels in IGF-1-deficient mice has been found to significantly reduce tumour number as well as decrease proliferation and increase apoptosis (Olivo-Marston et al., 2009). Therefore GLP-2 and IGF-1 both play a critical role in CRC, while the actions of GLP-2 via IGF-1 are controlled through the regulatory action of DPP4 protease activity. The increased tumorigenesis associated with DPP4 ablation in Dpp4-/- mice may be as a result of increase in active GLP-2 and IGF-1, measurement of these DPP4 substrates was outside the scope of this thesis but warrants further investigation in context of DPP4 during the promotion and progression of CRC.

Using the AOM mouse models targeted at initiation, promotion and progression, serum levels of GLP-2 and IGF-1 could be measured to provide a comparison between DPP4 knockout, DPP4 inhibitor treated WT and WT control mice. To maximise detection of GLP-2(1-33) or IGF-1 differences, animals will need to be fasted for five hrs prior to kill and then given a glucose bolus before blood collection. In addition to identification of GLP-2(1-33) and

IGF-1 in serum, DPP4 substrate cleavage could be performed on colon tissue in situ and in serum using nano-structured surface-assisted laser desorption/ionization (SALDI).

Matrix-assisted laser desorption/ionisation (MALDI) mass spectrometry imaging (MSI) MALDI-MSI has been used in pathological description of gastrointestinal tumour types and associated markers from gastric and colon cancers (Balluff et al., 2012, 2011; Mirnezami et al., 2014; Rudd et al., 2019). This however has limitations when analysing small molecules such as those coming from peptide cleavage products due to the requirement for a matrix compound which interfere with the detection of lower abundance molecules. The use of SALDI would allow investigation into the changes in tissue-specific spatial distribution for proteins and peptides. Matrix-free MSI methods use functionalised nanostructured substrates for surface-assisted ionisation (SALDI) of low abundance small molecules, including metabolites (Lowe et al., 2009; Svatoš, 2010), and can be used to detect intact and cleaved forms of GLP-2 and IGF-1 in situ in colon tissue and in serum to learn more about spatial localisation of these peptides during early and later stages of tumorigenesis.

5.1.5 Changes in inflammatory response and metabolism in Fap-/- mice may impact tumorigenesis

Inflammation and metabolism both play a role in CRC and both are altered in the absence of DPP4 and FAP. In chapter four saline treated Fap-/- mice show a similar increase in inflammatory and metabolic markers as mice with diet induced obesity which may be why an increase in tumour penetrance and size is seen in AOM treated Fap-/- mice compared to WT controls. In chapter four saline treated Fap-/- mice were shown to have a similar phenotype to mice with diet induced obesity used by Olivo-Marston et al., (2014) presenting with significantly increased inflammatory cytokines TNF-α and IL-1b as well as significantly increased leptin when compared to WT controls (Table 5.1). The similarity between the inflammatory and metabolic markers in Fap-/- and obese mice may be the driver for the increased tumorigenesis seen in AOM treated Fap-/- mice and may also be related to their increased body weight. Obese mice used in the work presented by Olivo-Marston et al., (2014) were four to five grams heavier in total body weight compared to normal diet controls, this is similar to the weight difference between Fap-/- and WT mice in chapter four where saline treated Fap-/- mice are on average three to four grams heavier that WT controls. This indicates that the similarity between the Fap-/- and obese phenotypes may be due to the increased body weight in Fap-/- mice which has been related to the reduced cage density, required to eliminate instances of aggression and in cage fighting, driving increased food consumption and higher body weight (Paigen et al., 2012).

Table 5.1. Fap-/- mice have increased inflammatory and metabolic markers consistent with an obese phenotype. Outline of shift in inflammatory cytokines and metabolic hormones in saline treated Dpp4-/- and Fap-/- mice at 28-30 weeks of age. Arrow denotes significant ↑ increase or ↓ decrease compared to WT control by ANOVA: P ≤ 0.05 (↓), P ≤ 0.01 (↓↓) or (↑↑) and P ≤ 0.005 (↑↑↑).

	Dpp4-/-	Fap-/-
GIP		↑↑↑
GLP-1	↑↑↑	↑↑↑
Glucagon	↓↓	
Leptin		↑↑↑
PYY		↑↑↑
VEGF		↑↑↑
IL-1b		↑↑
TNF-α		↑↑↑
IP-10 (CXCL10)	↓	
RANTES (CCL)	↓	↓↓

Table 5.2. Progression of AOM driven tumorigenesis in Fap-/- mice alters inflammatory and metabolic markers of obesity. Outline of shift in inflammatory cytokines and metabolic hormones Dpp4-/- and Fap-/- mice 14 weeks after 6th AOM treatment. Arrow denotes significant ↑ increase or ↓ decrease compared to WT control or significant ↑ increase compared to saline treated phenotype matched control by ANOVA: P ≤ 0.05 (↓) or (↑) or (↑), P ≤ 0.01 (↓↓) or (↑↑) and P ≤ 0.005 (↓↓↓) or (↑↑↑).or (↑↑↑).

	WT	Dpp4-/-	Fap-/-
GLP-1		↑	↑↑↑
Leptin		↓	
PYY		↑	↑↑
IL-10	↑		↓↓
IP-10	↑↑↑	↓↓↓	↓↓↓

In addition to the increase in inflammatory cytokines and metabolic markers associated with obesity driven tumorigenesis, Fap-/- mice also have significantly increased peptide tyrosine tyrosine (PYY), and vascular endothelial growth factor (VEGF). PYY is a gut hormone involved in stimulation of colonic epithelial cell growth (Persaud and Bewick, 2014), and VEGF is an endothelial cell-specific mitogen that is associated with protumorigenic protection of tumour cells from apoptosis and increased resistance to chemotherapy and radiotherapy (Duffy et al., 2004). Elevated serum levels of both PYY and VEGF are also linked to obesity so the significant increase in both factors may be related to Fap-/- mice presenting with an obese phenotype. The elevation in TNF-α and IL-1b and leptin is not seen in AOM treated Fap-/- mice (Table 5.2), the presence of tumours in these mice may mean that the response to increased body mass is taken over by CRC disease progression. It appears that the reduced cage density required for Fap-/- mice in chapter four may have resulted in an obese phenotype and the increase in tumorigenesis seen in these mice with AOM treatment may be related to the significant increase in body mass. To determine if these results are related to cage density follow on work using the 20 week AOM model in WT and Fap-/- mice at consistently low cage densities of two to three mice per cage could be undertaken with measurement of inflammatory and metabolic markers to determine if lower cage density also produces an obese phenotype in WT mice.

5.1.6 Increase in PYY in Dpp4-/- and Fap-/- mice may be tumour promotive

In addition to the significant decrease in IP-10 in AOM treated Dpp4-/- and Fap-/- mice as well as decrease in IL-10 in Fap-/- mice indicating a reduced tumour immune response, AOM treated Dpp4-/- and Fap-/- mice both have increased serum levels of PYY (Table 5.2) which may be correlated to the increased tumour presence and size in these mice. PYY is a regulatory peptide released after meals from the endocrine cells of the small intestine and colon and is involved in modulation of gastrointestinal function (Holzer et al., 2012; Karra et al., 2009). PYY is a known substrate of DPP4 and FAP, removal of the N-terminal dipeptide of PYY by DPP4 or FAP increases cellular proliferation and resistance to apoptosis through altered receptor specificity (Karra et al., 2009; Keane et al., 2011; Mentlein et al., 1993). PYY acts through five G-protein-coupled receptors (Y1 through 5), it is resistant to general aminopeptidase degradation but is N-terminally truncated by DPP4 and FAP which is shown to alter the receptor affinity (Mentlein et al., 1993). Activation of the Y1 receptor through coupling of full length PYY(1-36) is shown to stimulate colonic epithelial cell growth and protect cells from programmed cell death, this action is constrained by N-terminal dipeptidase removal as enzymatically cleaved PYY(3-36) has no affinity for the Y1 receptor (Kim et al., 2014; Persaud and Bewick, 2014). The removal of both DPP4 and FAP

enzymatic activity in knockout mice would result in greater presence of PYY(1-36) and increased activation of the Y1 receptor, the resulting stimulation of colonic epithelial cell growth and decrease in apoptotic response may be playing a role in the increased tumorigenesis in the colons of Dpp4-/- and Fap-/- mice.

5.1.7 The AOM model and efficacy of use with Dpp4-/- and Fap-/- mice

While animal studies cannot fully replace human clinical trials, they provide preclinical outcomes that allow targeted diagnostic and therapeutic design for human trials. Animal models such as the AOM model allow insight into the mechanisms of CRC pathophysiology and are useful tools for developing a deeper understanding of the tumour response to novel therapeutic strategies. Carcinogen-induced models of CRC in rodents are a highly reliable way to recapitulate human tumour initiation and progression. The AOM model is one of the most widely used chemically induced modes of CRC due to the simple mode of application, reproducibility and demonstrated ability to induce colon tumours with pathological features similar to that seen in sporadic human disease (De Robertis et al., 2011; Neufert et al., 2007). AOM promotes carcinogenesis through lesions induced by K-ras, APC, and p53 mutations that are similar to CRC in humans but are reported to also be found in other organs such as liver, small intestine and peritoneum (Bird, 1987; Bird and Good, 2000; Roncucci et al., 2000). Burlamaqui et al., (2013) have reported that rats exposed to weekly intraperitoneal injections of AOM have increased hepatocyte proliferation leading to preneoplastic lesions in the liver that evolved proportionally to the dose and duration of exposure (Burlamaqui et al., 2013). Furthermore, Ward, (1975) reported formation of tumours of both the liver and kidney in rats given single intraperitoneal injections of 3.4, 4.3 and 5.1 mg of AOM although noted that no formation of tumours was seen with doses under 3.4 mg (Ward, 1975). This is reflective of results presented in chapter three where treatment with AOM was associated with increase in markers of both hepatic and renal damage. Liver and renal injury has been reported in association with AOM ingestion in humans, rats, and livestock since the early 1960s (Laqueur et al., 1963). Given the successful use of this model for several decades these additional complications do not invalidate its use but should be taken into consideration during experimental design and end point analysis (Bissahoyo et al., 2012). Additionally, genetic predisposition, difference in localised environment and intestinal microflora influence susceptibility to AOM tumour development (Neufert et al., 2007). In chapter three we show that in our hands and within the localised environment of our animal facility, tumour development after treatment with AOM is faster than the reported 26 to 30 week timeline with our mice presenting with advanced tumours by 14 weeks post treatment (Bissahoyo et al., 2012; Neufert et al., 2007). This highlights the variability of response to

AOM and the need to perform pilot studies to optimise the timeline based on the facility specific and strain specific dose-response.

5.2 Conclusions and future direction

The work presented in this thesis confirms the multifunctional actions of DPP4 in relation to cancer. Inhibition of DPP4 activity was correlated with anti-neoplastic actions through AMPK-dependent increase in catabolic metabolism, growth inhibition and cell cycle arrest. While removal of both DPP4 and FAP in knockout mice was pro-neoplastic with Dpp4-/- mice developing a significantly increased number of adenomas and adenocarcinomas and both Dpp4-/- and Fap-/- mice presenting with significantly increased tumour growth and penetrance after exposure to AOM.

This is also some of the first work to report on the use of the AOM model of CRC in Dpp4-/- and Fap-/- mice establishing the efficacy of the use of this model of colorectal cancer in DPP4 and FAP genetic knockout mice and substantiating these phenotypes in a longer term model over a 20 week trial timeline. In addition, this work identified a refinement of the monitoring and ethics parameters to eliminate mice presenting with AOM derived liver damage and resulting weight loss early, reducing animal suffering and confounding variable factors in end point results.

To develop a better understanding of the role of DPP4 in tumorigenesis follow on work should be undertaken using the AOM-CRC model to compare DPP4 inhibition with knockout across differently timed AOM-rodent models targeted at the three different stages of the tumorigenic process, initiation, promotion and progression as described above. Analysis of the gene expression patterns in AOM induced tumours and preoplastic legions through quantitative real-time PCR, or transcriptomics methods like RNAseq, and/or proteomics methods would help to develop a better understanding of the impact of DPP4 and FAP ablation and inhibition and help to correlate specific gene expression patterns with tumour development. This would allow for identification of key insights into the individual roles of both the enzyme activity and protein binding actions of DPP4 and FAP in the three main stages of CRC. While further work using measurement of cellular bioenergetics in immune cells but also primary intestinal epithelial cells sourced from WT as well as DPP4 and FAP knockout mice could be used alongside semi quantitative RT-PCR to help to identify the pathway through which their inhibition or knockdown controls cell metabolism and identify the impact this has on intestinal proliferation.

The results taken from this thesis comprise an original significant contribution to our current understanding of the role of DPP4 and FAP in cancer and metabolism. DPP4 and FAP are clearly major players in tumorigenesis warranting further work in understanding this role and whether selective inhibitors at market for DPP4 and in design for FAP could be retargeted for use in cancer therapy. While the work here provides some reassurance that DPP4 inhibitors may be protective against colorectal and immune cancers further work is still required.

References

Abbott, C.A., McCaughan, G.W., Baker, E., Sutherland, G.R., 1994. Genomic organization, exact localization, and tissue expression of the human CD26 (dipeptidyl peptidase IV) gene. Immunogenetics 40, 331–338.

Abbott, C.A., McCaughan, G.W., Gorrell, M.D., 1999. Two highly conserved glutamic acid residues in the predicted beta propeller domain of dipeptidyl peptidase IV are required for its enzyme activity. FEBS Lett. 458, 278–284.

Abbott, C.A., Yu, D., McCaughan, G.W., Gorrell, M.D., 2006. Post Proline Cleaving Peptidases Having DP IV Like Enzyme Activity. In: Cellular Peptidases in Immune Functions and Diseases 2. pp. 103–109.

Abe, M., Havre, P., Urasaki, Y., Ohnuma, K., Morimoto, C., Dang, L., Dang, N., 2011. Mechanisms of confluence-dependent expression of CD26 in colon cancer cell lines. BMC Cancer 11, 51.

Abraham, R.T., Weiss, A., 2004. Jurkat T cells and development of the T-cell receptor signalling paradigm. Nat. Rev. Immunol. 4, 301–308.

Adams, J.M., Harris, A.W., Pinkert, C.A., Corcoran, L.M., Alexander, W.S., Cory, S., Palmiter, R.D., Brinster, R.L., 1985. The c-myc oncogene driven by immunoglobulin enhancers induces lymphoid malignancy in transgenic mice. Nature 318, 533–538.

Aertgeerts, K., Ye, S., Tennant, M.G., Kraus, M.L., Rogers, J.O.E., Sang, B., Skene, R.J., Webb, D.R., Prasad, G.S., 2004. Crystal structure of human dipeptidyl peptidase IV in complex with a decapeptide reveals details on substrate specificity and tetrahedral intermediate formation. Protein Sci. 13, 412–421.

Agilent Technologies, 2019a. How to run an assay [WWW Document]. XF Cell Mito Stress Test with Neo-Jurkat Cells. URL https://www.agilent.com/en/products/cell-analysis/how-to-run-an-assay

Agilent Technologies, 2019b. Agilent User Manuals [WWW Document]. Agil. Seahorse XF Cell Mito Stress Test User Guid. URL https://www.agilent.com/cs/library/usermanuals/public/XF_Cell_Mito_Stress_Test_Kit_User_Guide.pdf (accessed 10.4.19).

Ahmed, R.L., Schmitz, K.H., Anderson, K.E., Rosamond, W.D., Folsom, A.R., 2006. The metabolic syndrome and risk of incident colorectal cancer. Cancer 107, 28–36.

Amatya, V.J., Takeshima, Y., Kushitani, K., Taketo, Y., Chikao, M., Inai, K., 2011. Overexpression of CD26/DPPIV in mesothelioma tissue and mesothelioma cell lines. Oncol. Rep. 26, 1369–1375.

Angermayr, M., Strobel, G., Zollner, A., Korber, D., Bandlow, W., 2001. Two parameters improve efficiency of mitochondrial uptake of adenylate kinase: Decreased folding velocity and increased propensity of N-terminal α-helix formation. FEBS Lett. 508, 427–432.

Ansorge, S., Nordhoff, K., Heimburg, A., Julius, H., Breyer, D., Thielitz, A., Reinhold, D., Tager, M., 2011. Novel aspects of cellular action of dipeptidyl peptidase IV/CD26. Biol. Chem. 392, 153–168.

Aoe, K., Amatya, V.J., Fujimoto, N., Ohnuma, K., Hosono, O., Hiraki, A., Fujii, M., Yamada, T., Dang, N.H., Takeshima, Y., Inai, K., Kishimoto, T., Morimoto, C., 2012. CD26 overexpression is associated with prolonged survival and enhanced chemosensitivity in malignant pleural mesothelioma. Clin. Cancer Res. 18, 1447–1456.

Aono, M., Sato, Y., 2016. Dipeptidyl peptidase 4 inhibitor linagliptin can decrease the dosage of erythropoiesis-stimulating agents in patients on hemodialysis. Ren. Replace. Ther. 2, 44.

Ariga, N., Sato, E., Ohuchi, N., Nagura, H., Ohtani, H., 2001. Stromal expression of fibroblast activation protein/seprase, a cell membrane serine proteinase and gelatinase, is associated with longer survival in patients with invasive ductal carcinoma of breast. Int. J. Cancer 95, 67–72.

Armaghany, T., Wilson, J.D., Chu, Q., Mills, G., 2012. Genetic alterations in colorectal cancer. Gastrointest. Cancer Res. 5, 19–27.

Arscott, W.T., LaBauve, A.E., May, V., Wesley, U. V., 2009. Suppression of neuroblastoma growth by dipeptidyl peptidase IV: Relevance of chemokine regulation and caspase activation. Oncogene 28, 479–491.

Asada, Y., Aratake, Y., Kotani, T., Marutsuka, K., Araki, Y., Ohtaki, S., Sumiyoshi, A., 1993. Expression of dipeptidyl aminopeptidase IV activity in human lung carcinoma. Histopathology 23, 265–270.

Ashton-Rickardt, P.G., Dunlop, M.G., Nakamura, Y., Morris, R.G., Purdie, C.A., Steel, C.M., Evans, H.J., Bird, C.C., Wyllie, A.H., 1989. High frequency of APC loss in sporadic

colorectal carcinoma due to breaks clustered in 5q21-22. Oncogene 4, 1169–1174.

Australian Institute of Health and Welfare, 2020. Cancer data in Australia [WWW Document]. Cancer Compend. Inf. trends by cancer type. URL https://www.aihw.gov.au/reports/cancer/cancer-compendium-information-and-trends-by-cancer-type/report-contents/colorectal-cancer-in-australia

Aytac, U., Claret, F.-X.X., Ho, L., Sato, K., Ohnuma, K., Mills, G.B., Cabanillas, F., Morimoto, C., Dang, N.H., 2001. Expression of CD26 and Its Associated Dipeptidyl Peptidase IV Enzyme Activity Enhances Sensitivity to Doxorubicin-induced Cell Cycle Arrest at the G 2/M Checkpoint. Cancer Res. 61, 7204–7210.

Aytac, U., Sato, K., Yamochi, T., Yamochi, T., Ohnuma, K., Mills, G.B., Morimoto, C., Dang, N.H., 2003. Effect of CD26/dipeptidyl peptidase IV on Jurkat sensitivity to G2/M arrest induced by topoisomerase II inhibitors. Br. J. Cancer 88, 455–462.

Baggio, L.L., Varin, E.M., Koehler, J.A., Cao, X., Lokhnygina, Y., Stevens, S.R., Holman, R.R., Drucker, D.J., 2020. Plasma levels of DPP4 activity and sDPP4 are dissociated from inflammation in mice and humans. Nat. Commun. 11, 1–12.

Bailoo, J.D., Murphy, E., Boada-Saña, M., Varholick, J.A., Hintze, S., Baussière, C., Hahn, K.C., Göpfert, C., Palme, R., Voelkl, B., Würbel, H., 2018. Effects of cage enrichment on behavior, welfare and outcome variability in female mice. Front. Behav. Neurosci. 12, 232.

Ballard, F.J., Wallace, J.C., Francis, G.L., Read, L.C., Tomas, F.M., 1996. Des(1-3)IGF-I: A truncated form of insulin-like growth Factor-I. Int. J. Biochem. Cell Biol. 28, 1085–1087.

Balluff, B., Rauser, S., Ebert, M.P., Siveke, J.T., Höfler, H., Walch, A., 2012. Direct molecular tissue analysis by MALDI imaging mass spectrometry in the field of gastrointestinal disease. Gastroenterology 143, 544–549.

Balluff, B., Rauser, S., Meding, S., Elsner, M., Schöne, C., Feuchtinger, A., Schuhmacher, C., Novotny, A., Jtting, U., MacCarrone, G., Sarioglu, H., Ueffing, M., Braselmann, H., Zitzelsberger, H., Schmid, R.M., Höfler, H., Ebert, M.P., Walch, A., 2011. MALDI imaging identifies prognostic seven-protein signature of novel tissue markers in intestinal-type gastric cancer. Am. J. Pathol. 179, 2720–2729.

Barbero, S., Bonavia, R., Bajetto, A., Porcile, C., Pirani, P., Ravetti, J.L., Zona, G.L., Spaziante, R., Florio, T., Schettini, G., 2003. Stromal cell-derived factor 1α stimulates

human glioblastoma cell growth through the activation of both extracellular signal-regulated kinases 1/2 and Akt. Cancer Res. 63, 1969–1974.

Barkan, D., Chambers, A.F., 2011. β1-integrin: A potential therapeutic target in the battle against cancer recurrence. Clin. Cancer Res. 17, 7219–7223.

Barnes, J.L., Gorin, Y., 2011. Myofibroblast differentiation during fibrosis: role of NAD(P)H oxidases. Kidney Int. 79, 944–956.

Barone, I., Catalano, S., Gelsomino, L., Marsico, S., Giordano, C., Panza, S., Bonofiglio, D., Bossi, G., Covington, K.R., Fuqua, S.A.W., Andò, S., 2012. Leptin mediates tumor-stromal interactions that promote the invasive growth of breast cancer cells. Cancer Res. 72, 1416–1427.

Batandier, C., Guigas, B., Detaille, D., El-Mir, M., Fontaine, E., Rigoulet, M., Leverve, X.M., 2006. The ROS production induced by a reverse-electron flux at respiratory-chain complex 1 is hampered by metformin. J. Bioenerg. Biomembr. 38, 33–42.

Bauer, S., Jendro, M.C., Wadle, A., Kleber, S., Stenner, F., Dinser, R., Reich, A., Faccin, E., Gödde, S., Dinges, H., Müller-Ladner, U., Renner, C., 2006. Fibroblast activation protein is expressed by rheumatoid myofibroblast-like synoviocytes. Arthritis Res. Ther. 8, 171.

Baxmann, A.C., Ahmed, M.S., Marques, N.C., Menon, V.B., Pereira, A.B., Kirsztajn, G.M., Heilberg, I.P., 2008. Influence of muscle mass and physical activity on serum and urinary creatinine and serum cystatin C. Clin. J. Am. Soc. Nephrol. 3, 348–354.

Beckenkamp, A., Willig, J.B., Santana, D.B., Nascimento, J., Paccez, J.D., Zerbini, L.F., Bruno, A.N., Pilger, D.A., Wink, M.R., Buffon, A., 2015. Differential expression and enzymatic activity of DPPIV/CD26 affects migration ability of cervical carcinoma cells. PLoS One 10.

Benninghoff, A.D., Hintze, K.J., Monsanto, S.P., Rodriguez, D.M., Hunter, A.H., Phatak, S., Pestka, J.J., Van Wettere, A.J., Ward, R.E., 2020. Consumption of the total western diet promotes colitis and inflammation-associated colorectal cancer in mice. Nutrients 12, 1–17.

Berster, J.M., Göke, B., 2008. Type 2 diabetes mellitus as risk factor for colorectal cancer. Arch. Physiol. Biochem. 114, 84–98.

Bird, R.P., 1987. Observation and quantification of aberrant crypts in the murine colon treated with a colon carcinogen: Preliminary findings. Cancer Lett. 37, 147–151.

Bird, R.P., 1995. Role of aberrant crypt foci in understanding the pathogenesis of colon cancer. Cancer Lett. 93, 55–71.

Bird, R.P., Good, C.K., 2000. The significance of aberrant crypt foci in understanding the pathogenesis of colon cancer. Toxicol. Lett. 112–113, 395–402.

Bishnoi, R., Hong, Y.R., Shah, C., Ali, A., Skelton, W.P., Huo, J., Dang, N.H., Dang, L.H., 2019. Dipeptidyl peptidase 4 inhibitors as novel agents in improving survival in diabetic patients with colorectal cancer and lung cancer: A Surveillance Epidemiology and Endpoint Research Medicare study. Cancer Med. 8, 3918–3927.

Bissahoyo, A., Pearsall, R.S., Hanlon, K., Amann, V., Hicks, D., Godfrey, V.L., Threadgill, D.W., 2012. Azoxymethane is a genetic background-dependent colorectal tumor initiator and promoter in mice: Effects of dose, route, and diet. Carcinogenesis 4, 1998–2004.

Blay, J., White, T.D., Hoskin, D.W., 1997. The extracellular fluid of solid carcinomas contains immunosuppressive concentrations of adenosine. Cancer Res. 57, 2602–2605.

Bogenrieder, T., Finstad, C.L., Freeman, R.H., Papandreou, C.N., Scher, H.I., Albino, A.P., Reuter, V.E., Nanus, D.M., 1997. Expression and localization of aminopeptidase A, aminopeptidase N and dipeptidyl peptidase IV in benign and malignant human prostate tissue. Prostate 33, 225.

Boonacker, E., Van Noorden, C.J.F., 2003. The multifunctional or moonlighting protein CD26/DPPIV. Eur. J. Cell Biol. 82, 53–73.

Bosshart, H., Heinzelmann, M., 2016. THP-1 cells as a model for human monocytes. Ann. Transl. Med. 4, 1–4.

Bray, F., Ferlay, J., Soerjomataram, I., Siegel, R.L., Torre, L.A., Jemal, A., 2018. Global cancer statistics 2018: GLOBOCAN estimates of incidence and mortality worldwide for 36 cancers in 185 countries. CA. Cancer J. Clin. 68, 394–424.

Breen, E.J., Tan, W., Khan, A., 2016. The Statistical Value of Raw Fluorescence Signal in Luminex xMAP Based Multiplex Immunoassays. Sci. Rep. 6, 1–13.

Brennen, W.N., Isaacs, J.T., Denmeade, S.R., 2012. Rationale behind targeting fibroblast

activation protein-expressing carcinoma-associated fibroblasts as a novel chemotherapeutic strategy. Mol. Cancer Ther. 11, 257–266.

Bruce, W.R., Giacca, A., Medline, A., 2000. Possible mechanisms relating diet and risk of colon cancer. Cancer Epidemiol. Biomarkers Prev. 9, 1271–1279.

Bühling, F., Junker, U., Reinhold, D., Neubert, K., Jäger, L., Ansorge, S., 1995. Functional role of CD26 on human B lymphocytes. Immunol. Lett. 45, 47–51.

Buhling, F., Kunz, D., Reinhold, D., Ulmer, A.J., Ernst, M., Flad, H.D., Ansorge, S., 1994. Expression and functional role of dipeptidyl peptidase IV (CD26) on human natural killer cells. Nat. Immun. 13, 270–279.

Burlamaqui, I.M.B., Dornelas, C.A., Almeida, P.R.C., Jamacaru, F.V.F., Mota, D.M.C., Mesquita, F.J.C., Brito, L.A. de, Veras, L.B., Rodrigues, L.V., 2013. Hepatic repercussions of azoxymethane-induced colorectal carcinogenesis. Rev. Col. Bras. Cir. 40, 137–141.

Busek, P., Sedo, A., 2013. Dipeptidyl Peptidase-IV and Related Proteases in Brain Tumors. In: Evolution of the Molecular Biology of Brain Tumors and the Therapeutic Implications. InTech, pp. 235–269.

Bušek, P., Stremeňová, J., Křepela, E., Šedo, A., 2008. Modulation of substance P signaling by dipeptidyl peptidase-IV enzymatic activity in human glioma cell lines. Physiol. Res. 57, 443–449.

Busek, P., Stremenova, J., Sromova, L., Hilser, M., Balaziova, E., Kosek, D., Trylcova, J., Strnad, H., Krepela, E., Sedo, A., 2012. Dipeptidyl peptidase-IV inhibits glioma cell growth independent of its enzymatic activity. Int. J. Biochem. Cell Biol. 44, 738–747.

Busher, J.T., 1990. Serum Albumin and Globulin. In: Clinical Methods: The History, Physical, and Laboratory Examinations. Butterworths.

Cairns, P., 2011. Renal cell carcinoma. Cancer Biomarkers 9, 461–473.

Carbone, A., Gloghini, A., Zagonel, V., Aldinucci, D., Gattei, V., Degan, M., Improta, S., Sorio, R., Monfardini, S., Pinto, A., 1995. The expression of CD26 and CD40 ligand is mutually exclusive in human T- cell non-Hodgkin's lymphomas/leukemias. Blood 86, 4617–4626.

Caunt, C.J., Sale, M.J., Smith, P.D., Cook, S.J., 2015. MEK1 and MEK2 inhibitors and

cancer therapy: The long and winding road. Nat. Rev. Cancer 15, 577–592.

Cavalli, L.R., Varella-Garcia, M., Liang, B.C., 1997. Diminished tumorigenic phenotype after depletion of mitochondrial DNA. Cell Growth Differ. 8, 1189–1198.

Chang, J.H., Cheng, C.W., Yang, Y.C., Chen, W.S., Hung, W.Y., Chow, J.M., Chen, P.S., Hsiao, M., Lee, W.J., Chien, M.H., 2018. Downregulating CD26/DPPIV by apigenin modulates the interplay between Akt and Snail/Slug signaling to restrain metastasis of lung cancer with multiple EGFR statuses. J. Exp. Clin. Cancer Res. 37.

Château, M.-T., Rabesandratana, H., Caravano, R., 1996. Differentiated U937 cells and human monocytes exhibit a differential production of extracellular oxygen species: $O_2 \cdot {}^-$ excretion versus H_2O_2 diffusion. FEMS Immunol. Med. Microbiol. 13, 19–28.

Chen, H., Yang, W.W., Wen, Q.T., Xu, L., Chen, M., 2009. TGF-β-induced fibroblast activation protein expression, fibroblast activation protein expression increases the proliferation, adhesion, and migration of HO-8910PM. Exp. Mol. Pathol. 87, 189–194.

Chen, J., Huang, X.F., 2009. The signal pathways in azoxymethane-induced colon cancer and preventive implications. Cancer Biol. Ther. 8, 1313–1317.

Chen, W., An, D., Xu, H., Cheng, X., Wang, S., Yu, W., Yu, D., Zhao, D., Sun, Y., Deng, W., Tang, Y., Yin, S., 2016. Effects of social isolation and re-socialization on cognition and ADAR1 (p110) expression in mice. PeerJ 4, e2306.

Chen, Y.-C., Chen, T.-H., Sun, C.-C., Chen, J.-Y., Chang, S.-S., Yeung, L., Tsai, Y.-W., 2020. Dipeptidyl peptidase-4 inhibitors and the risks of autoimmune diseases in type 2 diabetes mellitus patients in Taiwan: a nationwide population-based cohort study. Acta Diabetol. 57, 1.

Cheng, H.C., Abdel-Ghany, M., Elble, R.C., Pauli, B.U., 1998. Lung endothelial dipeptidyl peptidase IV promotes adhesion and metastasis of rat breast cancer cells via tumor cell. J Biol Chem 273, 24207–24215.

Cheng, H.C., Abdel-Ghany, M., Pauli, B.U., 2003. A Novel Consensus Motif in Fibronectin Mediates Dipeptidyl Peptidase IV Adhesion and Metastasis. J. Biol. Chem. 278, 24600–24607.

Cheng, J.D., Dunbrack, R.L., Valianou, M., Rogatko, A., Alpaugh, R.K., Weiner, L.M., 2002. Promotion of tumor growth by murine fibroblast activation protein, a serine protease, in

an animal model. Cancer Res. 62, 4767–4772.

Cheng, J.D., Valianou, M., Canutescu, A.A., Jaffe, E.K., Lee, H.O., Wang, H., Lai, J.H., Bachovchin, W.W., Weiner, L.M., 2005. Abrogation of fibroblast activation protein enzymatic activity attenuates tumor growth. Mol. Cancer Ther. 4, 351–360.

Cheng, Y., Ling, Z., Li, L., 2020. The Intestinal Microbiota and Colorectal Cancer. Front. Immunol. 11, 3100.

Cheong, J.H., Park, E.S., Liang, J., Dennison, J.B., Tsavachidou, D., Nguyen-Charles, C., Cheng, K.W., Hall, H., Zhang, D., Lu, Y., Ravoori, M., Kundra, V., Ajani, J., Lee, J.S., Hong, W.K., Mills, G.B., 2011. Dual inhibition of tumor energy pathway by 2-deoxyglucose and metformin is effective against a broad spectrum of preclinical cancer models. Mol. Cancer Ther. 10, 2350–2362.

Chodak, W., Chang, C., Li, A., Chodak, G.W., 1992. Basic Fibroblast Growth Factor in Human Prostate Cancer Cells. Cancer Res. 52, 571–577.

Chowdhury, S., Song, S., Zhang, H.E., Wang, X.M., Gall, M.G., Tse Yu, D.M., Lay, A.J., Wen Xiang, M.S., Evans, K.A., Wetzel, S., Liu, Y., Yau, B., Coppage, A.L., Lo, L., Stokes, R.A., Hawthorne, W.J., Cooney, G.J., McLennan, S. V, Gunton, J.E., Bachovchin, W.W., Turner, N., Kebede, M.A., McCaughan, G.W., Twigg, S.M., Gorrell, M.D., 2018. Fibroblast activation protein enzyme deficiency prevents liver steatosis, insulin resistance and glucose intolerance and increases fibroblast growth factor-21 in diet induced obese mice, bioRxiv.

Chrostek, L., Supronowicz, L., Panasiuk, A., Cylwik, B., Gruszewska, E., Flisiak, R., 2014. The effect of the severity of liver cirrhosis on the level of lipids and lipoproteins. Clin. Exp. Med. 14, 417–421.

Chu, T.M., Murphy, G.P., Kawinski, E., Mirand, E.A., 1983. Lncap model of human prostatic carcinoma. Cancer Res. 43, 1809–1818.

Coburn, M.C., Hixson, D.C., Reichner, J.S., 1994. In vitro immune responsiveness of rats lacking active dipeptidylpeptidase IV. Cell. Immunol. 158, 269–280.

Cohen, J., Chesa, P.G., Beresford, H.R., Feickert, H.J., Jennings, M.T., Oettgen, H.F., Old, L.J., 1986. Differential Expression of Cell Surface Antigens and Glial Fibrillary Acidic Protein in Human Astrocytoma Subsets1. Cancer Res. 46, 6406–6412.

Cohen, R.D., 2003. Role of Dipeptidyl Peptidase IV/CD26 in Inflammatory bowel disease. In: Karoui, S. (Ed.), Inflammatory Bowel Disease : Diagnosis and Therapeutics. Humana Press, p. 364.

Cohen, S.J., Alpaugh, R.K., Palazzo, I., Meropol, N.J., Rogatko, A., Xu, Z., Hoffman, J.P., Weiner, L.M., Cheng, J.D., 2008. Fibroblast activation protein and its relationship to clinical outcome in pancreatic adenocarcinoma. Pancreas 37, 154–158.

Collins, P.J., McMahon, G., O'Brien, P., O'Connor, B., 2004. Purification, identification and characterisation of seprase from bovine serum. Int. J. Biochem. Cell Biol. 36, 2320–2333.

Conarello, S.L., Li, Z., Ronan, J., Roy, R.S., Zhu, L., Jiang, G., Liu, F., Woods, J., Zycband, E., Moller, D.E., Thornberry, N.A., Zhang, B.B., 2003. Mice lacking dipeptidyl peptidase IV are protected against obesity and insulin resistance 100, 6825–6830.

Constantinides, C., Mean, R., Janssen, B.J., 2011. Effects of isoflurane anesthesia on the cardiovascular function of the C57BL/6 mouse. ILAR J. 52, 21–31.

Cordero, O.J., Ayude, D., Nogueira, M., Rodriguez-Berrocal, F.J., de la Cadena, M.P., 2000. Preoperative serum CD26 levels: diagnostic efficiency and predictive value for colorectal cancer. Br. J. Cancer 83, 1139–1146.

Cordero, O.J., Salgado, F.J., Nogueira, M., 2009. On the origin of serum CD26 and its altered concentration in cancer patients. Cancer Immunol. Immunother. 58, 1723–1747.

Costa, A., Kieffer, Y., Scholer-Dahirel, A., Pelon, F., Bourachot, B., Cardon, M., Sirven, P., Magagna, I., Fuhrmann, L., Bernard, C., Bonneau, C., Kondratova, M., Kuperstein, I., Zinovyev, A., Givel, A.M., Parrini, M.C., Soumelis, V., Vincent-Salomon, A., Mechta-Grigoriou, F., 2018. Fibroblast Heterogeneity and Immunosuppressive Environment in Human Breast Cancer. Cancer Cell 33, 463-479.e10.

Cro, L., Morabito, F., Zucal, N., Fabris, S., Lionetti, M., Cutrona, G., Rossi, F., Gentile, M., Ferrario, A., Ferrarini, M., Molica, S., Neri, A., Baldini, L., 2009. CD26 expression in mature B-cell neoplasia: Its possible role as a new prognostic marker in B-CLL. Hematol. Oncol. 27, 140–147.

Cunningham, D.F., O'Connor, B., 1997. Proline specific peptidases. Biochim. Biophys. Acta 1343, 160–186.

Cutró, A.C., Montich, G.G., Roveri, O.A., 2014. Effect of carbonylcyanide-4-(trifluoromethoxy)phenylhydrazone (FCCP) on the interaction of 1-anilino-8-naphthalene sulfonate (ANS) with phosphatidylcholine liposomes. J. Bioenerg. Biomembr. 46, 119–125.

Dang, N.A.M.H., Torimoto, Y., Deusch, K.A.I., Morimot, C., Schlossman, F., 1990. Comitogenic effect of solid-phase immobilized anti-1F7 on human CD4 T cell activation via CD3 and CD2 pathways. J. Immunol. 6, 4092–4100.

Dang, N.H., Aytac, U., Sato, K., O'Brien, S., Melenhorst, J., Morimoto, C., Barrett, A.J., Molldrem, J.J., 2003. T-large granular lymphocyte lymphoproliferative disorder: Expression of CD26 as a marker of clinically aggressive disease and characterization of marrow inhibition. Br. J. Haematol. 121, 857–865.

Darmoul, D., Lacasa, M., Baricault, L., Marguet, D., Sapin, C., Trotot, P., Barbat, A., Trugnan, G., 1992. Dipeptidyl peptidase IV (CD 26) gene expression in enterocyte-like colon cancer cell lines HT-29 and Caco-2. Cloning of the complete human coding sequence and changes of dipeptidyl peptidase IV mRNA levels during cell differentiation. J. Biol. Chem. 267, 4824–4833.

Darmoul, D., Voisin, T., Couvineau, A., Rouyer-Fessard, C., Salomon, R., Wang, Y., Swallow, D.M., Laburthe, M., 1994. Regional Expression of Epithelial Dipeptidyl Peptidase IV in the Human Intestines. Biochem. Biophys. Res. Commun. 203, 1224–1229.

De Chiara, L., Rodríguez-Piñeiro, A.M., Cordero, O.J., Vázquez-Tuñ, L., Ayude, D., Rodríguez-Berrocal, F.J., De La Cadena, M.P., 2014. Postoperative serum levels of sCD26 for surveillance in colorectal cancer patients. PLoS One 9, e107470.

De La Fuente, I.M., Cortés, J.M., Valero, E., Desroches, M., Rodrigues, S., Malaina, I., Martínez, L., 2014. On the dynamics of the adenylate energy system: Homeorhesis vs homeostasis. PLoS One 9, e108676.

De La Haba-Rodríguez, J., Macho, A., Calzado, M.A., Blázquez, M. V, Gómez, M.A., Munoz, E.E., Aranda, E., 2002. Soluble dipeptidyl peptidase IV (CD-26) in serum of patients with colorectal carcinoma. Neoplasma 49, 307–311.

De La Luz Sierra, M., Yang, F., Narazaki, M., Salvucci, O., Davis, D., Yarchoan, R., Zhang, H.H., Fales, H., Tosato, G., 2004. Differential processing of stromal-derived factor-1α and stromal-derived factor-1β explains functional diversity. Blood 103, 2452–2459.

De Meester, I., Korom, S., Van Damme, J., Scharpé, S., 1999. CD26, let it cut or cut it down. Immunol. Today 20, 367–75.

De Robertis, Mariangela, Massi, E., Poeta, M.L., Carotti, S., Morini, S., Cecchetelli, L., Signori, E., Fazio, V.M., Robertis, MariangelaDe, Massi, E., Poeta, M.L., Carotti, S., Morini, S., Cecchetelli, L., Signori, E., De Robertis, Mariangela, Massi, E., Poeta, M.L., Carotti, S., Morini, S., Cecchetelli, L., Signori, E., Fazio, V.M., Robertis, MariangelaDe, Massi, E., Poeta, M.L., Carotti, S., Morini, S., Cecchetelli, L., Signori, E., 2011. The AOM/DSS murine model for the study of colon carcinogenesis: From pathways to diagnosis and therapy studies. J. Carcinog. 10, 9.

De, S., Banerjee, S., Kumar, S.K.A., Paira, P., 2018. Critical Role of Dipeptidyl Peptidase IV: A Therapeutic Target for Diabetes and Cancer. Mini-Reviews Med. Chem. 19, 88–97.

Deacon, C.F., Lebovitz, H.E., 2016. Comparative review of dipeptidyl peptidase-4 inhibitors and sulphonylureas. Diabetes, Obes. Metab. 18, 333–347.

DeCensi, A., Puntoni, M., Goodwin, P., Cazzaniga, M., Gennari, A., Bonanni, B., Gandini, S., 2010. Metformin and cancer risk in diabetic patients: A systematic review and meta-analysis. Cancer Prev. Res. 3, 1451–1461.

Di Gregorio, C., Losi, L., Fante, R., Modica, S., Ghidoni, M., Pedroni, M., Tamassia, M.G., Gafà, L., Ponz de Leon, M., Roncucci, L., 1997. Histology of aberrant crypt foci in the human colon. Histopathology 30, 328–334.

Divakaruni, A.S., Paradyse, A., Ferrick, D.A., Murphy, A.N., Jastroch, M., 2014. Analysis and interpretation of microplate-based oxygen consumption and pH data. In: Methods in Enzymology. Academic Press, pp. 309–354.

Dolznig, H., Schweifer, N., Puri, C., Kraut, N., Rettig, W.J., Kerjaschki, D., Garin-Chesa, P., 2005. Characterization of cancer stroma markers: In silico analysis of an mRNA expression database for fibroblast activation protein and endosialin. Cancer Immun. 5, 1–9.

Dong, C.X., Zhao, W., Solomon, C., Rowland, K.J., Ackerley, C., Robine, S., Holzenberger, M., Gonska, T., Brubaker, P.L., 2014. The intestinal epithelial insulin-like growth factor-1 receptor links glucagon-like peptide-2 action to gut barrier function. Endocrinology 155, 370–379.

Dow, J.K., Devere White, R.W., 2000. Fibroblast growth factor 2: Its structure and property,

paracrine function, tumor angiogenesis, and prostate-related mitogenic and oncogenic functions. Urology 55, 800–806.

Dowling, R.J.O., Zakikhani, M., Fantus, I.G., Pollak, M., Sonenberg, N., 2007. Metformin inhibits mammalian target of rapamycin-dependent translation initiation in breast cancer cells. Cancer Res. 67, 10804–10812.

Dranka, B.P., Zielonka, J., Kanthasamy, A.G., Kalyanaraman, B., 2012. Alterations in bioenergetic function induced by Parkinson's disease mimetic compounds: Lack of correlation with superoxide generation. J. Neurochem. 122, 941–951.

Drucker, D.J., 2003. Therapeutic potential of dipeptidyl peptidase IV inhibitors for the treatment of type 2 diabetes. Expert Opin. Investig. Drugs 12, 87–100.

Drucker, D.J., Ehrlich, P., Asa, S.L., Brubaker, P.L., 1996. Induction of intestinal epithelial proliferation by glucagon-like peptide 2. Proc. Natl. Acad. Sci. U. S. A. 93, 7911–7916.

Drucker, D.J., Shi, Q., Crivici, A., Sumner-Smith, M., Tavares, W., Hill, M., DeForest, L., Cooper, S., Brubaker, P.L., 1997. Regulation of the biological activity of glucagon-like peptide 2 in vivo by dipeptidyl peptidase IV. Nat Biotechnol 15, 673–677.

Dubé, P.E., Rowland, K.J., Brubaker, P.L., 2008. Glucagon-like peptide-2 activates β-catenin signaling in the mouse intestinal crypt: Role of insulin-like growth factor-I. Endocrinology 149, 291–301.

Dubois, V., Van Ginneken, C., De Cock, H., Lambeir, A.-M.M., Van der Veken, P., Augustyns, K., Chen, X., Scharpé, S., De Meester, I., 2009. Enzyme activity and immunohistochemical localization of dipeptidyl peptidase 8 and 9 in male reproductive tissues. J. Histochem. Cytochem. 57, 531–41.

Ducarouge, B., Pelissier-Rota, M., Powell, R., Buisson, A., Bonaz, B., Jacquier-Sarlin, M., 2017. Involvement of CRF2 signaling in enterocyte Differentiation. World J. Gastroenterol. 23, 5127–5145.

Duffy, A.M., Bouchier-Hayes, D.J., Harmey, J.H., 2004. Vascular Endothelial Growth Factor (VEGF) and Its Role in Non-Endothelial Cells: Autocrine Signalling by VEGF. In: VEGF and Cancer. Landes Bioscience, pp. 133–144.

Dzeja, P., Terzic, A., 2009. Adenylate Kinase and AMP Signaling Networks: Metabolic Monitoring, Signal Communication and Body Energy Sensing. Int. J. Mol. Sci. 10,

1729–1772.

Eager, R.M., Cunningham, C.C., Senzer, N., Richards, D.A., Raju, R.N., Jones, B., Uprichard, M., Nemunaitis, J., 2009. Phase II trial of talabostat and docetaxel in advanced non-small cell lung cancer. Clin. Oncol. (R. Coll. Radiol). 21, 464–72.

El-Mir, M.Y., Nogueira, V., Fontaine, E., Avéret, N., Rigoulet, M., Leverve, X., 2000. Dimethylbiguanide inhibits cell respiration via an indirect effect targeted on the respiratory chain complex I. J. Biol. Chem. 275, 223–228.

Engel, M., Hoffmann, T., Wagner, L., Wermann, M., Heiser, U., Kiefersauer, R., Huber, R., Bode, W., Demuth, H.U., Brandstetter, H., 2003. The crystal structure of dipeptidyl peptidase IV (CD26) reveals its functional regulation and enzymatic mechanism. Proc. Natl. Acad. Sci. U. S. A. 100, 5063–5068.

Enz, N., Vliegen, G., De Meester, I., Jungraithmayr, W., 2019. CD26/DPP4 - a potential biomarker and target for cancer therapy. Pharmacol. Ther. 198, 135–159.

Esmaeelian, B., Abbott, C.A., Le Leu, R.K., Benkendorff, K., 2014. 6-Bromoisatin found in muricid mollusc extracts inhibits colon cancer cell proliferation and induces apoptosis, preventing early stage tumor formation in a colorectal cancer rodent model. Mar. Drugs 12, 17–35.

Feig, C., Jones, J.O., Kraman, M., Wells, R.J.B., Deonarine, A., Chan, D.S., Connell, C.M., Roberts, E.W., Zhao, Q., Caballero, O.L., Teichmann, S.A., Janowitz, T., Jodrell, D.I., Tuveson, D.A., Fearon, D.T., 2013. Targeting CXCL12 from FAP-expressing carcinoma-associated fibroblasts synergizes with anti-PD-L1 immunotherapy in pancreatic cancer. Proc. Natl. Acad. Sci. U. S. A. 110, 20212–20217.

Femia, A. Pietro, Paulsen, J.E., Dolara, P., Alexander, J., Caderni, G., 2008. Correspondence between flat aberrant crypt foci and mucin-depleted foci in rodent colon carcinogenesis. Anticancer Res. 28, 3771–3775.

Femia, A. Pietro, Raimondi, L., Maglieri, G., Lodovici, M., Mannucci, E., Caderni, G., 2013. Long-term treatment with Sitagliptin, a dipeptidyl peptidase-4 inhibitor, reduces colon carcinogenesis and reactive oxygen species in 1,2- dimethylhydrazine-induced rats. Int. J. Cancer 133, 2498–2503.

Fenwick, N., Griffin, G., Gauthier, C., 2009. The welfare of animals used in science: how the "Three Rs" ethic guides improvements. Can. Vet. J. 50, 523–530.

Fernandez-De-Cossio-DIaz, J., Vazquez, A., 2018. A physical model of cell metabolism. Sci. Rep. 8, 1–13.

Fernández-Ramos, A.A., Marchetti-Laurent, C., Poindessous, V., Antonio, S., Petitgas, C., Ceballos-Picot, I., Laurent-Puig, P., Bortoli, S., Loriot, M.A., Pallet, N., 2017. A comprehensive characterization of the impact of mycophenolic acid on the metabolism of Jurkat T cells. Sci. Rep. 7, 1–11.

Fernandis, A.Z., Cherla, R.P., Ganju, R.K., 2003. Differential regulation of CXCR4-mediated T-cell chemotaxis and mitogen-activated protein kinase activation by the membrane tyrosine phosphatase, CD45. J. Biol. Chem. 278, 9536–9543.

Finger, Y., Habich, M., Gerlich, S., Urbanczyk, S., Logt, E., Koch, J., Schu, L., Lapacz, K.J., Ali, M., Petrungaro, C., Salscheider, S.L., Pichlo, C., Baumann, U., Mielenz, D., Dengjel, J., Brachvogel, B., Hofmann, K., Riemer, J., 2020. Proteasomal degradation induced by DPP9-mediated processing competes with mitochondrial protein import. EMBO J. 39, e103889.

Fleischer, B., 1994. CD26: A surface protease involved in T-cell activation. Immunol. Today 15, 180–184.

Floridon, C., Nielsen, O., Hølund, B., Sunde, L., Westergaard, J.G., Thomsen, S.G., Teisner, B., 2000. Localization of E-cadherin in villous, extravillous and vascular trophoblasts during intrauterine, ectopic and molar pregnancy. Mol. Hum. Reprod. 6, 943–950.

Franklin, C.L., Ericsson, A.C., 2017. Microbiota and reproducibility of rodent models. Lab Anim. (NY). 46, 114–122.

Fu, S.K., Lawrance, I.C., 2015. Animal models of IBD-Associated CRC and colorectal cancer tumorigenesis. Clin. Med. Insights Ther. 7, 1–9.

Fujita, M., Zhu, X., Ueda, R., Sasaki, K., Kohanbash, G., Kastenhuber, E.R., McDonald, H.A., Gibson, G.A., Watkins, S.C., Muthuswamy, R., Kalinski, P., Okada, H., 2009. Effective Immunotherapy against Murine Gliomas Using Type 1 Polarizing Dendritic Cells—Significant Roles of CXCL10. Cancer Res. 69, 1587–1595.

Fullár, A., Dudás, J., Oláh, L., Hollósi, P., Papp, Z., Sobel, G., Karászi, K., Paku, S., Baghy, K., Kovalszky, I., 2015. Remodeling of extracellular matrix by normal and tumor-associated fibroblasts promotes cervical cancer progression. BMC Cancer 15.

Gall, M.G., Chen, Y., Vieira de Ribeiro, A.J., Zhang, H., Bailey, C.G., Spielman, D.S., Yu, D.M.T., Gorrell, M.D., 2013. Targeted Inactivation of Dipeptidyl Peptidase 9 Enzymatic Activity Causes Mouse Neonate Lethality. PLoS One 8, e78378.

Gandomani, H.S., Yousefi, S.M., Aghajani, M., Mohammadian-Hafshejani, A., Tarazoj, A.A., Pouyesh, V., Salehiniya, H., 2017. Colorectal cancer in the world: incidence, mortality and risk factors. Biomed. Res. Ther. 4, 1656–1675.

Garin-Chesa, P., Old, L.J., Rettig, W.J., 1990. Cell surface glycoprotein of reactive stromal fibroblasts as a potential antibody target in human epithelial cancers. Proc. Natl. Acad. Sci. U. S. A. 87, 7235–7239.

Gemei, M., Di Noto, R., Mirabelli, P., Del Vecchio, L., 2013. Cytometric profiling of CD133+ cells in human colon carcinoma cell lines identifies a common core phenotype and cell type-specific mosaics. Int. J. Biol. Markers 28, 267–273.

Ghani, F.I., Yamazaki, H., Iwata, S., Okamoto, T., Aoe, K., Okabe, K., Mimura, Y., Fujimoto, N., Kishimoto, T., Yamada, T., Xu, C.W., Morimoto, C., 2011. Identification of cancer stem cell markers in human malignant mesothelioma cells. Biochem. Biophys. Res. Commun. 404, 735–742.

Ghatei, M.A., Goodlad, R.A., Taheri, S., Mandir, N., Brynes, A.E., Jordinson, M., Bloom, S.R., 2001. Proglucagon-derived peptides in intestinal epithelial proliferation: Glucagon-like peptide-2 is a major mediator of intestinal epithelial proliferation in rats. Dig. Dis. Sci. 46, 1255–1263.

Ghersi, G., Dong, H., Goldstein, L.A., Yeh, Y., Hakkinen, L., Larjava, H.S., Chen, W.T., 2002. Regulation of fibroblast migration on collagenous matrix by a cell surface peptidase complex. J. Biol. Chem. 277, 29231–29241.

Ghersi, G., Zhao, Q., Salamone, M., Yeh, Y., Zucker, S., Chen, W.T., 2006. The protease complex consisting of dipeptidyl peptidase IV and seprase plays a role in the migration and invasion of human endothelial cells in collagenous matrices. Cancer Res. 66, 4652–4661.

Giovannucci, E., Harlan, D.M., Archer, M.C., Bergenstal, R.M., Gapstur, S.M., Habel, L.A., Pollak, M., Regensteiner, J.G., Yee, D., 2010. Diabetes and Cancer: A Consensus Report. CA. Cancer J. Clin. 60, 207–221.

Giri, D., Ropiquet, F., Ittmann, M., 1999. Alterations in expression of basic fibroblast growth

factor (FGF) 2 and its receptor FGFR-1 in human prostate cancer. Clin. Cancer Res. 5, 1063–1071.

Givel, A.M., Kieffer, Y., Scholer-Dahirel, A., Sirven, P., Cardon, M., Pelon, F., Magagna, I., Gentric, G., Costa, A., Bonneau, C., Mieulet, V., Vincent-Salomon, A., Mechta-Grigoriou, F., 2018. miR200-regulated CXCL12β promotes fibroblast heterogeneity and immunosuppression in ovarian cancers. Nat. Commun. 9.

Goldstein, L.A., Ghersi, G., Piñeiro-Sánchez, M.L., Salamone, M., Yeh, Y., Flessate, D., Chen, W.T., 1997. Molecular cloning of seprase: A serine integral membrane protease from human melanoma. Biochim. Biophys. Acta - Mol. Basis Dis. 1361, 11–19.

Gong, C., Nie, Y., Qu, S., Liao, J.Y., Cui, X., Yao, H., Zeng, Y., Su, F., Song, E., Liu, Q., 2014. miR-21 induces myofibroblast differentiation and promotes the malignant progression of breast phyllodes tumors. Cancer Res. 74, 4341–4352.

Goodman, J.D., Rozypal, T.L., Kelly, T., 2003. Seprase, a membrane-bound protease, alleviates the serum growth requirement of human breast cancer cells. Clin. Exp. Metastasis 20, 459–470.

Gorrell, M.D., 2005. Dipeptidyl peptidase IV and related enzymes in cell biology and liver disorders. Clin. Sci. (Lond). 108, 277–292.

Gorrell, M.D., Gysbers, V., McCaughan, G.W., 2001. CD26: A multifunctional integral membrane and secreted protein of activated lymphocytes. Scand. J. Immunol. 54, 249–264.

Gorrell, M.D., Park, J.E., 2013. Fibroblast Activation Protein α. In: Handbook of Proteolytic Enzymes. Academic Press, pp. 3395–3401.

Gorrell, M.D., Song, S., Wang, X., 2010. Novel Metabolic Disease Therapy.

Gossrau, R., 1979. Histochemical and biochemical distribution of dipeptidylpeptidase IV (DPP IV). Histochemistry 60, 231–248.

Gowda, S., Desai, P.B., Hull, V. V, Math, A.A.K., Vernekar, S.N., Kulkarni, S.S., 2009. A review on laboratory liver function tests. Pan Afr. Med. J. 3, 17.

Gutschmidt, S., Gossrau, R., 1981. A quantitative histochemical study of dipeptidylpeptidase IV (DPP IV). Histochemistry 73, 285–304.

Hagan, C., 2019. When Are Mice Considered Old? [WWW Document]. Jackson Labs. URL https://www.jax.org/news-and-insights/jax-blog/2017/november/when-are-mice-considered-old (accessed 1.8.21).

Hagenbeek, T.J., Spits, H., 2008. T-cell lymphomas in T-cell-specific Pten-deficient mice originate in the thymus. Leukemia 22, 608–619.

Hahn-Windgassen, A., Nogueira, V., Chen, C.C., Skeen, J.E., Sonenberg, N., Hay, N., 2005. Akt activates the mammalian target of rapamycin by regulating cellular ATP level and AMPK activity. J. Biol. Chem. 280, 32081–32089.

Hall, J.M., Korach, K.S., 2003. Stromal cell-derived factor 1, a novel target of estrogen receptor action, mediates the mitogenic effects of estradiol in ovarian and breast cancer cells. Mol. Endocrinol. 17, 792–803.

Hanahan, D., Weinberg, R.A., 2011. Hallmarks of cancer: the next generation. Cell 144, 646–674.

Hardie, D.G., Hawley, S.A., 2001. AMP-activated protein kinase: The energy charge hypothesis revisited. BioEssays 23, 1112–1119.

Hardie, D.G., Schaffer, B.E., Brunet, A., 2016. AMPK: An Energy-Sensing Pathway with Multiple Inputs and Outputs. Trends Cell Biol. 26, 190–201.

Hardie, D.G., Scott, J.W., Pan, D.A., Hudson, E.R., 2003. Management of cellular energy by the AMP-activated protein kinase system. FEBS Lett. 546, 113–120.

Hartmann, B., Harr, M.B., Jeppesen, P.B., Wojdemann, M., Deacon, C.F., Mortensen, P.B., Holst, J.J., 2000a. In vivo and in vitro degradation of glucagon-like peptide-2 in humans. J. Clin. Endocrinol. Metab. 85, 2884–2888.

Hartmann, B., Thulesen, J., Kissow, H., Thulesen, S., Orskov, C., Physiology, M., Anatomy, J.T., 2000b. Dipeptidyl Peptidase IV Inhibition Enhances the Intestinotrophic Effect of Glucagon-Like Peptide-2 in Rats and Mice. Endocrinology 141, 4013–4020.

Havre, P.A., Abe, M., Urasaki, Y., Ohnuma, K., Morimoto, C., Dang, N.H., 2008. The role of CD26/dipeptidyl peptidase IV in cancer. Front. Biosci. 13, 1634–1645.

Havre, P.A., Abe, M., Urasaki, Y., Ohnuma, K., Morimoto, C., Dang, N.H., 2009. CD26 expression on T cell lines increases SDF-1-α-mediated invasion. Br. J. Cancer 101, 983–991.

Havre, P.A., Dang, L.H., Ohnuma, K., Iwata, S., Morimoto, C., Dang, N.H., 2013. CD26 Expression on T-Anaplastic Large Cell Lymphoma (ALCL) Line Karpas 299 is associated with increased expression of Versican and MT1-MMP and enhanced adhesion. BMC Cancer 13, 1–11.

Hawley, S.A., Gadalla, A.E., Olsen, G.S., Grahame Hardie, D., 2002. The antidiabetic drug metformin activates the AMP-activated protein kinase cascade via an adenine nucleotide-independent mechanism. Diabetes 51, 2420–2425.

Hawley, S.A., Pan, D.A., Mustard, K.J., Ross, L., Bain, J., Edelman, A.M., Frenguelli, B.G., Hardie, D.G., 2005. Calmodulin-dependent protein kinase kinase-β is an alternative upstream kinase for AMP-activated protein kinase. Cell Metab. 2, 9–19.

Hawley, S.A., Ross, F.A., Chevtzoff, C., Green, K.A., Evans, A., Fogarty, S., Towler, M.C., Brown, L.J., Ogunbayo, O.A., Evans, A.M., Hardie, D.G., 2010. Use of cells expressing γ subunit variants to identify diverse mechanisms of AMPK activation. Cell Metab. 11, 554–565.

Hayashi, J.I., Takemitsu, M., Nonaka, I., 1992. Recovery of the missing tumorigenicity in mitochondrial DNA-less HeLa cells by introduction of mitochondrial DNA from normal human cells. Somat. Cell Mol. Genet. 18, 123–129.

He, L., Wondisford, F.E., 2015. Metformin action: Concentrations matter. Cell Metab. 21, 159–162.

Heijstek, M.W., Kranenburg, O., Rinkes, I.H.M.B., 2005. Mouse models of colorectal cancer and liver metastases. Dig. Surg. 22, 16–25.

Henry, L.R., Lee, H.-O., Lee, J.S., Klein-Szanto, A., Watts, P., Ross, E.A., Chen, W.-T., Cheng, J.D., 2007. Clinical Implications of Fibroblast Activation Protein in Patients with Colon Cancer. Clin. Cancer Res. 13, 1736–1741.

Herman, G.A., Bergman, A., Liu, F., Stevens, C., Wang, A.Q., Zeng, W., Chen, L., Snyder, K., Hilliard, D., Tanen, M., Tanaka, W., Meehan, A.G., Lasseter, K., Dilzer, S., Blum, R., Wagner, J.A., 2006. Pharmacokinetics and Pharmacodynamic Effects of the Oral DPP-4 Inhibitor Sitagliptin in Middle-Aged Obese Subjects. J. Clin. Pharmacol. 46, 876–886.

Herman, G.A., Mistry, G.C., Yi, B., Bergman, A.J., Wang, A.Q., Zeng, W., Chen, L., Snyder, K., Ruckle, J.L., Larson, P.J., Davies, M.J., Langdon, R.B., Gottesdiener, K.M., Wagner, J.A., 2011. Evaluation of pharmacokinetic parameters and dipeptidyl

peptidase-4 inhibition following single doses of sitagliptin in healthy, young Japanese males. Br. J. Clin. Pharmacol. 71, 429–436.

Herrera, C., Morimoto, C., Blanco, J., Mallol, J., Arenzana, F., Lluis, C., Franco, R., 2001. Comodulation of CXCR4 and CD26 in Human Lymphocytes. J. Biol. Chem. 276, 19532–19539.

Herrmann, H., Sadovnik, I., Cerny-Reiterer, S., Rülicke, T., Stefanzl, G., Willmann, M., Hoermann, G., Bilban, M., Blatt, K., Herndlhofer, S., Mayerhofer, M., Streubel, B., Sperr, W.R., Holyoake, T.L., Mannhalter, C., Valent, P., 2014. Dipeptidylpeptidase IV (CD26) defines leukemic stem cells (LSC) in chronic myeloid leukemia. Blood 123, 3951–3962.

Herzig, S., Shaw, R.J., 2018. AMPK: Guardian of metabolism and mitochondrial homeostasis. Nat. Rev. Mol. Cell Biol. 19, 121–135.

Holst, J.J., 2007. The Physiology of Glucagon-like Peptide 1. Physiol. Rev. 87, 1409–1439.

Holzer, P., Reichmann, F., Farzi, A., 2012. Neuropeptide Y, peptide YY and pancreatic polypeptide in the gut-brain axis. Neuropeptides 46, 261–274.

Hong, W., Petell, J.K., Swank, D., Sanford, J., Hixson, D.C., Doyle, D., 1989. Expression of dipeptidyl peptidase IV in rat tissues is mainly regulated at the mRNA levels. Exp. Cell Res. 182, 256–266.

Hopsu-Havu, V.K., Glenner, G.G., 1966. A new dipeptide naphthylamidase hydrolyzing glycyl-prolyl-beta-naphthylamide. Histochemie 7, 197–201.

Hori, T., Chen, F., Baine, A.-M.T., Gardner, L.B., Nguyen, J.H., 2011. Fulminant liver failure model with hepatic encephalopathy in the mouse. Ann. Gastroenterol. 24, 294–306.

Houghton, A.N., Albino, A.P., Cordon-Cardo, C., Davis, L.J., Eisinger, M., 1988. Cell surface antigens of human melanocytes and melanoma. Expression of adenosine deaminase binding protein is extinguished with melanocyte transformation. J. Exp. Med. 167, 197–212.

Howell, J.J., Hellberg, K., Turner, M., Talbott, G., Kolar, M.J., Ross, D.S., Hoxhaj, G., Saghatelian, A., Shaw, R.J., Manning, B.D., 2017. Metformin Inhibits Hepatic mTORC1 Signaling via Dose-Dependent Mechanisms Involving AMPK and the TSC Complex. Cell Metab. 25, 463–471.

Hu, Y., Le Leu, R.K., Christophersen, C.T., Somashekar, R., Conlon, M.A., Meng, X.Q., Winter, J.M., Woodman, R.J., McKinnon, R., Young, G.P., 2015. Manipulation of the gut microbiota using resistant starch is associated with protection against colitis-associated colorectal cancer in rats. Carcinogenesis 37, 366–375.

Hu, Y., Le Leu, R.K., Young, G.P., 2005. Sulindac corrects defective apoptosis and suppresses azoxymethane-induced colonic oncogenesis in p53 knockout mice. Int. J. Cancer 116, 870–875.

Hua, H., Zhang, Z., Qian, Y., Yuan, H., Ge, W., Huang, S., Zhang, A., Zhang, Y., Jia, Z., Ding, G., 2019. Inhibition of the mitochondrial complex-1 protects against carbon tetrachloride-induced acute liver injury. Biomed. Pharmacother. 115, 108948.

Hwang, H.J., Chung, H.S., Jung, T.W., Ryu, J.Y., Hong, H.C., Seo, J.A., Kim, S.G., Kim, N.H., Choi, K.M., Choi, D.S., Baik, S.H., Yoo, H.J., 2015a. The dipeptidyl peptidase-IV inhibitor inhibits the expression of vascular adhesion molecules and inflammatory cytokines in HUVECs via Akt- and AMPK-dependent mechanisms. Mol. Cell. Endocrinol. 405, 25–34.

Hwang, H.J., Jung, T.W., Kim, B.H., Hong, H.C., Seo, J.A., Kim, S.G., Kim, N.H., Choi, K.M., Choi, D.S., Baik, S.H., Yoo, H.J., 2015b. A dipeptidyl peptidase-IV inhibitor improves hepatic steatosis and insulin resistance by AMPK-dependent and JNK-dependent inhibition of LECT2 expression. Biochem. Pharmacol. 98, 157–166.

Hwang, H.J., Jung, T.W., Ryu, J.Y., Hong, H.C., Choi, H.Y., Seo, J.A., Kim, S.G., Kim, N.H., Choi, K.M., Choi, D.S., Baik, S.H., Yoo, H.J., 2014. Dipeptidyl petidase-IV inhibitor (gemigliptin) inhibits tunicamycin-induced endoplasmic reticulum stress, apoptosis and inflammation in H9c2 cardiomyocytes. Mol. Cell. Endocrinol. 392, 1–7.

Hwang, Jung Hwan, Hwang, Jin Hee, Chung, H.K., Kim, D.W., Hwang, E.S., Suh, J.M., Kim, H., You, K.H., Kwon, O.Y., Ro, H.K., Jo, D.Y., Shong, M., 2003. CXC chemokine receptor 4 expression and function in human anaplastic thyroid cancer cells. J. Clin. Endocrinol. Metab. 88, 408–416.

Iakoubov, R., Lauffer, L.M., Trivedi, S., Kim, Y.I.J., Brubaker, P.L., 2009. Carcinogenic effects of exogenous and endogenous glucagon-like peptide-2 in azoxymethane-treated mice. Endocrinology 150, 4033–4043.

Ichii, S., Takeda, S., Horii, A., Nakatsuru, S., Miyoshi, Y., Emi, M., Fujiwara, Y., Koyama, K., Furuyama, J., Utsunomiya, J., Nakamura, Y., 1993. Detailed analysis of genetic

alterations in colorectal tumors from patients with and without familial adenomatous polyposis (FAP). Oncogene 8, 2399–2405.

Inamoto, T., Yamada, T., Ohnuma, K., Kina, S., Takahashi, N., Yamochi, T., Inamoto, S., Katsuoka, Y., Hosono, O., Tanaka, H., Dang, N.H., Morimoto, C., 2007. Humanized anti-CD26 monoclonal antibody as a treatment for malignant mesothelioma tumors. Clin. Cancer Res. 13, 4191–200.

Inamoto, T., Yamochi, T., Ohnuma, K., Iwata, S., Kina, S., Inamoto, S., Tachibana, M., Katsuoka, Y., Dang, N.H., Morimoto, C., 2006. Anti-CD26 monoclonal antibody-mediated G1-S arrest of human renal clear cell carcinoma caki-2 is associated with retinoblastoma substrate dephosphorylation, cyclin-dependent kinase 2 reduction, p27kip1 enhancement, and disruption of binding to the extrace. Clin. Cancer Res. 12, 3470–3477.

Ishii, T., Ohnuma, K., Murakami, A., Takasawa, N., Kobayashi, S., Dang, N.H., Schlossman, S.F., Morimoto, C., 2001. CD26-mediated signaling for T cell activation occurs in lipid rafts through its association with CD45RO. PNAS 98, 12138–12143.

Iwaki-Egawa, S., Watanabe, Y., Kikuya, Y., Fujimoto, Y., 1998. Dipeptidyl Peptidase IV from Human Serum: Purification, Characterization, and N-Terminal Amino Acid Sequence. J. Biochem. 124, 428–433.

Jacobs, S.R., Herman, C.E., Maciver, N.J., Wofford, J.A., Wieman, H.L., Hammen, J.J., Rathmell, J.C., 2008. Glucose uptake is limiting in T cell activation and requires CD28-mediated Akt-dependent and independent pathways. J. Immunol. 180, 4476–86.

Jang, J.H., Janker, F., De Meester, I., Arni, S., Borgeaud, N., Yamada, Y., Bazo, I.G., Weder, W., Jungraithmayr, W., 2019. The CD26/DPP4-inhibitor vildagliptin suppresses lung cancer growth via macrophage-mediated NK cell activity. Carcinogenesis 40, 324–334.

Javidroozi, M., Zucker, S., Chen, W.T., 2012. Plasma seprase and DPP4 levels as markers of disease and prognosis in cancer. Dis. Markers 32, 309–320.

Jensen, T., Kiersgaard, M., Sørensen, D., Mikkelsen, L., 2013. Fasting of mice: a review. Lab. Anim. 47, 225–240.

Jiang, X., Lu, X., Hu, P., Liu, R., 2009. Improved therapeutic efficacy using vaccination with glioma lysate-pulsed dendritic cells combined with IP-10 in murine glioma. Vaccine 27,

6210–6216.

Jin, X., Iwasa, S., Okada, K., Mitsumata, M., Ooi, A., 2003. Expression patterns of seprase, a membrane serine protease, in cervical carcinoma and cervical intraepithelial neoplasm. Anticancer Res. 23, 3195–3198.

Jones, A.M., Mitter, R., Springall, R., Graham, T., Winter, E., Gillett, C., Hanby, A.M., Tomlinson, I.P.M., Sawyer, E.J., Walker, R., Pinder, S., Jones, L., Ellis, I., Puay, H.T., Macartney, J., Green, D., Hales, S., Harding-Mackean, C., Colclough, A., MacNeil, F., Rowlands, D., Smith, C., Fentiman, I., Cane, P., Desai, A., Goderya, R., Nerurkar, A., Kissin, M., Jackson, P., 2008. A comprehensive genetic profile of phyllodes tumours of the breast detects important mutations, intra-tumoral genetic heterogeneity and new genetic changes on recurrence. J. Pathol. 214, 533–544.

Jones, B., Adams, S., Miller, G.T., Jesson, M.I., Watanabe, T., Wallner, B.P., 2003. Hematopoietic stimulation by a dipeptidyl peptidase inhibitor reveals a novel regulatory mechanism and therapeutic treatment for blood cell deficiencies. Blood 102, 1641–1648.

Jones, R.G., Plas, D.R., Kubek, S., Buzzai, M., Mu, J., Xu, Y., Birnbaum, M.J., Thompson, C.B., 2005. AMP-activated protein kinase induces a p53-dependent metabolic checkpoint. Mol. Cell 18, 283–293.

Joshi, S., Liu, M., Turner, N., 2015. Diabetes and its link with cancer: providing the fuel and spark to launch an aggressive growth regime. Biomed Res. Int. 2015, 390863.

Kaighn, M.E., Narayan, K.S., Ohnuki, Y., Lechner, J.F., Jones, L.W., 1979. Establishment and characterization of a human prostatic carcinoma cell line (PC-3). Invest. Urol. 17, 16–23.

Kajiyama, H., Kikkawa, F., Khin, E.E., Shibata, K., Ino, K., Mizutani, S., 2003. Dipeptidyl peptidase IV overexpression induces up-regulation of E-cadherin and tissue inhibitors of matrix metalloproteinases, resulting in decreased invasive potential in ovarian carcinoma cells. Cancer Res. 63, 2278–2283.

Kajiyama, H., Kikkawa, F., Suzuki, T., 2002. Prolonged Survival and Decreased Invasive Activity Attributable to Dipeptidyl Peptidase IV Overexpression in Ovarian Carcinoma Advances in Brief Prolonged Survival and Decreased Invasive Activity Attributable to Dipeptidyl. Cancer Res. 62, 2753–2757.

Kajiyama, H., Shibata, K., Ino, K., Mizutani, S., Nawa, A., Kikkawa, F., 2010. The expression of dipeptidyl peptidase IV (DPPIV/CD26) is associated with enhanced chemosensitivity to paclitaxel in epithelial ovarian carcinoma cells. Cancer Sci. 101, 347–354.

Kalender, A., Selvaraj, A., Kim, S.Y., Gulati, P., Brûlé, S., Viollet, B., Kemp, B.E., Bardeesy, N., Dennis, P., Schlager, J.J., Marette, A., Kozma, S.C., Thomas, G., 2010. Metformin, independent of AMPK, inhibits mTORC1 in a rag GTPase-dependent manner. Cell Metab. 11, 390–401.

Kalluri, R., 2016. The biology and function of fibroblasts in cancer. Nat. Rev. Cancer 16, 582–598.

Kalyanaraman, B., Cheng, G., Hardy, M., Ouari, O., Lopez, M., Joseph, J., Zielonka, J., Dwinell, M.B., 2018. A review of the basics of mitochondrial bioenergetics, metabolism, and related signaling pathways in cancer cells: Therapeutic targeting of tumor mitochondria with lipophilic cationic compounds. Redox Biol. 14, 316–327.

Kanasaki, K., 2018. The role of renal dipeptidyl peptidase-4 in kidney disease: Renal effects of dipeptidyl peptidase-4 inhibitors with a focus on linagliptin. Clin. Sci. 132, 489–507.

Kanazawa, I., Tanaka, K.I., Sugimoto, T., 2014. DPP-4 inhibitors improve liver dysfunction in type 2 diabetes mellitus. Med. Sci. Monit. 20, 1662–1667.

Kannen, V., Garcia, S.B., Stopper, H., Waaga-Gasser, A.M., 2013. Glucagon-like peptide 2 in colon carcinogenesis: possible target for anti-cancer therapy? Pharmacol. Ther. 139, 87–94.

Karra, E., Chandarana, K., Batterham, R.L., 2009. The role of peptide YY in appetite regulation and obesity. In: Journal of Physiology. Blackwell Publishing Ltd, pp. 19–25.

Keane, F.M., Chowdhury, S., Yao, T.W., Nadvi, N.A., Gall, M.G., Chen, Y., Osborne, B., Vieira de Ribeiro, A.J., Church, W.B., McCaughan, G.W., Gorrell, M.D., Yu, D.M.T., 2012. Targeting dipeptidyl peptidase-4 (DPP-4) and fibroblast activation protein (FAP) for diabetes and cancer therapy. In: Dunn, B.M. (Ed.), Proteinases as Drug Targets. Royal Society of Chemistry, United Kingdom, p. 275.

Keane, F.M., Nadvi, N.A., Yao, T.W., Gorrell, M.D., 2011. Neuropeptide Y, B-type natriuretic peptide, substance P and peptide YY are novel substrates of fibroblast activation protein-α. FEBS J. 278, 1316–1332.

Keane, F.M., Yao, T.W., Seelk, S., Gall, M.G., Chowdhury, S., Poplawski, S.E., Lai, J.H., Li, Y., Wu, W., Farrell, P., Vieira de Ribeiro, A.J., Osborne, B., Yu, D.M.T., Seth, D., Rahman, K., Haber, P., Topaloglu, A.K., Wang, C., Thomson, S., Hennessy, A., Prins, J., Twigg, S.M., McLennan, S. V., McCaughan, G.W., Bachovchin, W.W., Gorrell, M.D., 2014. Quantitation of fibroblast activation protein (FAP)-specific protease activity in mouse, baboon and human fluids and organs. FEBS Open Bio 4, 43–54.

Kehlen, A., Göhring, B., Langner, J., Riemann, D., 1998. Regulation of the expression of aminopeptidase A, aminopeptidase N/CD13 and dipeptidylpeptidase IV/CD26 in renal carcinoma cells and renal tubular epithelial cells by cytokines and cAMP-increasing mediators. Clin. Exp. Immunol. 111, 435–441.

Kelly, T., Huang, Y., Simms, A.E., Mazur, A., 2012. Fibroblast Activation Protein-α. A Key Modulator of the Microenvironment in Multiple Pathologies. In: International Review of Cell and Molecular Biology. Elsevier Inc., pp. 83–116.

Khin, E.E., Kikkawa, F., Ino, K., Kajiyama, H., Suzuki, T., Shibata, K., Tamakoshi, K., Nagasaka, T., Mizutani, S., 2003. Dipeptidyl peptidase IV expression in endometrial endometrioid adenocarcinoma and its inverse correlation with tumor grade. Am. J. Obstet. Gynecol. 188, 670–676.

Khokha, R., Waterhouse, P., Yagel, S., Lala, P.K., Overall, C.M., Norton, G., Denhardt, D.T., 1989. Antisense RNA-induced reduction in murine TIMP levels confers oncogenicity on Swiss 3T3 cells. Science (80-.). 243, 947–950.

Kikkawa, F., Kajiyama, H., Ino, K., Shibata, K., Mizutani, S., 2003. Increased adhesion potency of ovarian carcinoma cells to mesothelial cells by overexpression of dipeptidyl peptidase IV. Int. J. Cancer 105, 779–783.

Kikkawa, F., Kajiyama, H., Shibata, K., Ino, K., Nomura, S., Mizutani, S., 2005. Dipeptidyl peptidase IV in tumor progression. In: Biochimica et Biophysica Acta - Proteins and Proteomics. pp. 45–51.

Kikkawa, F., Tamakoshi, K., Nawa, A., Shibata, K., Yamagata, S., Yamagata, T., Suganuma, N., 1997. Positive correlation between inhibitors of matrix metalloproteinase 1 and matrix metalloproteinases in malignant ovarian tumor tissues. Cancer Lett. 120, 109–115.

Kim, D., Wang, L., Beconi, M., Eiermann, G.J., Fisher, M.H., He, H., Hickey, G.J., Kowalchick, J.E., Leiting, B., Lyons, K., Marsilio, F., Mccann, M.E., Patel, R.A., Petrov,

A., Scapin, G., Patel, S.B., Roy, R.S., Wu, J.K., Wyvratt, M.J., Zhang, B.B., Zhu, L., Thornberry, N.A., Weber, A.E., 2005. (2R)-4-Oxo-4-[3-(Trifluoromethyl)-5,6-dihydro[1,2,4]triazolo[4,3-a]pyrazin- 7(8H)-yl]-1-(2,4,5-trifluorophenyl)butan-2-amine: A Potent, Orally Active Dipeptidyl Peptidase IV Inhibitor for the Treatment of Type 2 Diabetes. J. Med. Chem. 141, 141–151.

Kim, N.H., Yu, T., Lee, D.H., 2014. The nonglycemic actions of dipeptidyl peptidase-4 inhibitors. Biomed Res. Int. 2014, 68703.

Kim, W.R., Flamm, S.L., Di Bisceglie, A.M., Bodenheimer, H.C., 2008. Serum activity of alanine aminotransferase (ALT) as an indicator of health and disease. Hepatology 47, 1363–1370.

Kimoto, T., 1998. Pathological observations during treatment with the biological response modifier Maruyama vaccine in cancer: Implications for collagen production in the prevention of cancer invasion and metastasis. Cancer Detect. Prev. 22, 340–349.

Kirby, M., Yu, D.M., O'Connor, S., Gorrell, M.D., 2010. Inhibitor selectivity in the clinical application of dipeptidyl peptidase-4 inhibition. Clin Sci 118, 31–41.

Kishton, R.J., Barnes, C.E., Nichols, A.G., Cohen, S., Gerriets, V.A., Siska, P.J., Macintyre, A.N., Goraksha-Hicks, P., De Cubas, A.A., Liu, T., Warmoes, M.O., Abel, E.D., Yeoh, A.E.J., Gershon, T.R., Rathmell, W.K., Richards, K.L., Locasale, J.W., Rathmell, J.C., 2016. AMPK Is Essential to Balance Glycolysis and Mitochondrial Metabolism to Control T-ALL Cell Stress and Survival. Cell Metab. 23, 649–662.

Kissow, H., Hartmann, B., Holst, J.J., Viby, N.E., Hansen, L.S., Rosenkilde, M.M., Hare, K.J., Poulsen, S.S., 2012. Glucagon-like peptide-1 (GLP-1) receptor agonism or DPP-4 inhibition does not accelerate neoplasia in carcinogen treated mice. Regul. Pept. 179, 91–100.

Kitlinska, J., Abe, K., Kuo, L., Pons, J., Yu, M., Li, L., Tilan, J., Everhart, L., Lee, E.W., Zukowska, Z., Toretsky, J.A., 2005. Differential effects of neuropeptide Y on the growth and vascularization of neural crest-derived tumors. Cancer Res. 65, 1719–1728.

Klemann, C., Wagner, L., Stephan, M., von Hörsten, S., 2016. Cut to the chase: a review of CD26/dipeptidyl peptidase-4's (DPP4) entanglement in the immune system. Clin. Exp. Immunol. 185, 1–21.

Klepinin, A., Zhang, S., Klepinina, L., Rebane-Klemm, E., Terzic, A., Kaambre, T., Dzeja, P.,

2020. Adenylate Kinase and Metabolic Signaling in Cancer Cells. Front. Oncol. 10, 660.

Kobayashi, H., Enomoto, A., Woods, S.L., Burt, A.D., Takahashi, M., Worthley, D.L., 2019. Cancer-associated fibroblasts in gastrointestinal cancer. Nat. Rev. Gastroenterol. Hepatol. 16, 282–295.

Koehler, J.A., Kain, T., Drucker, D.J., 2011. Glucagon-like peptide-1 receptor activation inhibits growth and augments apoptosis in murine CT26 colon cancer cells. Endocrinology 152, 3362–3372.

Komiya, E., Ohnuma, K., Yamazaki, H., Hatano, R., Iwata, S., Okamoto, T., Dang, N.H., Yamada, T., Morimoto, C., 2014. CD26-mediated regulation of periostin expression contributes to migration and invasion of malignant pleural mesothelioma cells. Biochem. Biophys. Res. Commun. 447, 609–615.

Kornelius, E., Lin, C.L., Chang, H.H., Li, H.H., Huang, W.N., Yang, Y.S., Lu, Y.L., Peng, C.H., Huang, C.N., 2015. DPP-4 Inhibitor Linagliptin Attenuates Aβ-induced Cytotoxicity through Activation of AMPK in Neuronal Cells. CNS Neurosci. Ther. 21, 549–557.

Kotackova, L., Balaziova, E., Šedo, A., Kotačková, L., Balážiová, E., Šedo, A., 2009. Expression pattern of dipeptidyl peptidase IV activity and/or structure homologues in cancer. Folia Biol. (Praha). 55, 77–84.

Kovacic, S., Soltys, C.L.M., Barr, A.J., Shiojima, I., Walsh, K., Dyck, J.R.B., 2003. Akt activity negatively regulates phosphorylation of AMP-activated protein kinase in the heart. J. Biol. Chem. 278, 39422–39427.

Lahl, M., Fisher, V.L., Laschinger, K., 2008. Ewing's sarcoma family of tumors: An overview from diagnosis to survivorship. Clin. J. Oncol. Nurs. 12, 89–97.

Lam, C.S.-C.C., Cheung, A.H.-K.K., Wong, S.K.-M.M., Wan, T.M.-H.H., Ng, L., Chow, A.K.-M.M., Cheng, N.S.-M.M., Pak, R.C.-H.H., Li, H.-S.S., Man, J.H.-W.W., Yau, T.C.-C.C., Lo, O.S.-H.H., Poon, J.T.-C.C., Pang, R.W.-C.C., Law, W.L., 2014. Prognostic significance of CD26 in patients with colorectal cancer. PLoS One 9, e98582.

Lambeir, A., Durinx, C., Scharpe, S., De Meester, I., 2003. Dipeptidyl-peptidase IV from bench to bedside : An update on structural properties , functions. Crit. Rev. Clin. Lab. Sci. 40, 209–294.

Lambeir, A.M., Proost, P., Durinx, C., Bal, G., Senten, K., Augustyns, K., Scharpé, S., Van

Dammes, J., De Meester, I., 2001. Kinetic Investigation of Chemokine Truncation by CD26/Dipeptidyl Peptidase IV Reveals a Striking Selectivity within the Chemokine Family. J. Biol. Chem. 276, 29839–29845.

Lamont, B.J., Andrikopoulos, S., 2014. Hope and fear for new classes of type 2 diabetes drugs: Is there preclinical evidence that incretin-based therapies alter pancreatic morphology? J. Endocrinol. 221, 43–61.

Laouar, A., Bauvois, B., 1992. Characterization and modulation of cell surface proteases on human mycloblastic (HL-60) cells and comparison to normal mycloid cells. Immunol. Lett. 34, 257–265.

Laqueur, G.L., Mickelsen, O., Whiting, M.G., Kurland, L.T., 1963. Carcinogenic properties of nuts from Cycas Circinalis L. Indigenous to Guam. J. Natl. Cancer Inst. 31, 919–51.

Laron, Z., 2001. Insulin-like growth factor 1 (IGF-1): A growth hormone. J. Clin. Pathol. - Mol. Pathol. 54, 311–316.

Larrinaga, G., Blanco, L., Sanz, B., Perez, I., Gil, J., Unda, M., Andrés, L., Casis, L., López, J.I., 2012. The impact of peptidase activity on clear cell renal cell carcinoma survival. Am. J. Physiol. - Ren. Physiol. 303, F1584-91.

Larrinaga, G., Perez, I., Sanz, B., Beitia, M., Errarte, P., Fernández, A., Blanco, L., Etxezarraga, M.C., Gil, J., López, J.I., 2015. Dipeptidyl-peptidase IV activity is correlated with colorectal cancer prognosis. PLoS One 10, 1–17.

Lay, A.J., Zhang, H.E., McCaughan, G.W., Gorrell, M.D., 2019. Fibroblast activation protein in liver fibrosis. Front. Biosci. - Landmark 24, 1–17.

LeBleu, V.S., Kalluri, R., 2018. A peek into cancer-associated fibroblasts: Origins, functions and translational impact. DMM Dis. Model. Mech. 11.

Lee, K.N., Jackson, K.W., Christiansen, V.J., Lee, C.S., Chun, J.G., McKee, P.A., 2006. Antiplasmin-cleaving enzyme is a soluble form of fibroblast activation protein. Blood 107, 1397–1404.

Lee, S., Kang, K.P., Kang, S.K., 2006. Clinical usefulness of the serum anion gap. Electrolyte Blood Press. 4, 44–46.

Lefort, É.C., Blay, J., 2010. The dietary flavonoid apigenin enhances the activities of the anti-metastatic protein CD26 on human colon carcinoma cells. Clin. Exp. Metastasis 28,

337–349.

Leiphrakpam, P.D., Agarwal, E., Mathiesen, M., Haferbier, K.L., Brattain, M.G., Chowdhury,
S., 2014. In vivo analysis of insulin-like growth factor type 1 receptor humanized
monoclonal antibody MK-0646 and small molecule kinase inhibitor OSI-906 in
colorectal cancer. Oncol. Rep. 31, 87–94.

Levy, M.T., McCaughan, G.W., Marinos, G., Gorrell, M.D., 2002. Intrahepatic expression of
the hepatic stellate cell marker fibroblast activation protein correlates with the degree of
fibrosis in hepatitis C virus infection. Liver 22, 93–101.

Leystra, A.A., Clapper, M.L., 2019. Gut microbiota influences experimental outcomes in
mouse models of colorectal cancer. Genes (Basel). 10, 900.

Li, M., Li, X., Zhang, H., Lu, Y., 2018. Molecular Mechanisms of Metformin for Diabetes and
Cancer Treatment. Front. Physiol. 9, 1039.

Liang, J., Xu, Z.X., Ding, Z., Lu, Y., Yu, Q., Werle, K.D., Zhou, G., Park, Y.Y., Peng, G.,
Gambello, M.J., Mills, G.B., 2015. Myristoylation confers noncanonical AMPK functions
in autophagy selectivity and mitochondrial surveillance. Nat. Commun. 6, 7926.

Lijinsky, W., Saavedra, J.E., Reuber, M.D., 1985. Organ-specific Carcinogenesis in Rats by
Methyl- and Ethylazoxyalkanes. Cancer Res. 45, 76–79.

Liu, F., Qi, L., Liu, B., Liu, J., Zhang, H., Che, D.H., Cao, J.Y., Shen, J., Geng, J.X., Bi, Y.,
Ye, L.G., Pan, B., Yu, Y., 2015. Fibroblast activation protein overexpression and clinical
implications in solid tumors: A meta-analysis. PLoS One 10, e0116683.

Liu, H., Jiang, Y., Luo, Y., Jiang, W., 2006. A Simple and Rapid Determination of ATP, ADP
and AMP Concentrations in Pericarp Tissue of Litchi Fruit by High Performance Liquid
Chromatography. Food Technol. Biotechnol. 44, 531–534.

Liu, H., Pu, Y., Amina, Q., Wang, Q., Zhang, M., Song, J., Guo, J., Mardan, M., 2019.
Prognostic and therapeutic potential of Adenylate kinase 2 in lung adenocarcinoma.
Sci. Rep. 9, 17757.

Liu, M., Guo, S., Stiles, J.K., 2011. The emerging role of CXCL10 in cancer. Oncol. Lett. 2,
583–589.

Liu, R., Li, H., Liu, L., Yu, J., Ren, X., 2012. Fibroblast activation protein: A potential
therapeutic target in cancer. Cancer Biol. Ther. 13, 123–129.

Lloyd, R. V., Erickson, L.A., Jin, L., Kulig, E., Qian, X., Cheville, J.C., Scheithauer, B.W., 1999. p27(kip1): A multifunctional cyclin-dependent kinase inhibitor with prognostic significance in human cancers. Am. J. Pathol. 154, 313–323.

Loetscher, M., Loetscher, P., Brass, N., Meese, E., Moser, B., 1998. Lymphocyte-specific chemokine receptor CXCR3: regulation, chemokine binding and gene localization. Eur. J. Immunol. 28, 3696–3705.

Lovshin, J.A., Drucker, D.J., 2009. Incretin-based therapies for type 2 diabetes mellitus. Nat. Rev. Endocrinol. 5, 262–269.

Lowe, R.D., Guild, G.E., Harpas, P., Kirkbride, P., Hoffmann, P., Voelcker, N.H., Kobus, H., 2009. Rapid drug detection in oral samples by porous silicon assisted laser desorption/ionization mass spectrometry. Rapid Commun. Mass Spectrom. 23, 3543–3548.

Lu, C., Tilan, J.U., Everhart, L., Czarnecka, M., Soldin, S.J., Mendu, D.R., Jeha, D., Hanafy, J., Lee, C.K., Sun, J., Izycka-Swieszewska, E., Toretsky, J.A., Kitlinska, J., 2011. Dipeptidyl peptidases as survival factors in ewing sarcoma family of tumors: Implications for tumor biology and therapy. J. Biol. Chem. 286, 27494–27505.

Lu, X., Jiang, X., Liu, R., Zhang, S., 2008. The enhanced anti-angiogenic and antitumor effects of combining flk1-based DNA vaccine and IP-10. Vaccine 26, 5352–5357.

Lu, Z., Qi, L., Bo, X.J., Liu, G.D., Wang, J.M., Li, G., 2013. Expression of CD26 and CXCR4 in prostate carcinoma and its relationship with clinical parameters. J. Res. Med. Sci. 18, 647–652.

Luo, J., Lubaroff, D.M., Hendrix, M.J.C., 1999. Suppression of prostate cancer invasive potential and matrix metalloproteinase activity by E-cadherin transfection. Cancer Res. 59, 3552–3556.

Ma, X., Jin, M., Cai, Y., Xia, H., Long, K., Liu, J., Yu, Q., Yuan, J., 2011. Mitochondrial electron transport chain complex III is required for antimycin A to inhibit autophagy. Chem. Biol. 18, 1474–1481.

Mareš, V., Stremeňová, J., Lisá, V., Kozáková, H., Marek, J., Syrůček, M., Šoula, O., Šedo, A., 2012. Compartment- and malignance-dependent up-regulation of γ-glutamyltranspeptidase and dipetidylpeptidase-IV activity in human brain gliomas. Histol. Histopathol. 27, 931–940.

Marguet, D., Baggio, L., Kobayashi, T., Bernard, A.-M., Pierres, M., Nielsen, P.F., Ribel, U., Watanabe, T., Drucker, D.J., Wagtmann, N., 2000. Enhanced insulin secretion and improved glucose tolerance in mice lacking CD26. Proc. Natl. Acad. Sci. 97, 6874–6879.

Mathew, S., Scanlan, M.J., Mohan Raj, B.K., Murty, V.V.V.S., Garin-Chesa, P., Old, L.J., Rettig, W.J., Chaganti, R.S.K., 1995. The gene for fibroblast activation protein α (FAP), a putative cell surface-bound serine protease expressed in cancer stroma and wound healing, maps to chromosome band 2q23. Genomics 25, 335–337.

Matkowskyj, K.A., Marrero, J.A., Carroll, R.E., Danilkovich, A. V, Green, R.M., Benya, R. V, 1999. Azoxymethane-induced fulminant hepatic failure in C57BL/6J mice: characterization of a new animal model. Am. J. Physiol. Liver Physiol. 277, 455–462.

Matsuno-Yagi, A., Hatefi, Y., 1985. Studies on the mechanism of oxidative phosphorylation. J. Biol. Chem. 260, 14424–14427.

Matteucci, E., Giampietro, O., 2009. Dipeptidyl peptidase-4 (CD26): knowing the function before inhibiting the enzyme. Curr. Med. Chem. 16, 2943–2951.

McGinley, J.N., Thompson, M.D., Thompson, H.J., 2010. A method for serial tissue processing and parallel analysis of aberrant crypt morphology, mucin depletion, and beta-catenin staining in an experimental model of colon carcinogenesis. Biol. Proced. Online 12, 118–130.

McGuinness, C., Wesley, U. V., 2008. Dipeptidyl peptidase IV (DPPIV), a candidate tumor suppressor gene in melanomas is silenced by promoter methylation. Front. Biosci. 13, 2435–2443.

Ménétrier-Caux, C., Ray-Coquard, I., Blay, J.Y., Caux, C., 2019. Lymphopenia in Cancer Patients and its Effects on Response to Immunotherapy: An opportunity for combination with Cytokines? J. Immunother. Cancer 7, 1–15.

Mentlein, R., 1988. Proline residues in the maturation and degradation of peptide hormones and neuropeptides. FEBS Lett. 234, 251–256.

Mentlein, Rolf, Dahms, P., Grandt, D., Krüger, R., 1993. Proteolytic processing of neuropeptide Y and peptide YY by dipeptidyl peptidase IV. Regul. Pept. 49, 133–144.

Mentlein, R, Gallwitz, B., Schmidt, W., 1993. Dipeptidyl-peptidase IV hydrolyses gastric

inhibitory polypeptide, glucagon-like peptide-1(7-36)amide, peptide histidine methionine and Is Responsible for Their Degradation in Human Serum. Eur. J. Biochem. 0215, 829–835.

Merck Sharp & Dohme Corp., 2015. Januvia (sitagliptin) Tablets [WWW Document]. Highlights Prescr. Inf. URL https://www.accessdata.fda.gov/drugsatfda_docs/label/2019/021995s046lbl.pdf (accessed 4.30.21).

Milner, J.M., Kevorkian, L., Young, D.A., Jones, D., Wait, R., Donell, S.T., Barksby, E., Patterson, A.M., Middleton, J., Cravatt, B.F., Clark, I.M., Rowan, A.D., Cawston, T.E., 2006. Fibroblast activation protein alpha is expressed by chondrocytes following a pro-inflammatory stimulus and is elevated in osteoarthritis. Arthritis Res. Ther. 8, 1–8.

Mirnezami, R., Spagou, K., Vorkas, P.A., Lewis, M.R., Kinross, J., Want, E., Shion, H., Goldin, R.D., Darzi, A., Takats, Z., Holmes, E., Cloarec, O., Nicholson, J.K., 2014. Chemical mapping of the colorectal cancer microenvironment via MALDI imaging mass spectrometry (MALDI-MSI) reveals novel cancer-associated field effects. Mol. Oncol. 8, 39–49.

Misumi, Y., Hayashi, Y., Arakawa, F., Ikehara, Y., 1992. Molecular cloning and sequence analysis of human dipeptidyl peptidase IV , a serine proteinase on the cell surface. Biochim. Biophys. Acta 1131, 333–336.

Miyamoto, T., Rho, E., Sample, V., Akano, H., Magari, M., Ueno, T., Gorshkov, K., Chen, M., Tokumitsu, H., Zhang, J., Inoue, T., 2015. Compartmentalized AMPK Signaling Illuminated by Genetically Encoded Molecular Sensors and Actuators. Cell Rep. 11, 657–670.

Mizoguchi, E., Kanneganti, M., Mino-Kenudson, M., 2011. Animal models of colitis-associated carcinogenesis. J. Biomed. Biotechnol. 2011, 342637.

Mizokami, Y., Kajiyama, H., Shibata, K., Ino, K., Kikkawa, F., Mizutani, S., 2004. Stromal cell-derived factor-1α-induced cell proliferation and its possible regulation by CD26/dipeptidyl peptidase IV in endometrial adenocarcinoma. Int. J. Cancer 110, 652–659.

Moawad Mahmoud, A., Abdella, E., Mahmoud, A.M., El-derby, A.M., M Elsayed, K.N., Abdella, E.M., 2014. Brown Seaweeds Ameliorate Renal Alterations in Mice Treated with the Carcinogen Azoxymethane. Artic. Int. J. Pharm. Pharm. Sci. 6, 365–369.

Monsky, W.L., Lin, C.Y., Aoyama, A., Kelly, T., Akiyama, S.K., Mueller, S.C., Chen, W.T., 1994. A Potential Marker Protease of Invasiveness, Seprase, Is Localized on Invadopodia of Human Malignant Melanoma Cells. Cancer Res. 54, 5702–5710.

Monteran, L., Erez, N., 2019. The dark side of fibroblasts: Cancer-associated fibroblasts as mediators of immunosuppression in the tumor microenvironment. Front. Immunol. 10, 1835.

Montesinos, M.C., Desai, A., Chen, J.F., Yee, H., Schwarzschild, M.A., Fink, J.S., Cronstein, B.N., 2002. Adenosine promotes wound healing and mediates angiogenesis in response to tissue injury via occupancy of A2A receptors. Am. J. Pathol. 160, 2009–2018.

Morais, R., Zinkewich-Péotti, K., Parent, M., Wang, H., Zollinger, M., Babai, F., 1994. Tumor-forming Ability in Athymic Nude Mice of Human Cell Lines Devoid of Mitochondrial DNA. Cancer Res. 54, 3889–3896.

Morimoto, C., Torimoto, Y., Levinson, G., Rudd, C.E., Schrieber, M., Dang, N.H., Letvin, N.L., Schlossman, S.F., 1989. 1F7 , A Novel Cell Surface Molecule, Involved in helper function of CD4 Cells. J. Immunol. 143, 3430–3439.

Morrison, M.E., Vijayasaradhi, S., Engelstein, D., Albino, A.P., Houghton, A.N., 1993. A marker for neoplastic progression of human melanocytes is a cell surface ectopeptidase. J. Exp. Med. 177, 1135–1143.

Morton, D.B., Jennings, M., Buckwell, A., Ewbank, R., Godfrey, C., Holgate, B., Inglis, I., James, R., Page, C., Sharman, I., Verschoyle, R., Westall, L., Wilson, A.B., 2001. Refining procedures for the administration of substances. Lab. Anim. 35, 1–41.

Mujoomdar, M., Bennett, A., Hoskin, D., Blay, J., 2004. Adenosine stimulation of proliferation of breast carcinoma cell lines: Evaluation of the [3H]thymidine assay system and modulatory effects of the cellular microenvironment in vitro. J. Cell. Physiol. 201, 429–438.

Mulsow, F.W., 1953. Cancer incidence and mortality. J. Iowa State Med. Soc. 43, 176–178.

Mulvihill, E.E., Drucker, D.J., 2014. Pharmacology, physiology, and mechanisms of action of dipeptidyl peptidase-4 inhibitors. Endocr. Rev. 35, 992–1019.

Muñoz, M., Gómez-Ramírez, S., Martín-Montañez, E., Auerbach, M., 2014. Perioperative

anemia management in colorectal cancer patients: A pragmatic approach. World J. Gastroenterol. 20, 1972–1985.

Nakhoul, G.N., Huang, H., Arrigain, S., Jolly, S.E., Schold, J.D., Nally, J. V, Navaneethan, S.D., Navaneethan, S.D., 2015. Serum Potassium, End-Stage Renal Disease and Mortality in Chronic Kidney Disease. Am. J. Nephrol. 41, 456–463.

Nardini, M., Dijkstra, B., 1999. α / β Hydrolase fold enzymes : the family keeps growing. Curr. Opin. Struct. Biol. 9, 732–737.

National Research Council, 1995. Nutrient Requirements of the Mouse. In: Nutrient Requirements of Laboratory Animals. National Academies Press (US), pp. 80–102.

Nazarian, A., Lawlor, K., Yi, S.S., Philip, J., Ghosh, M., Yaneva, M., Villanueva, J., Saghatelian, A., Assel, M., Vickers, A.J., Eastham, J.A., Scher, H.I., Carver, B.S., Lilja, H., Tempst, P., 2014. Inhibition of circulating dipeptidyl peptidase 4 activity in patients with metastatic prostate cancer. Mol. Cell. Proteomics 13, 3082–3096.

Nemunaitis, J., Vukelja, S.J., Richards, D., Cunningham, C., Senzer, N., Nugent, J., Duncan, H., Jones, B., Haltom, E., Uprichard, M.J., 2006. Phase I trial of PT-100 (PT-100), a cytokine-inducing small molecule, following chemotherapy for solid tumor malignancy. Cancer Invest. 24, 553–61.

Neufert, C., Becker, C., Neurath, M.F., 2007. An inducible mouse model of colon carcinogenesis for the analysis of sporadic and inflammation-driven tumor progression. Nat. Protoc. 2, 1998–2004.

Newmark, H.L., Yang, K., Kurihara, N., Fan, K., Augenlicht, L.H., Lipkin, M., 2009. Western-style diet-induced colonic tumors and their modulation by calcium and vitamin D in C57Bl/6 mice: A preclinical model for human sporadic colon cancer. Carcinogenesis 30, 88–92.

Niedermeyer, J., Garin-Chesa, P., Kriz, M., Hilberg, F., Mueller, E., Bamberger, U., Rettig, W.J., Schnapp, A., 2001. Expression of the fibroblast activation protein during mouse embryo development. Int. J. Dev. Biol. 45, 445–447.

Niedermeyer, J., Kriz, M., Hilberg, F., Garin-Chesa, P., Bamberger, U., Lenter, M.C., Park, J., Viertel, B., Puschner, H., Mauz, M., Rettig, W.J., Schnapp, A.A., Püschner, H., Mauz, M., Rettig, W.J., Schnapp, A.A., Kriz, † M, Hilberg, F., Garin-Chesa, P., Bamberger, U., Lenter, M.C., Park, J., Viertel, B., Pu¨schner, H., Pu¨schner, P., Mauz,

M., Rettig, W.J., Schnapp, A.A., 2000. Targeted Disruption of Mouse Fibroblast Activation Protein. Mol. Cell. Biol. 20, 1089–1094.

Noma, T., 2005. Dynamics of nucleotide metabolism as a supporter of life phenomena. J. Med. Investig. 52, 127–136.

Novellasdemunt, L., Antas, P., Li, V.S.W., 2015. Targeting Wnt signaling in colorectal cancer. A Review in the Theme: Cell Signaling: Proteins, Pathways and Mechanisms. Am. J. Physiol. - Cell Physiol. 309, 511–521.

O'Brien, P., O'Connor, B.F., 2008. Seprase: An overview of an important matrix serine protease. Biochim. Biophys. Acta - Proteins Proteomics 1784, 1130–1145.

O'callaghan, J.P., 2018. Pierce BCA Protein Assay Protocol V.2 [WWW Document]. PLoS One. URL https://dx.doi.org/10.17504/protocols.io.hswb6fe (accessed 1.11.21).

O'Leary, H., Ou, X., Broxmeyer, H.E., 2013. The role of dipeptidyl peptidase 4 in hematopoiesis and transplantation. Curr. Opin. Hematol. 20, 314–319.

O'Neill, L.A.J., Kishton, R.J., Rathmell, J., 2016. A guide to immunometabolism for immunologists. Nat. Rev. Immunol. 16, 553–565.

Ogata, S., Misumi, Y., Ikehara, Y., 1989. Primary structure of rat liver dipeptidyl peptidase IV deduced from its cDNA and identification of the NH2-terminal signal sequence as the membrane-anchoring domain. J. Biol. Chem. 264, 3596–601.

Ohnuma, K., Dang, N.H., Morimoto, C., 2008. Revisiting an old acquaintance: CD26 and its molecular mechanisms in T cell function. Trends Immunol. 29, 295–301.

Ohnuma, K., Ishii, T., Iwata, S., Hosono, O., Kawasaki, H., Uchiyama, M., Tanaka, H., Yamochi, T., Dang, N.H., Morimoto, C., 2002. G1/S cell cycle arrest provoked in human T cells by antibody to CD26. Immunology 107, 325–333.

Ohnuma, K., Morimoto, C., 2013. DPP4 (dipeptidyl-peptidase 4). Atlas Genet. Cytogenet. Oncol. Haematol. 17, 301–312.

Okamoto, T., Iwata, S., Yamazaki, H., Hatano, R., Komiya, E., Dang, N.H., Ohnuma, K., Morimoto, C., 2014. CD9 negatively regulates CD26 expression and inhibits CD26-mediated enhancement of invasive potential of malignant mesothelioma cells. PLoS One 9, e86671.

Olivo-Marston, S.E., Hursting, S.D., Lavigne, J., Perkins, S.N., Maarouf, R.S., Yakar, S., Harris, C.C., 2009. Genetic reduction of circulating insulin-like growth factor-1 inhibits azoxymethane-induced colon tumorigenesis in mice. Mol. Carcinog. 48, 1071–1076.

Olivo-Marston, S.E., Hursting, S.D., Perkins, S.N., Schetter, A., Khan, M., Croce, C., Harris, C.C., Lavigne, J., 2014. Effects of Calorie Restriction and Diet-Induced Obesity on Murine Colon Carcinogenesis, Growth and Inflammatory Factors, and MicroRNA Expression. PLoS One 9, e94765.

Orlando, F.A., Tan, D., Baltodano, J.D., Khoury, T., Gibbs, J.F., Hassid, V.J., Ahmed, B.H., Alrawi, S.J., 2008. Aberrant crypt foci as precursors in colorectal cancer progression. J. Surg. Oncol. 98, 207–213.

Ospelt, C., Mertens, J.C., Jüngel, A., Brentano, F., Maciejewska-Rodriguez, H., Huber, L.C., Hemmatazad, H., Wüest, T., Knuth, A., Gay, R.E., Michel, B.A., Gay, S., Renner, C., Bauer, S., 2010. Inhibition of fibroblast activation protein and dipeptidylpeptidase 4 increases cartilage invasion by rheumatoid arthritis synovial fibroblasts. Arthritis Rheum. 62, 1224–1235.

Owen, M.R., Doran, E., Halestrap, A.P., 2000. Evidence that metformin exerts its anti-diabetic effects through inhibition of complex 1 of the mitochondrial respiratory chain. Biochem. J. 348, 607–614.

Paigen, B., Svenson, K.L., Von Smith, R., Marion, M.A., Stearns, T., Peters, L.L., Smith, A.L., 2012. Physiological effects of housing density on C57BL/6J mice over a 9-month period. J. Anim. Sci. 90, 5182–92.

Palmqvist, R., Hallmans, G., Rinaldi, S., Biessy, C., Stenling, R., Riboli, E., Kaaks, R., 2002. Plasma insulin-like growth factor 1, insulin-like growth factor binding protein 3, and risk of colorectal cancer: A prospective study in northern Sweden. Gut 50, 642–646.

Pang, R., Law, W.L., Chu, A.C.Y., Poon, J.T., Lam, C.S.C., Chow, A.K.M., Ng, L., Cheung, L.W.H., Lan, X.R., Lan, H.Y., Tan, V.P.Y., Yau, T.C., Poon, R.T., Wong, B.C.Y., 2010. A subpopulation of CD26 + cancer stem cells with metastatic capacity in human colorectal cancer. Cell Stem Cell 6, 603–615.

Pelletier, M., Billingham, L.K., Ramaswamy, M., Siegel, R.M., 2014. Extracellular flux analysis to monitor glycolytic rates and mitochondrial oxygen consumption. In: Methods in Enzymology. Elsevier Inc., pp. 125–149.

Perla, F., Prelati, M., Lavorato, M., Visicchio, D., Anania, C., 2017. The Role of Lipid and Lipoprotein Metabolism in Non-Alcoholic Fatty Liver Disease. Children 4, 46.

Persaud, S.J., Bewick, G.A., 2014. Peptide YY: More than just an appetite regulator. Diabetologia 57, 1762–1769.

Pethiyagoda, C.L., Welch, D.R., Fleming, T.P., 2000. Dipeptidyl peptidase IV (DPPIV) inhibits cellular invasion of melanoma cells. Clin. Exp. Metastasis 18, 391–400.

Pfortmueller, C.A., Uehlinger, D., von Haehling, S., Schefold, J.C., 2018. Serum chloride levels in critical illness-the hidden story. Intensive care Med. Exp. 6, 10.

Piazza, G. a, Callanan, H.M., Mowery, J., Hixson, D.C., 1989. Evidence for a role of dipeptidyl peptidase IV in fibronectin-mediated interactions of hepatocytes with extracellular matrix. Biochem. J. 262, 327–34.

Pitman, M.R., 2009. Dipeptidyl peptidase 8 and 9 - guilty by association? Front. Biosci. 1, 3619–3633.

Plitzko, B., Loesgen, S., 2018. Measurement of Oxygen Consumption Rate (OCR) and Extracellular Acidification Rate (ECAR) in Culture Cells for Assessment of the Energy Metabolism. BIO-PROTOCOL 8.

Pro, B., Dang, N.H., 2004. CD26/dipeptidyl peptidase IV and its role in cancer. Histol. Histopathol. 19, 1345–51.

Puré, E., Blomberg, R., 2018. Pro-tumorigenic roles of fibroblast activation protein in cancer: back to the basics. Oncogene 37, 4343–4357.

Qin, S., Rottman, J.B., Myers, P., Kassam, N., Weinblatt, M., Loetscher, M., Koch, A.E., Moser, B., Mackay, C.R., 1998. The chemokine receptors CXCR3 and CCR5 mark subsets of T cells associated with certain inflammatory reactions. J. Clin. Invest. 101, 746–754.

Quail, D.F., Joyce, J.A., 2013. Microenvironmental regulation of tumor progression and metastasis. Nat. Med. 2013 1911 19, 1423–1437.

Quinn, B.J., Kitagawa, H., Memmott, R.M., Gills, J.J., Dennis, P.A., 2013. Repositioning metformin for cancer prevention and treatment. Trends Endocrinol. Metab. 24, 469–480.

Ramirez-Montagut, T., Blachere, N.E., Sviderskaya, E. V., Bennett, D.C., Rettig, W.J., Garin-Chesa, P., Houghton, A.N., 2004. FAPα, a surface peptidase expressed during wound healing, is a tumor suppressor. Oncogene 23, 5435–5446.

Rathmell, J.C., Elstrom, R.L., Cinalli, R.M., Thompson, C.B., 2003. Activated Akt promotes increased resting T cell size, CD28-independent T cell growth, and development of autoimmunity and lymphoma. Eur. J. Immunol. 33, 2223–2232.

Rausch, P., Basic, M., Batra, A., Bischoff, S.C., Blaut, M., Clavel, T., Gläsner, J., Gopalakrishnan, S., Grassl, G.A., Günther, C., Haller, D., Hirose, M., Ibrahim, S., Loh, G., Mattner, J., Nagel, S., Pabst, O., Schmidt, F., Siegmund, B., Strowig, T., Volynets, V., Wirtz, S., Zeissig, S., Zeissig, Y., Bleich, A., Baines, J.F., 2016. Analysis of factors contributing to variation in the C57BL/6J fecal microbiota across German animal facilities. Int. J. Med. Microbiol. 306, 343–355.

Rawla, P., Sunkara, T., Barsouk, A., 2019. Epidemiology of colorectal cancer: Incidence, mortality, survival, and risk factors. Prz. Gastroenterol. 14, 89–103.

Reinhold, D., Bank, U., Buhling, F., Lendeckel, U., Faust, J., Neubertt, K., 1997. Inhibitors of dipeptidyl peptidase iv induce secretion of transforming growth factor-β1 in PWM-stimulated PBMC and T cells. Immunology 91, 354–360.

Reinhold, D., Bank, U., Entz, D., Goihl, A., Stoye, D., Wrenger, S., Brocke, S., Thielitz, A., Stefin, S., Nordhoff, K., Heimburg, A., Ta¨ger, M., Ansorge, S., 2011. PETIR-001, a dual inhibitor of dipeptidyl peptidase IV (DP IV) and aminopeptidase N (APN), ameliorates experimental autoimmune encephalomyelitis in SJL/J mice. Biol. Chem. 392, 233–237.

Reinhold, D., Kähne, T., Steinbrecher, A., Gerber, A., Preller, V., Gornickel, B., Wrenger, S., Ansorge, S., Brocke, S., 2005. The role of dipeptidyl peptidase IV (DP IV , CD26) in T cell activation and multiple sclerosis. Signal Transduct. 5, 258–265.

Reinhold, D., Vetter, R.W., Mnich, K., Bühling, F., Lendeckel, U., Born, I., Faust, J., Neubert, K., Gollnick, H., Ansorge, S., 1998. Dipeptidyl peptidase IV (DP IV, CD26) is involved in regulation of DNA synthesis in human keratinocytes. FEBS Lett. 428, 100–4.

Rena, G., Hardie, D.G., Pearson, E.R., 2017. The mechanisms of action of metformin. Diabetologia 60, 1577–1585.

Rettig, W.J., Garin-Chesa, P., Beresford, H.R., Oettgen, H.F., Melamed, M.R., Old, L.J.,

1988. Cell-surface glycoproteins of human sarcomas: differential expression in normal and malignant tissues and cultured cells. Proc. Natl. Acad. Sci. U. S. A. 85, 3110–3114.

Rettig, W.J., Garin-chesa, P., Healey, J.H., Albino, A.P., Old, L.J., 1993. Regulation and Heteromeric Structure of the Fibroblast Activation Protein in Normal and Transformed Cells of Mesenchymal and Neuroectodermal Origin Regulation and Heteromeric Structure of the Fibroblast Activation Protein in Normal and Transformed Cells o 3327–3335.

Riss, T.L., Moravec, R.A., Niles, A.L., Duellman, S., Benink, H.A., Worzella, T.J., Minor, L., 2004. Cell Viability Assays. In: Assay Guidance Manual. Eli Lilly & Company and the National Center for Advancing Translational Sciences.

Robert, F., Fendri, S., Hary, L., Lacroix, C., Andréjak, M., Lalau, J.D., 2003. Kinetics of plasma and erythrocyte metformin after acute administration in healthy subjects. Diabetes Metab. 29, 279–283.

Roberts, E.W., Deonarine, A., Jones, J.O., Denton, A.E., Feig, C., Lyons, S.K., Espeli, M., Kraman, M., McKenna, B., Wells, R.J.B., Zhao, Q., Caballero, O.L., Larder, R., Coll, A.P., O'Rahilly, S., Brindle, K.M., Teichmann, S.A., Tuveson, D.A., Fearon, D.T., 2013. Depletion of stromal cells expressing fibroblast activation protein-α from skeletal muscle and bone marrow results in cachexia and anemia. J. Exp. Med. 210, 1137–1151.

Roger Yazbeck, Sulda, M., Howarth, G., J Holst, H.D., Abbott, C., 2008. Resolving how inhibition of dipeptidyl peptidase activity can ameliorate DSS induced colitis in mice. J. Gastroenterol. Hepatol. 23, A210.

Rolf, J., Zarrouk, M., Finlay, D.K., Foretz, M., Viollet, B., Cantrell, D.A., 2013. AMPKα1: A glucose sensor that controls CD8 T-cell memory. Eur. J. Immunol. 43, 889–896.

Roncucci, L., Pedroni, M., Vaccina, F., Benatti, P., Marzona, L., De Pol, A., 2000. Aberrant crypt foci in colorectal carcinogenesis. Cell and crypt dynamics. Cell Prolif.

Rosenberg, D.W., Giardina, C., Tanaka, T., 2009. Mouse models for the study of colon carcinogenesis. Carcinogenesis 30, 183–196.

Rosenblum, J.S., Kozarich, J.W., 2003. Prolyl peptidases: a serine protease subfamily with high potential for drug discovery. Curr. Opin. Chem. Biol. 7, 496–504.

Rowland, K.J., Brubaker, P.L., 2011. The "cryptic" mechanism of action of glucagon-like

peptide-2. Am. J. Physiol. - Gastrointest. Liver Physiol. 301, G1–G8.

Rudd, D.A., Benkendorff, K., Chahal, C., Guinan, T., Gustafsson, O.J.R., Esmaeelian, B., Krysinska, H., Pogson, L., Voelcker, N.H., Abbott, C.A., 2019. Mapping insoluble indole metabolites in the gastrointestinal environment of a murine colorectal cancer model using desorption/ionisation on porous silicon imaging. Sci. Rep. 9, 12342.

Russell, H. V, Hicks, J., Okcu, M.F., Nuchtern, J.G., 2004. CXCR4 expression in neuroblastoma primary tumors is associated with clinical presentation of bone and bone marrow metastases. J. Pediatr. Surg. 39, 1506–1511.

Ryabtsova, O., Jansen, K., Van Goethem, S., Joossens, J., Cheng, J.D., Lambeir, A.M., De Meester, I., Augustyns, K., Van Der Veken, P., 2012. Acylated Gly-(2-cyano)pyrrolidines as inhibitors of fibroblast activation protein (FAP) and the issue of FAP/prolyl oligopeptidase (PREP)-selectivity. Bioorganic Med. Chem. Lett. 22, 3412–3417.

S, K., I, D.M., TH, S., A, C., M, S., MH, S., A, B., A, H., S, S., JW, K.-W., 1997. Inhibition of CD26/dipeptidyl peptidase IV activity in vivo prolongs cardiac allograft survival in rat recipients. Transplantation 63, 1495–1500.

Saigusa, S., Toiyama, Y., Tanaka, K., Yokoe, T., Okugawa, Y., Fujikawa, H., Matsusita, K., Kawamura, M., Inoue, Y., Miki, C., Kusunoki, M., 2011. Cancer-associated fibroblasts correlate with poor prognosis in rectal cancer after chemoradiotherapy. Int. J. Oncol. 38, 655–663.

Saito, Y., Chapple, R.H., Lin, A., Kitano, A., Nakada, D., 2015. AMPK Protects Leukemia-Initiating Cells in Myeloid Leukemias from Metabolic Stress in the Bone Marrow. Cell Stem Cell 17, 585–596.

Sallusto, F., Lenig, D., Mackay, C.R., Lanzavecchia, A., 1998. Flexible programs of chemokine receptor expression on human polarized T helper 1 and 2 lymphocytes. J. Exp. Med. 187, 875–83.

Sánchez-Garrido, M.A., Habegger, K.M., Clemmensen, C., Holleman, C., Müller, T.D., Perez-Tilve, D., Li, P., Agrawal, A.S., Finan, B., Drucker, D.J., Tschöp, M.H., DiMarchi, R.D., Kharitonenkov, A., 2016. Fibroblast activation protein (FAP) as a novel metabolic target. Mol. Metab. 5, 1015–1024.

Sanli, T., Steinberg, G.R., Singh, G., Tsakiridis, T., 2014. AMP-activated protein kinase

(AMPK) beyond metabolism: A novel genomic stress sensor participating in the DNA damage response pathway. Cancer Biol. Ther. 15, 156–169.

Sarkar, M., Dey, S., Giri, B., 2017. Antiproliferative and apoptogenic efficacy of antidiabetic drugs metformin and sitagliptin against mcf7 and hepg2 cancer cells: a comparative molecular study. J. Drug Deliv. Ther. 7, 11–21.

Sato, K., Aytac, U., Yamochi, T., Yamochi, T., Ohnuma, K., McKee, K.S., Morimoto, C., Dang, N.H., 2003. CD26/dipeptidyl peptidase IV enhances expression of topoisomerase II alpha and sensitivity to apoptosis induced by topoisomerase II inhibitors. Br. J. Cancer 89, 1366–1374.

Sato, T., Yamochi, Tadanori, Yamochi, Toshiko, Aytac, U., Ohnuma, K., McKee, K.S., Morimoto, C., Dang, N.H., 2005. CD26 regulates p38 mitogen-activated protein kinase-dependent phosphorylation of integrin β1, adhesion to extracellular matrix, and tumorigenicity of T-anaplastic large cell lymphoma Karpas 299. Cancer Res. 65, 6950–6956.

Sato, Y., Fujiwara, H., Higuchi, T., Shinya, Y., Keiji, T., Maeda, M., Fujii, S., 2002. Involvement of Dipeptidyl Peptidase IV in Extravillous Trophoblast Invasion and Differentiation. J. Clin. Endocrinol. Metab. 87, 4287–4296.

Schmelzle, T., Hall, M.N., 2000. TOR, a central controller of cell growth. Cell 103, 253–62.

Schnell, M.A., Hardy, C., Hawley, M., Propert, K.J., Wilson, J.M., 2002. Effect of Blood Collection Technique in Mice on Clinical Pathology Parameters. Hum. Gene Ther. 13, 155–161.

Schoene, N.W., Kamara, K.S., 1999. Population doubling time, phosphatase activity, and hydrogen peroxide generation in Jurkat cells. Free Radic. Biol. Med. 27, 364–369.

Scholz, W., Mentlein, R., Heymann, E., Feller, A.C., Ulmer, A.J., Flad, H., 1985. Interleukin 2 Production Antibodies by Human T Lymphocytes identified by to Dipeptidyl Peptidase IV. Cell. Immunol. 93, 199–211.

Schon, E., Demuth, H.U., Bar-tht, A., Ansorge, S., Magdeburg, M.A., Klinik, M., Immunologie, A.E., 1984. Dipeptidyl peptidase IV of human lymphocytes 223, 255–258.

Schricker, R., Angermayr, M., Strobel, G., Klinke, S., Korber, D., Bandlow, W., 2002. Redundant mitochondrial targeting signals in yeast adenylate kinase. J. Biol. Chem.

277, 28757–28764.

Schuiveling, M., Vazirpanah, N., Radstake, T.R.D.J., Zimmermann, M., Broen, J.C.A., 2018. Metformin, A New Era for an Old Drug in the Treatment of Immune Mediated Disease? Curr. Drug Targets 19, 945–959.

Scotton, C.J., Wilson, J.L., Scott, K., Stamp, G., Wilbanks, G.D., Fricker, S., Bridger, G., Balkwill, F.R., 2002. Multiple actions of the chemokine CXCL12 on epithelial tumor cells in human ovarian cancer. Cancer Res. 62, 5930–5938.

Servais, C., Erez, N., 2013. From sentinel cells to inflammatory culprits: cancer-associated fibroblasts in tumour-related inflammation. J. Pathol. 229, 198–207.

Shafaee, A., Dastyar, D.Z., Islamian, J.P., Hatamian, M., 2015. Inhibition of tumor energy pathways for targeted esophagus cancer therapy. Metabolism. 64, 1193–1198.

Shao, S., Xu, Q., Yu, X., Pan, R., Chen, Y., 2020. Dipeptidyl peptidase 4 inhibitors and their potential immune modulatory functions. Pharmacol. Ther. 209, 107503.

Shih, L.-M., Hsu, M.-Y., Kurmanab, R.J., Old, R.J., Meenhard, H., Gearhart, J.D., Kurmanab, R.J., 2002. The Role of E-cadherin in the Motility and Invasion of Implantation Site Intermediate Trophoblast. Placenta 23, 706–715.

Short, J.D., Dere, R., Houston, K.D., Cai, S.L., Kim, J., Bergeron, J.M., Shen, J., Liang, J., Bedford, M.T., Mills, G.B., Walker, C.L., 2010. AMPK-mediated phosphorylation of murine p27 at T197 promotes binding of 14-3-3 proteins and increases p27 stability. Mol. Carcinog. 49, 429–439.

Silberg, D.G., Swain, G.P., Suh, E.R., Traber, P.G., Eun Ran Suh, Traber, P.G., 2000. Cdx1 and Cdx2 expression during intestinal development. Gastroenterology 119, 961–971.

Silva, M., Gomes, S., Peixoto, A., Torres-Ramalho, P., Cardoso, H., Azevedo, R., Cunha, C., Macedo, G., 2015. Nutrition in Chronic Liver Disease. GE Port. J. Gastroenterol. 22, 268–276.

Singh, O., Raleng, I., Surbala, L., Debashree, N., 2017. A promising anti-neoplastic drug - Metformin (an AMPK activator) for the future. Int. J. Pharm. Sci. Res. 8, 435–439.

Sinnathurai, P., Lau, W., Vieira de Ribeiro, A.J., Bachovchin, W.W., Englert, H., Howe, G., Spencer, D., Manolios, N., Gorrell, M.D., 2018. Circulating fibroblast activation protein and dipeptidyl peptidase 4 in rheumatoid arthritis and systemic sclerosis. Int. J. Rheum.

Dis. 21, 1915–1923.

Six, E., Lagresle-Peyrou, C., Susini, S., De Chappedelaine, C., Sigrist, N., Sadek, H., Chouteau, M., Cagnard, N., Fontenay, M., Hermine, O., Chomienne, C., Reynier, P., Fischer, A., André-Schmutz, I., Ueguen, N., Cavazzana, M., 2015. AK2 deficiency compromises the mitochondrial energy metabolism required for differentiation of human neutrophil and lymphoid lineages. Cell Death Dis. 6, 1856.

Smokelin, I.S., Mizzoni, C., Erndt-Marino, J., Kaplan, D., Georgakoudi, I., 2020. Optical changes in THP-1 macrophage metabolism in response to pro- and anti-inflammatory stimuli reported by label-free two-photon imaging. J. Biomed. Opt. 25, 014512.

Snyder, V., Reed-Newman, T.C., Arnold, L., Thomas, S.M., Anant, S., 2018. Cancer stem cell metabolism and potential therapeutic targets. Front. Oncol. 8, 1–9.

Sparks, A.B., Morin, P.J., Vogelstein, B., Kinzler, K.W., 1998. Mutational Analysis of the APC / Beta-Catenin / Tcf Pathway in Colorectal Cancer. Am. Assoc. Cancer Res. 58, 1130–1135.

Starr, T., Bauler, T.J., Malik-Kale, P., Steele-Mortimer, O., 2018. The phorbol 12-myristate-13-acetate differentiation protocol is critical to the interaction of THP-1 macrophages with Salmonella Typhimurium. PLoS One 13, e0193601.

Stock, U., Matter, H., Diekert, K., Dörner, W., Dröse, S., Licher, T., 2013. Measuring interference of drug-like molecules with the respiratory chain: Toward the early identification of mitochondrial uncouplers in lead finding. Assay Drug Dev. Technol. 11, 408–422.

Stremenova, J., Krepela, E., Mares, V., Trim, J., Dbaly, V., Marek, J., Vanickova, Z., Lisa, V., Yea, C., Sedo, A., 2007. Expression and enzymatic activity of dipeptidyl peptidase-IV in human astrocytic tumours are associated with tumour grade. Int. J. Oncol. 31, 785–792.

Strobel, G., Zollner, A., Angermayr, M., Bandlow, W., 2002. Competition of spontaneous protein folding and mitochondrial import causes dual subcellular location of major adenylate kinase. Mol. Biol. Cell 13, 1439–1448.

Stulc, T., Sedo, A., 2010. Inhibition of multifunctional dipeptidyl peptidase-IV: Is there a risk of oncological and immunological adverse effects? Diabetes Res. Clin. Pract. 88, 125–131.

Sulda, M.L., 2009. Investigation of biological targets for prognostication and therapy in B-cell chronic lymphocytic leukaemia. Flinders University.

Sulda, M.L., Abbott, C.A., Hildebrandt, M., 2006. DPIV/CD26 and FAP in cancer: a tale of contradictions. In: Advances in Experimental Medicine and Biology. pp. 197–206.

Sun, Y.-X., Schneider, A., Jung, Y., Wang, Jianhua, Dai, J., Wang, Jingcheng, Cook, K., Osman, N.I., Koh-Paige, A.J., Shim, H., Pienta, K.J., Keller, E.T., McCauley, L.K., Taichman, R.S., 2005. Skeletal localization and neutralization of the SDF-1(CXCL12)/CXCR4 axis blocks prostate cancer metastasis and growth in osseous sites in vivo. J. Bone Miner. Res. 20, 318–29.

Sun, Y.X., Pedersen, E.A., Shiozawa, Y., Havens, A.M., Jung, Y., Wang, J., Pienta, K.J., Taichman, R.S., 2008. CD26/dipeptidyl peptidase IV regulates prostate cancer metastasis by degrading SDF-1/CXCL12. Clin. Exp. Metastasis 25, 765–776.

Sun, Y.X., Wang, J., Shelburne, C.E., Lopatin, D.E., Chinnaiyan, A.M., Rubin, M.A., Pienta, K.J., Taichman, R.S., 2003. Expression of CXCR4 and CXCL12 (SDF-1) in human prostate cancers (PCa) in vivo. J. Cell. Biochem. 89, 462–473.

Svatoš, A., 2010. Mass spectrometric imaging of small molecules. Trends Biotechnol. 28, 425–434.

Szczesny, G., Veihelmann, A., Massberg, S., Nolte, D., Messmer, K., 2004. Long-term anaesthesia using inhalatory iso urane in different strains of mice — the haemodynamic effects. Lab. Anim. 38, 64–69.

Taichman, R.S., Cooper, C., Keller, E.T., Pienta, K.J., Taichman, N.S., McCauley, L.K., 2002. Use of the stromal cell-derived factor-1/CXCR4 pathway in prostate cancer metastasis to bone. Cancer Res. 62, 1832–1837.

Takahashi, M., Wakabayashi, K., 2004. Gene mutations and altered gene expression in azoxymethane-induced colon carcinogenesis in. Cancer Sci. 95, 475–480.

Takeichi, M., 1993. Cadherins in cancer: implications for invasion and metastasis. Curr. Opin. Cell Biol. 5, 806–811.

Tan, B., Xiao, H., Li, F., Zeng, L., Yin, Y., 2015. The profiles of mitochondrial respiration and glycolysis using extracellular flux analysis in porcine enterocyte IPEC-J2. Anim. Nutr. 1, 239–243.

Tan, C.W., Lee, Y.H., Tan, H.H., Lau, M.S.K., Choolani, M., Griffith, L., Chan, J.K.Y., 2014. CD26/DPPIV down-regulation in endometrial stromal cell migration in endometriosis. Fertil. Steril. 102, 167–177.

Tan, E.Y., Mujoomdar, M., Blay, J., 2004. Adenosine down-regulates the surface expression of dipeptidyl peptidase IV on HT-29 human colorectal carcinoma cells: implications for cancer cell behavior. Am. J. Pathol. 165, 319–30.

Tanaka, T., 1993. Cloning and functional expression of the T cell activation antigen CD26. J. Immunol. 149, 481–486.

Teichgräber, V., Monasterio, C., Chaitanya, K., Boger, R., Gordon, K., Dieterle, T., Jäger, D., Bauer, S., 2015. Specific inhibition of fibroblast activation protein (FAP)-alpha prevents tumor progression in vitro. Adv. Med. Sci. 60, 264–272.

Terzić, J., Grivennikov, S., Karin, E., Karin, M., 2010. Inflammation and Colon Cancer. Gastroenterology 138, 2101–2114.

Teslaa, T., Teitell, M.A., 2014. Techniques to monitor glycolysis. In: Methods in Enzymology. Academic Press, pp. 91–114.

The Jackson Laboratory, 2007. Physiological Data Summary - C57BL/6J (000664) [WWW Document]. JAX Mice Database. URL http://cheval.pratique.free.fr/STAGE ENVL/m%E9moire/C57BL6J/B6data000664%5B1%5D.pdf

The Jackson Laboratory, 2019. Body weight information for C57BL/6J (000664) [WWW Document]. JAX Mice Serv. URL https://www.jax.org/jax-mice-and-services/strain-data-sheet-pages/body-weight-chart-000664#

The Jackson Laboratory, 2021. C57BL/6 Mice [WWW Document]. URL https://www.jax.org/strain/000664

Thongprayoon, C., Cheungpasitporn, W., Kashani, K., 2016. Serum creatinine level, a surrogate of muscle mass, predicts mortality in critically ill patients. J. Thorac. Dis. 8, E305-311.

Thornberry, N., Weber, A., 2007. Discovery of JANUVIA™ (Sitagliptin), a Selective Dipeptidyl Peptidase IV Inhibitor for the Treatment of Type2 Diabetes. Curr. Top. Med. Chem. 7, 557–568.

Thulesen, J., Hartmann, B., Hare, K.J., Kissow, H., Ørskov, C., Holst, J.J., Poulsen, S.S.,

2004. Glucagon-like peptide 2 (GLP-2) accelerates the growth of colonic neoplasms in mice. Gut 53, 1145–1150.

Tilan, J.U., Lu, C., Galli, S., Izycka-Swieszewska, E., Earnest, J.P., Shabbir, A., Everhart, L.M., Wang, S., Martin, S., Horton, M., Mahajan, A., Christian, D., O'Neill, A., Wang, H., Zhuang, T., Czarnecka, M., Johnson, M.D., Toretsky, J.A., Kitlinska, J., 2013. Hypoxia shifts activity of neuropeptide Y in Ewing sarcoma from growth-inhibitory to growth-promoting effects. Oncotarget 4, 2487–2501.

Torimoto, Y., Dang, N.H., Vivier, E., Tanaka, T., Schlossman, S.F., Morimoto, C., 1991. Coassociation of CD26 (dipeptidyl peptidase IV) with CD45 on the surface of human T lymphocytes. J. Immunol. 147, 2514–2517.

Toyama, E.Q., Herzig, S., Courchet, J., Lewis, T.L., Losón, O.C., Hellberg, K., Young, N.P., Chen, H., Polleux, F., Chan, D.C., Shaw, R.J., 2016. Metabolism: AMP-activated protein kinase mediates mitochondrial fission in response to energy stress. Science (80-.). 351, 275–281.

Trivedi, S., Wiber, S.C., El-Zimaity, H.M., Brubaker, P.L., 2012. Glucagon-like peptide-2 increases dysplasia in rodent models of colon cancer. AJP Gastrointest. Liver Physiol. 302, G840–G849.

Tsuchiya, S., Minegishi, N., Minegishi, M., Sato, T., Konno, T., 1986. Adaptation of a Human Monocytic Leukemia Cell Line (THP-1) in a Protein-Free Chemically Defined Medium. Tohoku J. Exp. Med. 150, 455–465.

Tsuchiya, S., Yamabe, M., Yamaguchi, Y., Kobayashi, Y., Konno, T., Tada, K., 1980. Establishment and characterization of a human acute monocytic leukemia cell line (THP-1). Int. J. Cancer 26, 171–176.

Tsujimoto, H., Nishizuka, S., Redpath, J.L., Stanbridge, E.J., 1999. Differential gene expression in tumorigenic and nontumorigenic HeLa � normal human fibroblast hybrid cells. Mol. Carcinog. 26, 298–304.

Tudzarova, S., Osman, M.A., 2015. The double trouble of metabolic diseases: The diabetes-cancer link. Mol. Biol. Cell 26, 3129–3139.

U, M.-L., C, O., S, G., O, D., T, P., 2007. Cells of the synovium in rheumatoid arthritis. Synovial fibroblasts. Arthritis Res. Ther. 9.

Ukpo, G.E., Ebuehi, O.A.T., Kareem, A.A., 2012. Evaluation of moxifloxacin-induced biochemical changes in mice. Indian J. Pharm. Sci. 74, 454–457.

US Food and Drug Administration, 2016. FDA approves new treatment for inhalation anthrax [WWW Document]. FDA news release. URL http://www.fda.gov/NewsEvents/Newsroom/PressAnnouncements/ucm491470.htm

van der Windt, G.J.W., Chang, C.H., Pearce, E.L., 2016. Measuring bioenergetics in T cells using a seahorse extracellular flux analyzer. Curr. Protoc. Immunol. 113, 3.16B.1-3.16B.14.

van der Windt, G.J.W., Pearce, E.L., 2012. Metabolic switching and fuel choice during T-cell differentiation and memory development. Immunol. Rev. 249, 27–42.

Vander Heiden, M.G., Cantley, L.C., Thompson, C.B., 2009. Understanding the Warburg Effect: The Metabolic Requirements of Cell Proliferation. Science (80-.). 324, 1029–1033.

Vangoitsenhoven, R., Mathieu, C., Van Der Schueren, B., 2012. GLP1 and cancer: Friend or foe? Endocr. Relat. Cancer 19, F77-88.

Vanhoof, G., De Meester, I., Hendriks, D., Goossens, F., Van Sande, M., Scharpe, S., Yaron, A., 1992. Proline-specific aminopeptidases: Potential role in bradykinin degradation. Agents Actions 38, 120–127.

Vanhoof, G., Goossens, F., De Meester, I., Hendriks, D., Scharpé, S., 1995. Proline motifs in peptides and their biological processing. FASEB J. 9, 736–44.

Vara-Ciruelos, D., Dandapani, M., Gray, A., Egbani, E.O., Mark Evans, A., Grahame Hardie, D., 2018. Genotoxic Damage Activates the AMPK-a1 Isoform in the Nucleus via Ca2þ/CaMKK2 Signaling to Enhance Tumor Cell Survival. Mol. Cancer Res. 16, 345–357.

Vara-Ciruelos, D., Dandapani, M., Russell, F.M., Grzes, K.M., Atrih, A., Foretz, M., Viollet, B., Lamont, D.J., Cantrell, D.A., Hardie, D.G., 2019a. Phenformin, But Not Metformin, Delays Development of T Cell Acute Lymphoblastic Leukemia/Lymphoma via Cell-Autonomous AMPK Activation. Cell Rep. 27, 690–698.

Vara-Ciruelos, D., Russell, F.M., Grahame Hardie, D., 2019b. The strange case of AMPK and cancer: Dr Jekyll or Mr Hyde? Open Biol. 9, 190099.

Varona, A., Blanco, L., Perez, I., Gil, J., Irazusta, J., López, J.I., Candenas, M.L., Pinto, F.M., Larrinaga, G., 2010. Expression and activity profiles of DPP IV/CD26 and NEP/CD10 glycoproteins in the human renal cancer are tumor-type dependent. BMC Cancer 10, 1–11.

Vazirinejad, R., Ahmadi, Z., Kazemi Arababadi, M., Hassanshahi, G., Kennedy, D., 2014. The Biological Functions, Structure and Sources of CXCL10 and Its Outstanding Part in the Pathophysiology of Multiple Sclerosis. Neuroimmunomodulation 21, 322–330.

Vigneri, P., Frasca, F., Sciacca, L., Pandini, G., Vigneri, R., 2009. Diabetes and cancer. Endocr. Relat. Cancer 16, 1103–1123.

Vijayan, V., Pradhan, P., Braud, L., Fuchs, H.R., Gueler, F., Motterlini, R., Foresti, R., Immenschuh, S., 2019. Human and murine macrophages exhibit differential metabolic responses to lipopolysaccharide - A divergent role for glycolysis. Redox Biol. 22, 101147.

Vita, M., Henriksson, M., 2006. The Myc oncoprotein as a therapeutic target for human cancer. Semin. Cancer Biol.

Wagner, L., Klemann, C., Stephan, M., von Hörsten, S., 2016. Unravelling the immunological roles of dipeptidyl peptidase 4 (DPP4) activity and/or structure homologue (DASH) proteins. Clin. Exp. Immunol. 184, 265–283.

Waldele, S., Koers-Wunrau, C., Beckmann, D., Korb-Pap, A., Wehmeyer, C., Pap, T., Dankbar, B., 2015. Deficiency of fibroblast activation protein alpha ameliorates cartilage destruction in inflammatory destructive arthritis. Arthritis Res. Ther. 17, 1–7.

Wang, Jianhua, Shiozawa, Y., Wang, Jincheng, Wang, Y., Jung, Y., Pienta, K.J., Mehra, R., Loberg, R., Taichman, R.S., 2008. The role of CXCR7/RDC1 as a chemokine receptor for CXCL12/SDF-1 in prostate cancer. J. Biol. Chem. 283, 4283–4294.

Wang, W., Yang, X., De Silanes, I.L., Carling, D., Gorospe, M., 2003. Increased AMP:ATP ratio and AMP-activated protein kinase activity during cellular senescence linked to reduced HuR function. J. Biol. Chem. 278, 27016–27023.

Warburg, O., 1956. On the Origin of Cancel Cells. Science (80-.). 123, 309–314.

Ward, J.M., 1975. Dose Response to a Single Injection of Azoxymethane in Rats: Induction of Tumors in the Gastrointestinal Tract, Auditory Sebaceous Glands, Kidney, Liver and

Preputial Gland. Vet. Pathol. 12, 165–177.

Wargovich, M.J., Brown, V.R., Morris, J., 2010. Aberrant crypt foci: The case for inclusion as a biomarker for colon cancer. Cancers (Basel). 2, 1705–1716.

Watanabe, K., Kubo, S., 1982. Mitochondrial Adenylate Kinase from Chicken Liver: Purification, characterization and Its Cell-Free Synthesis. Eur. J. Biochem. 123, 587–592.

Waterston, R.H., Lindblad-Toh, K., Birney, E., Rogers, J., Abril, J.F., Agarwal, P., Agarwala, R., Ainscough, R., Alexandersson, M., An, P., Antonarakis, S.E., Attwood, J., Baertsch, R., Bailey, J., Barlow, K., Beck, S., Berry, E., Birren, B., Bloom, T., Bork, P., Botcherby, M., Bray, N., Brent, M.R., Brown, D.G., Brown, S.D., Bult, C., Burton, J., Butler, J., Campbell, R.D., Carninci, P., Cawley, S., Chiaromonte, F., Chinwalla, A.T., Church, D.M., Clamp, M., Clee, C., Collins, F.S., Cook, L.L., Copley, R.R., Coulson, A., Couronne, O., Cuff, J., Curwen, V., Cutts, T., Daly, M., David, R., Davies, J., Delehaunty, K.D., Deri, J., Dermitzakis, E.T., Dewey, C., Dickens, N.J., Diekhans, M., Dodge, S., Dubchak, I., Dunn, D.M., Eddy, S.R., Elnitski, L., Emes, R.D., Eswara, P., Eyras, E., Felsenfeld, A., Fewell, G.A., Flicek, P., Foley, K., Frankel, W.N., Fulton, L.A., Fulton, R.S., Furey, T.S., Gage, D., Gibbs, R.A., Glusman, G., Gnerre, S., Goldman, N., Goodstadt, L., Grafham, D., Graves, T.A., Green, E.D., Gregory, S., Guigó, R., Guyer, M., Hardison, R.C., Haussler, D., Hayashizaki, Y., Hillier, L.W., Hinrichs, A., Hlavina, W., Holzer, T., Hsu, F., Hua, A., Hubbard, T., Hunt, A., Jackson, I., Jaffe, D.B., Johnson, L.S., Jones, M., Jones, T.A., Joy, A., Kamal, M., Karlsson, E.K., Karolchik, D., Kasprzyk, A., Kawai, J., Keibler, E., Kells, C., Kent, W.J., Kirby, A., Kolbe, D.L., Korf, I., Kucherlapati, R.S., Kulbokas, E.J., Kulp, D., Landers, T., Leger, J.P., Leonard, S., Letunic, I., Levine, R., Li, J., Li, M., Lloyd, C., Lucas, S., Ma, B., Maglott, D.R., Mardis, E.R., Matthews, L., Mauceli, E., Mayer, J.H., McCarthy, M., McCombie, W.R., McLaren, S., McLay, K., McPherson, J.D., Meldrim, J., Meredith, B., Mesirov, J.P., Miller, W., Miner, T.L., Mongin, E., Montgomery, K.T., Morgan, M., Mott, R., Mullikin, J.C., Muzny, D.M., Nash, W.E., Nelson, J.O., Nhan, M.N., Nicol, R., Ning, Z., Nusbaum, C., O'Connor, M.J., Okazaki, Y., Oliver, K., Overton-Larty, E., Pachter, L., Parra, G., Pepin, K.H., Peterson, J., Pevzner, P., Plumb, R., Pohl, C.S., Poliakov, A., Ponce, T.C., Ponting, C.P., Potter, S., Quail, M., Reymond, A., Roe, B.A., Roskin, K.M., Rubin, E.M., Rust, A.G., Santos, R., Sapojnikov, V., Schultz, B., Schultz, J., Schwartz, M.S., Schwartz, S., Scott, C., Seaman, S., Searle, S., Sharpe, T., Sheridan, A., Shownkeen, R., Sims, S., Singer, J.B., Slater, G., Smit, A., Smith, D.R., Spencer, B., Stabenau, A., Stange-Thomann, N., Sugnet, C., Suyama, M., Tesler, G., Thompson, J., Torrents, D.,

Trevaskis, E., Tromp, J., Ucla, C., Ureta-Vidal, A., Vinson, J.P., Von Niederhausern, A.C., Wade, C.M., Wall, M., Weber, R.J., Weiss, R.B., Wendl, M.C., West, A.P., Wetterstrand, K., Wheeler, R., Whelan, S., Wierzbowski, J., Willey, D., Williams, S., Wilson, R.K., Winter, E., Worley, K.C., Wyman, D., Yang, S., Yang, S.-P., Zdobnov, E.M., Zody, M.C., Lander, E.S., 2002. Initial sequencing and comparative analysis of the mouse genome. Nature 420, 520–562.

Waumans, Y., Baerts, L., Kehoe, K., Lambeir, A.M., De Meester, I., 2015. The dipeptidyl peptidase family, prolyl oligopeptidase and prolyl carboxypeptidase in the immune system and inflammatory disease, including atherosclerosis. Front. Immunol. 6, 387.

Wen, Y., Wang, C.T., Ma, T.T., Li, Z.Y., Zhou, L.N., Mu, B., Leng, F., Shi, H.S., Li, Y.O., Wei, Y.Q., 2010. Immunotherapy targeting fibroblast activation protein inhibits tumor growth and increases survival in a murine colon cancer model. Cancer Sci. 101, 2325–2332.

Weihofen, W.A.,Liu, J., Reutter, W., Saenger, W., Fan, H., 2004. Crystal structure of CD26/dipeptidyl-peptidase IV in complex with adenosine deaminase reveals a highly amphiphilic interface. J. Biol. Chem. 279, 43330–43335.

Wesley, U., Albino, A., Tiwari, S., Houghton, A., 1999. A role for dipeptidyl peptidase IV in suppressing the malignant phenotype of melanocytic cells. J. Exp. Med. 190, 311–322.

Wesley, U., McGroarty, M., Homoyouni, A., 2005. Dipeptidyl peptides inhibits malignant phenotype of prostate cancer cells by blocking basic fibroblast growth factor signaling pathway. Cancer Res. 65, 1325–1334.

Wesley, U., Tiwari, S., Houghton, A., 2004. Role for dipeptidyl peptidase IV in tumor suppression of human non small cell lung carcinoma cells. Int. J. Cancer 109, 855–66.

Wesley, U. V, Mcgroarty, M., Homoyouni, A., 2005. Dipeptidyl Peptidase Inhibits Malignant Phenotype of Prostate Cancer Cells by Blocking Basic Fibroblast Growth Factor Signaling Pathway Dipeptidyl Peptidase Inhibits Malignant Phenotype of Prostate Cancer Cells by Blocking Basic Fibroblast Growth Factor S. Cancer Res. 65, 1325–1334.

Wight, T.N., Kang, I., Evanko, S.P., Harten, I.A., Chang, M.Y., Pearce, O.M.T., Allen, C.E., Frevert, C.W., 2020. Versican—A Critical Extracellular Matrix Regulator of Immunity and Inflammation. Front. Immunol. 11, 512.

Wikberg, M.L., Edin, S., Lundberg, I. V, Van Guelpen, B., Dahlin, A.M., Rutegård, J.,

Stenling, R., Öberg, A., Palmqvist, R., 2013. High intratumoral expression of fibroblast activation protein (FAP) in colon cancer is associated with poorer patient prognosis. Tumor Biol. 1–8.

Williams, K.H., Viera De Ribeiro, A.J., Prakoso, E., Veillard, A.S., Shackel, N.A., Bu, Y., Brooks, B., Cavanagh, E., Raleigh, J., Mclennan, S. V, Mccaughan, G.W., Bachovchin, W.W., Keane, F.M., Zekry, A., Twigg, S.M., Gorrell, M.D., 2015. Lower serum fibroblast activation protein shows promise in the exclusion of clinically significant liver fibrosis due to non-alcoholic fatty liver disease in diabetes and obesity. Diabetes Res. Clin. Pract. 108, 466–472.

Wilson, C.H., Abbott, C.A., 2012. Expression profiling of dipeptidyl peptidase 8 and 9 in breast and ovarian carcinoma cell lines. Int. J. Oncol. 41, 919–932.

Wilson, C.H., Indarto, D., Doucet, A., Pogson, L.D., Pitman, M.R., McNicholas, K., Menz, I.R., Overall, C.M., Abbott, C.A., 2013. Identifying natural substrates for dipeptidyl peptidases 8 and 9 using terminal amine isotopic labeling of substrates (TAILS) reveals in vivo roles in cellular homeostasis and energy metabolism. J. Biol. Chem. 288, 13936–13949.

Wilson, M.J., Ruhland, A.R., Quast, B.J., Reddy, P.K., Ewing, S.L., Sinha, A.A., 2000. Dipeptidylpeptidase IV activities are elevated in prostate cancers and adjacent benign hyperplastic glands. J. Androl. 21, 220–226.

Won, J.H., Park, S., Hong, S., Son, S., Yu, J.W., 2015. Rotenone-induced Impairment of Mitochondrial Electron Transport Chain Confers a Selective Priming Signal for NLRP3 Inflammasome Activation. J. Biol. Chem. 290, 27425–27437.

Wong, A.K.F., Howie, J., Petrie, J.R., Lang, C.C., 2009. AMP-activated protein kinase pathway: A potential therapeutic target in cardiometabolic disease. Clin. Sci. 116, 607–620.

Woods, A., Dickerson, K., Heath, R., Hong, S.P., Momcilovic, M., Johnstone, S.R., Carlson, M., Carling, D., 2005. Ca2+/calmodulin-dependent protein kinase kinase-β acts upstream of AMP-activated protein kinase in mammalian cells. Cell Metab. 2, 21–33.

Wronkowitz, N., Görgens, S.W., Romacho, T., Villalobos, L.A., Sánchez-Ferrer, C.F., Peiró, C., Sell, H., Eckel, J., 2014. Soluble DPP4 induces inflammation and proliferation of human smooth muscle cells via protease-activated receptor 2. Biochim. Biophys. Acta - Mol. Basis Dis. 1842, 1613–1621.

Wu, C., Hu, S., Wang, N., Tian, J., 2017. Dipeptidyl peptidase-4 inhibitor Sitagliptin prevents high glucose-induced apoptosis via activation of AMP-activated protein kinase in endothelial cells. Mol. Med. Rep. 15, 4346–4351.

Wu, D., Li, L., Liu, C., 2014. Efficacy and safety of dipeptidyl peptidase-4 inhibitors and metformin as initial combination therapy and as monotherapy in patients with type 2 diabetes mellitus: a meta-analysis. Diabetes, Obes. Metab. 16, 30–37.

Wu, L., Zhou, B., Oshiro-Rapley, N., Li, M., Paulo, J.A., Webster, C.M., Mou, F., Kacergis, M.C., Talkowski, M.E., Carr, C.E., Gygi, S.P., Zheng, B., Soukas, A.A., 2016. An Ancient, Unified Mechanism for Metformin Growth Inhibition in C. elegans and Cancer. Cell 167, 1705-1718.e13.

Wu, Y., Yakar, S., Zhao, L., Hennighausen, L., LeRoith, D., 2002. Circulating insulin-like growth factor-I levels regulate colon cancer growth and metastasis. Cancer Res. 62, 1030–1035.

Wullschleger, S., Loewith, R., Hall, M.N., 2006. TOR signaling in growth and metabolism. Cell 124, 471–484.

Xin, M.W., Yao, T.W., Nadvi, N.A., Osborne, B., McCaughan, G.W., Gorrell, M.D., 2008. Fibroblast activation protein and chronic liver disease. Front. Biosci. 13, 3168–3180.

Yabluchanskiy, A., Ma, Y., Iyer, R.P., Hall, M.E., Lindsey, M.L., 2013. Matrix metalloproteinase-9: Many shades of function in cardiovascular disease. Physiology 28, 391–403.

Yamaguchi, U., Nakayama, R., Honda, K., Ichikawa, H., Hasegawa, T., Shitashige, M., Ono, M., Shoji, A., Sakuma, T., Kuwabara, H., Shimada, Y., Sasako, M., Shimoda, T., Kawai, A., Hirohashi, S., Yamada, T., 2008. Distinct gene expression-defined classes of gastrointestinal stromal tumor. J. Clin. Oncol. 26, 4100–4108.

Yamamoto, J., Ohnuma, K., Hatano, R., Okamoto, T., Komiya, E., Yamazaki, H., Iwata, S., Dang, N.H., Aoe, K., Kishimoto, T., Yamada, T., Morimoto, C., 2014. Regulation of somatostatin receptor 4-mediated cytostatic effects by CD26 in malignant pleural mesothelioma. Br. J. Cancer 110, 2232–2245.

Yamazaki, H., Naito, M., Ghani, F.I., Dang, N.H., Iwata, S., Morimoto, C., 2012. Characterization of cancer stem cell properties of CD24 and CD26-positive human malignant mesothelioma cells. Biochem. Biophys. Res. Commun. 419, 529–536.

Yamochi, Toshiko, Yamochi, Tadanori, Aytac, U., Sato, T., Sato, K., Ohnuma, K., McKee, K.S., Morimoto, C., Dang, N.H., 2005. Regulation of p38 phosphorylation and topoisomerase IIα expression in the B-cell lymphoma line Jiyoye by CD26/dipeptidyl peptidase IV is associated with enhanced in vitro and in vivo sensitivity to doxorubicin. Cancer Res. 65, 1973–1983.

Yan, S., Marguet, D., Dobers, J., Reutter, W., Fan, H., 2003. Deficiency of CD26 results in a change of cytokine and immunoglobin secretion after stimulation by pokeweed mitogen. Eur. J. Immunol. 33, 1519–1527.

Yang, J., Nie, J., Ma, X., Wei, Y., Peng, Y., Wei, X., 2019. Targeting PI3K in cancer: Mechanisms and advances in clinical trials. Mol. Cancer 18, 1–28.

Yang, X., Zhang, X., Wu, R., Huang, Q., Jiang, Y., Qin, J., Yao, F., Jin, G., Zhang, Y., 2017. DPPIV promotes endometrial carcinoma cell proliferation, invasion and tumorigenesis. Oncotarget 8, 8679–8692.

Yazbeck, R., Howarth, G.S., Abbott, C.A., 2009. Dipeptidyl peptidase inhibitors, an emerging drug class for inflammatory disease? Trends Pharmacol. Sci. 30, 600–607.

Yazbeck, R., Jaenisch, S.E., Abbott, C.A., 2018. Potential disease biomarkers: dipeptidyl peptidase 4 and fibroblast activation protein. Protoplasma 255, 375–386.

Yazbeck, R., Jaenisch, S.E., Abbott, C.A., 2021. Dipeptidyl peptidase 4 inhibitors: Applications in innate immunity? Biochem. Pharmacol. 188, 114517.

Yazbeck, R., Sulda, M.L., Howarth, G.S., Bleich, A., Raber, K., Von Hörsten, S., Holst, J.J., Abbott, C.A., 2010. Dipeptidyl peptidase expression during experimental colitis in mice. Inflamm. Bowel Dis. 16, 1340–1351.

Yeung, T.M., Gandhi, S.C., Wilding, J.L., Muschel, R., Bodmer, W.F., 2010. Cancer stem cells from colorectal cancer-derived cell lines. Proc. Natl. Acad. Sci. U. S. A. 107, 3722–3727.

Yizhak, K., Le Devedec, S.E., Rogkoti, V.M., Baenke, F., de Boer, V.C., Frezza, C., Schulze, A., van de Water, B., Ruppin, E., 2014. A computational study of the Warburg effect identifies metabolic targets inhibiting cancer migration. Mol. Syst. Biol. 10, 744–744.

Yu, D.M.T., Slaitini, L., Gysbers, V., Riekhoff, a G.M., Kähne, T., Knott, H.M., De Meester, I., Abbott, C. a, McCaughan, G.W., Gorrell, M.D., 2011. Soluble CD26/dipeptidyl

peptidase IV enhances human lymphocyte proliferation in vitro independent of dipeptidyl peptidase enzyme activity and adenosine deaminase binding. Scand. J. Immunol. 73, 102–11.

Yu, D.M.T., Wang, X.M., McCaughan, G.W., Gorrell, M.D., 2006. Extraenzymatic functions of the dipeptidyl peptidase IV-related proteins DP8 and DP9 in cell adhesion, migration and apoptosis. FEBS J. 273, 2447–2460.

Yu, D.M.T., Yao, T.-W., Chowdhury, S., Nadvi, N.A., Osborne, B., Church, W.B., McCaughan, G.W., Gorrell, M.D., 2010. The dipeptidyl peptidase IV family in cancer and cell biology. FEBS J. 277, 1126–44.

Yu, L., Lu, M., Jia, D., Ma, J., Ben-Jacob, E., Levine, H., Kaipparettu, B.A., Onuchic, J.N., 2017. Modeling the genetic regulation of cancer metabolism: Interplay between glycolysis and oxidative phosphorylation. Cancer Res. 77, 1564–1574.

Zakikhani, M., Dowling, R., Fantus, I.G., Sonenberg, N., Pollak, M., 2006. Metformin is an AMP kinase-dependent growth inhibitor for breast cancer cells. Cancer Res. 66, 10269–10273.

Zeng, Y., Li, C., Guan, M., Zheng, Z., Li, J., Xu, W., Wang, L., He, F., Xue, Y., 2014. The DPP-4 inhibitor sitagliptin attenuates the progress of atherosclerosis in apolipoprotein-E-knockout mice via AMPK- and MAPK-dependent mechanisms. Cardiovasc. Diabetol. 13, 1–10.

Zhang, C.S., Hawley, S.A., Zong, Y., Li, M., Wang, Z., Gray, A., Ma, T., Cui, J., Feng, J.W., Zhu, M., Wu, Y.Q., Li, T.Y., Ye, Z., Lin, S.Y., Yin, H., Piao, H.L., Hardie, D.G., Lin, S.C., 2017. Fructose-1,6-bisphosphate and aldolase mediate glucose sensing by AMPK. Nature 548, 112–116.

Zhang, H.-H., Guo, X.-L., 2016. Combinational strategies of metformin and chemotherapy in cancers. Cancer Chemother. Pharmacol. 78, 13–26.

Zhang, M., Qiao, Y., Suo, Z., 2008. Correlation of DPPIV expression with clinicopathological features and prognosis in epithelial ovarian carcinoma. Zhonghua Zhong Liu Za Zhi 30, 848–852.

Zhang, M., Xu, L., Wang, X., Sun, B., Ding, J., 2015. Expression levels of seprase/FAPα and DPPIV/CD26 in epithelial ovarian carcinoma. Oncol. Lett. 10, 34–42.

Zhang, S., Sheng, H., Zhang, X., Qi, Q., Chan, C.B., Li, L., Shan, C., Ye, K., 2019. Cellular energy stress induces AMPK-mediated regulation of glioblastoma cell proliferation by PIKE-A phosphorylation. Cell Death Dis. 10, 222.

Zhang, Y., Hildegund, C.J.., 2016. Depletion of FAP+ cells reduces immunosuppressive cells and improves metabolism and functions CD8+T cells within tumors. Oncotarget 7, 23282–23299.

Zhou, G., Myers, R., Li, Y., Chen, Y., Shen, X., Fenyk-Melody, J., Wu, M., Ventre, J., Doebber, T., Fujii, N., Musi, N., Hirshman, M.F., Goodyear, L.J., Moller, D.E., 2001. Role of AMP-activated protein kinase in mechanism of metformin action. J. Clin. Invest. 108, 1167–1174.

Ziani, L., Chouaib, S., Thiery, J., 2018. Alteration of the Antitumor Immune Response by Cancer-Associated Fibroblasts. Front. Immunol. 9.

Zwerschke, W., Mazurek, S., Stöckl, P., Hütter, E., Eigenbrodt, E., Jansen-Dürr, P., 2003. Metabolic analysis of senescent human fibroblasts reveals a role for AMP in cellular senescence. Biochem. J. 376, 403–411.

Appendix A

A.1 Bioenergetic analysis using the XF Extracellular Flux Analyser

The Seahorse XF Extracellular Flux Analyzer provides the ability to simultaneously quantify the cellular oxygen consumption rate (OCR) as a measure of oxidative phosphorylation and the extracellular acidification rate (ECAR) as a measure of glycolytic metabolism (Kalyanaraman et al., 2018). For this work we used the 96-well instrument with the XF assay kit containing a disposable sensor cartridge embedded with pairs of fluorescence biosensors coupled to a fibre optic waveguide for measurement of oxygen (532 nm/650 nm) and pH (470 nm/530 nm). In the 96-well cartridge each well is equipped with four reagent delivery chambers for direct delivery of various compounds used to examine the bioenergetic profile of cells during assays. The nature of the Seahorse XF Extracellular Flux Analyzer allows bioenergetic measurements to be made repeatedly over time using the same cell population, detailed.

A.1.1 Mitochondrial stress test

The extracellular flux analyser coupled with sequential injection of electron transport chain (ETC) inhibitors is a reliable method for assessing mitochondrial function (Dranka et al., 2012). Sequential injection of the ETC inhibitors, oligomycin, FCCP, rotenone and antimycin A are used to determine multiple mitochondrial parameters including basal OCR, ATP-linked OCR, proton leak, maximal respiratory capacity, and mitochondrial reserve respiratory capacity. Measurement of mitochondrial function is assessed in four stages (Figure 4.2) with three measurements taken three minutes apart at each stage. Stage one of the process runs between the 0- and 12-minute mark, this is the measurement of basal OCR taken over three readings from cells prior to the addition of ETC modulators.

Stage two is initiated via an injection of 1mM of oligomycin A performed at the 18-minute time point. Oligomycin is an inhibitor of ATP synthase and stops oxidative phosphorylation of ADP to ATP through the blockage of the F0 subunit proton channel (complex V, Figure 4.1) (Matsuno-Yagi and Hatefi, 1985; Stock et al., 2013). The inhibition of ATP synthesis by oligomycin A will eliminate electron flow through the electron transport chain but some electron flow associated with proton leak or mitochondrial uncoupling will still be evident in the overall OCR measurement. The injection of 1mM oligomycin A and subsequent OCR measurements allow for quantification of mitochondrial respiration required to satisfy the basal cellular ATP demand. The level of energy production driven by oxidative phosphorylation is determined by comparison of basal OCR levels to those seen after oligomycin injection (Divakaruni et al., 2014).

Stage three performed at the 36-minute time point is the injection of 2mM carbonyl cyanide-4-(trifluoromethoxy) phenylhydrazone or FCCP. FCCP is an ionophore or a mobile ion carrier, it is an uncoupling agent and disrupts ATP synthesis by transporting hydrogen ions through the inner mitochondrial cell membrane before they can be used to provide the energy for oxidative phosphorylation (Figure 4.1) (Cutró et al., 2014). The injection of 2mM FCCP provides a measure of the maximal mitochondrial respiration rate and the difference between the basal OCR and the maximal respiration OCR reflects the spare respiratory capacity of the cell (Divakaruni et al., 2014).

Stage four is performed at the 54-minute time point and is the addition of 1mM of both rotenone and antimycin A. Rotenone and antimycin A individually inhibit components of the mitochondrial electron transport chain, rotenone inhibits the transfer of electrons from iron-sulfur centers in complex I to ubiquinone and antimycin A inhibits the oxidation of ubiquinol in complex III through binding to the Qi site of cytochrome c reductase (Figure 4.1) (Hua et al., 2019; Ma et al., 2011; Won et al., 2015). The actions of both inhibitory agents create a back-up of electrons within the inner mitochondria disrupting the formation of the proton gradient across the inner membrane. The disruption results in no proton flow through the ATP synthase complex which completely shuts down mitochondrial respiration and abolishes the production of ATP via oxidative phosphorylation. The OCR measurement taken after addition of rotenone and antimycin A provides a quantification for any non-mitochondrial respiration within the cell (Divakaruni et al., 2014).

For development of a bioenergetic profile for the cell, basal respiration is calculated by subtracting the non-mitochondrial OCR taken after addition of rotenone and antimycin A from the initial three readings taken without the addition of ETC modulators. ATP linked or coupled respiration is calculated by subtracting the OCR after addition of oligomycin from the basal respiration OCR. Proton leak is calculated from the difference between OCR measured after oligomycin treatment and the non-mitochondrial OCR determined after addition of rotenone and antimycin A and maximal respiration is the OCR recorded after the addition of FCCP (Divakaruni et al., 2014). OCR readings were taken at 3-minute intervals and three interval readings were taken after the addition of each ETC modulator.
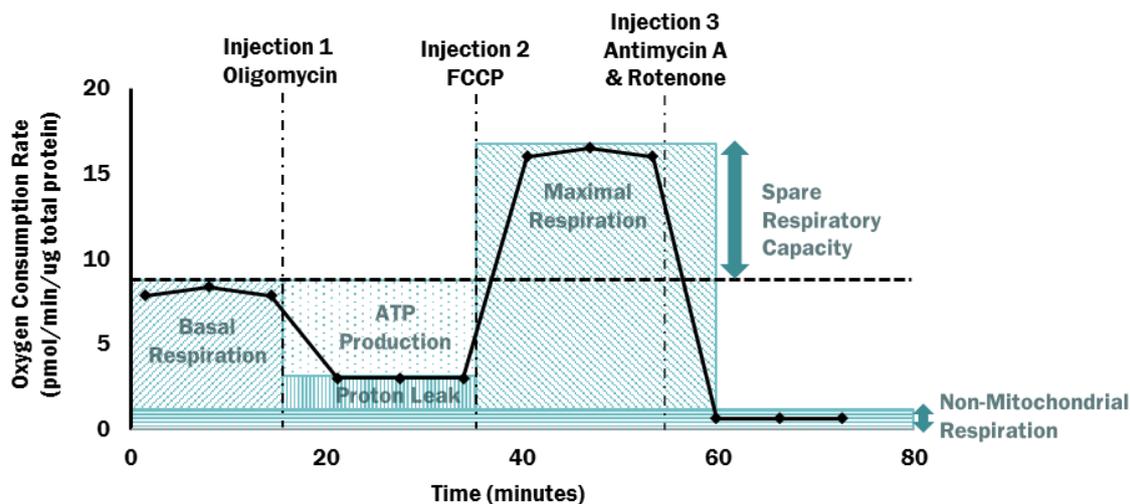
Figure A.1. The expected profile of oxygen consumption rate over time for an Xfe analyser mitochondrial stress test. First three readings determine basal mitochondrial metabolism. Injection 1: performed at the 18-minute time point is 1mM of Oligomycin A which is an inhibitor of ATP synthase. Some electron flow is still evident, as depicted above, through a process known as proton leak or mitochondrial uncoupling. ATP production is determined via a comparison of basal OCR levels to those seen after Oligomycin injection. Injection 2: performed at the 36-minute time point is 2mM FCCP or Carbonyl cyanide-4-(trifluoromethoxy) phenylhydrazone. FCCP is an ionophore or a mobile ion carrier. It is an uncoupling agent and disrupts ATP synthesis by transporting hydrogen ions through the inner mitochondrial cell membrane before they can be used to provide the energy for oxidative phosphorylation. The injection of 2mM FCCP provides a measure of the maximal respiration of the cell and the difference between the Basal OCR level and the maximal respiration level reflects the spare respiratory capacity. Injection 3: performed at the 54 minute time point is 1mM of both rotenone and antimycin A. Rotenone and antimycin A individually inhibit components of the mitochondrial electron transport chain. Rotenone inhibits the transfer of electrons from iron-sulfur centres in complex I to ubiquinone and antimycin A inhibits the oxidation of ubiquinol through binding to the Qi site of cytochrome c reductase. The actions of both inhibitory agents create a back-up of electrons within the inner mitochondria disrupting the formation of the proton gradient across the inner membrane. The injection of 1mM rotenone and antimycin A completely shuts down mitochondrial respiration and any oxygen consumption requirements of the cell allowing for a measurement of the maximal respiration as well as an indication of the portion of non-mitochondrial respiration responsible for ATP production.

A.1.2 Glycolysis stress test

For this work a measurement of the variation in extracellular H^+ concentration or extracellular acidification rate (ECAR) was taken to determine the basal and maximal glycolytic capacity of the cell. This measurement was done in two stages and requires the use of the ETC modulator oligomycin A. Stage one uses the first three ECAR readings taken without the addition of ETC modulators to determine the basal level of glycolysis within the cell (Figure 4.3). This is a measurement of the level of glycolytic activity required by the cell for basal ATP production. In non-cancerous cells performing optimum levels of aerobic respiration, the glycolytic level will be that which provides enough pyruvate and $NADH^+ H^+$ to feed into the TCA cycle for further ATP production via mitochondrial respiration. Basal glycolysis will be increased in cancerous cells due to production of ATP through heightened aerobic glycolysis.

Stage two is performed at the 18-minute time point and like the OCR measurement requires the addition of 1mM of oligomycin A (Figure 4.3). As oligomycin blocks ATP synthase activity meaning the cell can no longer rely on oxidative phosphorylation for energy production and must rely solely on glycolysis for its energy needs. The injection of 1mM oligomycin A and subsequent ECAR measurements reflect maximal glycolytic capacity of the cell as the ATP production capacity of the cell through mitochondrial respiration has been blocked. This measure of glycolytic activity via extracellular acidification utilizes stage one and two of the OCR protocol and is run in conjunction with the OCR measurements to produce a complete bioenergetic analysis. For quantification of ECAR injection 2 and 3 of 2mM FCCP and 1mM each of rotenone and antimycin A respectively have no further effect on the ECAR measurement. After the use of oligomycin A, glycolysis is already at its maximal level. The use of these uncoupling agents to further disrupt mitochondrial ATP synthesis simply ensures that the cells are relying on aerobic glycolysis for their energy needs, this is reflected by minimal change in the ECAR measurement once glycolytic capacity is reached after injection of oligomycin A.
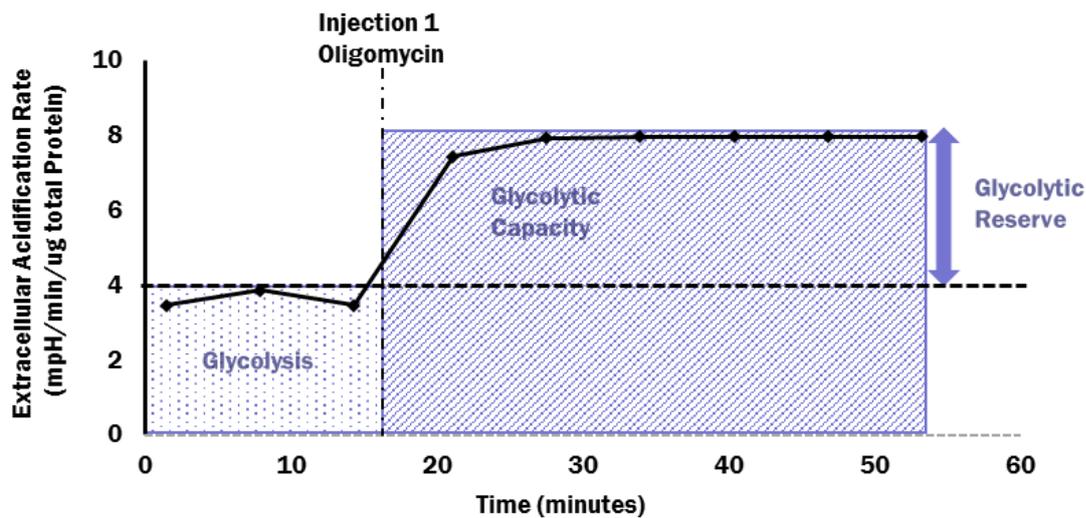
Figure A.2. The expected profile of extracellular acidification rate (ECAR) over time for an XFe analyser glycolysis stress test. ECAR is taken as a measurement of the variation in extracellular H^+ concentration. The first three readings determine the basal level of glycolysis within the cell. This is a measurement of the level of glycolytic activity required by the cell for basal ATP production. In non-cancerous cells performing optimum levels of aerobic respiration, the glycolytic level will be that which provides enough pyruvate and $NADH^+$ H^+ to feed into the TCA cycle for further ATP production via mitochondrial respiration. Basal glycolysis will be increased in cancerous cells due to production of ATP through heightened aerobic glycolysis. Injection 1: performed at the 18-minute time point is 1mM of oligomycin A which is an inhibitor of ATP synthase. Oligomycin stops oxidative phosphorylation of ADP to ATP through the inhibition of ATP synthase which is required for oxidative phosphorylation (energy production). The injection of 1mM oligomycin A and subsequent ECAR measurements reflect maximal glycolytic capacity of the cell as the ATP production capacity of the cell through mitochondrial respiration has been blocked. Injection 2 and 3, seen in Figure 2.1.but not depicted here, of 2mM FCCP and 1mM each of rotenone and antimycin A respectively have no further effect on the ECAR measurement. After the use of oligomycin A, glycolysis is already at its maximal level. The use of these uncoupling agents to further disrupt mitochondrial ATP synthesis simply ensures that the cells are relying on aerobic glycolysis for the majority of their energy needs, this is reflected by minimal change in the ECAR measurement once glycolytic capacity is reached through injection of oligomycin A.

A.2 Mouse Diet Composition

GORDONS SPECIALTY FEEDS
RAT AND MOUSE PREMIUM BREEDER DIET 23% PROTEIN

A complete diet for rats and mice. Suitable for intensive breeding and all stages of development (breeding/gestation/lactation/growth). A high protein and high energy diet. Available in standard, autoclavable and irradiated forms. A fixed formula diets.

Ingredients
Wheat
Sorghum
Soybean meal
Pollard
Bran
Meat and bone meal
Bloodmeal
Fish meal
Lucerne meal
Vegetable oil
Sunflower meal
Salt
Vitamin and mineral premix
Lysine
Choline chloride
(Additional premixes for irradiated pellets and for autoclavable pellets)

Proximate Analysis
Min. Crude Protein………….23% Max. Crude Fibre……….5%
Min. Crude Fat ……………… 6% M.E. (Min.)…………13mj/kg

Calculated Analysis Results:

Amino Acids

Lysine	9.8g/kg
Methionine & Cystine	5.9g/kg
Threonine	8.4g/kg
Histidine	5.0g/kg
Leucine	15.2g/kg
Arginine	12.1g/kg
Valine	10.2g/kg
Isoleucine	8.0g/kg
Phenylaline & Tyrosine	16.4g/kg
Tryptophan	3.7g/kg

Minerals

Calcium	10.1g/kg
Phosphorus	7.7g/kg
Potassium	5.4g/kg

Magnesium	1.8g/kg
Iron	97.0mg/kg
Copper	10.6mg/kg
Manganese	87.4mg/kg
Zinc	48.1mg/kg
Iodine	1.15mg/kg
Selenium	0.1mg/kg
Sodium	0.3%

Fats

Saturated Fat	14.9g/kg
Mono-unsaturated	18.1g/kg
Poly-unsaturated w6	22.0g/kg
Poly-unsaturated w3	6.5g/kg

Vitamins

Vitamin A	170µg/100g
Vitamin B1 (Thiamine)	4mg/kg
Vitamin B2 (Riboflavin)	5mg/kg
Vitamin B6 (Pyridoxine)	6mg/kg
Vitamin B12 (Cyanocobalamin)	0.005mg/kg
Vitamin C (Ascorbic Acid)	150mg/kg
Vitamin D	200i.u/kg
Vitamin E (Tocopherol Acetate)	50mg/kg
Vitamin K (menadione)	13mg/kg
Niacin	10mg/kg
Pantothenate	12mg/kg
Folic Acid	10mg/kg
Biotin	0.06mg/kg

The diet is a fixed formula. This proximate analysis is calculated on published and analytical testing data for raw ingredients. There may be variations in the nutrient values which are inherent in natural ingredients.

Data updated on 10.3.16